UNIVERSITÀ DEGLI STUDI DI PADOVA

Università degli Studi di Padova

Dipartimento di Scienze Biomediche

CORSO DI DOTTORATO DI RICERCA IN SCIENZE BIOMEDICHE SPERIMENTALI

CICLO: XXX

Neuroeffector coupling in the heart: determinants of function and survival of cardiac sympathetic neurons

Tesi redatta con il contributo finanziario di:
Comunità Europea (EUTrigTreat); Association Francaise des Miopaties (AFM, TG19956)

Coordinatore: Ch.mo Prof. Paolo Bernardi

Supervisore: Ch.mo Prof. Marco Mongillo

Co-Supervisore: Ch.ma Dott. ssa Tania Zaglia

Dottoranda : Valentina Prando

INDICE

ABBREVIATIONS

2-AFG3L2	ATPase family gene 3-like protein
6-OH-DA	6-Hydroxy-DopAmine
α-MyHC	alpha-Myosin Heavy Chain
AC	Adenylyl Cyclase
ACh	Acetylcholin
ADOA	Dominant Optic Atrophy
AKAR3	A-kinase activity reporter
ALS	Autophagy-Lysosome System
ANS	Autonomic Nervous System
AP	Action Potential
ATP	Adenosine-1,4,5,-TriPhosphate
AV	Atrioventricular
AVN	Atrioventricular Node
β-AR	beta-Adrenergic Receptor
BSA	Bovine Serum Albumin
cAMP	Cyclic-Adenosine Monophosphate
CHMP2B	Charged Multivesicular Body protein 2B
ChR2	ChannelRhodopsin-2
CICR	Calcium-Induced Calcium Release
CM	Cardiomyocyte
cSN	cardiac Sympathetic Neurons
Cy3	Cyanine-3
Cx	Connexin
DA	Dopamine
DA-β-OH	Dopamine β-hydroxylase
DAPI	4,6-Diamidino-2-Phenyl-Indole
DNA	Deoxyribonucleid Acid
Drp1	Dynamin-Related Protein-1
DSI	Data Science International
DTI	Diffusion Tensor Cardiovascular Magnetic Resonance

DTT	Dithiotreitol
ECC	Excitation Contraction Coupling
ECG	Electrocardiogram
EDTA	Ethilenediaminetetraacetic Acid
EF	Ejection Fraction
ENDO	*Subendocardium*
EPAC1	Exchange Protein directly Activated by cAMP
EPI	*Subepicardium*
ESC	Embryonic stem cell
ESCRT	Endosomal Sorting Complexes Required for Transport
FBS	Fetal Bovine Serum
FFPE	Formalin-fixed paraffin-embedded
FITC	Fluorescein Isothiocyanate
FOXO	Forkhead box O
FRET	Föster Resonance Energy Transfer
FS	Fractional Shortening
GAPDH	GlycerAldehyde 3-Phosphate DeHydrogenase
GP	Gap Junction
GPCR	G protein-coupled receptor
HCN	Hyperpolarization activated cyclic-nucleotide gated channels
hFis-1	Mitochondrial Fission-1
HR	Heart Rate
HRV	Heart Rate Variability
HS	Horse Serum
IF	Immunofluorescence
IMM	Inner Mitochondrial Membrane
ITS	Insuline-trasferrin-selenium
IVS	Interventricular Septum
LA	Left Atrium
LAD	Left Anterior Descending
LBB	left bundle branch
LED	Light Emitting Diode
LV	Left Ventricle
m-AAA	mitochondrial ATPases Associated with diverse cellular Activities

MAFbx	Muscle Atrophy F-box
MFN	Mitofusin
MID	*Midmyocardium*
MOPS	4-MorpholinePropane Sulfonic acid
mTOR	mammalian Target Of Rapamycin
MTS	Signal for Mitochondrial import
MuRF1	Muscle Ringfinger protein 1
NCX	Na^{+}/Ca^{2+} exchanger
NE	Norepinephrine
NEAA	Non essential amminoacid
NGF	Nerve Growth Factor
NMJ	Neuromuscular Junction
NPY	Neuropeptide-Y
NT	Neurotransmitter
NT-3	NeuroTrophin-3
OCT	Optimal Cutting Temperature embedding matrix
OMA1	m-AAA protease
OMM	outer Mitochondrial Membrane
Opa1	Optic Atrophy Protein 1
OPT	Optical Projection Tomography
OXPHOS	Oxidative Phosphorylation
p75	p75 neurotrophin receptor
PARL	Presenilin-associated rhomboid-like
PBS	Phosphate Buffered Saline
PCR	Polymerase Chain Reaction
PF	Purkinje Fiber
PFA	Para-Formaldehyde
PKA	Protein Kinase A
PLB	Phopsholamban
PNS	Parasympathetic Nervous System
PVDF	Polyvynilidene Fluoride
PVC	Premature Ventricular Complex
RA	Right Atrium
RBB	Right Bundle Branch

RNA	Ribonucleic Acid
ROI	Region of interest
ROS	Reactive Oxygen Species
RT	Room Temperature
RT-qPCR	Real Time Quantitative Polymerase Chain Reaction
RV	Right Ventricle
RyR2	Ryanodine Receptor 2
SAN	Sinoatrial Node
SCGN	Superior Cervical Ganglia Neuron
SDNN	Standard Deviation N-N interval
SDS	Sodium Dodecyl Sulfate
SEM	Standard Error Mean
Sema-3A	Semaphorine -3A
SERCA	Sarco-Endoplasmic Reticulum Calcium ATPase
SMA	Smooth Muscle Actin
SMC	Smooth Muscle cells
SN	Sympathetic Neuron
SNAP25	Synaptosomal-associated protein 25
SNS	Sympathetic Nervous System
SR	Sarcoplasmic Reticulum
SYN1a	Synapsin 1a
TBS	Tris Buffered Saline
Tn-C	Troponin-C
TnI	Troponin-I
Tn-T	Troponin-T
TOH	Tyrosine Hydroxylase
TRITC	Tetrametil Rhodamine IsoThioCyanato
TrkA	Tyrosine kinases ReceptorA
TTBS	Tween20-Tris Buffered Saline
UPS	Ubiquitin Proteasome System
VIP	Vasointestinal peptide
WB	Western Blot
WGA	Wheat Germ Agglutinin
YME1L	ATP-dependent metalloprotease

SUMMARY

Rationale: The sympathetic branch of the autonomic nervous system (ANS) operates continuous control on the function and structure of cardiac cells (Bers *et al.,* 2009). In basal conditions, neuronal input to sino-atrial node (SAN) cardiomyocytes (CM) is responsible for the fine regulation of heart rate (HR), and in parallel, it influences the balance between protein synthesis and degradation in working CMs, thus determining the resting cellular trophism (Zaglia *et al.,* 2013). It is also commonly appreciated that sympathetic neurons (SNs) are rapidly activated upon strenuous exercise or emotional stresses characterizing the so-called 'fight-or-flight' response, resulting in the recruitment of maximal cardiac performance through positive inotropic and chronotropic effects (Li *et al.*, 2000). While these general mechanisms of regulation of heart physiology are commonly recognized and have been thoroughly investigated in the last decades in both normal and disease conditions (Franzoso *et al.,* 2016), the relationship between the fine anatomy of the myocardial neuronal network and its function, as well as the biophysics of the neuro-effector communication remain largely uncovered.

Purposes: In our initial studies, we used various imaging methods to investigate the morphological aspects of myocardial innervation. Our results demonstrate that the heart of most mammals, including humans, is highly innervated by SN processes, which distribute throughout the different heart regions with a conserved, specie-specific pattern, and display regular varicosities (i.e. active neurotransmitter release sites), which appear in close contact with the target CM membranes. Furthermore, ultrastructural analysis showed that such contacts have features similar to those described for the well-known neuromuscular junction (NMJ), which, remarkably, include the accumulation of mitochondria in the "presynaptic" varicosities (Slater, 2003; Levitan *et al.,* 2015).

This data prompted us to study:

i) the biophysics of neuro-cardiac communication, which was addressed using both *in vitro* and *in vivo* models, with the aim to determine the role of direct intercellular contact in the dynamics of neuro-effector coupling;

ii) whether dysfunction in SN mitochondria, as addressed in a newly developed murine model of Optic Atrophy Factor-1 (Opa1)

haploinsufficiency (TOH-Opa1$^{+/-}$), may affect the neurogenic control of the heart.

Results: *i)* Dynamics of neuro-effector coupling at 'cardiac sympathetic' synapses.

Sympathetic neurons operate through norepinephrine (NE) release, that by activating CM β-adrenergic receptors (β-ARs), increase intracellular cyclic-Adenosine MonoPhosphate (cAMP) and activate Protein Kinase A (PKA) and its downstream targets involved in the regulation of Ca^{2+} oscillations, thereby enhancing HR and sarcomere shortening velocity (Rochais *et al.,* 2004). The 'classic' view on the neurogenic control of heart function implicates the release of NE in the myocardial interstitium, and its diffusion to the β-AR expressing CM membranes (Levy and Martin, 1989). However, this model fails to explain the rapidity, efficiency and potency of the control exerted by the sympathetic nervous system (SNS) on cardiac function, which would be better achieved through direct intercellular contact.

To address whether SN signal to CM directly, we developed an *in vitro* model using co-cultures between superior cervical ganglia neurons (SCGNs) and neonatal rat CMs, to analyzed the dynamics of intercellular coupling at the single cell level. Once established, the SN-CM contact sites were characterized, alike the *in vivo* observations, by reduced intermembrane distance (≅ 67±16, in nm), which remained stable in time, supporting the structural basis of the neuro-cardiac interaction. In mature co-cultures, the topology of interactions established between neurons and CMs was classified into three categories: *type i)* cells in direct contact with the neuronal varicosities, identified as round shaped enlargements of the axon within the CM area; *type ii)* cells close to neuronal varicosities, that are found outside the CM area, and *type iii)* CMs passed over by the neuronal processes devoid of varicosities. As β-AR stimulation causes cardiac effects through cAMP dependent signaling, we used real time cAMP imaging in CMs expressing the FRET based Epac1-camps biosensor in co-culture, to analyze the CM responses to SN activation. Changes in intracellular [cAMP] were assessed at the single cell level by monitoring the variation of CFP/YFP emission upon CFP illumination (a.k.a. sensitized emission ratio method). Depolarization of SNs, as obtained by briefly perfusing cells with 50 mmol/L KCl, caused an increase in intracellular [cAMP] that was only detected in the innervated CMs (*type i*), while no changes

were observed in non-innervated cells on the same coverslip (type *ii and iii*), or in CMs cultured alone ($\Delta R/R_0$, innervated CMs: 9.3±0.92; non-innervated CMs: 0.23±0.08, in %). All groups showed comparable cAMP responses to direct application of NE. Addition of the cell bathing solution, collected after neuronal depolarization, to Epac1-cAMPs expressing CMs did not induce any cAMP response, indicating that the NE concentration ([NE]) in the bulk medium was too low to activate CM β-ARs. To further define the spatial range of action of NE, we investigated cAMP responses in adjacent CMs, and observed that activation of β-ARs was confined to the innervated cell. In addition, cAMP changes were faster and higher in proximity to the neuro-cardiac interaction site, thus supporting that neuronally-released NE activates only a confined pool of β-ARs/adenylyl cyclases in the post-synaptic CM membrane. Taken together, all these data support that activated SN communicate to CM by discharging NE in a 'diffusion-restricted' extracellular signalling domain at the interface between the two cell types. We thus used the principle of competition binding assay, and we estimated that neuronally released NE reaches, into the synaptic cleft, an effective concentration in the order of 100 nMol/L, which, interestingly, corresponds to the k_d of β-ARs.

To determine if the effects of sympathetic activation, *in vivo*, reflect the direct cell-cell communication observed in the *in vitro* system, we exploited optogenetics to control SN activity, while monitoring HR. The method is based on expression of Channelrhodopsin-2 (ChR2), a microbial-derived, light-activated ion channel, permeable to Na^+, in SNs (Stieber *et al.*, 2003). Illumination of ChR2-expressing neurons generates an inward current enabling cell depolarization and neurotransmitter release, with millisecond resolution (Boyden *et al*., 2005; Zhang *et al.,* 2007). Transgenic mice with the *ChR2-H134R-tdTomato* gene under control of the Tyrosine Hydroxylase (TOH) promoter, had structurally and functionally normal hearts, and expressed ChR2 in SCGN, which enabled neuronal action potentials (APs) to be triggered using short depolarizing light flashes (10 ms, 470 nm), as shown in cultured neurons. We thus used the hardware and protocols previously developed for cardiac specific optogenetics (Zaglia *et al.,* 2015), to assess the effect of SN activation on HR, by scanning the epicardial heart surface with the tip of a fiber optic probe, during delivery of light flashes. Photoactivation of a restricted region, approximately 1-2 mm wide, on the right atrial epicardium, reproducibly induced sinusal tachycardia. The underlying myocardium was marked

with dermographic ink and analysed with immunofluorescence (IF), which revealed a region with CMs expressing the *bona fide* marker of SAN myocytes, HCN4 (Liu *et al.,* 2007), interacting closely with SNs. No effect on HR was detected with photostimulation of the atrial regions immediately neighboring the SAN region, despite the dense innervation of the whole atrial myocardium, indicating a stringent target discrimination of specific groups of cardiac SNs, and suggesting that neuronally-released NE has a very limited spatial action range in the intact myocardium. To estimate the effective [NE] activating SAN β-ARs during sympathetic activity, we analyzed the effects of neuronal photostimulation in mice treated with the competitive β-AR antagonist propranolol (4 mg/kg). At this dose, propranolol decreased resting HR by about 30%. Remarkably, the response to sympathetic photoactivation was almost unchanged in propranolol treated mice, suggesting that the inhibitory effect of the antagonist was overcome by the high $[NE]_{cleft}$. These results are in line with the concept purported by our *in vitro* experiments that sympatho-cardiac coupling uses neuro-cardiac junctions. In summary, our *in vivo* data, showing the rapidity of the onset and termination of SAN responses to sympathetic stimulation, and the efficiency of neuro-cardiac coupling, are all in support of the working model whereby the establishment of a specialized extracellular domain enables sympathetic neurotransmission to the heart to occur in a 'quasi-synaptic' fashion.

Our data indicate that sympathetic modulation of CM signaling requires direct cell-cell contact, which brings together the 'neuronal NE-releasing' and the 'CM NE-sensing membranes'. Such interaction defines a low-volume extracellular space in which high [NE] is reached with only a few thousands of molecules (i.e. few vesicles), as estimated by numerical simulation obtained in neuro-effector junctions with comparable geometry. Such restricted signaling domains promote the activation of only a fraction of β-ARs within the contacted CM membrane, as supported by the stringent ***selectivity*** of neuronal target activation, and allow high ***efficiency*** enabling CM responses to minimal neuronal activation. These results fit well with the observation that signaling complexes of the cAMP/PKA pathway, including β1-ARs, as well as PKA anchoring proteins and targets, cluster within the CM membrane at the neuronal interaction site (Shcherbakova *et al.,* 2007). Our imaging data describe the consequences of such arrangement, showing that cAMP synthesis initiates, upon neuronal stimulation, at the innervated CM site,

and identify the complex formed by the neuronal varicosity and post-synaptic CM membrane as the functional signaling unit in the neurogenic regulation of the heart. This working model was corroborated by our *in vivo* findings using optogenetics, which was exploited to achieve non-invasive control of cardiac SNs, avoiding direct effects on heart electrophysiology. This property, together with the high spatial resolution in ChR2 activation, provided a flexible tool to probe the function of restricted groups of cardiac neurons *in vivo*, and address neuro-effector signaling kinetics. Although there are differences between the cellular environment *in vitro* and the intact innervated heart, the results of the *in vivo* experiments support the working model whereby neurogenic regulation of heart rhythm is underpinned by high-efficiency metabotropic synapses. The elevated speed and single beat precision of the neural control of SAN automaticity is further sustained by previous numerical modelling of agonist kinetics in a neuro-effector junction of comparable morphology, showing $[NE]_{cleft}$ rise and decay time of only few msec (Bennett *et al.,* 1995). Taken together, *in vitro* and *in vivo* evidences suggest that the morphological and functional arrangement of the neuro-cardiac junction enables the SNS to regulate heart function with high precision.

This data are part of a manuscript currently under review at the *Journal of Physiology*, in which I am co-first author.

ii) *Role of the mitochondrial protein Opa1 in the regulation of the cardiac SN physiology.*

In the study of neuro-cardiac interactions described above, we were intrigued by the observation that mitochondria accumulated in SN varicosities, and specifically concentrated in the subspace of the presynaptic membrane. Neuronal mitochondria are fundamental for several cellular functions, including neuro-exocytosis, neurotransmitter reuptake and maintenance of neuronal process trophism, but their specific role in cardiac SNs is largely unexplored.

We thus sought to determine whether dysfunctional mitochondria would compromise the neurogenic control of the heart. To this aim, we exploited a murine model generated in our laboratory, characterized by the haploinsufficiency of Opa1 gene (Hoppins *et al.,* 2007), selectively in SNs. Opa1 is a key protein implicated in mitochondrial dynamics, and its deficiency causes an inherited neurodegenerative disease characterized by retinal ganglion cell death known as Autosomal Dominant Optic Atrophy (ADOA), leading to visual loss. Interestingly,

ADOA patients also display peripheral neuropathy and cardiac rhythm abnormalities (Spiegel *et al.,* 2016) suggesting the hypothesis that dysfunctional mitochondria may affect not only central but also peripheral neurons, and remarkably, the autonomic neurons innervating the heart (Yu-Wai Man *et al.,* 2016). To address this hypothesis, we focused on cardiac sympathetic innervation in both adult and aged Opa1 haploinsufficient mice (TOH-Opa1$^{+/-}$) mice, which was studied using morphological and functional assays.

Our transgenic mice showed, in SNs, a 50% reduction of Opa1 mRNA level resulting in the congruous decrease in Opa1 protein content. No changes in Opa1 content were observed in other cell types, including CMs. Hearts from TOH-Opa1$^{+/-}$ mice were normal in function and morphology, as assessed by echocardiography and standard histological analyses, respectively. However, when we looked at heart innervation, we observed a marked decrease in the density of SNs, which also display profound alterations in both their morphology and distribution pattern.

In detail, by combining IF and morphometric analyses, we estimated a (38±2%) decrease in SN density in the left ventricle of adult Opa1 haploinsufficient mice, compared to sex- and aged- matched controls, and such dysinnervation is maintained during ageing. Similar features were detected in the atria, and in both heart regions, the remainder neuronal processes, were thinner, fragmented and displayed increased sprouting, as compared to the normal ones.

Therefore such alteration in SN morphology and density could impact on the control of heart rhythm (atrial component) and on the propensity to develop electrophysiological abnormalities (ventricular component) (Rubart *et al.,* 2005).

To evaluate the functional consequence of heart dysinnervation, we performed ECG analysis by telemetry in freely-moving mice. To assess the effect of atrial denervation, we compared the average heart rate and its beat-to-beat variability (HRV) during 24 hours. While no significant changes in the basal HR were detected, we recorded a significant reduction in the variability of HR, which was already evident in the adult and aged mice (SDNN, adult Control: 6.17±0.36 *vs* adult TOH-Opa1$^{+/-}$: 3.62±0.46; aged Control: 3.86±0.60 *vs* aged TOH-Opa1$^{+/-}$: 1.17±0.19, in msec). HRV is a parameter reflecting the balance of the activity of the sympathetic and parasympathetic components of the autonomic nervous system on SAN cells, and our results indicate therefore that dysfunctional control

of HR occurred in Opa1 haploinsufficient mice, and may be ascribed to the progressive SAN dysinnervation.

In further support of the reduction of the sympathetic input to SAN cells, the increase in HR elicited by blocking the effect of parasympathetic neurons with atropine, was significantly blunted in the TOH-Opa1$^{+/-}$ mice as compared to controls (Δ, adult control: 19.89±2.23 *vs* adult TOH-Opa1$^{+/-}$: 13.68±1.68; aged TOH-cre$^{+/-}$: 11.3±3.2 vs TOH-Opa1$^{+/-}$: 6.7±1.2, in %). Both the morphological and functional abnormalities observed in the aged TOH-Opa1$^{+/-}$ mice overlapped to the physiologic neurodegeneration occurring spontaneously in aged hearts.

In line with the dysinnervation of the ventricular myocardium, atropine administration caused increased number of arrhythmic beats (premature ventricular contractions, PVCs), similar to those detected in ADOA patients. These phenomena have previously been attributed to unbalanced sympathetic discharge in different regions of the heart, and are thus consistent with the alterations in ventricular SN morphology. The findings accrued in the murine model suggest altogether, that the degeneration of peripheral SNs, including those innervating the heart, occurs when neurons have reduced Opa1 expression. This data support the concept whereby functioning mitochondrial dynamics are essential to maintain the correct myocardial sympathetic innervation, which reflects on the physiological neurogenic control of heart function. In addition when extrapolated to the human disease pathogenesis, these findings suggest that the cardiac rhythm abnormalities observed in ADOA patients may be the consequence of the degeneration of cardiac sympathetic neurons.

To test this hypothesis we analyzed the morphology and density of peripheral SNs in skin biopsies collected from a cohort of 25 ADOA patients (from 20 to 70 years old) in a collaborative study with Prof Valerio Carelli at the IRCCS Istituto delle Scienze Neurologiche, Bologna. In line with our preclinical data, skin biopsies, which represent an easily accessible viewpoint on peripheral autonomic innervation, showed significant reduction in the density of sympathetic processes, which was more pronounced in the older subjects. This preliminary data suggest that peripheral sympathetic neurons are degenerated in ADOA patients. To specifically assess the functional state of cardiac innervation, we have recently started a clinical study in which ADOA patients and healthy control subjects will undergo ECG Holter monitoring and analysis and cardiac scintigraphy. At study

completion, this data will be included in a manuscript in preparation, in which I am first author.

Conclusions: Collectively, the data from these two projects, pose the bases for future studies aimed at defining whether a primary alteration in the SN-CM contact contribute to the pathogenesis of several cardiovascular disorders and at clarifying the molecular mechanisms whereby defective mitochondrial dynamics causes SN degeneration.

RIASSUNTO

Razionale: Il sistema nervoso simpatico, componente del sistema nervoso autonomo (ANS), opera un continuo controllo della funzione e sulla struttura delle cellule cardiache. In condizioni basali, l'*input* neuronale ai cardiomiociti (CMs) del nodo seno-atriale (SAN) è responsabile della regolazione della frequenza cardiaca (HR) e, in parallelo, influenza l'equilibrio tra la sintesi e la degradazione proteica nei CM di lavoro, determinando così il trofismo cellulare (Zaglia *et al.,* 2013). È anche comunemente noto che i neuroni simpatici (SNs) si attivano rapidamente dopo l' esercizio fisico o dopo stress emozionali che caratterizzano la cosiddetta risposta "*fight-or-flight*", con conseguente aumento delle prestazioni cardiache massime attraverso effetti inotropici e cronotropici positivi (Li *et al.*, 2000). Mentre questi meccanismi generali di regolazione della fisiologia del cuore sono comunemente riconosciuti e sono stati accuratamente studiati negli ultimi decenni sia nelle condizioni normali che in quelle patologiche (Franzoso *et al.,* 2016), il rapporto tra la fine organizzazione della rete neuronale nel miocardio e la sua funzione, così come la biofisica della comunicazione neuro-cardiaca rimane in gran parte non nota.

Scopo della tesi: Nei nostri studi iniziali, abbiamo utilizzato diversi metodi di *imaging* per indagare gli aspetti morfologici dell'innervazione del miocardio. I nostri risultati dimostrano che il cuore della maggior parte dei mammiferi, compresi gli esseri umani, è altamente innervato dalle fibre simpatiche, che si distribuiscono nelle varie regioni del cuore con un *pattern* ben conservato, specie-specifico e mostrano varicosità (ovvero siti di rilascio di neurotrasmettitori attivi) regolari a stretto contatto con le membrane dei CMs *target*. Inoltre, l'analisi ultrastrutturale ha dimostrato che tali contatti hanno caratteristiche simili a quelle descritte per la nota giunzione neuromuscolare (NMJ), che comprendono tra le altre, l'accumulo di mitocondri nelle varicosità "presinaptiche" (Slater, 2003; Levitan *et al.,* 2015).

Questi dati ci hanno spinto a studiare:

i) la biofisica della comunicazione neurocardiaca, che è stata affrontata con modelli sia *in vitro* che *in vivo*, al fine di determinare il ruolo del contatto diretto intercellulare nelle dinamiche di accoppiamento neuro-cardiaco;

ii) se la disfunzione nei mitocondri che si trovano nei SNs, valutata in un modello murino recentemente sviluppato nel laboratorio del mio PhD aploinsufficiente per la proteina Opa1 (Optic Atrophy Factor-1) (TOH-Opa1$^{+/-}$), possa influenzare il controllo neurogenico del cuore.

Risultati: *i)* Dinamiche dell'accoppiamento neuro-cardiaco a livello della "sinapsi cardiaca".

I neuroni simpatici funzionano attraverso il rilascio di norepinefrina (NE) che, attivando i recettori β-adrenergici (β-AR) sulla membrana dei CM, aumenta l' AMP ciclico (cAMP) intracellulare e attiva la Protein Chinasi A (PKA) ed i suoi bersagli a valle coinvolti nella regolazione delle oscillazioni del Ca^{2+}, migliorando così la frequenza cardiaca e la contrazione dei sarcomeri (Rochais *et al.,* 2004). La visione "classica" sul controllo neurogenico della funzione cardiaca implica il rilascio di NE nell'*interstitium* cardiaco e la sua diffusione alla membrane dei CM che esprimono i β-AR (Levy and Martin, 1989). Tuttavia, questo modello non riesce a spiegare la rapidità, l'efficienza e la potenza del controllo esercitato dal SNS sulla funzione cardiaca, che sarebbe meglio realizzato attraverso un diretto contatto intercellulare. Per capire se il segnale tra SN e CM sia un segnale diretto e localizzato, abbiamo sviluppato un modello *in vitro* utilizzando co-colture tra i neuroni gangliari cervicali superiori (SCGNs) ed CM neonatali di ratto, per analizzare le dinamiche di interazione intercellulare a livello di singola cellula. Una volta stabilito, il sito di contatto tra SN-CM è caratterizzato, analogamente alle osservazioni *in vivo*, dalla ridotta distanza intermembranale (≅ 67±16, in nm), che rimane stabile nel tempo, sostenendo la base strutturale dell'interazione neuro-cardiaca. Nelle colture mature, la topologia delle interazioni stabilite tra i neuroni e i CMs è stata classificata in tre categorie: i) le cellule in contatto diretto con le varicosità neuronali, identificate come ingrandimenti rotondi dell'assone a contatto con la membrana dei CM; tipo ii) cellule vicine alle varicosità neuronali, che si trovano al di fuori dell'area dei CMs e tipo iii) CMs in cui i processi neuronali passano ma senza formare varicosità. Poiché la stimolazione β-AR provoca effetti sul cuore tramite la segnalazione dipendente da cAMP, abbiamo utilizzato l'*imaging* di cAMP in tempo reale nei CMs in co-cultura che esprimono il sensore per la FRET Epac1, per analizzare le risposte dei CMs dopo l'attivazione dei SNs. Le variazioni della concentrazione di cAMP sono state valutate a livello di singola cellula monitorando la variazione dell'emissione della CFP/YFP dopo

l'illuminazione della CFP (metodo del rapporto di emissione sensibilizzato). La depolarizzazione dei SNs, ottenuta mediante un breve tempo di perfusione delle cellule con 50 mmol/L di KCl, ha causato un aumento del [cAMP] intracellulare che è stato rilevato solo nei CMs innervati (tipo i), mentre nessuna modifica è stata osservata in cellule non innervate sullo stesso vetrino di coltura (tipo ii e iii), o in CMs in coltura da soli (ΔR/R0, CM innervati: 9.3±0.92, CM non innervati: 0.23±0.08, in%). Tutti i gruppi analizzati hanno mostrato risposte paragonabili in termini di crescita dell' cAMP dopo l' applicazione diretta di NE. L'aggiunta della soluzione di coltura, raccolta dopo la depolarizzazione neuronale, non ha indotto una risposta dell' cAMP nei CMs che esprimono Epac1, indicando che la concentrazione di NE nel mezzo di coltura era troppo bassa per attivare i β-AR nei CMs. Per definire ulteriormente il *range* di azione della NE nello spazio, abbiamo studiato le risposte dell' cAMP in CMs adiacenti e abbiamo osservato che l'attivazione dei β-ARs era limitata alla cellula innervata. Inoltre, i cambiamenti di cAMP sono stati più veloci e più elevati in prossimità del sito di interazione neuro-cardiaca, sostenendo quindi che la NE rilasciata dai neuroni attiva solo un *pool* confinato di β-AR/adenilat ciclasi nella membrana post-sinaptica dei CMs. Considerati insieme, tutti questi dati supportano che i SNs attivati comunicano con i CMs scaricando NE in un dominio di segnalazione extracellulare ristretto all'interfaccia tra i due tipi di cellule. Abbiamo quindi utilizzato il saggio di inibizione competitiva e abbiamo stimato che la NE rilasciata dai neuroni raggiunge, nella fessura sinaptica, una concentrazione effettiva nell'ordine di 100 nmol/L, che corrisponde alla kd dei β-ARs. Per determinare se gli effetti dell'attivazione simpatica, *in vivo*, riflettono la comunicazione diretta delle cellule, osservate nel sistema *in vitro*, abbiamo sfruttato l'optogenetica per controllare l'attività dei SNs mentre si monitora la frequenza cardiaca. Il metodo è basato sull'espressione di *Channelrhodopsin-2* (ChR2), un canale ionico microbico, luce-attivato, permeabile al Na^+, nei SNs (Stieber *et al.*, 2003). L'illuminazione dei neuroni esprimenti ChR2 genera una corrente interna che consente la depolarizzazione delle cellule e il rilascio del neurotrasmettitore, con una risoluzione in millisecondi (Boyden *et al*., 2005; Zhang *et al.,* 2007). I topi transgenici con il gene ChR2-H134R-tdTomato sotto il controllo del promotore TOH, presentano cuori strutturalmente e funzionalmente normali e esprimevano ChR2 in SCGN, che consentivano l'innesco di potenziali d'azione (AP) neuronali usando brevi *flash* di luce

depolarizzanti (10 ms, 470 nm) come mostrato nei neuroni in coltura. Abbiamo quindi utilizzato l'*hardware* e i protocolli precedentemente sviluppati per l'optogenetica cardiaca (Zaglia *et al.,* 2015), per valutare l'effetto dell' attivazione dei SNs sulla frequenza cardiaca, abbiamo scansionato la superficie epicardica del cuore con la punta di una sonda a fibra ottica durante l'emissione di *flash* di luce. La foto-attivazione di una regione limitata, larga circa 1-2mm, sulla superficie epicardica dell'atrio di destra, ha indotto una riproducibile tachicardia sinusale. Il miocardio sottostante è stato marcato con inchiostro dermografico e analizzato con IF, che ha rivelato una regione in cui i CMs esprimono *bona fide marker* dei miociti del SAN, HCN4 (Liu *et al.,* 2007), che interagisce strettamente con i SNs. Nessun effetto sulla frequenza cardiaca è stato rilevato con la fotostimolazione delle regioni atriali immediatamente vicine alla regione del SAN, nonostante la fitta innervazione di tutto il miocardio atriale, indicando una rigorosa discriminazione di *target* di gruppi specifici di SNs cardiaci e suggerendo che la NE rilasciata dai neuroni ha una limitata azione spaziale nel miocardio murino. Per stimare l'effettiva concentrazione di NE che serve per attivare i β-ARs durante l'attivazione simpatica, abbiamo analizzato gli effetti della fotostimolazione neuronale nei topi trattati con l' antagonista dei β-AR, propranololo (4mg/kg). A questa dose, il propranololo diminuisce la frequenza cardiaca di riposo di circa il 30%. È interessante notare che, la risposta alla fotoattivazione simpatica era quasi invariata nei topi trattati con propranololo, suggerendo che l'effetto inibitorio dell'antagonista venisse superato dall'elevata concentrazione di NE nel *cleft* sinaptico. Questi risultati sono in linea con il concetto sostenuto dai nostri esperimenti *in vitro* che indicano che l'interazione tra SN-CM usa giunzioni neuro-cardiache. In sintesi, i nostri dati *in vivo*, mostrando la rapidità dell'insorgenza e del termine delle risposte del SAN alla stimolazione simpatica e l'efficienza dell'interazione neuro-cardiaca, sono tutti a sostegno del modello di lavoro in base al quale la creazione di un dominio extracellulare specializzato rende possibile la la neurotrasmissione tra SNs e cuore e si manifesta in modo quasi sinaptico. I nostri dati indicano che la modulazione simpatica del *signalling* dei CMs richiede il contatto diretto tra le cellule, che riunisce sia il rilascio della NE da parte dei neuroni sia le membrane dei CMs sensibili al rilascio di NE. Tale interazione definisce uno spazio extracellulare a basso volume in cui la NE raggiunge un' elevata concentrazione con poche migliaia di molecole (cioè poche vescicole),

come stimato dalla simulazione numerica ottenuta in giunzioni tra neuroni e cellule effettrici con geometria comparabile. Tali domini di segnalazione limitati promuovono l'attivazione di una sola frazione di β-ARs all'interno della membrana dei CMs contattata dai neuroni, come sostenuto dalla stretta selettività dell'attivazione del *target* neuronale e consentono un' elevata efficienza che consente risposte dei CMs ad una minima attivazione neuronale. Questi risultati si adattano bene all'osservazione che i complessi di segnalazione del *pathway* cAMP/PKA, inclusi i β1-ARs, come pure le proteine di ancoraggio e i *targets* della PKA, sono clusterizzati all'interno della membrana dei CMs sul sito di interazione con i neuroni (Shcherbakova *et al.,* 2007). I nostri dati di *imaging* descrivono le conseguenze di tale organizzazione, mostrando che la sintesi di cAMP inizia, dopo la stimolazione neuronale, al sito di contatto tra CMs e neuroni, identificando lì il complesso formato dalla varicosità neuronale e dalla membrana post-sinaptica dei CMs come unità di segnalazione funzionale nella regolazione neurogenica del cuore. Questo modello di lavoro è stato corroborato dai nostri risultati *in vivo* utilizzando l'optogenetica, che è stata sfruttata per ottenere un controllo non invasivo dei SNs cardiaci, evitando effetti diretti sull'elettrofisiologia del cuore. Questa tecnica, insieme all'elevata risoluzione spaziale nell'attivazione di ChR2, ha fornito uno strumento flessibile per sondare *in vivo* la funzione di gruppi ristretti di neuroni cardiaci e capire la cinetica di segnalazione neuro-effetrice. Anche se esistono differenze tra le condizioni *in vitro* ed il cuore innervato intatto, i risultati degli esperimenti *in vivo* supportano il modello di lavoro per cui la regolazione neurogenica del ritmo cardiaco è sostenuta da sinapsi metabotropicche ad alta efficienza. L'elevata velocità e la precisione del singolo battito del controllo neuronale dell'automatismo del SAN è ulteriormente sostenuta dai precedenti modelli numerici delle cinetiche dell'agonista in una giunzione neuro-effetrice di morfologia comparabile, che mostra che la concentrazione di NE raggiunta nel *cleft* sinaptico cresce e cala con tempistiche di soli pochi millisecondi. (Bennett *et al.,* 1995). Valutando nell'insieme, le evidenze *in vitro* e *in vivo* suggeriscono che l'organizzazione morfologica e funzionale della giunzione neuro-cardiaca consente al SNS di regolare la funzione del cuore con grande precisione. Questi dati fanno parte di un manoscritto attualmente in fase di revisione presso il "Journal of Physiology", in cui sono co-primo autore.

***ii)* Ruolo della proteina mitocondriale Opa1 nella regolazione della fisiologia dei neuroni simpatici cardiaci.**

Nello studio delle interazioni neuro-cardiache descritte in precedenza, siamo stati intrigati dall'osservazione che i mitocondri si accumulavano nelle varicosità dei SNs e specificamente si concentravano nello spazio attorno alla membrana presinaptica. I mitocondri dei neuroni sono fondamentali per molte funzioni cellulari, tra cui la neuro-esocitosi, il recupero del neurotrasmettitore ed il mantenimento del trofismo del processo neuronale, ma il loro ruolo specifico nei SN cardiaci è in gran parte inesplorato. Abbiamo quindi cercato di determinare se mitocondri disfunzionali compromettessero il controllo neurogenico del cuore. A questo scopo, abbiamo sfruttato un modello murino generato nel nostro laboratorio, caratterizzato dall' aploinsufficienza del gene che codifica per la proteina Optic Atrophy Factor-1 (Opa1) (Hoppins *et al.,* 2007), selettivamente nei SNs. Opa1 è una proteina chiave implicata nelle dinamiche mitocondriali e la sua carenza causa una malattia neurodegenerativa ereditaria caratterizzata dalla morte delle cellule ganglionari retiniche, nota come Atrofia ottica autosomica dominante (ADOA), con conseguente perdita visiva. È interessante notare che i pazienti affetti da ADOA presentano anche neuropatia periferica e anomalie del ritmo cardiaco (Spiegel *et al.,* 2016), suggerendo l'ipotesi che i mitocondri disfunzionali possono influenzare non solo i neuroni centrali ma anche periferici e, in modo notevole, i neuroni autonomici che innervano il cuore (Yu-Wai Man *et al.,* 2016). Per indagare questa ipotesi, ci siamo concentrati sull'innervazione simpatica cardiaca sia nei topi aploinsufficienti per Opa1 (TOH-Opa1$^{+/-}$) adulti che vecchi, utilizzando saggi morfologici e funzionali. I nostri topi transgenici hanno mostrato, nei SNs, una riduzione del 50% del livello di mRNA di Opa1, con conseguente riduzione congrua del suo contenuto proteico. Nessuna alterazione del contenuto di Opa1 è stata osservata in altri tipi di cellule, tra cui i CMs. I cuori dei topi TOH-Opa1$^{+/-}$ erano normali in funzione e morfologia, valutati rispettivamente da ecocardiografia e analisi istologiche standard. Tuttavia, quando abbiamo guardato l'innervazione cardiaca, abbiamo osservato una marcata diminuzione della densità delle fibre simpatiche, che mostrano anche profonde alterazioni sia nella loro morfologia che nella distribuzione. In dettaglio, combinando l'immunofluorescenza con analisi morfometriche, abbiamo stimato una diminuzione (38±2%) della densità dei SNs nel ventricolo sinistro nei topi

TOH-Opa1$^{+/-}$ adulti (6 mo.), confrontati con i controlli della stessa età e similmente la disinnivazione è presente durante l'invecchiamento (24 mo.). Caratteristiche simili sono state rilevate negli atrii, e in entrambe le regioni del cuore, i processi neuronali si presentano più sottili, frammentati e mostrano un aumento delle ramificazioni, rispetto ai normali. Quindi è possibile pensare che l' alterazione nella morfologia dei SNs e nella loro densità possa influire sul controllo del ritmo cardiaco (componente atriale) e sulla propensione a sviluppare anomalie elettrofisiologiche (componente ventricolare) (Rubart *et al.,* 2005) . Per valutare le conseguenze funzionali della disinnervazione del cuore abbiamo eseguito un'analisi elettrocardiografica (ECG) mediante telemetria in topi che si possono muovere liberamente. Per valutare l'effetto della denervazione atriale, abbiamo confrontato la frequenza cardiaca media e la sua variabilità battito-battito (HRV) per 24 ore. Mentre non sono stati rilevati cambiamenti significativi nella frequenza cardiaca (HR) basale, abbiamo registrato una significativa riduzione della variabilità della HR, che era evidente sia nei topi adulti che vecchi (SDNN, Controllo adulti: 6.17±0.36 *vs* TOH-Opa1$^{+/-}$ adulti: 3.62±0.46; Controllo vecchio: 3.86±0.60 *vs* TOH-Opa1$^{+/-}$ vecchi: 1.17±0.19, in msec). La HRV è un parametro che riflette l'equilibrio dell'attività delle componenti simpatica e parasimpatica del sistema nervoso autonomo sulle cellule del SAN e i nostri risultati indicano quindi che nei topi Opa1 haploinsufficienti c'è un controllo disfunzionale dell'HR e può essere attribuito alla disinnervazione progressiva del SAN. In ulteriore sostegno alla riduzione dell'*input* simpatico alle cellule del SAN, l'aumento dell' HR ottenuto bloccando l'effetto dei neuroni parasimpatici con atropina, è stato significativamente ridotto nei topi TOH-Opa1$^{+/-}$ rispetto ai controlli (Δ, aduti controlli: 19.89±2.23 *vs* TOH-Opa1$^{+/-}$: 13.68±1.68; vecchi controlli: 11.3±3.2 *vs* TOH-Opa1$^{+/-}$: 6.7±1.2, in%). Sia le anomalie morfologiche che funzionali osservate nei topi TOH-Opa1$^{+/-}$ vecchi si sono sovrapposte alla neurodegenerazione fisiologica che avviene spontaneamente durante l'invecchiamento. In linea con la disinnervazione del miocardio ventricolare, la somministrazione di atropina ha causato un aumento del numero di battiti aritmici (contrazioni ventricolari premature, PVC), simili a quelle rilevate nei pazienti ADOA. Questi fenomeni sono stati precedentemente attribuiti a scariche squilibrate dei neuroni simpatici in diverse regioni del cuore e sono quindi coerenti con le alterazioni della morfologia dei SNs ventricolari. I risultati ottenuti nel modello murino suggeriscono che la

degenerazione delle fibre simpatiche periferiche, incluse quelle che innervano il cuore, si verifica quando i neuroni hanno una ridotta espressione di Opa1. Questi dati supportano il concetto secondo cui la funzionalità delle dinamiche mitocondriali è essenziale per mantenere l'innervazione simpatica del miocardio, che si riflette nel controllo fisiologico della funzione cardiaca. Inoltre, quando estrapolati alla patogenesi della malattia umana, questi risultati suggeriscono che le alterazioni del ritmo cardiaco, osservate nei pazienti ADOA, possono essere la conseguenza della degenerazione dei SNs cardiaci. Per verificare questa ipotesi, abbiamo analizzato la morfologia e la densità dei SNs periferici in biopsie cutanee raccolte da una coorte di 25 pazienti ADOA (da 20 a 70 anni) in uno studio in collaborazione con il Prof. Carelli presso l'IRCCS Istituto delle Scienze Neurologiche di Bologna. In linea con i nostri dati preclinici, le biopsie cutanee, che rappresentano un punto di vista facilmente accessibile sull'innervazione autonomica periferica, hanno mostrato una significativa riduzione della densità dei processi simpatici, più pronunciata nei soggetti più anziani. Questi dati preliminari suggeriscono che i neuroni simpatici periferici sono degenerati nei pazienti ADOA. Per valutare specificamente lo stato funzionale dell'innervazione cardiaca, abbiamo recentemente avviato uno studio clinico in cui pazienti ADOA e soggetti di controllo sani saranno sottoposti a monitoraggio e analisi ECG Holter e scintigrafia cardiaca. Al completamento dello studio, questi dati saranno inclusi in un manoscritto in preparazione, in cui sono il primo autore.

Conclusioni: Complessivamente, i dati di questi due progetti forniscono le basi per studi futuri finalizzati a definire se un' alterazione primaria nel contatto tra SN-CM contribuisca alla patogenesi di diversi disturbi cardiovascolari e al chiarimento dei meccanismi molecolari in cui un difetto nelle dinamiche mitocondriali possa provocare la degenerazione dei SNs.

INTRODUCTION

1. The heart: structure and function

1.1 Gross anatomy

The heart, by pumping the blood from the lungs to the systemic circulation and back to the lungs, is responsible for the propulsion of blood to all cells in the organism, and the delivery of oxygen and nutrients. The mammalian heart is divided in the *right and left sections*, which sustain the pulmonary and systemic circulation, respectively and are formed by atria (LA, RA) and ventricles (LV, RV). At the interface between the atria and ventricles there are the *atrioventricular* (AV) *valves* (i.e. the *tricuspid valve* for the right section and the *mitral valve* for the left section), which guarantee the unidirectional flow of blood from the atria to the ventricles. The *semilunar valves* are located at the interface between ventricles and the great arteries with the same function (**Fig. I**).

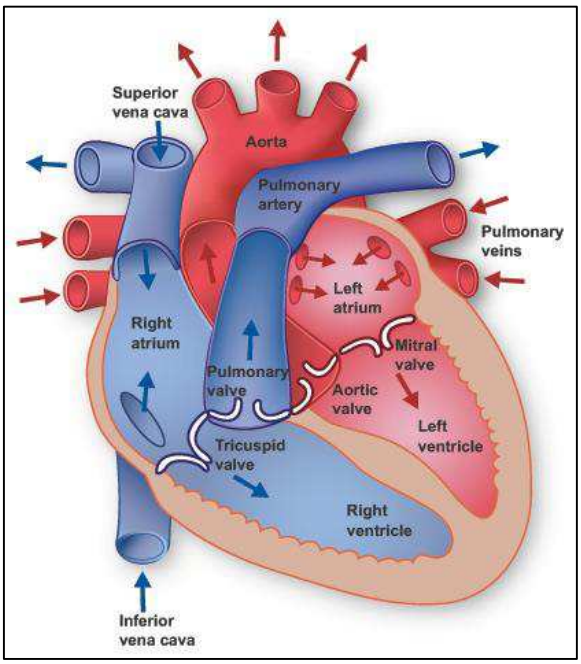

Figure I: *Gross anatomy of the heart.*

The heart valves lie in a plane within a scaffold of connective tissue, which electrically insulates the atria from the ventricles. The *AV bundle* (also called *His bundle*), is a strand of specialized ventricular myocardium, which penetrates this

barrier and constitutes the electrically-conducting pathway between the atria and the ventricles, forming the *AV node* at the level of the atrial-ventricular junction (Katz, 2011).

The larger cusps of the mitral and tricuspid valves are bound to fibrous structures called *chordae tendinae,* which link the valve leaflet to *papillary muscles*, projecting into the right and left ventricular cavities (Becker *et al.,* 1979).

The four chambers of the heart have peculiar shape and morphology: in particular, the RA and LA have an almost rounded shape, while the LV and RV possess a thicker wall compared to the atria. In detail, the LV is thicker than the RV, and has a cone shaped chamber, which accepts blood from the mitral valve and pumps it through the semilunar valve. The RV chamber is smaller and has a crescent shape when observed transversally (Katz, 2011). The portion of myocardium that lies between the RV and the LV is called *interventricular septum* (IVS). A fibrous sac called *pericardium,* encapsulates externally the heart and its inner surface is in contact with the *epicardium,* a layer of mesotelial cells lying just above the myocardium. A similar layer of endothelial cells called *endocardium*, instead, lines the cavity of atria and ventricles (Brutsaert, 1989).

Blood supply to the heart is provided by large epicardial coronary arteries, namely the left main coronary artery which divides into the left anterior descending (LAD) and circumflex; the right coronary artery which in most cases gives origin to the posterior descending coronary artery. The branches of each large vessel penetrate into the myocardium and distribute to warrant homogenous perfusion of the muscle.

1.2 Histology and cytoarchitecture of the myocardium

The myocardium is a complex cellular network composed by different cell populations including: *cardiomyocytes* (CMs), *fibroblasts*, *endothelial cells*, *smooth muscle cells* and *neurons* (see below). CMs are the cells responsible for heart contraction and although the only account for 30% of the total number of myocardial cells, they constitute the highest fraction of the myocardial mass.

CMs can be divided into two main populations: *the working CMs*, which are responsible for the contractile activity and *the conducting CMs*, specialized cells that initiate and propagate the electrical impulse triggering heart contraction.

The working CMs can be subdivided into atrial, smaller in size, and ventricular CMs. Moreover, inside the ventricular walls three subtypes of ventricular CMs can be found, which are distinguished for their different electrophysiological properties (Antzelevitch *et al.,* 1991; Liu *et al.,* 1993; Moseley *et al.,* 1993). These cells are organized in the transmural direction into three juxtaposed layers, with different orientation, which, from the outer to inner part of the heart wall, are called: *subepicardium* (EPI), *midmyocardium* (MID) and *subendocardium* (ENDO). Recent studies in the murine heart, using the technique of "diffusion tensor cardiovascular magnetic resonance" (DTI) (Moseley *et al.,* 1993; Basser *et al.,* 1994), allowed to precisely define the CMs orientation. In EPI and ENDO regions, CM have their long axis aligned parallel to the base-to-apex direction, while CMs in MID have an orientation that progressively changes moving from the border zone with EPI to the one with ENDO (Healy *et al.,* 2011; Jiang *et al.,* 2004; Schmitt *et al., 2009;* Angeli *et al., 2014;* Sands *et al., 2008)* (**Fig. II**).

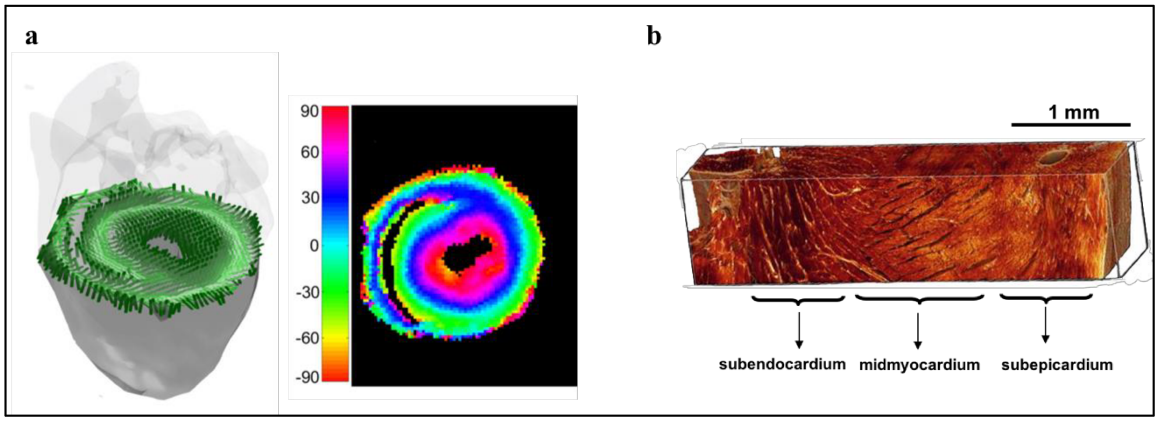

Figure II: (a) *3D reconstruction of the myocardial fiber orientation in the ventricles of mouse heart, obtained with DTI* ***(left panel)****. False color map indicating the angle formed by the intersection of the long axis of CMs and the transversal plane* ***(right panel)****.* ***(b)*** *3D reconstruction of a ventricular myocardial section showing the complex cytoarchitecture of the tissue with highlighted the three regions composing the ventricular wall (Healy, 2011; Sands, 2008).*

Conducting CMs are connected and form a complex network which distributes to all myocardial regions allowing achieve the sequential and coordinated contraction of atrial and ventricular CMs. Conducting CMs are divided into two subtypes: The *Nodal cells*, found in the *sinoatrial node* (SAN) and atrio-ventricular *node (AVN),* are small in size and possess spontaneous automaticity;

the *Purkinje fibers* (PF)*,* depart from the AV bundle, and form the anatomically distinct *right* (RBB) and *left bundle branch* (LBB), which distribute throughout the ENDO in the terminal PF network.

1.3 Ultrastructure of cardiomyocytes

More than 50% of the volume of working CMs is occupied by contractile proteins, organized in myofibrils. The remaining volume is mainly occupied by mitochondria (≈35%) and by the other subcellular organelles, including the nucleus, *sarcoplasmic reticulum* (SR) and all remainder. Contractile proteins are organized into fundamental units called *sarcomeres,* which are composed by overlapping thick and thin filaments. The **thick filaments** are made of polymers of *myosin* that interact with the **thin filaments**, made of double-stranded polymers *of actin* and other interacting proteins, namely *tropomyosin* and *troponins*. There are three different types of troponins: troponin I (TnI), troponin C (TnC) and troponin T (TnT), that are found in complex bound to tropomyosin. In relaxed muscles (diastolic phase of cardiac cycle), the troponin/tropomyosin complex inhibits the acto-myosin interaction, thus preventing contraction. Sarcomere shortening takes place when Ca^{2+} rises into the cytoplasm and binds to TnC, thus inducing a conformational change in the troponin complex relieving the inhibitory effect of tropomyosin on acto-myosin interaction. TnI exposes a site on the actin molecule that binds the myosin ATPase located on the myosin head. Such event results in ATP hydrolysis that supplies energy for a conformational change to occur in the actomyosin complex: the actin and myosin filaments slide along each other, thereby shortening the sarcomere length and thus inducing cell contraction (systolic phase of cardiac cycle). The length of thick and thin filaments remains constant during the phases of contraction and relaxation, and cell shortening is solely due to the overlap between the filaments (Hanson *et al.,* 1953). The rise in cellular Ca^{2+} activating contraction is the result of the complex organization of plasma membrane-localized Ca^{2+} channels and intracellular Ca^{2+} stores, mainly the SR (Bers, 2002).

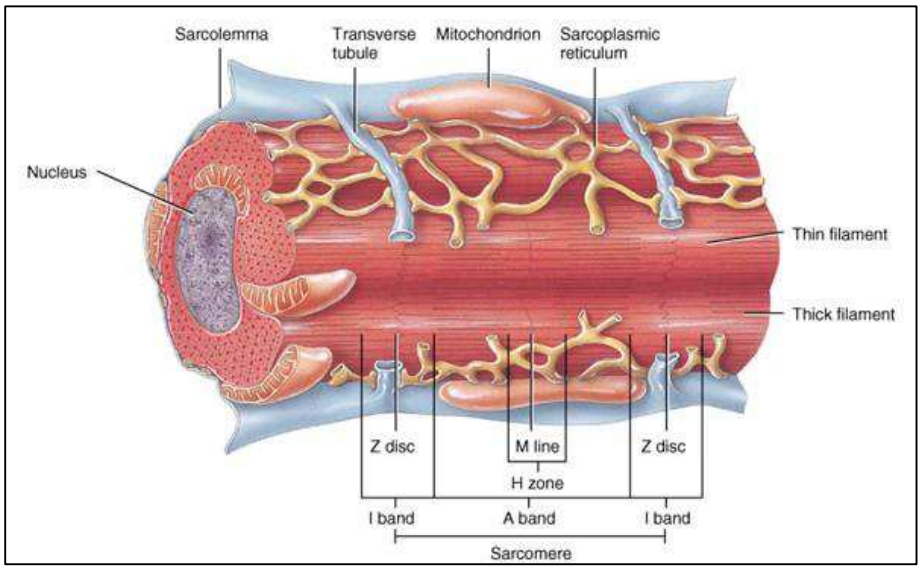

Figure III: *Structure of a cardiac myofiber (Grazia A.).*

The plasma membrane of CM is called *sarcolemma* and possesses particular invaginations called *transverse tubules* (*t-tubules*), which are enriched in Ca^{2+} entry sites (i.e. L-type Calcium channel) facing the terminal SR *cisternae* and in close apposition with sarcomeres. (**Figure III**).

The membrane depolarization initiated by the cardiac activation wave causes voltage-gated L-type Ca^{2+} channels, located in the t-tubules, to open (Bers *et al.,* 2002). The resulting Ca^{2+} influx in the cytoplasm activates a much larger release of Ca^{2+} from the SR through the Ryanodine Receptor intracellular Ca^{2+} release channels (RyR-2) (Zalk *et al.,* 2015), in a process known as called calcium-induced-calcium-release (CICR) (Fabiato *et al.,* 1979). The rise in intracellular [Ca^{2+}] is thus able to trigger sarcomere shortening. At the end of contraction, cytosolic [Ca^{2+}] is restored by the activity of *sarcoendoplasmic reticulum calcium ATP-ase pump* (SERCA) which pumps it back into the SR, and the *sodium-calcium exchanger* (NCX), which extrudes the remainder Ca^{2+} from the cell membrane. Remarkably, at each contractile cycle, a fraction of cytosolic Ca^{2+} is taken up by mitochondria (**Fig.IV**).

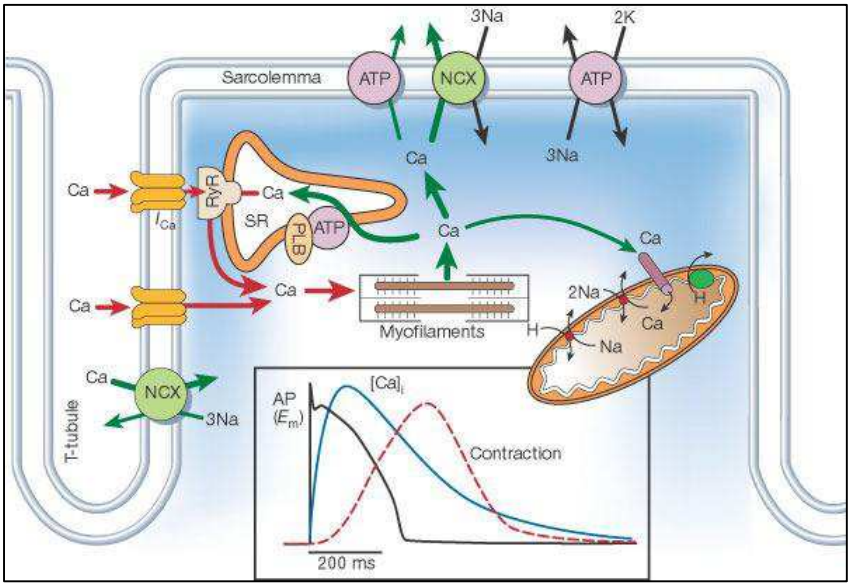

Figure IV: *Excitation contraction coupling model in the cardiomyocyte (Bers, 2002).*

1.4 Electrical conduction of the heart

The myocardium is a functional syncytium, as CMs are tightly connected mechanically and electrically to each other thanks to specialized structures called *intercalated disks* (Hoyt *et al.,* 1989; Veeraraghavan *et al.,* 2014; Weidmann, 1966; Weingart, 1974). The mechanical tethering is provided by the interaction of sarcomeric and cytoskeletal actin, and by *desmosomes*, structures where *intermediate filaments* of adjacent CMs are bound together (Franke *et al.,* 2006).

The electrical connection between adjacent CMs is operated by *gap junctions* (GJ), nonselective channels that allow ions and small molecules to diffuse freely between the cytosol of connected CMs. These channels reduce internal electrical resistance, thus creating a functional syncytium in which all CMs are electrically coupled (Veeraraghavan *et al.,* 2014; Peters *et al.,* 1996) (**Fig. V**).

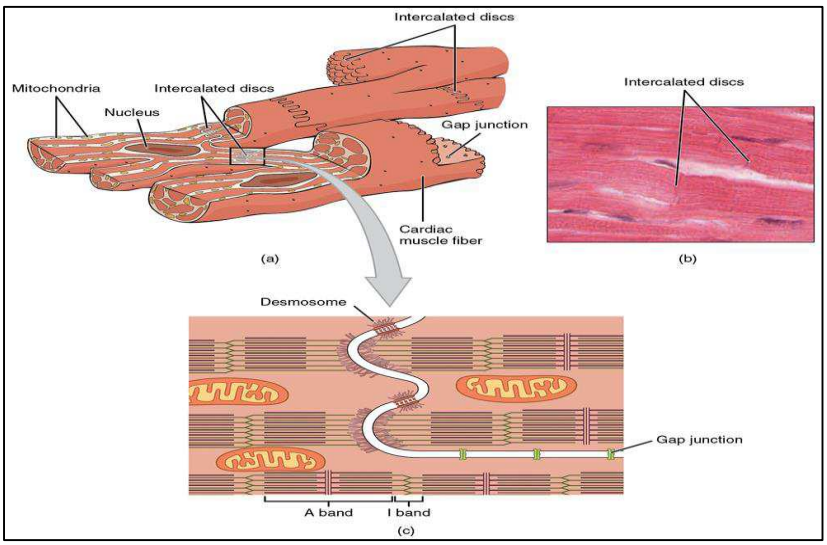

Figure V: *Complex arrangement of cardiomyocytes in the myocardium: structural and mechanical connections between them.*

Gap junctions (GJ) are constituted by proteins called *connexins* (Cx), which are arranged in examers at the sarcolemma to form a non selective channel known as connexon, which represents half of the complete GJ (Franke *et al.,* 2006) (**Fig. VI**). In the heart many different connexin isoforms are described, the most abundant being: connexin 43 (Cx43), connexin 40 (Cx40) and connexin 45 (Cx45). GJs formed by the different isoforms of connexin present different permeability to ions thus conducting electrical impulse with different efficiency. Since GJs are the links between each single CM, this means that the speed of propagation of electrical stimuli is determined by the connexin type expressed (Gros *et al.,* 1994). Cx43 is the most abundant and it is expressed by all working CMs and the distal PFs, while Cx40 is expressed in atrial working CMs, in coexistence with Cx43, and in PFs, and Cx45 is expressed almost exclusively in SAN and AVN, while a very low expression was also detected in PFs (Kirchhoff *et al.,* 2000; Miquerol *et al.,* 2010; Van Kempen *et al.,* 1996).

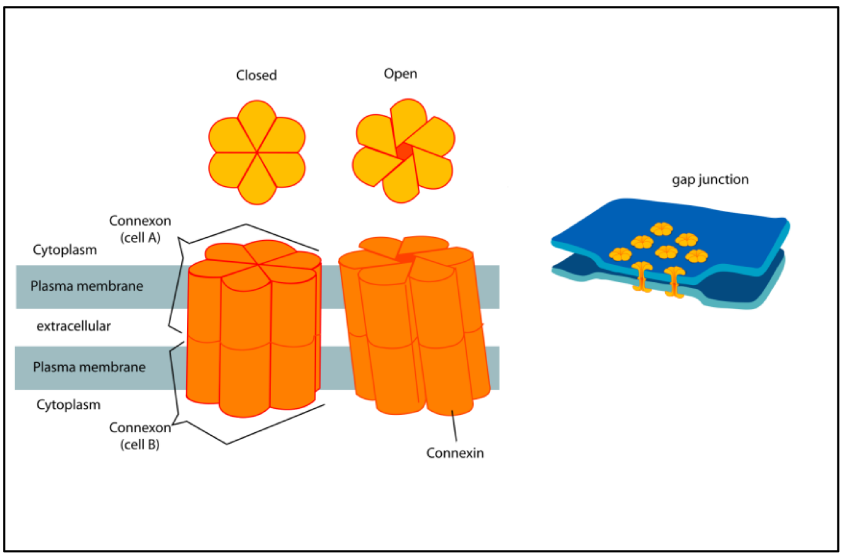

Figure VI: *Structure of the gap junctions formed by the connexins.*

Every heartbeat is initiated by the spontaneous depolarization of SAN cells, triggering an action potential (AP) spreading, through the other cells of the conduction system of the heart, to all working CMs. This depolarization wave opens the voltage gated Ca^{2+} channels in the sarcolemma of working CMs and starts the excitation contraction coupling (ECC), culminating in the systolic contraction. The cardiac AP is the result of the ordered opening and closing of the several different ion channels present in the sarcolemma of working and conductive CM. Each CM type, by expressing different patterns of ion channels, is characterized by unique AP kinetics, which reflect on the physiology of heart contractions.

The SAN is the physiologic pacemaker of the heart and is located in the RA. Every conductive CM possesses an intrinsic capacity of spontaneous depolarization, which is called *automaticity*. Since SAN cells exhibit the fastest spontaneous depolarization rate among all conductive CMs, this structure usually takes the lead and initiates heart depolarization waves.

After been propagated to both atria, the depolarization wave reaches the AV insulating region (see above) and can only propagate through the AVN, where it is slowed by the Cx45 expressing nodal cells. The delay that the depolarization wave encounters before passing to the ventricles is fundamental for the correct sequence of contraction of atria and ventricles. Once passed through the AVN the depolarization wave reaches the His bundle in the IVS, where it divides into the RBB and LBB, which propagate the electrical impulse to the distal part of the terminal PFs, which are, in turn, interspersed throughout the ENDO and contact the working ventricular CMs (Cunningham, 2002) (**Fig.VII**).

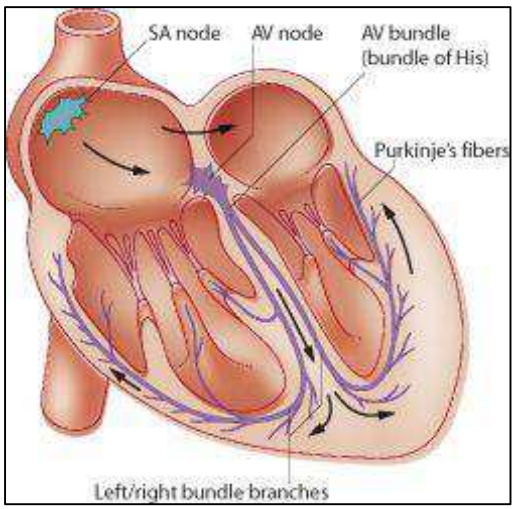

Figure VII: *Central conduction system of the heart (Cunningham, 2002).*

After the end of the activating AP, each heart cell is re-polarized by the action of a complex set of currents, restoring the membrane potential at its baseline negative value (Katz, 2001).

The rhythmic depolarization of the heart, described above, precedes every heart beat and it is defined *sinusal rhythm*. Depolarization waves following different paths result in *arrhythmic beats* also known as *ectopic* or *extrasystolic beats*, causing the so-called premature ventricular contractions (PVC). Repetitive PVCs define *arrhythmias*, which originate when such aberrant depolarizations are sustained and thus overcome the sinus rhythm (Myles *et al.,* 2012; Xie *et al.,* 2010). Arrhythmias can be divided, based on their location, into: *supraventricular* (arising from atria and nodal cells) and *ventricular* and, based on their effect on

heart rate (HR), into *tachycardia* (increasing HR) and *bradycardia* (decreasing HR). The most important in terms of epidemiology and severity of symptoms are tachycardia and, for their impact on cardiac mechanics and electrical stability, the ones with ventricular origin (Priori *et al.,* 2015).

2. Electrocardiography

Surface electrocardiography is a standard technique to record the electrical activity of the heart during a period of time, by using electrodes placed in well-defined positions on the chest wall and limbs. The electrocardiogram (ECG) is the trace of the difference in conducted electrical potentials between the exploring and the reference electrode, over time. It provides information on the HR and on the direction of cardiac depolarization and repolarization during the different phases of the heartbeat. Typically, an ECG trace is constituted by the repeated sequence of specific deflections, which represent the changes in electrical potential of defined heart regions. The first, in chronological order, is the so called "*p wave*" which arises from the depolarization of the atria, and is followed by the so-called "QRS complex", which represents the depolarization of the ventricles and the IVS. It is followed by the "T wave", corresponding to the ventricular repolarization (**Fig. VIII**). Although the activation of specific structures in the cardiac conduction system, e.g. the SAN or AVN is at the cellular level underlayed by electrical depolarization, these signals cannot be recorded because of the very low current they generate, given the very low number of cells involved. The morphology of the principal deflections in the ECG is similar between different species, while the amplitude and the length of each deflection and the intervals between them are very different. This applies, in particular, to small mammals, e.g. the rodents, that have fast HR and activation sequences, causing the interval between the end of the QRS complex and the start of the T wave to be so small that the T wave appears fused to the final part of the QRS (**Fig.VIII**).

The area under the curve of each deflection, or ECG segment, informs on the intensity of the underlying current, which in general terms corresponds to the activated tissue mass, while the length is influenced by the conduction velocity of cardiac activation waves. For example, defects in the conduction of the activation wave throughout the ventricular myocardium, as it happens for example after myocardial infarction when necrotic myocardium is substituted with an electrical inert fibrotic scar, result in the prolongation of the QRS complex. Wide QRS complexes are also feature of ectopic arrhythmic beats originating from the ventricular muscle outside the conduction system. The longer duration of the QRS complex of an arrhythmic beat is explained by its origin, indeed, it arises from the

focal depolarization of a small group of CMs, that generates a depolarizing wave that spreads throughout the ventricles, this event is slower than the physiologic depolarization of the ventricles, which occurs due to the simultaneous activation of CMs in multiple sites of contact between the distal part of the PFs network, and so it results in a wider QRS complex (**Fig.VIII**).

When the healthy heart is physiologically paced by sinusal rhythm, every “p wave” is followed by a QRS at a precise distance, reflecting the delaying filter of the AVN. When the AVN or bundle are not functioning correctly, the normal conduction from the atria to the ventricles might be interrupted, and this phenomenon is called AV block. Based on the severity, AV blocks are normally classified into three types, I, II and III, corresponding to incremental dysfunctions of the conduction system. Type III AV blocks are also known as complete AV block, highlighting that the heart rhythm is not initiated by the atria in the SAN, but ventricular contractions depend on the automaticity of ventricular cells. In the ECG, this condition is characterized by the appearance of “p waves” not followed regularly by QRS complexes, with the latter abnormally wide due to their ventricular origin.

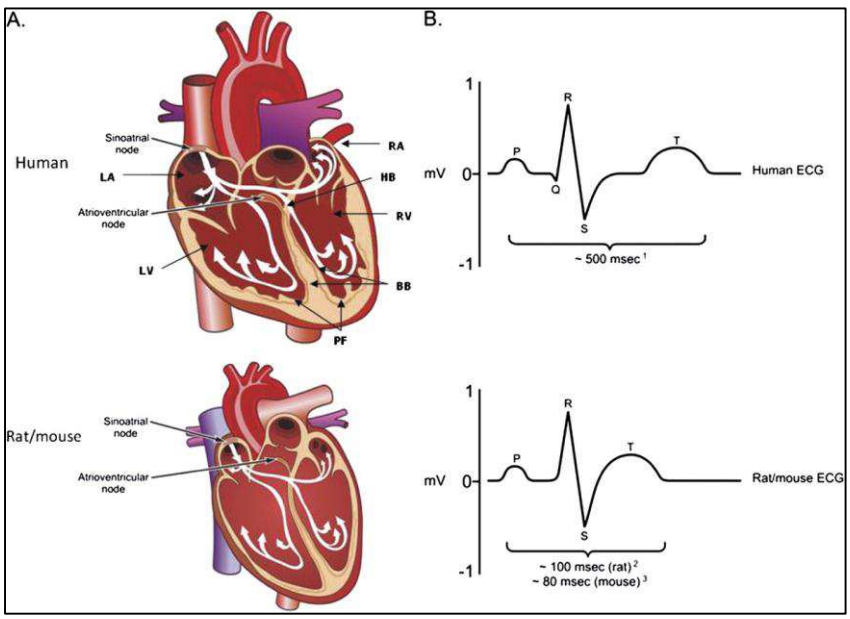

Figure VIII: ***(a)*** *Comparison between the anatomy of human and rodent heart and (**b**) respective deflections seen in the ECG.*

3. Anatomy and function of the Autonomic Nervous System

The Autonomic Nervous System (ANS) plays a crucial role in the maintenance of the systemic homeostasis, as it finely regulates the activity of all the bodily tissues and organs, spanning from the modulation of blood pressure, to the control of gastrointestinal responses to food intake, contraction of the urinary bladder, and thermoregulation (Guyton *et al.*, 2006). Interestingly, all these actions are regulated independently from the voluntary control, and as such the ANS is defined as an involuntary system (Bear *et al.*, 2007).

3.1 General organization of the ANS

The ANS operates through a two-neurons axis from the central nervous system to the target organs, organized in series: i) ***the pre-ganglionic neurons***, whose cell bodies originate from the lateral horn of the grey matter of the spinal cord, which contact ii) ***the post-ganglionic neuron***s, whose cell bodies are organized in peripheral ganglia and directly innervate the effector tissues with their terminal protions (Bear *et al.*, 2007).

3.2 Divisions of the ANS

The ANS comprises two branches which differ both for their fine anatomy and function: i) the Parasympathetic Nervous System (PNS) and ii) the Sympathetic Nervous Systems (SNS). These two branches are simultaneously represented in the majority of the body tissues, on which they exert opposite effects, resulting in the precise control of tissue homeostasis. While the PNS predominates during resting conditions, the SNS is activated during the so-called “fight or flight” response and exercise (Guyton *et al.*, 2006).

3.2.1 The Parasympathetic division of the ANS

The preganglionic neurons of the PNS originate from several cranial nerves nuclei and from the sacral segments of the spinal cord (S_2-S_4). The long axons of the parasympathetic neurons establish synaptic contacts with postganglionic neurons, whose cell bodies are organized in ganglia close to- or embedded into

the effector tissues. As a consequence, the axons of the postganglionic neurons are normally short (Guyton *et al.*, 2006).

Parasympathetic neurons enclosed in different nerves are targeted to specific organs, and, in detail, among the cranial nerves, the oculomotor nerve (III) innervates the eyes; the facial nerve (VII) innervates the lacrimal gland, the salivary glands and the mucus membranes of the nasal cavity; the glossopharyngeal nerve (IX) innervates the parotid (salivary) gland; and the vagus nerve (X) innervates the viscera of the thorax and the abdomen (i.e. heart, lungs, stomach, pancreas, small intestine, upper half of the large intestine, and liver). However, most of the PNS fibers (about 75%) are in the vagus nerve.

The preganglionic neurons that arise from the sacral region of the spinal cord form the pelvic nerves. Parasympathetic neurons participating to these nerves innervate the viscera of the pelvic cavity (i.e. lower half of the large intestine and organs of the renal and reproductive systems) (**Fig. IX**).

3.2.2 The Sympathetic division of the ANS

The preganglionic neurons of the SNS start from the thoracic and lumbar regions of the spinal cord (segments T_1 through L_2) and establish synaptic contacts with several postganglionic neurons found in the sympathetic ganglia chains, which consist of 22 ganglia running along either side of the spinal cord. From these ganglia, localized at distance from the targets, long axons originate and innervate the effector tissues (Guyton *et al.*, 2006).

Other preganglionic neurons exit the spinal cord and pass through the ganglion chain without synapsing with a postganglionic neuron. Instead, the axons of these neurons travel more peripherally and synapse with postganglionic neurons in one of the sympathetic collateral ganglia. These ganglia are located about halfway between the central nervous system and the effector tissue.

In addition, a subset of preganglionic neurons are directed to the adrenal medulla. The cells of this gland have the same embryonic origin of the neural tissue and, in fact, function as modified postganglionic neurons. Instead of releasing neurotransmitters directly on the effector organ, they release them in the bloodstream, thus functioning as long-range neuroendocrine systems.

An important feature of this system, which is quite distinct from the parasympathetic, is that the postganglionic neurons of the sympathetic system

travel within each of the 31 pairs of spinal nerves. Interestingly, 8% of the fibers that constitute a spinal nerve are sympathetic. This allows for the dense distribution of sympathetic nerve fibers to the majority of effector organs, including the skin, its blood vessels and sweat glands. In fact, most innervated blood vessels in the entire body, primarily arterioles and veins, receive only sympathetic nerve fibers. Therefore, vascular tone and sweating are regulated by the sympathetic system only. (**Fig. IX**).

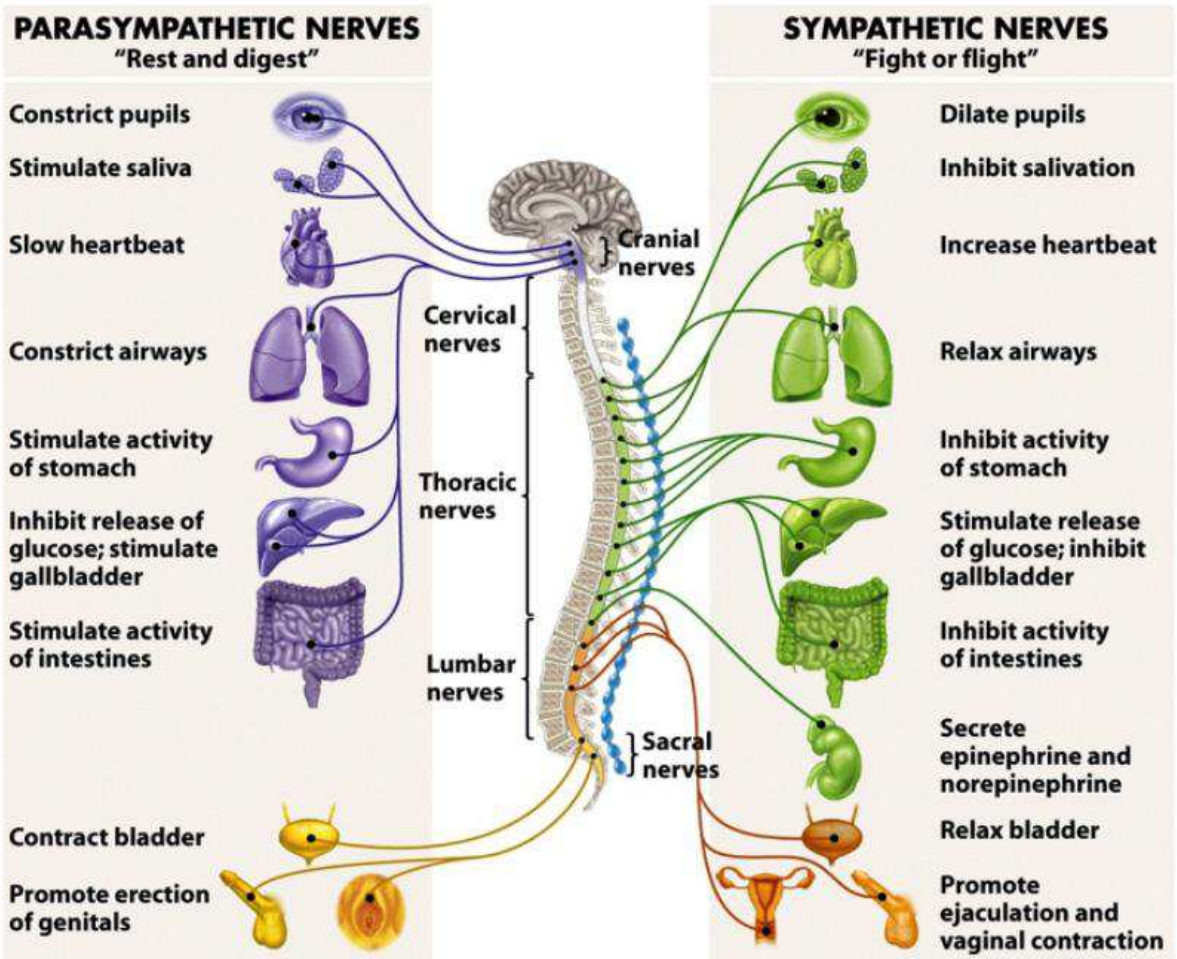

Figure IX: *structure and function of the ANS (Freeman, 2005)*

4. Autonomic innervation of the heart

4.1 Gross anatomy of heart innervation

The heart is densely innervated by the ANS, which comprises the SNS and the PNS, as previously described. The parasympathetic and the sympathetic branches of the ANS work in a reciprocal fashion to modulate heart activity by acting on HR (*chronotropy*) and conduction velocity (*dromotropy*) at the level of the cardiac conduction system. In addition, the SNS modulates heart contractility, by acting on the force of contraction (*inotropy*) and relaxation (*lusitropy*) at the level of working myocardium (Zipes *et al.,* 2008).

The parasympathetic neurons derive from cardiac neural crest cells, which migrate into the developing heart and form cardiac ganglia located the base of the atria. From these ganglia postganglionic cardiac parasympathetic nerves extend to the SAN, the AVN, the atria and heart's blood vessels, while the innervation of ventricular myocardium is limited. Parasympathetic neurons mainly use *acetylcholine* (ACh) as neurotransmitter.

The developmental origin of sympathetic neurons (SNs) is from trunk neural crest cells that migrate and form sympathetic ganglia where they proliferate and differentiate into mature neurons. Postganglionic SNs that innervate the heart have nearly all of their cell bodies in the middle-cervical and stellate ganglia, with the superior cervical and the 4^{th} to 6^{th} thoracic ganglia contributing to a little extent. From these ganglia, SNs extend their projections from the base of the heart throughout all the myocardium (Mitchell, 1953; Van Stee, 1978; Kimura *et al.,* 2012; Fukuda *et al*., 2015; Hasan, 2013) (**Fig.X**). Cardiac SN processes have a peculiar structure, which is quite different from other peripheral neurons, such as the motoneuron. Indeed, they show the typical "*pearl and necklace*" morphology, characterized by regular varicosities corresponding to the neurotransmitter releasing sites and contacting the target cells. Although SNs release a number of molecules (e.g. adenosine triphosphate, serotonin and histamine), the two main sympathetic neurotransmitters are *norepinephrine* (NE) and *neuropeptide Y* (NPY) that are stored in different vesicles, concentrated into the neuronal varicosities (Fukuda *et al.,* 2015). Effects of SN activation on CMs involve mainly NE, with NPY that seems to have a minor impact in the short term while it seems to have a role, in the long term in the regulation of CM ion currents (Protas *et al*., 1999;

Protas *et al.,* 2003). NPY is a peptide of 36 amminoacids and its receptors are coupled to Gi/Go proteins. NPY has been shown to regulate the expression of L-type Ca^{2+} channels during post-natal development, however its role in the regulation of heart homeostasis is still unclear (Herzog *et al.,* 1992; Heredia *et al.,* 2005).

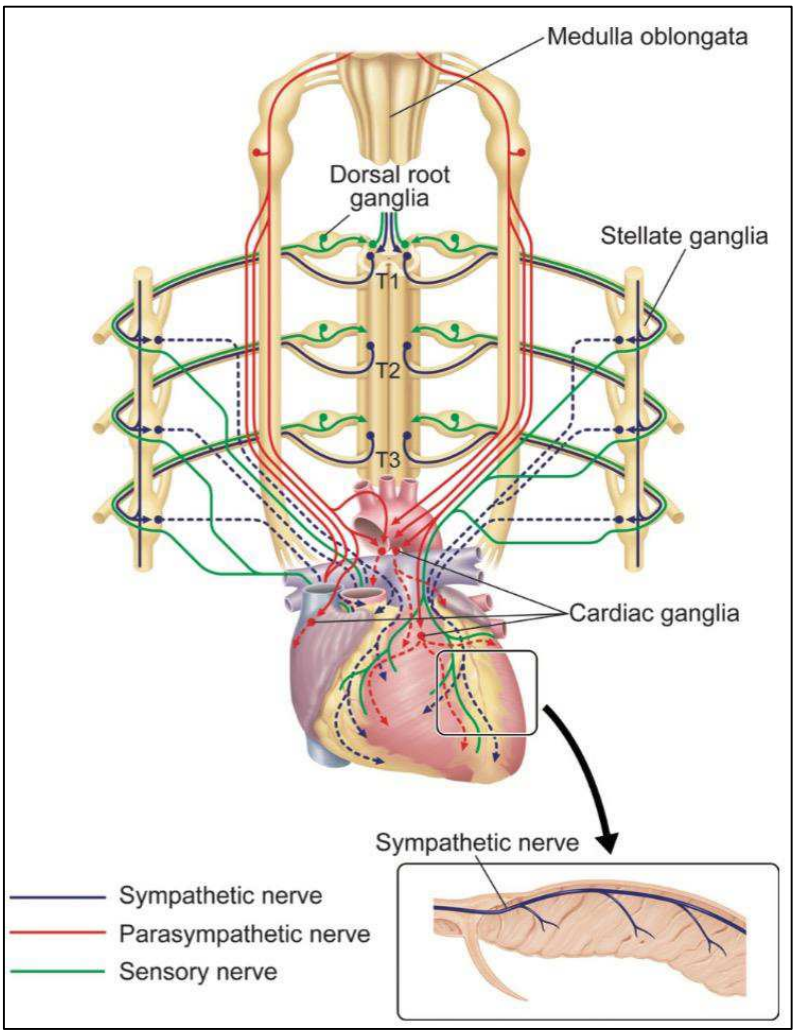

Figure X: *Anatomy of heart innervation (Kimura, 2012).*

4.2 Sympathetic innervation pattern

The myocardium starts to be innervated by SNs in the early post-natal weeks and axonal sprouting is guided by the balance between chemoattractant neurotrophins (e.g. nerve growth factor, NGF (Levi Montalcini *et al.,* 1986); neurotrophin-3, NT-3) and chemorepellent factors (e.g. semaphorin-3A, Sema-3A) released by target

myocardial cells. SN axons penetrate into myocardium, following blood vessels, an intermediate target, that express the neurotrophin-3 (NT-3). The neurotrophins NGF and NT-3 signal through the same receptors: the tropomyosin receptor kinase A (TrkA) and the p75 neurotrophin receptor (p75), to coordinate distinct stages of SN development (Kuruvilla *et al.,* 2004). NT-3 derived from vascular smooth muscle cells activates TrkA on sympathetic axons, allowing axonal extension along the vasculature. As axons approach the heart, and begin to acquire CM-derived NGF, the ensuing retrograde NGF/TrkA signaling promotes survival, anabolic responses, and expression of p75. The increase in p75, in turn, diminishes axonal responsiveness of TrkA to NT-3, enabling NGF to become the dominant axonal growth factor and so to establish a stable contact between CM and SN (Lockhart *et al.,* 1997).

Chemorepellent factors, such as Sema-3A, instead interfere with neuronal process growth, causing their retraction, and inhibit the interaction of the neuron with the target cells (Franzoso *et al.,* 2016). In the mouse heart, it is described that in the embryonic stages Sema-3A is expressed homogeneously by CMs of the nascent ventricles, while during the postnatal development, instead, it was observed a gradual decrease in the expression of Sema-3A that starts in the EPI CMs and progresses to ENDO ones. It has been demonstrated, indeed, that mice lacking Sema-3A showed an hyperinnervation of the myocardium and an unbalance of the innervation pattern, while mice overexpressing Sema-3A showed an almost denervated myocardium and are subjected to increased mortality due to sudden cardiac death (Chen *et al.,* 2007).

When the developmental process is completed, the balance between chemoattractant and chemorepellent factors generate a well-defined pattern of innervation in the heart. In the murine heart this pattern is well-described and shows a heterogeneous distribution among the four chambers. In detail, the highest density of nerve fibers is found in the atria, followed by the RV and LV, moreover inside the ventricular walls there is a decreasing gradient of SN density from the EPI region to the ENDO region (Randall *et al.,* 1968; Glebova *et al.,* 2004; Ieda *et al.,* 2007) Regarding other mammalian species, although it is described a peculiar organization of the SN, the innervation pattern is not so well characterized. In the case of the human heart, regional differences in innervation have been reported, mainly based on observational electron microscopy studies,

and similarly to the rodent heart, higher innervation density was observed in the atria compared to the ventricles, while on the contrary, no differences between the RV and LV have been reported. It has to be clarified, however, that these data come from post-mortem samples of patients, undergone prolonged medical treatments that might alter the SN patterning and further *ad hoc* studies are needed to define the SN distribution in normal human hearts (Franzoso *et al.,* 2016).

4.3 Modulation of cardiomyocyte activity by sympathetic neurons

Cardiac SNs exert a positive effect on force (*inotropy*) and frequency (*chronotropy*) of heart contraction, by the release of NE and the consequent activation of *β-adrenergic receptors* (β-ARs) on CMs. β-ARs are G protein-coupled receptor (GPCR) localized on the membrane of the CM. GPCRs contain seven transmembrane α-helices and a large cytosolic C-terminal loop. The ligand-binding sites include hydrophobic regions of α-helices, while the G proteins-binding sites include both transmembrane α-helices and the intracellular domain (Katz, 2001; Clapham, 2007; Luttrell, 2006). G proteins or *heterotrimeric GTP-binding proteins*, that mediate the response of these receptors, are composed of one member of each of three different protein families: Gα, Gβ and Gγ, organized as two separate units, one monomer of Gα and a dimer of Gβ-Gγ. Moreover, two types of Gα subunit are present in CMs: Gα_s and Gα_i exerting different functions. CMs express two major β-AR subtypes: β1 and β2. Both are members of the GPCR family of proteins, but, although are activated by the same agonist, the selective stimulation of one subtype leads to different downstream responses. Indeed β1-ARs are coupled to Gα_s stimulatory subunit only, and mediate the acute inotropic and chronotropic functional response while β2-AR seems to be coupled to Gα_s, mediating regulatory responses that are weaker than those initiated by β1-ARs and Gα_i, mediating counter-regulatory responses and anti-apoptotic effects (Chruscinski *et al.,* 1999; Bernstein *et al.,* 2005).

The increase in contraction force of CMs is exerted by SN at the level of the working CMs. Neuronally-released NE binds to CM β-AR leading to a cascade of downstream events: the activation of Gα_s, which in turns activates *adenylyl cyclase* (AC), the enzyme responsible for the production of the second messenger

cyclic-AMP (cAMP). cAMP activates its main effector, the *protein kinase A* (PKA), that phosphorylates the L-type Ca^{2+} channels and the RyR-2, enhancing the CICR and resulting in the increase of the cytoplasmic Ca^{2+} content. This increase leads finally to an augmented sarcomere contraction during systole. PKA activity is also essential in the control of Ca^{2+} reuptake in the SR during diastole, indeed, through the phosphorylation of *phospholamban* (PLB), a protein that positively modulates the activity of SERCA, PKA increases the speed of cytosolic Ca^{2+} clearance, thus resulting in the shortening of Ca^{2+} transient (**Fig.XI**) (Opie, 2004). This allows CMs also to be prone to increase the frequency of contraction.

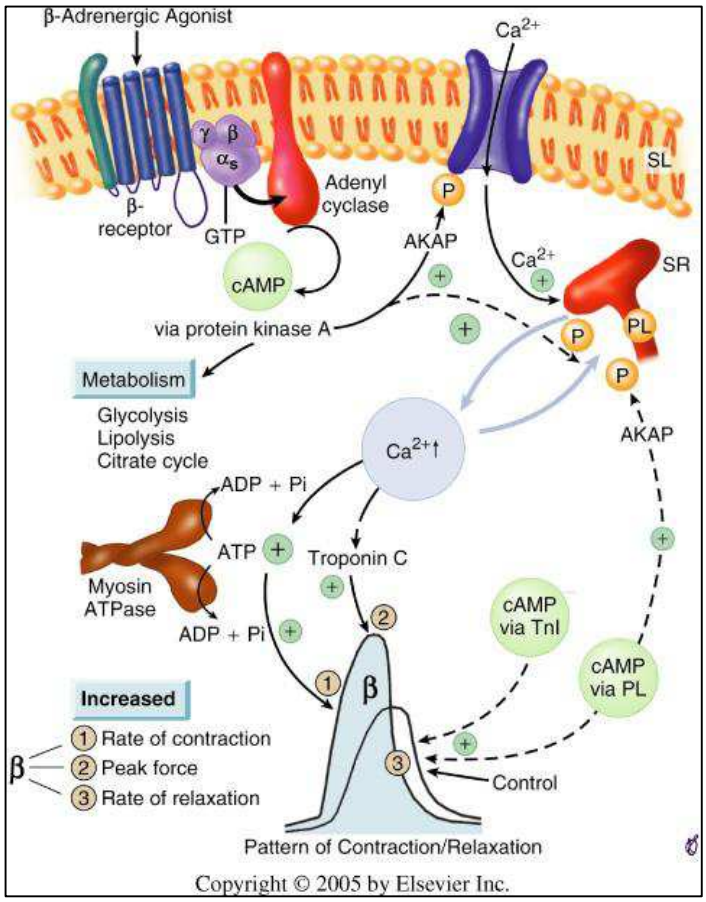

Figure XI: *Sympathetic nervous system positive modulation of CM contraction force (inotropy) (Opie, 2004).*

The frequency of heart contraction, that is dictated by SAN depolarization, is positively modulated by SNs innervating SAN cells. The SAN is the physiological pacemaker of the heart and SAN cells spontaneously depolarize through the activation of a number of different ion channels. The depolarization of

these cells starts with the opening of non specific cation channels called *hyperpolarization activated cyclic-nucleotide gated channels* (HCN), which open when the membrane potential is below -60/-70 mV and carry an inward depolarizing current called I_f. Then the L-type Ca^{2+} channels open and contribute to depolarize the cell. Moreover, the Ca^{2+} entered in the cytosol is extruded by NCX that, by exchanging each Ca^{2+} with three molecules of Na^+, generate an additional inward current. The repolarization, instead, is ensured by two potassium channels, which carry I_k and $I_{k,Ach}$ currents. $I_{k,Ach}$ is modulated by parasympathetic neurons, while I_k is controlled by SNS.

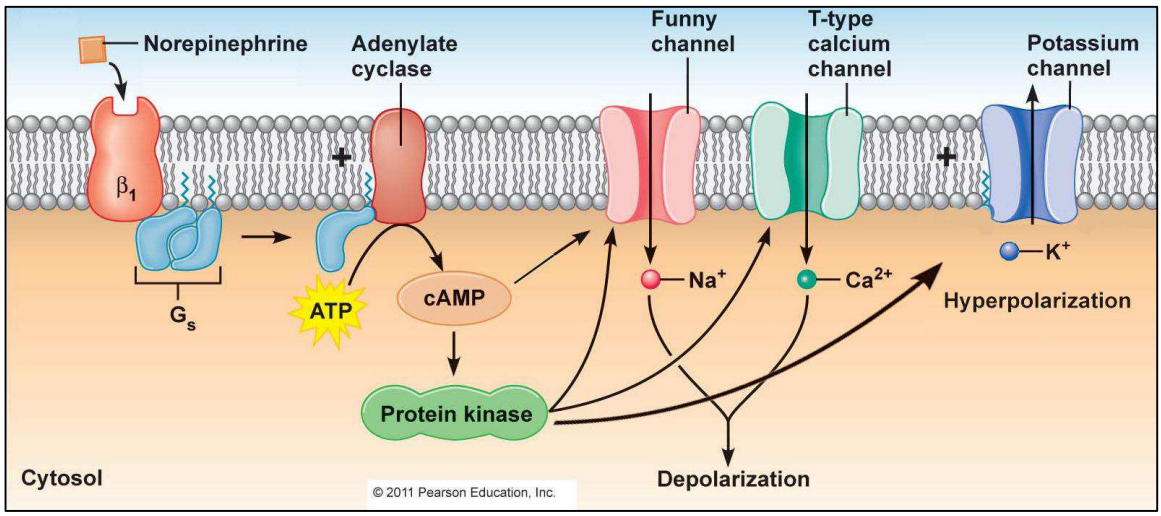

Figure XII: *Sympathetic nervous system positive modulation of heart frequency at the level of sinoatrial node (chronotropy).*

SNs innervating the SAN, accelerates its depolarization rate through the release of NE and activation of β-ARs in nodal cells. This leads to the increase of cAMP through the $G\alpha_s$/AC pathway that is able directly to positively modulate HCN opening and thus increase I_f. Moreover, cAMP mediated activation of PKA results in the phosphorylation of L-type Ca^{2+} channels and I_k channels, which increase depolarization and repolarization currents respectively, leading to the shortening of nodal cell action potential duration. This effects ultimately result in the increase of depolarization frequency of SAN that determines an increase in heart rate (**Fig.XII**).

The activation of the ANS (both sympathetic and parasympathetic

branches) generates changes in HR, that are seen in the ECG as variations in the distance between two consecutive QRS complexes, a phenomenon which is defined *heart rate variability* (HRV). The measure of HRV offers the possibility to quantify the amount of activation of the ANS in a specific situation.

Another important extrinsic modulator of heart activity is constituted by the release of catecholamines from the adrenal glands into the circulatory system, which reach the heart and activate β-ARs of CMs exerting a positive inotropic and chronotropic effect. This is the result of an endocrine signaling, which simultaneously targets various organs eliciting a systemic response in cases of elevated stress. SN modulation of heart activity, instead, is highly selective and is able to finely tune heart function with gradual responses to different stress conditions and also to physiological situations such as postural changes or exercise.

The textbook view of the cardiac SNS is best represented by the acute activation of neuronal discharge of NE in the so-called 'fight-or-flight' reaction to both intrinsic (hemodynamic, emotional) and extrinsic (fear, pain) stressors (Jansen *et al.,* 1995). However, it is worth reminding that SNs control heart functions, even in resting conditions (Lombardi *et al.,* 1996), by continuously tuning HR on a beat-to-beat basis, and controling long term signaling mechanisms involved in transcriptional control and cell division (Ogawa *et al.,* 2002; Zaglia *et al.,* 2013). It is remarkable, and yet unexplained, how information can be carried by the same neurons, encoded by a limited number of variables (amplitude and frequency of APs), and elicit responses as different as subtle or extreme modulation of HR, short-term control of inotropy (mostly mediated by β1-AR) and long-term regulation of cell size (controlled by β2-AR) (Jansen *et al.,* 1995; Zaglia *et al.,* 2013). Here, we will present evidence in support that such multiple abilities of SNS may be allowed by specific organization of the cell-cell contacts and the peculiar signaling dynamics underlying neuro-cardiac coupling.

4.4 The hypothesis of the ‘cardiac synapse’

Although the concept that the heart is innervated by the SNS was already known for decades, the diffusion of EM and the structural and functional discovery of the neuromuscular junction (NMJ), were an initial spark for the investigation of similar specific interactions between SNs and cardiac cells. Contiguities between CMs

and nerve processes enriched with electron-opaque granular vesicles, later identified as noradrenergic vesicles, were firstly described in cardiac sections from frogs (Thaemert, 1969). Structured contact sites between SN endings and CMs have been observed, although at low frequency, in the mammalian heart (Thaemert, 1969). To identify the molecular determinants of such interaction, subsequent studies have focused on proteins that typically participate in other intercellular junctions. Among these, vascular cell adhesion molecule-1 (VCAM1) and α4β1 integrins seem to play a role in the neurocardiac interaction during postnatal heart innervation. Consistently, treatment with antibodies to VCAM1 or anti-α4 integrins results in cardiac sympathetic denervation in neonatal rats (Wingerd *et al.,* 2002).

The neuro-cardiac interaction site was further studied using co-cultures between sympathetic ganglia neurons and CMs. Even if this cellular model cannot reproduce the complexity of the physiological innervation of the heart, such *in vitro* model is amenable for molecular manipulation. Recently, confocal immunofluorescence (IF) analyses demonstrated that the intercellular contact site is enriched in pre-synaptic markers (e. g. synapsin I and synaptotagmin), generic cell-to-cell adhesion molecules (i.e. cadherins and β catenin) and, importantly, post-synaptic specializations of the CM membrane, including accumulation of β-ARs and SAP97 (Shcherbakova *et al.,* 2007) all features resembling those of the well-known NMJ. In essence, the ***neuro-cardiac interaction*** resembles, for several structural and functional features, the NMJ. However, the definition of a neuro-cardiac junction was frustrated by several differences, including the variable and sometimes large distances between the neuron and CMs (Landis *et al.,* 1976) and the slow kinetics of the second messengers involved (Evellin *et al.,* 2004). Further research will be necessary to uncover the molecular determinants of the neuro-cardiac interaction and the complex properties of the neuronal network that grants autonomic control of the heart.

In this thesis, we will present evidence in support that the multiple abilities of cardiac SNS may be allowed by specific organization of the cell-cell contacts, and the peculiar signaling

5. The cardiac sympathetic nervous system plays a key role in the regulation of myocardial mass

5.1 The protein degradation systems

The myocardium is a post-mitotic tissue, indeed CMs stop divide few days after birth and, once the myocardium is fully developed, they cannot regenerate upon a tissue damage. Thus, CM health and ability to continuously adapt to intrinsic and extrinsic stresses of daily activities and ageing, is based on the removal of unfolded/misfolded proteins and their replacement with newly synthetized ones. This process is known as protein turnover.

The removal of damaged proteins and organelles is operated by the two main intracellular proteolytic machineries: the Ubiquitin Proteasome System (UPS) and the Autophagy-Lysosome System (ALS) (**Fig.XIII**).

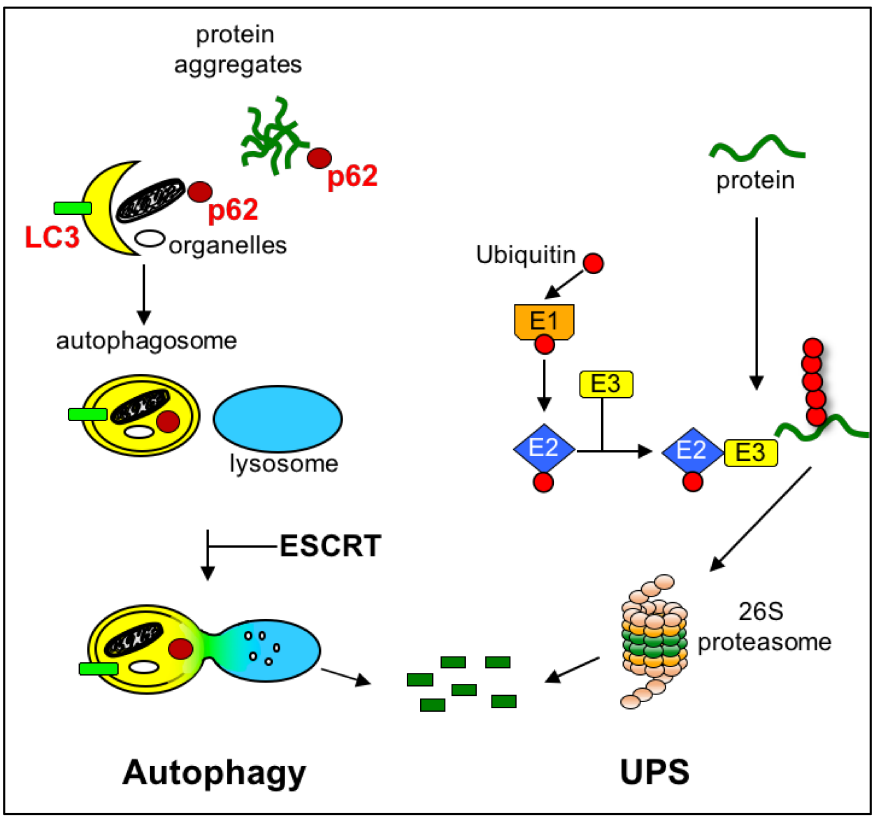

Figure XIII: *Protein degradation systems: Autophagy Lysosome System (ALS) and Ubiquitin Proteasome System (UPS).*

The UPS is responsible for the degradation of almost 90% of the sarcomeric proteins (Bucciantini *et al.,* 2002). This machinery degrades single proteins, which are tagged with a poly-ubiquitin chain through a multistep process

(Glickman *et al.,* 2002) (**Fig.XIII**) involving three families of enzymes called: E1, E2 and E3 (Ubiquitin activating, conjugating and ligating enzymes, respectively). The first step is the activation of ubiquitin by its binding to the activating enzyme E1. This is followed by the formation of the polyubiquitin chain, operated by the E2 conjugator enzyme, which is then transferred to the specific substrate, by the ubiquitin ligases (Frescas *et al.,* 2008; Jung *et al.,* 2009). Among the E3 enzymes selectively expressed in muscle cells, including CMs, Atrogin-1 (muscle atrophy F-box) and MuRF1 (muscle-specific RING finger 1) are the most studied (Willis *et al.,* 2006; Baehr *et al.,* 2014). Atrogin-1 has been originally identified as a key regulator of skeletal muscle trophism. However, recent works demonstrate that such ubiquitin ligase has also a key role in the regulation of cardiac proteostasis and participates to myocardial remodeling (Li *et al.,* 2007; Baskin *et al.,* 2014). In fact, high levels of Atrogin-1 suppress CM hypertrophy, induced by adrenergic stimulation and pressure overload, respectively, by degrading *calcineurin*, a Ca^{2+}-activated phosphatase which is a well recognized mediator of pathologic hypertrophy (Carrier *et al.,* 2010; Gomes *et al.,* 2001; Li *et al.,* 2004). MuRF1 controls the degradation of sarcomeric proteins (Bodine *et al.,* 2001; Willis *et al.,* 2007; Maejima *et al.,* 2014) e.g. cardiac troponin I (cTnI) (Kedar *et al.,* 2004) and myosin heavy chain (MyHC) (Clarke *et al.,* 2007) and its overexpression has been linked to post-LVAD atrophy (Willis *et al.,* 2009 a) and heart failure (Willis *et al.,* 2009 b).

Once the substrate to be removed is poly-ubiquitinated, it is targeted to the ***proteasome***, which degrades the protein into smaller peptides and aminoacids.

The ALS is a highly conserved process, mediating the degradation of complex cytoplasmic structures, such as protein aggregates and organelles. There are three types of autophagy that differ for the underling molecular mechanisms (Klionsky *et al.,* 2005; Massey *et al.,* 2006):

-the *chaperone-mediated autophagy*, which selective degrades cytosolic proteins expressing a peculiar aminoacidic domain (Bandyopadhyay *et al.,* 2010);

-the *microautophagy*, which is a mechanism of direct uptake of cytosolic components into the lysosome membrane, through invagination (Sahu *et al.,* 2011);

-the *macroautophagy* (referred to as *autophagy*), the most important one, which is characterized by the formation of a compartment delimited by a double membrane,

named *autophagosome*, engulfing the cytoplasmic material which will be delivered to the lysosome for its final degradation (Dargemont *et al.,* 2012). Among the autophagy players, LC3 and p62 are used as markers to assess the state of autophagy activation (McLeland *et al.,* 2011; Myeku *et al.,* 2011).

The UPS and the ALS have been considered for a long time two independent mechanisms. However, in a recent study, we identified a previously unrecognized role for Atrogin-1, as a mediator of the UPS-ALS cross-talk (Zaglia *et al.,* 2014). Indeed, we demonstrated that Atrogin-1 regulates the turnover of CHMP2B (*Charged Multivesicular Body protein 2B*), an ESCRTIII protein involved in the fusion between autophagosomes and lysosomes. Genetic ablation of Atrogin-1 thus compromises the turnover of CHMP2B, which accumulates and aggregates, leading to autophagy block, with proteotoxic CM death, which results in time in hypertrophic cardiomyopathy and sudden death (Powell*,* 2006).

5.2 Protein synthesis and degradation: the central role of the Akt pathway

Among the molecular mechanisms involved in the regulation of protein synthesis, the PI3K/Akt signaling pathway is fundamental. The protein kinase Akt, also known as protein kinase B (PKB), belongs to the family of the serine/threonine kinases (Robertson*,* 2005). Akt is the mediator of a wide spectrum of anabolic and catabolic stimuli, activating the synthesis of new proteins and blocking, at the same time, the proteolysis of the existing ones. Once activated by phosphorylation, Akt is responsible for the phosphorylation of mTOR (mammalian Target Of Rapamycin) (Nave *et al.,* 1999), another serine/threonine kinase critical for the transduction of a large number of hypertrophic stimuli (i.e. from nutrient stimulation to the activation of protein growth factors) (Glass*,* 2003). In parallel, Akt phosphorylates the FOXO (Forkhead box O) family of transcription factors, thus blocking their nuclear translocation and the transcriptional activation of the atrogenes, including Atrogin-1 and MuRF1 (Sandri *et al.,* 2004).

5.3 Roles of sympathetic innervation in the regulation of cardiac mass in postnatal growth and in the adult myocardium

The adrenergic stimulation has a key role in the early post-natal phases as neuronally-discharged NE, by acting on CM α-ARs, mediates the physiologic postnatal CM hypertrophic growth (Ieda *et al.,* 2007; Anversa *et al.,* 1986).

Recently, we demonstrated that also in the fully developed myocardium, constitutive neuronal inputs are required to maintain the correct cardiac mass (Zaglia *et al.,* 2013).

In this research we used an experimental model of cardiac SN ablation in normal adult mice, obtained by the administration of 6-hydroxy-dopamine (6-OH-DA), an analogue of dopamine that, once internalized by neurons, leads to neurodegeneration due to reactive oxygen species. SN ablation resulted in cardiac atrophic remodeling, with a reduction in heart weight of about 8% and 14% at 8 and 30 days after denervation, respectively. The decrease in cardiac mass was not due to the loss of the CMs, since no signs of CM death were detected, but rather to a reduction in cell size. In line with this, we demonstrated that the denervation-atrophy is mediated by the activation of the UPS, as we observed a significant induction in the expression levels of both Atrogin-1 and MuRF1. Interestingly, the increase in protein degradation was presumably accompanied by a decrease in protein synthesis. By combining *in vivo* to *in vitro* assays, we demonstrated that such effects are mediated by neuronally-released NE acting on CM β2-AR. Consistent with this, when we treated denervated mice with the β2- AR agonist, clenbuterol, the atrophic remodeling of the myocardium was totally prevented.

In conclusion, we identified a novel role for the cardiac SNS, as a regulator of the cardiac mass in the mature myocardium. In detail, the constitutive release of NE, by activating β2-AR, enhances protein synthesis and inhibits protein degradation, via PI3K/Akt/Foxo signaling pathway (**Fig. XIV**).

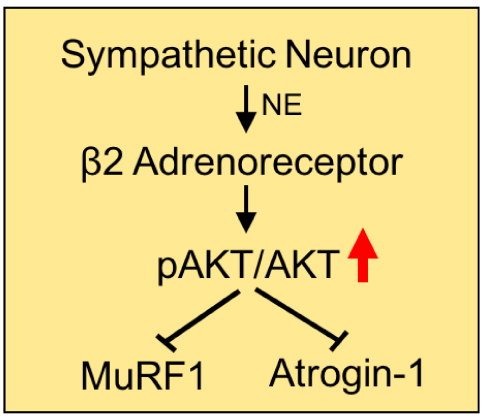

Figure XIV: *Molecular pathway through which SNs regulate CM size.*

6. Heart innervation and cardiovascular diseases

6.1 Impairment of sympathetic innervation and cardiovascular diseases

Physiological cardiac sympathetic innervation is crucial to modulate correctly heart function. In line with this, an unbalanced SN pattern and activity has been associated with several cardiac diseases, including arrhythmias, hypertrophy, heart failure, post-ischemic myocardial remodeling, diabetes, dystrophy and aging. The use of β-AR antagonists, or neuromodulation/removal of the sympathetic ganglia, represent the most common therapeutic options in such disease conditions, suggesting that dysfunction of the cardiac SNS may have a role in the disease mechanism (Shen *et al.,* 2014). In addition, the pathogenesis of the Takotsubo syndrome, a stress-cardiomyopathy, critically depends on the anatomy and function of SNs in the heart thus offering an additional viewpoint on the importance of sympathetic innervation in cardiac diseases. Although there are several disease conditions in which alteration in the SN patterning has been described, here we will focus on the Takotsubo syndrome, cardiac arrhythmias, heart failure and ageing.

6.1.1 Cardiac arrhythmias

The concept that an unbalanced NE discharge by cSNs has arrhythmogenic potential has been suggested a few decades ago and demonstrated since then in both structurally normal hearts of arrhythmic patients and ischemic hearts (Fukuda *et al.,* 2015; Zipes, 2015). The mechanism whereby regional heterogeneity of sympathetic discharge causes arrhythmia is associated with AP dispersion, an electrophysiological state favoring ventricular arrhythmias. Recently, it was shown in isolated perfused hearts that local injection of NE caused the onset of arrhythmic beats, at difference with the global perfusion (Myles *et al.,* 2012). To date, the mechanisms of regional control over cardiac activity by specific groups of cardiac sympathetic terminals are, however, largely unexplored in both physiological and disease states.

6.1.2 Takotsubo syndrome

Takotsubo cardiomyopathy is a transient cardiac syndrome that involves left ventricular apical akinesis and mimics acute coronary syndrome. It was first

described in Japan in 1990 by Sato *et al.* Patients often present with chest pain, have ST-segment elevation on ECG, and have elevated cardiac enzyme levels consistent with myocardial damage. Excess in catecholamine-dependent heart stimulation has been implicated in the disease pathogenesis, but the underling mechanisms are still unknown (Akashi *et al.,* 2015). The close temporal relationship between the triggering event (i.e. emotional stress associated to increased sympathetic neuron activity) and the onset of symptoms, together with the observation that the contractile dysfunction is confined at the heart apex, suggests that sympathetic nerves may have a key role in the disease onset (Akashi *et al.,* 2015). Indeed, Lyon and colleagues have hypothesized that hypersensitivity of the cardiac apical region to catecholamines may depend on the basal-apical differences in SN distribution and CM β-AR subtype expression levels. In particular, due to the switch of β2-AR coupling from Gs to Gi signaling, excess catecholamine stimulation may result in the regional contractile dysfunction (Lyon *et al.,* 2008).

6.1.3 Sympathetic dysfunction during aging

In addition to pathological hearts, impairment of the SNS is a common feature that occurs during aging and contributes to systolic hypertension together with a number of other causes (e.g. lower elasticity of the arterial walls). Interestingly, increased NE spillover and reduced re-uptake of the neurotransmitter by SNs have been detected in hearts from elderly people when compared to adults, suggesting that impaired resting activity of SNs occurs during aging (Seals *et al.,* 2000). Consistent with deregulated sympathetic activity, lower NGF levels were estimated in the sympathetic ganglia from old rats, (Bierl *et al.,* 2007), and might have a causal role in neurodegeneration in elders (Chow *et al.,* 2001).

In parallel, elder people display lower increase in HR upon administration of β-AR agonists due to the reduction of α- and β-AR sensitivity to NE stimulation (Lakatta, 1993), possible linked to AR desensitization as an adaptive effect of excessive sympathetic nerve tone.

It has been demonstrated that NMJ degeneration occurs during aging (Carnio *et al.,* 2014). Based on this evidence and on the data described in this thesis, and suggesting the existence of a specific neurocardiac junction, it is tempting to

speculate that impairment of the interaction between neurons and target CMs might be the primary cause of the sympathetic dysfunction in elderly people.

6.1.4 Heart failure (HF)

Sympathetic hyperactivity and NE spillover into the bloodstream are common findings in HF (Hasking *et al.,* 1986; Kaye *et al.,* 2005). Interestingly, paradoxical reduction of NGF levels and sympathetic innervation have been demonstrated in HF patients, which might be explained by a dynamic adaptive response to increased sympathetic activity (Kaye *et al.,* 2005). In a model of pulmonary hypertension-induced right ventricle hypertrophy, myocardial NGF expression was upregulated. Although such hypertrophic growth was accompanied by hyperinnervation, by TOH expressing neurons, reduced NE content and reuptake function, as well as re-expression of immature neuron-specific markers were demonstrated, supporting that sympathetic nerve 'rejuvenation' occurred in this model of HF (Kimura *et al.,* 2007). Reduced efficiency of neuro-cardiac communication, due to alterations in the specific contact structures, would therefore result in decreased activation of β-AR, NE spillover in the myocardial *interstitium* and depletion of NE stores, all of which are features commonly observed in failing hearts (Baker, 2014). In addition, it would decrease the trophic input to SNs, thus resulting with time, in heart denervation, another common feature of the failing hearts (Baker, 2014).

7. Optogenetics

7.1 Exciting cells with light: first approaches

The idea of stimulating excitable cells with light dates back to the early years of 21st century, with seminal papers on "caged" neurotransmitters (NT). This approach consisted in the neuronal delivery of NTs bound to inactivating molecules, which undergo conformational changes upon illumination, restoring the functionality of the NT (light assisted un-caging) (Volgraf *et al.,* 2006; Banghart *et al.,* 2004). This approach only allows NT-type dependent selectivity, which does not mean cell type specificity and selective activation of, for instance, a given type of neuron. Moreover, using this approach, the spatial control of activation required a stationary substrate, which made almost impossible its use in studies *in vivo*. These problems were circumvented by the pioneering studies of Miesenböck's group (Lima *et al.,* 2005) in 2005, in which insertion of a gene encoding an ATP-gated cation channel from the rat into the genome of *Drosophila*. Genetic engineering was used to restrict expression to only specific neurons of the fly. Subsequently, "caged" ATP was administered to the fly, and delivery of light, by uncaging ATP, activated a cation current in the cell. In so doing, the researchers succeeded in controlling membrane potential of specific classes of neurons in the fly, *in vivo*, with the delivery of light flashes.

7.2 ChannelRhodopsin: a new member of the rhodopsin family

Rhodopsins, is a family of light sensitive proteins expressed in eucariotic cells, like retinal photoreceptor cells, where they are implicated in light transduction, and in prokaryotes, in which they are involved in ionic homeostasis; in monocellular *algae* they control the flagellar movement and thus *phototaxis*. All these proteins are light-activated ion channels and, once active, they are able to change the membrane potential of the cell (Zhang *et al.,* 2011).

Channelrhodopsin-2 (ChR2) is a new member of the rhodopsin family of proteins, discovered by Bamberg and Hegemann's groups in 2002, in the green alga *Chlamydomonas* (Nagel *et al.,* 2003). ChR2 is a light-gated cation channel, sensitive to 470 nm light, composed of seven trans-membrane helices that form the ion channel and a long C-terminal extension of unknown function, which is omitted in the recombinant form of ChR2. The light-absorbing chromophore *retinal*,

a vitamin A derivative, is buried within the hydrophobic center of the seven helices. Light absorption by retinal leads to isomerization, followed by a protein conformational change and opening of the ion pore (Nagel *et al.,* 2003; Hegemann *et al.,* 2013) (**Fig.XV**). It was immediately clear, when these proteins were discovered, that their structural simplicity, with light sensor element and actuator channel linked and transcribed by a single gene, and their fast kinetic could turn them into a useful biotechnological tool.

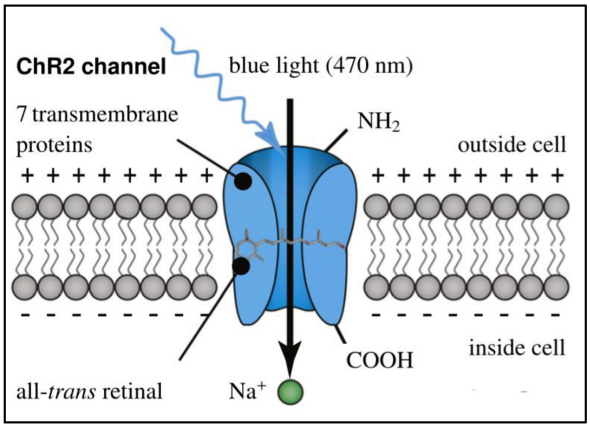

Figure XV: *ChannelRhodopsin-2 (ChR2) is a light gated cation channel (Nagel 2013).*

7.3 Optogenetics: a new field of study rises

At the same time of Miesenböck experiments, the group of Carl Deisseroth in Stanford (Boyden *et al.,* 2005), expressed ChR2 in specific neurons of the mouse brain and used this approach to control the membrane potential of these cells with the simple delivery of light flashes. The simplicity of such approach granted its success. Once the channel is inserted into the genome of the cell of interest, it is functional, although the addition of the co-factor retinal is necessary for the study of tissues that do not express it already at sufficient level. Moreover, by exploiting genetic tools for tissue-specific expression, such as neuronal-specific promoters, or the combination of these with the *Cre-Lox system*, the expression of the channel in a specific type of neuron inside a complex tissue, such as the brain, can be achieved.

This biotechnological strategy was described with the term "optogenetics", which combines the two main aspects of the method: the use of photo-activated channels to depolarize a cell and the genetics-driven expression of proteins in

specific cell types of interest (Miller, 2006). The innovative aspects of this technique, compared with the conventional electrophysiological methods, based on electrical stimulation, are the specificity of the stimulation, its non-invasiveness and its spatial and temporal accuracy. Cell-type specificity is particularly important when stimulation of only a subset of genetically identified neurons is needed, in a complex multicellular tissue in which many contiguous excitable cells are intermingled, such as the brain. This made possible to study the functionality of peculiar regions of the brain or even single neural circuits, without affecting the others (Deisseroth, 2011).

The additional possibility to photoactivate cells for prolonged time without perturbing or damaging them, is an incredible advancement for electrophysiological studies in neuroscience. Soon after optogenetics appeared, the optogenetic toolbox expanded with the exploitation of different rhodopsins, such as *Halorhodopsin* (Zhao *et al.,* 2008) which is a chloride channel that upon illumination iperpolarize the cell, offering the possibility to "switch off" single neurons or entire neural circuits (**Fig.XVI**).

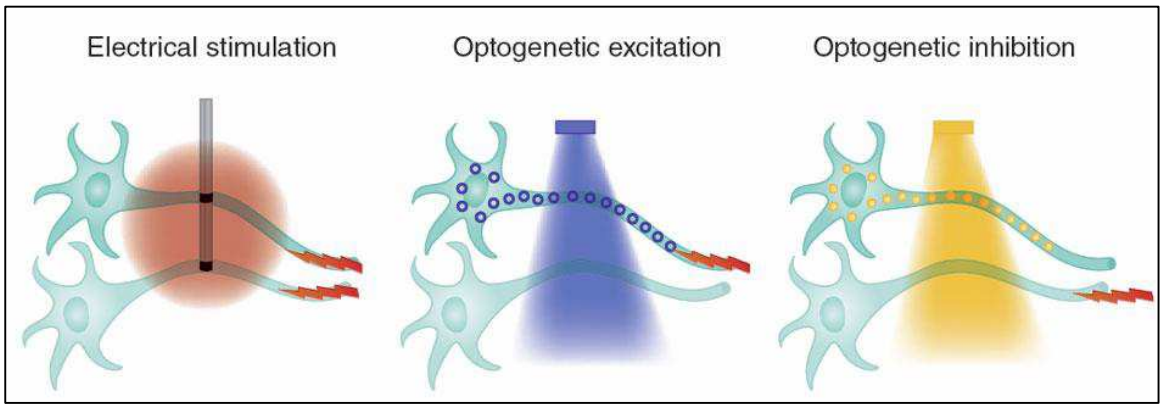

Figure XVI: *Advantages of optogenetics compared to electrical stimulation (Deisseroth, 2011).*

Our current knowledge of basal ganglia circuits and functions is strongly influenced by recent advances accomplished using optogenetic methods. For example, this technique has been used to unravel the contributions of the direct and indirect pathways to movement and reinforcement (Cui *et al., 2013*; Kravitz *et al.,* 2012), provide new descriptions of neuronal heterogeneity within the basal ganglia (Glajch *et al*., 2016; Sanders *et al., 2016*), help us understand the functional roles of nigrostriatal dopaminergic neurons (Howe and Dombeck,

2016; Tritsch *et al., 2012*), and provide new insights about the changes in the plasticity of basal ganglia circuits in pathological conditions (Chu *et al.,* 2015; Miguelez *et al., 2012*). Until now, advances enforced by the use of optogenetics have been achieved in rodent models. However, recent development of safe and efficient gene delivery strategies, currently undergoing several clinical trials, brings closer the possible clinical application of optogenetics for disease therapy. The first example is represented by a recently approved clinical trial testing the use of opsins in ganglionic retinal neurons for the treatment of a degenerative retinal disease, called *retinitis pigmentosa* (Busskamp *et al.*, 2012).

7.4 Cardiac optogenetics

Some years after the birth of optogenetics and its application to neuroscience field, the pioneering studies of Bruegmann (Bruegmann *et al.,* 2010) and Arrenberg (Arrenberg *et al.,* 2010) demonstrated that this technique could also be applied for the study of heart electrophysiology. In particular, Arrenberg and colleagues managed to express halorhodopsin and ChR2 in *zebrafish* CMs and using light sheet microscopy succeeded in controlling the HR of the animal *in vivo*, evoking episodes of tachycardia, bradycardia and also cardiac arrest (Arrenberg *et al.,* 2010). Bruegmann and colleagues, instead, generated a stable mouse embryonic stem cell line (ESC) and a transgenic mouse model expressing ChR2 under the constitutive synthetic promoter CAG (Bruegmann *et al.,* 2010). With the use of light emitted from the objective of a fluorescence microscope, they were able to influence heart rhythm by pacing heartbeats *in vivo*.

Despite these firsts proof of principle studies opened various fascinating perspectives, advancements in the new field of cardiac optogenetics lagged behind the following years, with only sparse but fundamental studies especially focused on *in vitro* models or computational approaches (Wong *et al.,* 2012; Boyle *et al.,* 2015). In particular, the group of Entcheva demonstrated *in vitro* the feasibility of obtaining optogenetic stimulation of CMs, through the delivery of non-excitable cells, expressing ChR2, that are capable of forming electrical coupling with CMs and conferring them the ability to be light stimulated (Jia *et al.,* 2011). Other *in vitro* studies tried different approaches to obtain ChR2 expression in CMs, using electroporation to express ChR2 in atrial cell line HL-1 (Hoffmann *et al.,* 2010) or lentiviral infection of human ESC that are then differentiated into CMs

(Abilez *et al.,* 2011). Moreover, Boyle and colleagues in 2013 provided a computational simulation of cardiac optogenetics, that took into account opsin channel kinetics, delivery mode and spatial distribution of light sensitive cells inside the heart, to study how these variables can be modulated to obtain low energy optical heart defibrillation (Boyle *et al.,* 2013).

Recently, in our group we developed *in vivo* cardiac optogenetic to investigate the tissue requirements to trigger arrhythmic beats, and the respective roles of common CM and conduction system CM in the generation of life-threatening ventricular arrhythmia in normal and ischemic hearts (Zaglia *et al.,* 2015).

It is worth reminding that CM are not the only excitable cell type in the myocardium, as the whole heart is highly innervated by SNs, which continuously modulate CM signalling and contractility. Optogenetics in cardiac SNs has recently been described in the pioneering study of Wengrowski and colleagues (Wengrowski *et al.,* 2015), who used optogenetics to investigate the physiology of the neurogenic control of heart function. By illuminating the epicardial surface of hearts isolated from transgenic mice expressing ChR2 under control of the sympathetic neuron promoter, tyrosine hydroxylase (TOH), this study provided the proof of principle that optogenetics could be used to modulate HR and contractile force through control of neuronal activity. Although this paper has pioneered the study of cardiac SNs with optogenetics, there are some limitations. In particular, the use of isolated-perfused hearts, in which post-ganglionic neuronal efferents were inevitably severed during the preparation, cannot ensure physiologic neurocardiac connectivity, and neither the normal pre- and afterload of a working heart. Recently, we implemented neuronal optogenetics in a mouse model obtained by CRE dependent recombination of a “double-floxed” ChR2 gene. This model was used to address, for the first time *in vivo*, the biophysics of neuro-cardiac coupling, in the experiments described in the current thesis.

AIMS OF THE PhD PROJECT

It is commonly appreciated that sympathetic neurons (SNs) are rapidly activated upon strenuous exercise or emotional stresses characterizing the so-called 'fight-or-flight' response, resulting in the recruitment of maximal cardiac performance through positive inotropic and chronotropic effects. While these general mechanisms of regulation of heart physiology are commonly recognized and have been thoroughly investigated in the last decades in both normal and disease conditions, the relationship between the fine anatomy of the myocardial neuronal network and its function, as well as the biophysics of the neuro-effector communication remain largely uncovered.

Given the physiologic and pathophysiologic implications of this aspect, research aimed at understanding the mechanisms underlying neurogenic control of heart function is of paramount importance.

Thus, the aim of the first PhD project was ***to study the biophysics of neuro-cardiac communication***, which was addressed using both *in vitro* and *in vivo* models, with the aim ***to determine the role of direct intercellular contact in the dynamics of neuro-effector coupling***.

In this first PhD project, we provided structural and functional evidence supporting that SNs communicate to cardiomyocytes (CMs) in a 'quasi synaptic' fashion.

When looking to the close apposition between SN processes and target CMs we were intrigued by the accumulation of mitochondria in the "pre-synaptic" varicosities. Mitochondria, in neurons, are fundamental for several cellular functions, including neuro-exocytosis, neurotransmitter reuptake and the preservation of cell trophism. However, at the time being, whether they have a role in the maintenance of cardiac sympathetic innervation is still unknown. On these bases, the second aim of this PhD thesis is ***to define whether dysfunction in SN mitochondria,*** as addressed in a newly developed murine model of Optic Atrophy Factor-1 (Opa1) haploinsufficiency (TOH-Opa1$^{+/-}$), ***may affect the neurogenic control of the heart.***

The PhD project results are organized into two sections, which present both data under revision (First PhD Project) and data which are part of a manuscript in preparation (Second PhD Project).
The common denominator of these parallel projects is the physiology of the cardiac autonomic innervation.

The ***first project***, whose data are part of a manuscript under revision in The Journal of Physiology, focus on ***the biophysics of the neuro-cardiac communication in vitro and in vivo systems***. Here, we present data which, contrary to the ancient view on neurocardiology, demonstrate that sympathetic neurons communciate to target cardiomyocytes in a 'quasi-synaptic' fashion.

The ***second project*** presents data which are part of a manuscript in preparation. The focus of this chapter is ***the role of the mitochondrial protein Opa1 in the maintenance of the cardiac autonomic innervation and the extrinsic control of heart function***.

Both chapters start with an introduction, followed by the method section, where the techniques used for each project are described; the result section supported by specific figures; and then the discussion and conclusions.

1st PhD PROJECT: Dynamics of neuro-effector coupling at 'cardiac sympathetic' synapses

1. Rationale

Intercellular communication between the sympathetic nervous system (SNS) and the heart underlies the most important extrinsic regulation of heart function. Sympathetic neurons (SNs) mainly operate through the release of norepinephrine (NE), activating cardiomyocyte (CM) β-adrenergic receptors (β-ARs) with subsequent increase in intracellular cyclic AMP (cAMP) (Zaccolo & Pozzan, 2002; Rochais *et al.*, 2004). SNs densely innervate the heart, and distribute to all regions, including atria, ventricles and several sectors of the conduction system. On ventricular CMs, positive inotropic effects are mediated by cAMP activation of protein kinase A (PKA), which increases Ca^{2+} availability (Bers, 2008), while chronotropic effects result from cAMP or cAMP/PKA dependent amplification of the inward current underlying diastolic depolarization in sino-atrial node (SAN) cells (Stieber *et al.*, 2003). Cardiac sympathetic stimulation is engaged at the greatest degree during acute stresses, commonly associated to the so-called *'fight-or-flight'* response (Jansen *et al.*, 1995). At the same time, SNs continuously tune heart rhythm, contributing to the non-random variation of the beat-to-beat intervals, referred to as physiological *'heart rate variability'* (Lombardi *et al.*, 1996). To comply with such a wide effect range, neurons must deliver their signals to CMs rapidly (for precise control of cardiac responses), efficiently (to minimize neurotransmitter disposal) and, if needed, potently (to maximize heart pumping). The existence of specialized sites for neurotrasmission based on direct coupling, has been demonstrated for the neuromuscular junction (NMJ), where high concentration of neurotransmitter binds to postsynaptic membrane receptors accumulated under the synaptic terminal together with channels, anchoring and signaling proteins required for muscle contraction (Slater, 2003). However, whether sympathetic control of heart function occurs through the activation of a fraction of the receptors localized at the neuro-cardiac interaction site or through the activation of all the receptors localized in the CM membrane is still debating. In fact, the 'textbook' view on the neurogenic control of heart function implicates the

release of NE in the myocardial *interstitium*, its diffusion to the CM membranes and interaction with β-ARs. Electron microscopy analysis demonstrated that in SN-CM co-cultures, neurons form varicosities containing synaptic vesicles along their axons 20-30 nm from the CM surface (Landis, 1976, Furshpan, 1986), and that SNs activation modulates CM beating rate (Oh *et al.*, 2016). More recently, it has been shown that in the CM membrane at the level of sympathetic terminals there is accumulation of anchoring and signaling proteins, supporting a model in which the neuro-cardiac interaction occurs through a well-organized structure similar to the NMJ (Shcherbakova *et al.,* 2007).

Abundant research has described the molecular details of AR signaling in the heart, and clearly identified that dysfunction of cardiac SNs is central to the pathogenesis of several cardiovascular disorders, but the dynamics of intercellular communication between SNs and CMs is much less understood. Here, we combined *in vitro* assays in co-cultures, and *in vivo* optogenetics of cardiac SNs, to investigate the neurogenic control of cardiac function, focusing on the interface between neurons and the heart. Live cell cAMP imaging was used to gain insight into the biophysics of neuro-cardiac communication dynamics *in vitro*. Optogenetics enabled us to assess neuro-cardiac coupling by selectively control of the activity of the SNs innervating the SAN of living mice.

2. Material and Methods

2.1 In Vivo analyses

2.1.1 Animal Models

Transgenic mice expressing cre-recombinase under the control of tyrosine hydroxylase (TOH) promoter B6.129X1-Th<tm1(cre)Te>/Kieg (Emma Laboratories, KCTT/EMMA/Johannes Wilbertz Stockholm SWEDEN) were bred with B6.Cg-Gt(ROSA)26Sor$^{tm27.1(CAG-COP4*H134R/tdTomato)Hze}$/J expressing mice (Jackson Lab. Bar Harbor, Maine, USA). The resulting offspring had the STOP cassette deleted in dopaminergic and adrenergic neurons, thus expressing the hChR2(H134R)-*td*Tomato fusion protein. TOH-cre$^{+/-}$ lines were used to maintain the colonies and used as littermate controls. In this study we also used C57BL/6J and α-MyHC/ChR2 mice (Zaglia *et al.*, 2015), as well as P1-P3 Sprague Dawley rats (from Charles River, Milan). All experimental procedures were approved by the local ethical committee (Authorization number C54) and communicated to Ministry of Health (Ufficio VI), in compliance of Italian Animal Welfare Law (Law n 116/1992 and subsequent modifications).

2.1.2 Neuronal optogenetics in living mice

Adult (3 mo.) TOHcre/ChR2 male mice were anesthetized with Zoletil (15mg/gr, i.p.), secured to the table in a supine position and intubated with a 24G needle for ventilation (tidal volume 0.4 ml; 120 strokes/min) using an artificial ventilator (SAR-830). Body temperature was constantly monitored during the entire experiment. Then, the skin was dissected by a lateral right sub-axillary 1.5 cm cut, subcutaneous muscles were removed and a 0.5 cm incision was performed at the level of the 1st intercostal space. Self-retaining microretractors were then used to separate the 1st and 2nd ribs enough to provide adequate exposure of the operating region. The right atrial surface was exposed and stimulated with a 1.5mm diameter fiber optic (Thorlabs, Germany), coupled to a 470 nm LED (Thorlabs, Germany), controlled by an ECG-coupled recording system (Powerlab 8/30, Bioamp and LabChart 7.1 software; AD Instruments). Photostimulation was performed by delivering trains (from 1 to 50 flashes) of 10 msec light pulses, at a

frequency ranging from 5 to 20 Hz. In these experiments we evaluated the increase of the heart frequency upon photostimulation and after the administration of different β-blockers antagonists, such as Propranolol (4-50mg/Kg, Sigma) and Metoprolol (4-40mg/Kg).

A single lead I ECG was recorded (Powerlab 8/30, Bioamp; AD Instruments) during the experiment. ECG parameters were calculated by using LabChart 7.1 software (AD Instruments). In particular, among the ECG parameters, we evaluated: *i)* the p-wave, that is an important index to determine the specificity of the SN stimulation; *ii)* QRS, RR interval, to analyse the ventricles contraction and *iii)* the heart rate (HR) to test if the photostimulation works, indeed we expected that upon the blue light flashes, the HR increases.

2.2 Ex Vivo analyses

2.2.1 Human heart sample processing and immunofluorescence

Human post-mortem samples were obtained thanks to an on-going collaboration with Prof. Cristina Basso, (Cardiovascular Pathological Anatomy Department). The samples were already anonymized when received and used in accordance with the relevant authority requirements. The samples analyzed in this study derived from adult male subjects died for extracardiac causes. Heart samples underwent prolonged formaline fixatio, followed by paraffin inclusion (PERINTELSINT RVG/2 KALTEK srl). Three microm sections were processed for immofluorescence (IF) analysis, following the procedure described in (Zaglia *et al.,* 2016).

2.2.2 Processing of murine heart samples and immunofluorescence

Hearts were harvested from adult mice, washed in 1X PBS to remove the blood, and the atria and the ventricles separated at the level of the atrio-ventricular junction.

Heart ventricles were fixed in 1% (vol/vol) paraformaldehyde (PFA) (Sigma) for 15 minutes (min.) at room temperature (RT), dehydrated in sucrose gradient at 4 °C, embedded in OCT and frozen in liquid nitrogen. On the contrary, atria underwent prolonged fixation (1h) in 2% PFA. Ten μm atrial and ventricular sections were obtained with a cryostat (Leica CM1850, Leica Microsystems GmbH) and

processed for standard histological and IF analyses. For IF analysis, ventricular heart sections were incubated with primary antibodies diluted in 1X PBS, supplemented with 1% BSA and 0.5% Triton, overnight at 4°C. For atrial sections the primary antibodies were diluted in 1X PBS, supplemented with 1% BSA and 2% Triton overnight at 4°C.

488- and Cy3-conjugated secondary antibodies, all from Jackson lab (UK), were used to detect primary antibodies. Secondary antibodies were diluted in 1X PBS, supplemented with 1% BSA and incubated on heart sections at 37°C for 30 minutes (min.). Heart sections were analyzed at the confocal microscope (TCS SP5 Leica, Leica Mikrosysteme Vertrieb GmbH). The primary antibodies used in this study are listed in **Table 1.**

2.2.3 Whole mount staining in murine and human thick heart tissue blocks

One mm^3 myocardial blocks were obtained from fresh harvested mouse hearts and autoptic human hearts.

After a brief wash in 1X PBS, the samples were fixed in 1% PFA for 5 min. in agitation at 4°C, followed by three washes (each of 5 min.) in 1X PBS. Heart samples were then incubated with the primary antibody diluted in 1X PBS, supplemented with 1% BSA and 2% Tritron X-100 (all from Sigma) for 4 consecutive days at 4°C. After this incubation, three washes of 1 hour in 1X PBS, supplemented with 1% BSA and 0.5%Triton X-100 were performed. This step was followed by the incubation with the secondary antibody diluted in 1X PBS, supplemented with 1%BSA and 0.5% Triton X-100 for 3 days at 4°C. Samples were then washed in 1X PBS (three times for 30 min) Samples were maintained in 1X PBS for imaging analysis at the multiphoton microscope (Olympus, Scientifica), equipped with a Ti-Sapphire laser (Chameleon, Coherent) and an 16x Objective (Nikon). 3D reconstructions were obtained with the software for 3D-rendering (Fiji, NIH Bethesda, USA).

2.2.4 *In vivo* electron microscopy analysis

Adult mice were anesthetized and the abdominal aorta was cannulated with a 22-G needle. The inferior *vena cava* was cut to allow the outflow of the fixative. Hearts were retrogradely perfused with 1X Tyrode Solution (in mmol/L, 136 NaCl, 5 Hepes, 0.33 $NaH_2PO_4(H_2O)$, 5.4 KCl, 1 $MgCl_2(6H_2O)$, 10 glucose, pH 7.4) at a

rate of 60ml/h, and fixed with 2.5% glutaraldehyde in 0.1 mol/L sodium cacodylate. Hearts were removed, the right and left ventricles dissected, minced in 1 mm^3 pieces and further fixed for 2 h at 4°C. Samples were then washed twice for 10 min. with 0.2 mol/L sucrose in 0.1mol/L sodium cacodylate. Post-fixation was carried out in 1% osmium tetroxide in 0.1 mol/L sodium cacodylate for 2h at 4°C. Samples were then treated with increasing ethanol concentrations, incubated with propylene oxide for 45 minutes and embedded in epoxy resin. Semi-thin sections were cut, stained with uranyl acetate, 50% ethanol and Reynolds lead citrate and examined with a FEI Tecnai 12 electron microscope.

2.3 In Vitro analyses

2.3.1 Primary culture of rat neonatal cardiomyocytes

Neonatal cardiomyocyte culture is a well-established cellular method to investigate signalling pathways and ion homeostasis in cardiac cells. Hearts were harvested from P1-P3 Sprague Dawley rats upon their sacrifice by cervical dislocation. Heart were quickly removed, atria were carefully excised, then ventricles were collected in a 50 mL tube half-filled with ice-cold ADS buffer (5 mM glucose, 106 mM NaCl, 5.3 mM KCl, 20 mM Hepes, 0.8 mM Na2HPO4, and 0.4 mM MgSO4, pH7.4). Under a sterile hood, ventricles were washed to remove excess of blood then minced in a 10 cm petri dish, placed on ice, in 5 mL of 1X ADS in order to obtain heart fragments around 1 mm^3. Ventricles mechanically minced were then transferred to a 50 mL sterile tube with a 5 mm magnetic stir bar. ADS Buffer was completely removed and replaced with 6 mL of Digestion Buffer (collagenase A (0.4 mg/ml) (Roche) and pancreatine (1.2 mg/ml) (Sigma)) and positioned on a magnetic stirrer inside a water-bath at 37°C. The first cycle of 5 min. allows to remove damaged cells so the supernatant was discarded at the end of this time. Another 6 mL of Digestion Buffer were added to the heart pieces for 20 min always at 37°C on a stirrer. To block the enzymatic activity, the surnatant of the cycle was transferred into 15mL tube cointaining Horse Serum (HS), and then centrifuged at 1250 rpm for 5 min. The supernatant was removed and cells were resuspended in 2.5 mL of first day medium composed by: MEM (88,8%, Gibco), Fetal Bovine Sereum (10%, FBS) (Gibco), Non Essential AmminoAcid

(0,1%, NEAA) (Gibco), 5-Bromo-2-desossiuridine (0,1%, Sigma) and antibiotics (0,1%, Gibco), and maintained in the incubator until the digestion cycles were completed. Non-digested heart pieces repeated the digestion step previously described; usually a total of 5-6 cycles are required to complete the enzymatic digestion of 10 hearts. At the end of the digestion cycles, isolated cells from the different cycles were mixed and seeded in a 10 cm tissue culture dish (BD Falcon) and maintained in the incubator at 37°C for 1 hour. This step is named “pre-plating” and allows to separate CMs from cardiac fibroblasts that are characterized by faster adhesion to the dish. After the pre-plating step, cells in suspension were collected and counted. The total number of cells obtained was determined diluting cells in 0.2% Trypan Blue and counting viable cells in a Bürker chamber. CMs were then plated on laminin-coated glass coverslips (1.8 µg/100 mm^2) at a density of 470 cells/mm^2 for live imaging and IF analysis. Twenty-four hours after plating, the medium was removed, cells washed twice with ADS Buffer, to remove dead cells, and incubated with second day medium (second day medium: 98,8% v:v MEM; 0,1% v:v Insuline-Transferrin-Selenium (ITS) (Gibco); 0,1% v:v 5-Bromo-2-desossiuridine (Sigma), 0,1% v:v NEAA (Gibco) and 0,1 % v:v antibiotics (Gibco)).

At the day of seeding, CMs were transfected with either the Förster Resonance Energy Transfer (FRET)-based sensor, GcAMPs (Nikolaev *et al.*, 2004) or the fluorescent PKA activity reporter AKAR3 (Allen and Zhang, 2006), by using transfectin (Bio Rad), as recommended by the manufacturer. In a subset of experiments, CMs were infected with an adenovirus (3.6×10^5 particle forming units) encoding for the FRET-based Camp sensor Epac-S^{H187} (Richards *et al.,* 2016). In detail CMs were maintained in the culture medium supplemented with the viral vector for 24 hours. Then, the medium was refreshed and cells used for long term co-culture experiments (Klarenbeek *et al*., 2015).

2.3.2 Isolation of Superior Cervical Ganglia Neuron and co-culture with cardiomyocytes

Superior Cervical Ganglia Neurons (SCGNs) were isolated from either P1-P3 Sprague Dawley rats or TOH/ChR2 mice. SCGNs were minced in RPMI, supplemented with 10% Horse Serum (HS) and enzymatically dissociated in 0.25% Trypsin with no EDTA (all from Thermo Fisher) for 30 min. at 37°C.

Rat SCGNs were co-cultured with rat neonatal CMs, in a 1:50 (SCGNs:CM) ratio. From the second day, cells were maintained in the CM culture medium, supplemented with 100 ng/ml Nerve Growth Factor (NGF) (Sigma) to maintain neuronal viability. The culture medium was refreshed every two days, and the co-cultures were followed for 2 weeks.

SCGNs isolated from TOH/ChR2 mice were cultured alone, on laminin-coated dishes, at a density of 25000 cells/cm^2 and were used for electrophysiological analysis (see below method “Electrophysiology on cultured neurons”).

2.3.3 Electrophysiology on cultured neurons

Whole cell current-clamp experiments were performed at RT (~23°C) on single cells visualized with an inverted microscope (Olympus IX50, Tokyo, Japan). Data were recorded using a EPC-7 amplifier (HEKA electronic, Lambrecht, Germany) and Axon Instruments pClamp10 software. Data are sampled at 10 kHz. Patch pipettes were prepared by pulling borosilicate glass capillaries (1.5 mm outer diameter and 1.16 mm inner diameter, Harvard Apparatus LTD, Massachusetts, United States) using a micropipette puller (Narishige, Japan). Pipette resistance is 2-4 MΩ when filled with intracellular solution. Extracellular solutions contained (in mmol/L): 125 NaCl, 5 KCl, 1 Na_3PO_4, 1 $MgSO_4$, 20 Hepes, 5.5 Glucose, 1.8 $CaCl_2$, pH 7.4 with NaOH. Intracellular solution was (in mmol/L): 100 K-gluconate, 20 KCl, 10 Hepes, 10 phosphocreatine, 4 Mg-ATP, 0.3 GTP, pH 7.3 with KOH. All membrane potential values are corrected for liquid junction potential, calculated as -14.5 mV.

2.3.4 Real time cAMP imaging in SN-CM co-cultures

FRET-based imaging experiments were performed in 15 days co-cultures. Cells, expressing the fluorescent cAMP sensor, were maintained in Hepes-buffered Ringer-modified saline (in mmol/L, 125 NaCl, 5 KCl, 1 Na_3PO_4, 1 $MgSO_4$, 5.5 glucose, 1.8 $CaCl_2$, 20 Hepes, pH 7.4) at RT and imaged on an inverted Olympus IX50 microscope coupled to a CCD camera (Sensicam QE, PCO) and a beam-splitter optical device (Microimager) (**Image 2**). Images were acquired using custom-made software and processed using ImageJ (National Institutes of Health). Variations in FRET efficiencies were measured by drawing a region of interest (ROI) in the cell cytosol and by monitoring changes in the 480nm/545 nm

fluorescence emission signals (R) on excitation at 430 nm after background subtraction. FRET values were expressed as $\Delta R/R_0$, where R_0 is the ratio at t=0 s and $\Delta R=R-R_0$. The beginning of FRET variations, indicative of intracellular cAMP concentration, was defined as the time of the first frame after which two consecutive values fell outside the standard deviation of values in basal condition. Membrane depolarization of SNs was obtained by applying high potassium solution (in mmol/L, 80 NaCl, 50 KCl, 1 Na_3PO_4, 1 $MgSO_4$, 5.5 glucose, 1.8 $CaCl_2$, 20 Hepes, pH 7.4) either via a perfusion system or via pulses delivered by means of a software-controlled pressurized micropipette (Eppendorf AG, Germany) in proximity of the analyzed cell.

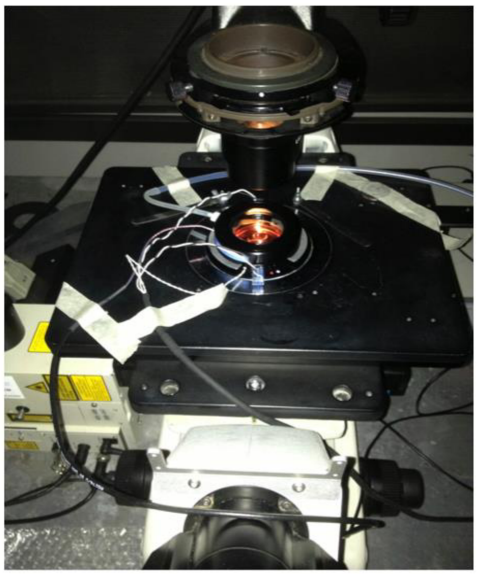

Image 2. *Microscope used for live imaging experiments*

2.3.5 Assessment of chronic SN-to-CM communication in co-cultures

To evaluate whether SN activity control CM size locally, we established co-cultures between CMs and SN-differentiated from PC12 cells. PC12 are a cell line derived from the rat pheochromocytoma, a tumor of chromaffin cells. These cells are easy to genetically and pharmacologically maintain and manipulate. In this work, we used a particular clone of PC12 cells, kindly gifted by Patrizia Rosa (CNR, Milan), that are highly responsive to NGF and actively release NE when stimulated.

PC12 cells were maintained in undifferentiated state in a medium composed by: DMEM-H16 (83%); HS (10%); FBS (5%) and antibiotics. When required, PC12

cells were put in co-culture with CMs following the protocol previously described for primary SCGN. In PC12-CM co-cultures, once the SN-CM contacts were established, cells were treated with nicotine (1μM) for 8h for 5 consecutive days.
At the end of the protocol, cells were fixed and processed with IF analysis to compare the areas of innervated *vs* non-innervated CMs.
A subset of PC12-CM co-culture was used to study cAMP dynamics.

2.3.6 *In vitro* immunofluorescence analysis

SN-CM co-cultures, as well as SNs cultured alone, were fixed in 3.7% formaldehyde for 30 min. at 4°C, followed by three washes (10 min. each) in 1X PBS. Cells were permeabilized with 1X PBS, supplemented with 0.1% Triton X-100 for 5 min. at RT and incubated with primary antibodies diluted in 1X PBS, supplemented with 1% BSA for 2 h at 37°C. Primary antibodies were revealed by a 30-min-long incubation with CY3- or Alexa 488-secondary antibodies. Cells were analyzed at the confocal microscope. The primary antibodies used for *in vitro* assays are listed in **Table 1.**

2.3.7 *In vitro* electron microscopy analysis

TEM analysis was performed on co-cultures. Cells were fixed with 2.5% glutaraldehyde in 0.1M sodium cacodylate for 1h at 4°C and washed twice for 30 min. with 0.2M sucrose, supplemented with 0.1M sodium cacodylate. Post-fixation was carried out in 1% osmium tetroxide, supplemented with 0.1M sodium cacodylate for 2 hours at 4°C. Samples were then treated with increasing ethanol concentrations, incubated with propylene oxide for 45 minutes and embedded in epoxy resin. The resin with the cells was extracted from the wells and semithin sections were cut, stained with uranyl acetate, 50% ethanol and Reynolds lead citrate and examined with a FEI Tecnai 12 electron microscope.

2.4 Statistics

Data are shown as ‘mean ± SEM’, unless differently indicated. For the analysis of significance, unpaired Student’s *t*-test was used, with P values <0.05 (*), < 0.01 (**) and < 0.001 (***) considered statistically significant. Curve fitting was performed with GraphPad Prism software; NE dose/response analyses were fitted

with non-linear regression sigmoidal dose-response; the goodness of fittings was assessed by the least-square method. We also used ANOVA statistical test in *in vivo* photostimulation experiments to compare two or more data groups by comparing the internal variability of these groups with the variability between the groups.

Table 1. Primary antibodies used in the study

Primary antibodies

Target	Company	Diluition	Host species
TOH	Millipore	1:600	rabbit
SYN1a	Millipore	1:1000	rabbit
TOH	Abcam	1:400	mouse
HCN4	Alomone Lab	1:100	Guinea Pig
Pan- cadherine	Abcam	1:600	rabbit
□-catenine	Abcam	1:400	rabbit
□-actinin	Sigma	1:200	mouse
dystrophin	Abcam	1:300	rabbit
Troponin I	Gift from Prof. Schiaffino, UNIPD (Saggin et al, 1990)	1:200	mouse
ChR2-tdTomato	SicGene Antibodies	1:300	Goat
SNAP25	Covance	1:200	mouse
FITC conjugated isolectin-b4	Vector laboratories	1:200	
Smooth muscle actin	Sigma	1:1000	mouse
Alexa Fluor 555 conjugate	Invitrogen	1:800	
RYR2	Sigma	1:200	rabbit
TOM 20	Santa Cruz	1:100	rabbit
Synaptotagmin	Abcam	1:200	mouse

3. Results

3.1 Characterization of the autonomic nervous system in the murine and human myocardium.

The heart innervation is a complex network intertwined between cardiomyocytes (CMs). Indeed, the mammalian heart is highly innervated by sympathetic neurons (SNs), which, from the anatomy textbooks, have been described to distribute, within the myocardial *interstitium*, along capillary vessels (Ieda *et al.,* 2007; Kimura *et al.,* 2012). However, at the time being, the fine anatomy of heart innervation remained underexplored (Zhou *et al.* 2004; Ieda *et al.* 2007; Clarke *et al.* 2010; Muhlfeld *et al.*, 2010). This is likely due to the imaging methods mostly used to visualize SNs in the cardiac tissue, such as electron microscopy, which focuses on ultrastructural details at the expense of a general vision of the neuronal network. Recent studies provide a description, based on immunofluorescence (IF) analysis, on heart sections, of cardiac innervation in the murine myocardium. Although these observations delineate the innervation pattern, they fail to provide a reliable reconstruction of the complex interactions between cardiac sympathetic neurons (cSNs) in the three dimensions (Baluk and Fujiwara,1984; Choate *et al.*, 1993; Ieda *et al.,* 2007; Pauza *et al.,* 2014).

To define the fine anatomy of the autonomic myocardial innervation, we used IF with antibodies specific for enzymes involved in the synthesis of norepinephrine (NE), such as dopamine β-hydroxylase (DA-β-OH) and tyrosine hydroxylase (TOH). While DA-β-OH selectively identifies cSNs, TOH antibody stains both cSNs and dopaminergic neurons, which are present in the heart, although at a very low density. In the experiements of this thesis, TOH will be used as *bona fide* marker of SNs, since by using double IF staining we observed that more than 95% of TOH positive neurons also express DA-β-OH (**Fig. 1A**). Cardiac sympathetic processes also express markers of neuroexocytosis (i.e. synapsin-1a, SNAP25, syntaxin and synaptotagmin) (**Fig. 1B-C**), which are predominantly found at the contact site with target cells including: i) CMs (**Fig. 2A**); ii) smooth muscle cells (SMC) of coronary vessels (**Fig. 2B**) and iii) endothelial cells of capillary vessels (**Fig. 2C**). To improve the characterization of sympathetic innervation in a 3D context, we develop a protocol of whole mount staining of cSN in 1mm^3 heart tissue blocks, which were then imaged at the multiphoton microscope (**Fig. 2D**). This analysis

showed that each CM is simultaneously innervated by more than one neuronal process. Thus, while the bi-dimensional analysis of heart sections suggests the coexistence, in the heart, of innervated and not-innervated CMs, our experiment indicates that all CMs are contacted by cSNs and what varies, in the different heart regions, is the total number of innervating neuronal processes received by each CM (TOH^+ fibre/CM, EPI: 0.45±0.06 *vs* ENDO: 0.15±0.02). In the 3D context we estimated from 2 to 4 neuronal process/CM in the *subendocardium* region (ENDO) of the left ventricle (LV), and from 6 to 8 SN processes/CM in the *subepicardium* (EPI). This data are totally in line with evidence described in the literature and confirmed by us that, in the mouse heart, the EPI is much more innervated than the ENDO (Fukuda *et al.,* 2005).

Interestingly, this concept holds true also in the human myocardium. Indeed, thanks to a collaboration with Prof. Cristina Basso (Pathological Anatomy of the University of Padova), we had the opportunity to process block of autoptic heart samples from patients died for extra-cardiac diseases and provided the first 3D reconstruction of the neuronal network in the normal human myocardium (**Fig. 3A**). This data prompted us to aim at defining the fine anatomy of cardiac innervation in the human heart, a piece of information still missing, notwithstanding the common use of pharmacological therapies based on blockade of adrenergic effects in cardiovascular diseases. A key step we employed to analyse neuronal distribution in FFPE samples from human post-mortem hearts, which are preserved in biobanks, has been represented by the implementation in the laboratory of a tissue processing protocol allowing IF studies at high resolution in these samples (Zaglia *et al.,* 2016). This strategy allowed to demonstrate that, in the human myocardium, the density of cSN is higher in the ENDO than the EPI region, and in both neurons are found in close apposition to CM, coronary and capillary vessels (**Fig. 3B-D**).

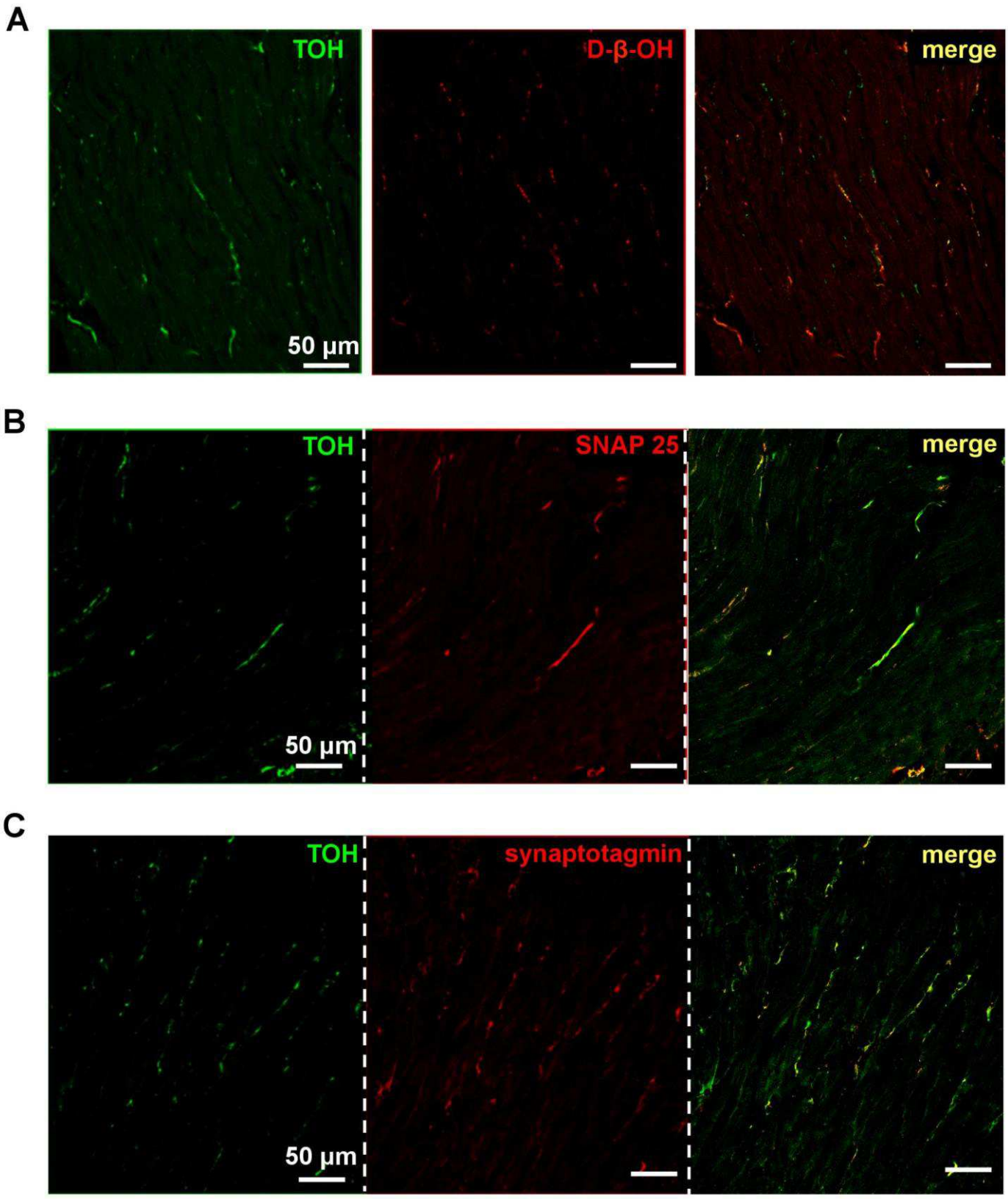

Figure 1. Characterization of the autonomic innervation of the adult murine myocardium.

(A-C) Confocal IF analysis of heart cryosections co-stained with an antibody to tyrosine hydroxylase (TOH) (green signal) and antibodies specific for: dopamine-β-hydroxylase (D- β-OH) (**A**), SNAP25 (**B**) and synaptotagmin (**C**) (all red signals). The right panels in (**A-C**) are the merge of the left and middle panels.

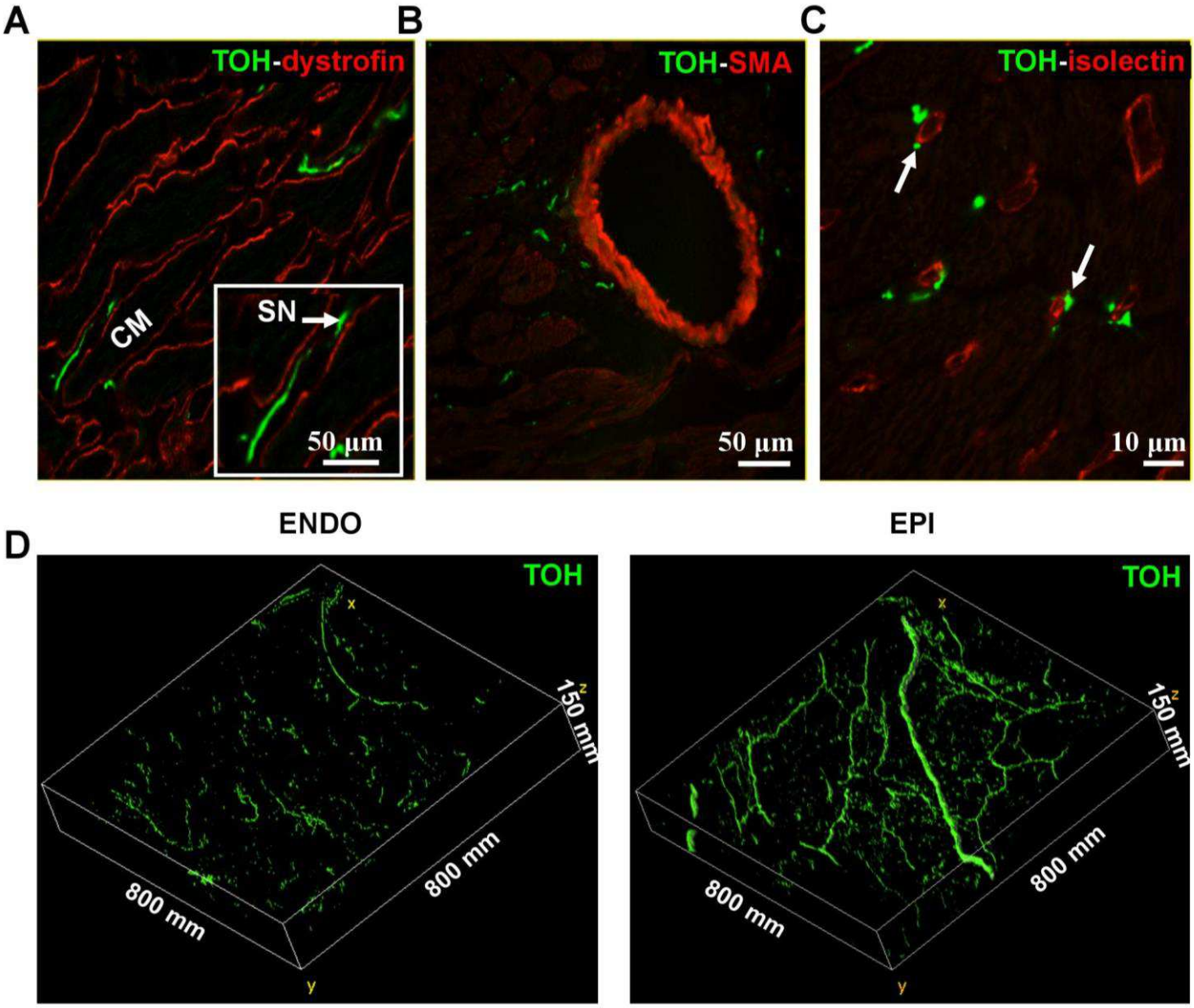

Figure 2. Characterization of the fine anatomy of the autonomic innervation of the adult murine myocardium.

(**A-C**) Confocal IF analysis of heart cryosections co-stained with an antibody to tyrosine hydroxylase (TOH) (green signal) and antibodies specific for: dystrophin (**A**), smooth muscle actin (SMA) (**B**) and isolectin (**C**) (all red signals). (**D**) 3D reconstruction at the multiphoton microscope of the neuronal network in 1mm^3 tissue blocks from the left ventricle *subendocardium* (left panel) and *subepicardium* (right panel). Whole mount staining, with an antibody to TOH, was used to identify sympathetic neuron processes.

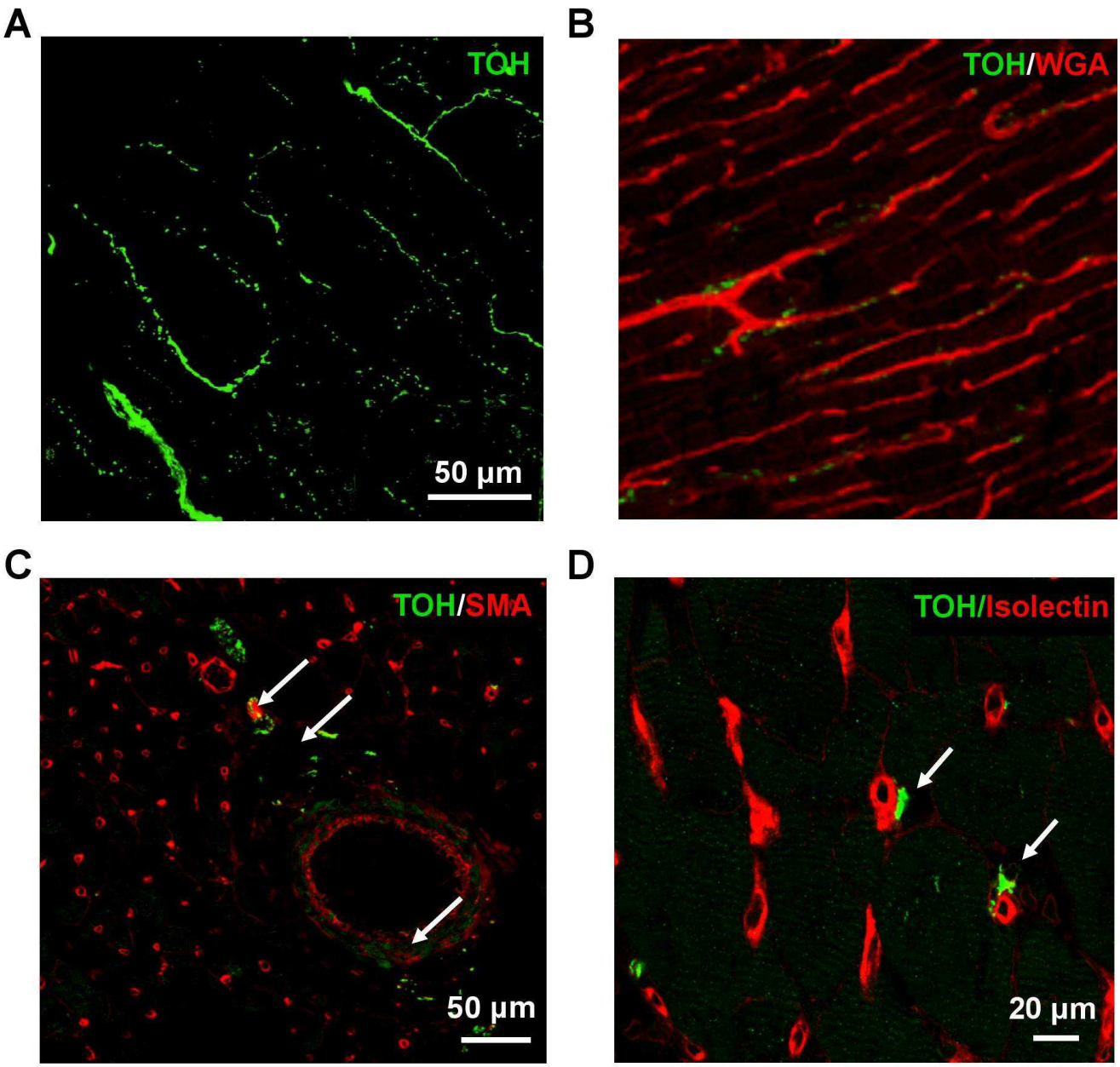

Figure 3. Characterization of the fine anatomy of the autonomic innervation of the adult healthy human myocardium.
(**A**) 3D reconstruction at the multiphoton microscope of the neuronal network in 1mm^3 tissue blocks from the left ventricle of the human myocardium. Whole mount staining with an antibody to TOH was used to identify sympathetic neuron processes. (**B-D**) Confocal IF analysis of heart cryosections stained with an antibody to tyrosine hydroxylase (TOH) (green signal) (**B**) and co-stained with an antibody to wheat germ agglutinin (WGA) and antibodies specific for: smooth muscle actin (SMA) (**C**) and isolectin (**D**) (all red signals).

3.2 Sympathetic neurons closely interact with cardiomyocytes *in vivo*

Confocal IF analysis on human and mouse heart ventricular sections revealed that neuronal varicosities are in close apposition with CM membrane (**Fig. 4A-C**). Ultrastructural analysis of murine heart sections identified sympathetic varicosities, in which NE vesicles are positioned close to the membrane on the side facing a juxtaposed CM, found at an inter-membrane distance of 67±16 nm (n=18) (**Fig. 4D**), a value consistent with that described for peripheral synapses. Additionally, we observed: i) the presence of flask-shaped membrane invaginations (caveolar-like) in the CM membrane juxtaposed to the neuronal varicosity ii) a thickening of the CM membrane at the innervated portion; iii) accumulation of dystrophin in portion of CM membrane directly in contact with the neuronal process (**Fig. 4D-E**). Interestingly, all these features are typical of the well-characterized neuromuscular junction (NMJ), and support the concept that a 'simil-synaptic' contact occurs between sympathetic neurons and target CMs.

To further analyse the specific cardiac structures, in which innervation plays a key physiologic role, we evaluated the neuronal interaction with sino-atrial node (SAN) cells. To this aim, the hearts were collected, the atria dissected and meticulously cleaned from vascular tissue debris and fat, to better isolate the putative area of interest. The tissue was fixed with PFA (2%, 1h at room temperature), dehydrated in sucrose gradient (O/N at 4°C), embedded in OCT and snap frozen in liquid nitrogen. After cryostat sectioning, samples were processed for IF analysis using the *bona fidae* marker HCN4 to identify SAN cells in combination with an antibody to TOH. In line with the results obtained in the ventricles, SN varicosities appeared in close contact with the membrane of HCN4 expressing SAN cells **(Fig. 4F)**. This is in line with published data, in which, by using electron microscopy analysis, close apposition between SN and CMs was suggested to occur non-randomly in SAN (Woods, 1970). Whether the morphological and structural features of the neuro-cardiac contacts are identical in atria and ventricles will be the object of further investigations.

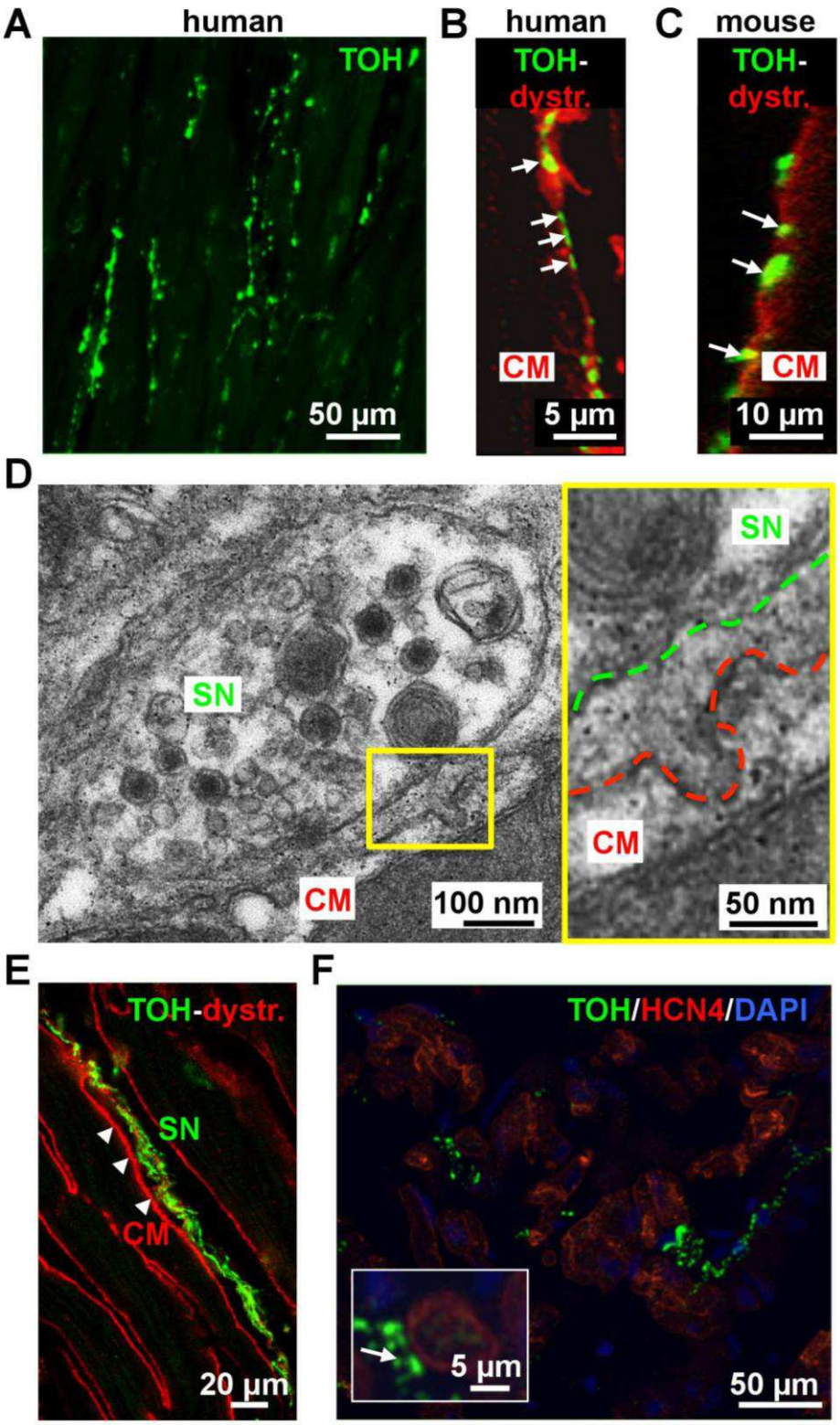

Figure 4. Interaction between sympathetic neurons and cardiomyocytes in the mammalian heart, *in vivo.*

Confocal immunofluorescence (IF) analysis on human (**A-B**) and mouse (**C**) hearts co-stained with antibodies for dystrophin and TOH. Close contacts between SN varicosities and CM membrane are highlighted by arrows. (**D**) Electron microscopy on mouse heart sections. Right panel is a detail of flask-shaped membrane invaginations of CM membrane. (**E**) Double IF with TOH and dystrophin antibodies. The image shows the accumulation of dystrophin in portion of CM membrane directly in contact with the neuronal process. **(F)** Confocal IF analysis of cryosections from the right atrium co-stained with antibodies to HCN4 (red signal) and TOH (green signal). The inset shows a high magnification of the interaction between SN and HCN4 expressing cells.

3.3 Setting up a protocol for *in vitro* maturation of neonatal cardiomyocytes

The data described above suggest the existence of a structured contact between SNs and CMs. Whether such intercellular displacement impacts on the dynamics of intercellular communication between cSNs and CMs, has not been assessed thus far. To this purpose, we set up co-cultures between SNs isolated from the superior cervical ganglia (SCG) of neonatal rats and neonatal rat CMs.

While primary culture of neonatal rat CMs are widely used in experimental cardiology (Mongillo *et al.*, 2007) as they can be easily isolated and amenable to genetic manipulation, we reckoned that this cell type would not be ideal for the purposes of our investigation. Indeed, neonatal CM display important morphological, functional and structural differences compared with the cells of adult hearts. Remarkably, these differences include the incomplete maturation of the cell membranes (i.e. lack of t-tubules) and of the membrane associated proteins centrally involved in cell-cell interactions, including the dystrophin/dystroglycan complex. We thus optimized current culture protocols to promote maturation of neonatal CMs, mainly by substituting the culture media initially used to maintain neonatal cells in culture. The main adjustments were: i) serum removal, aimed at avoiding cell proliferation and de-differentiation; ii) reduction of glucose content, to mimic the metabolic asset of the adult myocardium; iii) introduction of co-factors and trophic hormones, such as insulin; iv) addition of BrdU to inhibit fibroblast proliferation and avoid proliferating cells to secrete growth factors and matrix components, both promoting cell de-differentiation and hyperplastic growth. These manoeuvres increased the purity of the culture, allowing to maintain the cells in culture for several weeks and achieve a structural maturation reminiscent of the adult phenotype. Indeed, these mature CMs had more developed contractile apparatus, with regular sarcomeres, interfibrillar displacement of mitochondria, and enhanced translocation of dystrophin in the sarcolemma (**Fig. 5A-B**). In addition, IF staining of RyRs revealed that the protein appeared in clusters more regularly distributed along the short axis of the cell, which more closely mimics the phenotype observed in fully differentiated CMs, and suggests increased maturation of the SR (**Fig. 5C**). While additional studies are in progress to further characterize such novel cardiac cell culture at the structural and functional level, we concurred that these cells could be better suited for the study of intercellular communication.

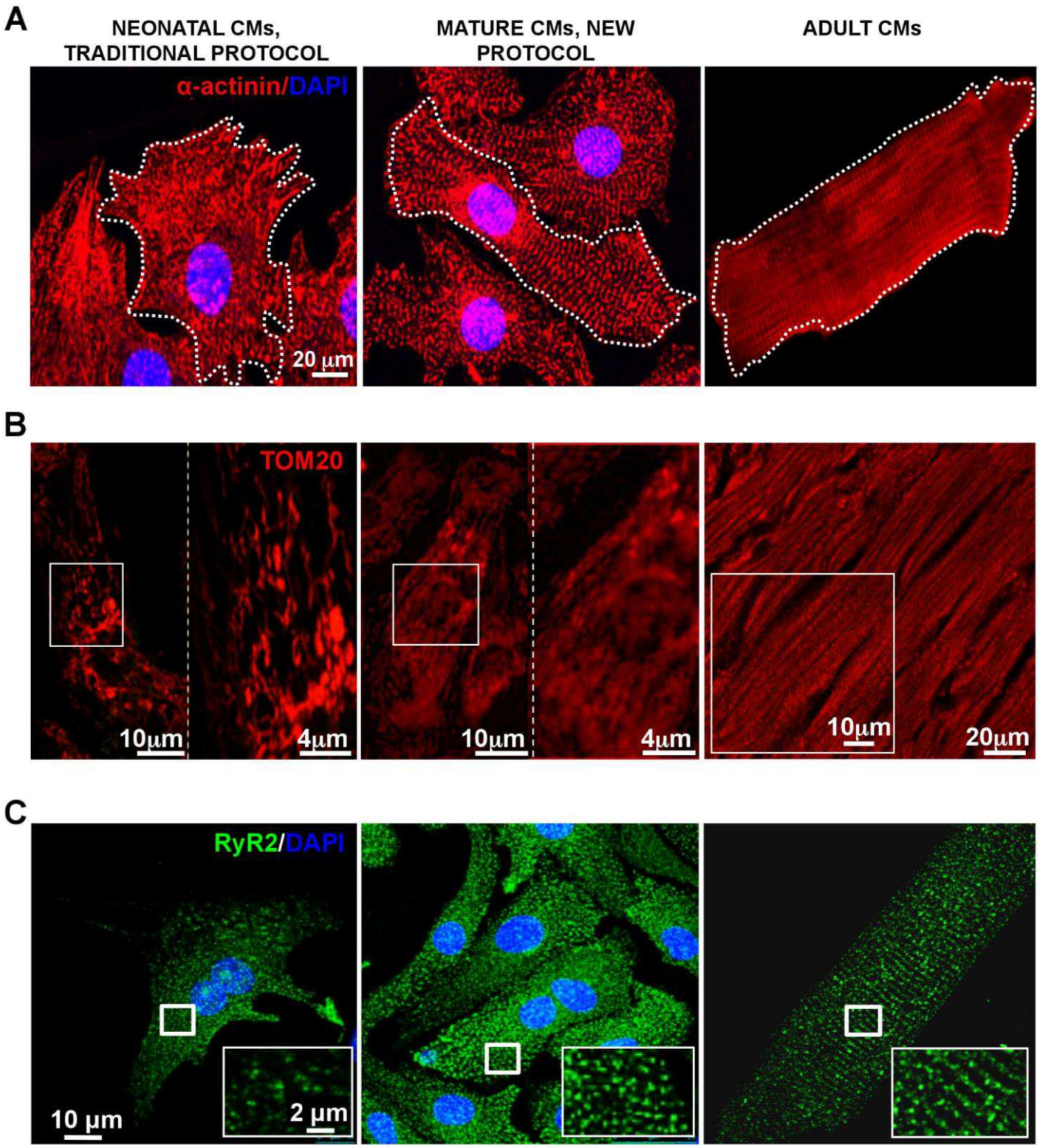

Figure 5. Comparison between different protocols to culture neonatal cardiomyocytes.

(**A-C**) Confocal IF analysis on cultured rat neonatal cardiomyocytes processed with the traditional (left panel) and the newly developed (middle panel) protocols. The right panels show freshly isolated adult cardiomyocytes. Cells were stained with antibodies to: α-actinin (**A**); TOM20 (**B**) and RyR2 (**C**).

3.4 Sympathetic neurons closely interact with cardiomyocytes *in vitro*

To analyze the dynamics of intercellular coupling between cSNs and CMs, at the single cell level, we used co-cultures between SCGNs and neonatal rat CMs (**Fig. 6**). In co-culture, the majority of SCGNs was adrenergic, co-expressing tyrosine hydroxylase (TOH) and dopamine-β-hydroxylase (D-β-OH) (92±4, in %, n=240 neurons from 3 cultures). Moreover, they developed synapsin-1a-expressing enlargements of the axonal processes, whose size increased with the time in culture (from 5 to 15 days), suggesting the progressive development of the neuronal apparatus at the contact site (**Fig. 7A**).

To further test the hypothesis of contact maturation, co-cultures were characterized for the enrichment of generic cell-to-cell adhesion molecules in the pre- and post- synaptic membranes, which is one of the main features of the contact site between neurons and innervated cellular targets, in both the central and peripheral nervous systems (Anderson and Cohen, 1977; Okabe *et al.*,1999; Sharma *et al.*, 2010). In particular, we focused on cadherins, which are Ca^{2+}-dependent homophilic cell adhesion molecules, linking the pre- and post-synaptic membranes, and β-catenin, which binds the cadherin-complex to the actin cytoskeleton. Our IF staining showed cadherins and β-catenin accumulation, at the SN-CM contact sites, progressing from 5 to 15 days, indicating that the interaction between cSNs and CMs is characterized by time-dependent maturation (**Fig. 7B-E**). No significant differences were observed between 15- and 20-day old co-cultures, suggesting that 2 weeks are sufficient to reach the structural maturation of the intercellular contact. Such results are totally in line with previous works showing that cadherins and β-catenin accumulate, with β1-AR, in the portion of CM membrane contacted by a sympathetic varicosity (Shcherbakova *et al.,* 2007). In addition, the linear correlation between TOH and cadherin or β-catenin enrichment supports that the enzyme involved in NE synthesis is enriched at the cell-to-cell interaction site.

In mature co-cultures, the topology of interactions established between neuronal processes and CMs was classified into three categories: ***type i)*** cells in direct contact with the neuronal varicosities, identified as round shaped enlargements of the axon within the CM area; ***type ii)*** cells close to neuronal varicosities, that are found outside the CM area and ***type iii)*** CMs passed over by the neuronal processes devoid of varicosities (**Fig. 8A**). Remarkably, in 15-day co-

cultures, the ***type i*** contacts showed morphological features similar to those observed in the intact heart, and were characterized by sites with reduced inter-membrane distance (42.3±7.1, in nm) between NE-containing varicosities and target CMs (**Fig.8B**)

A

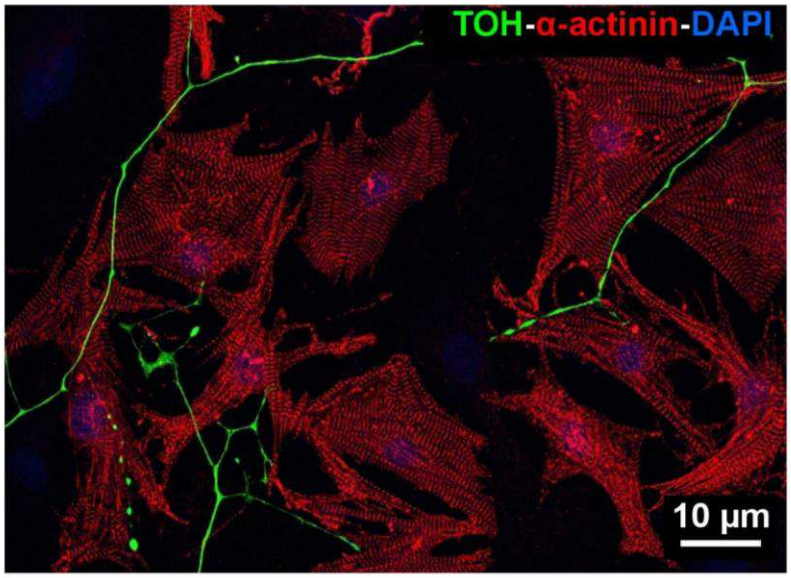

B

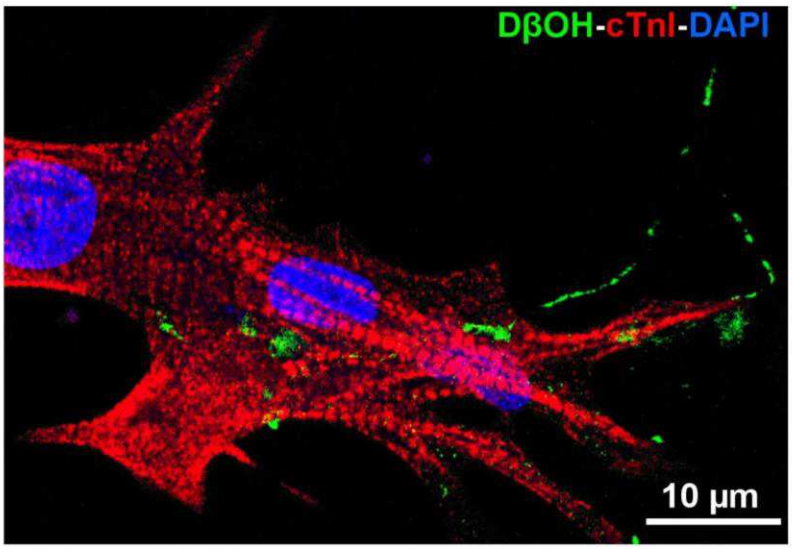

C

	SN properties
RMP (mV)	-55.7±1.6 (17)
C_m (pF)	29.6± 7.5 (17)
AP amplitude (mV)	59.1±14.3 (29)
AP D_{50} (ms)	10.8±8.1 (29)

Figure 6. Characterization of sympathetic neuron-cardiomyocyte co-cultures.

(**A-B**) IF analysis on 15-days co-cultures stained with antibodies to: TOH and sarcomeric actinin (α-actinin) (**A**) or dopamine-β-hydroxylase (D-β-OH) and cardiac troponin I (cTnI) (**B**). Nuclei were counterstained with DAPI. (**C**) Electrophysiological properties of SNs after 15 days in co-culture with CMs. RMP, resting membrane potential; C_m, membrane capacitance; AP, action potential; AP D_{50}, action potential half-width.

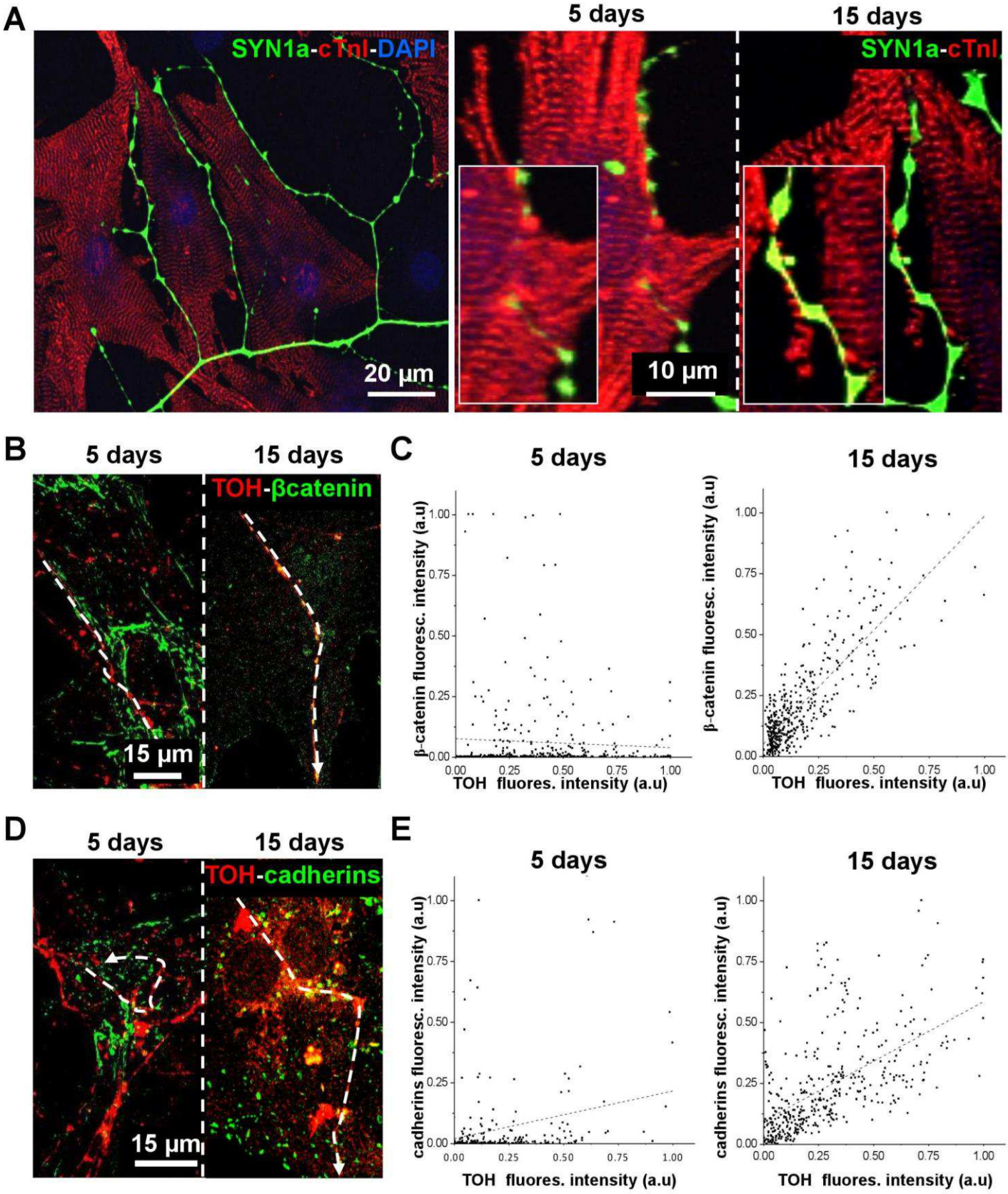

Figure 7. Interaction between sympathetic neurons and cardiomyocytes *in vitro*. (**A**) IF image of 15-days SN-CM co-cultures, co-stained with antibodies to cardiac troponin-I (cTnI) and synapsin-1a (syn1a). (**B** and **D**) Confocal IF analysis on five (left panels) and 15 days (right panels) SN-CM co-cultures co-stained with antibodies to TOH and: β-catenin (**B**) and pan-cadherins (**D**). (**C** and **E**) Plot profile showing time-dependent β-catenin and pan-cadherin accumulation at the SN-CM contact site.

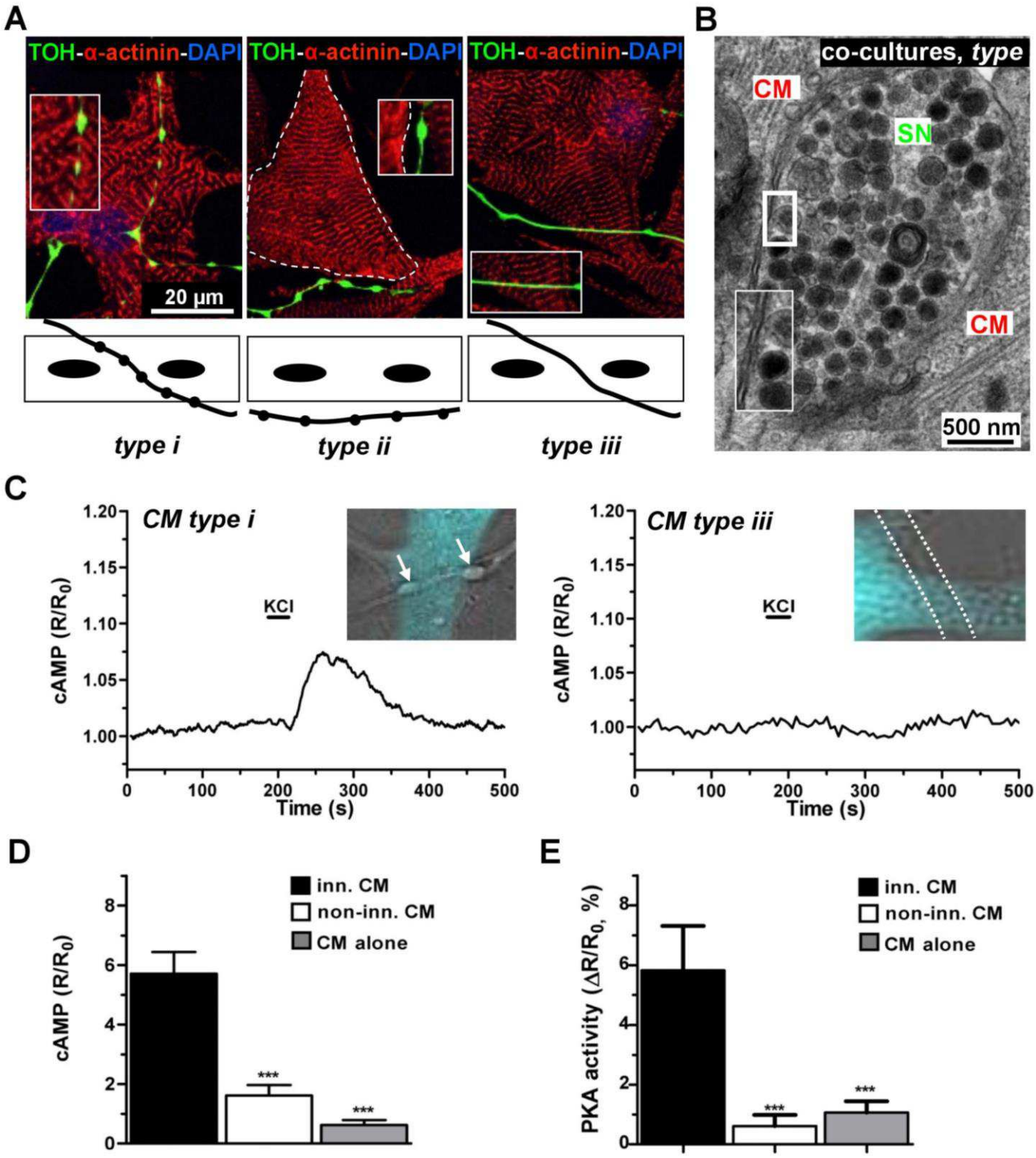

Figure 8. Selective signaling of sympathetic neurons to target innervated cardiomyocytes.

(**A**) IF staining of 15 days co-cultures stained with antibodies to: sarcomeric actinin (α-actinin) and TOH. Confocal images (top) and schematic representations (bottom) of the different types of SN-CM interactions observed in our experimental settings. (**B**) Electron microscopy on 15-days co-cultures. (**C**) cAMP changes in EPAC-camps expressing CMs upon SN depolarization by KCl, measured in innervated (*type i*), or non-innervated (*type iii*) CM (see text for details). (**D**) Statistics of cAMP responses in corresponding groups. (**E**) Statistics of the PKA activity in response to KCl stimulation of SCGNs, in differently innervated CMs. Bars indicate s.e.m. (***, $p<0.001$; n=100 CMs for each group).

3.5 Cell-to-cell contact is required for neuronal dependent cardiomyocyte stimulation, in co-cultures

As β-AR stimulation causes cardiac effects through cAMP dependent signalling, we used real-time cAMP measurements, in co-cultures, to analyze the CM responses to SN activation. This approach is usually performed by ratiometric FRET imaging. FRET is an event that describes a transfer of energy between two chromospheres: a donor chromophore, which is in the excited state, may give a part of the energy to excite the acceptor chromophore. The efficiency of the transfer depends on chromophores orientation, on the acceptor-donor distance and on fluorophore spectra that have to be overlapped. In our study, CMs were transfected with a FRET-based sensor, GcAMPs (Nikolaev *et al.*, 2004). EPAC1 (Exchange Protein directly Activated by cAMP) is a protein, activated by cAMP, fused with two fluorescence proteins suitable to making FRET (CFP, donor and YFP, acceptor) and it is expressed in cells by transient transfection. When the intracellular concentration of cAMP is low, EPAC1 is not activated and the two chromophores are one close to the other inducing high FRET signal. When intracellular cAMP increase, EPAC1 is activated and changed its conformation, augmenting the distance between the two chromophores, there is a decrease in the FRET signal. cAMP variation is measured as ratio between the fluorescence intensity of CFP and the fluorescence intensity of YFP. In a subset of experiments, we implemented the protocol for the evaluation of cAMP dynamics, infecting CMs with an adenovirally delivered FRET-based sensor, that referred cAMP concentration in cytoplasm, Epac-S^{H187} (Richards *et al.*, 2016), for 24 hours. Epac-S^{H187}, that is the high-affinity version of this sensor, is obtained by the mutation in Q270E in Epac1, which may cause a conformational shift that further increases FRET in these constructs. This allowed us to obtain about 100% expression of H187 in our cells and it offered also a substantially improvement in the analysis of the dynamic range for cAMP imaging.

Depolarization of a single SN, as obtained by brief perfusion with 50 mmol/L KCl, locally delivered with a pressurized micropipette, caused an increase in intracellular [cAMP] that was only detected in the innervated CMs (***type i***), while no changes were observed in non-innervated cells (**types *ii and iii***), or in KCl perfused CMs cultured alone ($\Delta R/R_0$, innervated CMs: 5.71±0.73; non-innervated CMs: 1.62±0.35%; CMs alone: 0.62±0.17, in %) (**Fig. 8C-D**). All groups showed

comparable cAMP responses to stimulation with NE. We then sought to determine whether the cAMP rise, elicited solely in coupled CMs by neuronal depolarization, was paralleled by activation of downstream β-AR/cAMP effectors. PKA activity was thus monitored with the fluorescence reporter AKAR3 (A-kinase activity reporter) (Allen and Zhang, 2006), under the experimental conditions used above. In line with the previous experiment, SN stimulation activated PKA only in directly contacted cells, while no effects were observed in non-innervated CMs or in CMs cultured alone ($\Delta R/R_0$, innervated CMs: 5.82±1.48; non-innervated CMs: 0.62±0.37; CMs alone: 1.07±0.38, in %) (**Fig. 8E**). We excluded that the cAMP responses observed upon neuronal stimulation were due to NE released in the culture medium, as addition of the cell bathing solution, collected after KCl perfusion of all neurons in the dish, failed to induce any cAMP response in Epac1-cAMPs expressing CMs ($\Delta R/R_0$, CMs plus conditioned medium: 0.54±0.16 *vs* non-treated CMs: 0.58±0.12, in %). In further support to the cell-to-cell contact between SN and CM, we observed that the innervated CM elicited a cAMP response upon the neuronal depolarizing *stimulus*, however if the SN axon, in contact with a CM, is detached, we can't observe any cAMP rise, although previously verified (**Fig. 9**).

Altogether, these data demonstrate that the establishment of a structured intercellular contact is required for the cSNs to provoke a response in the innervated CM.

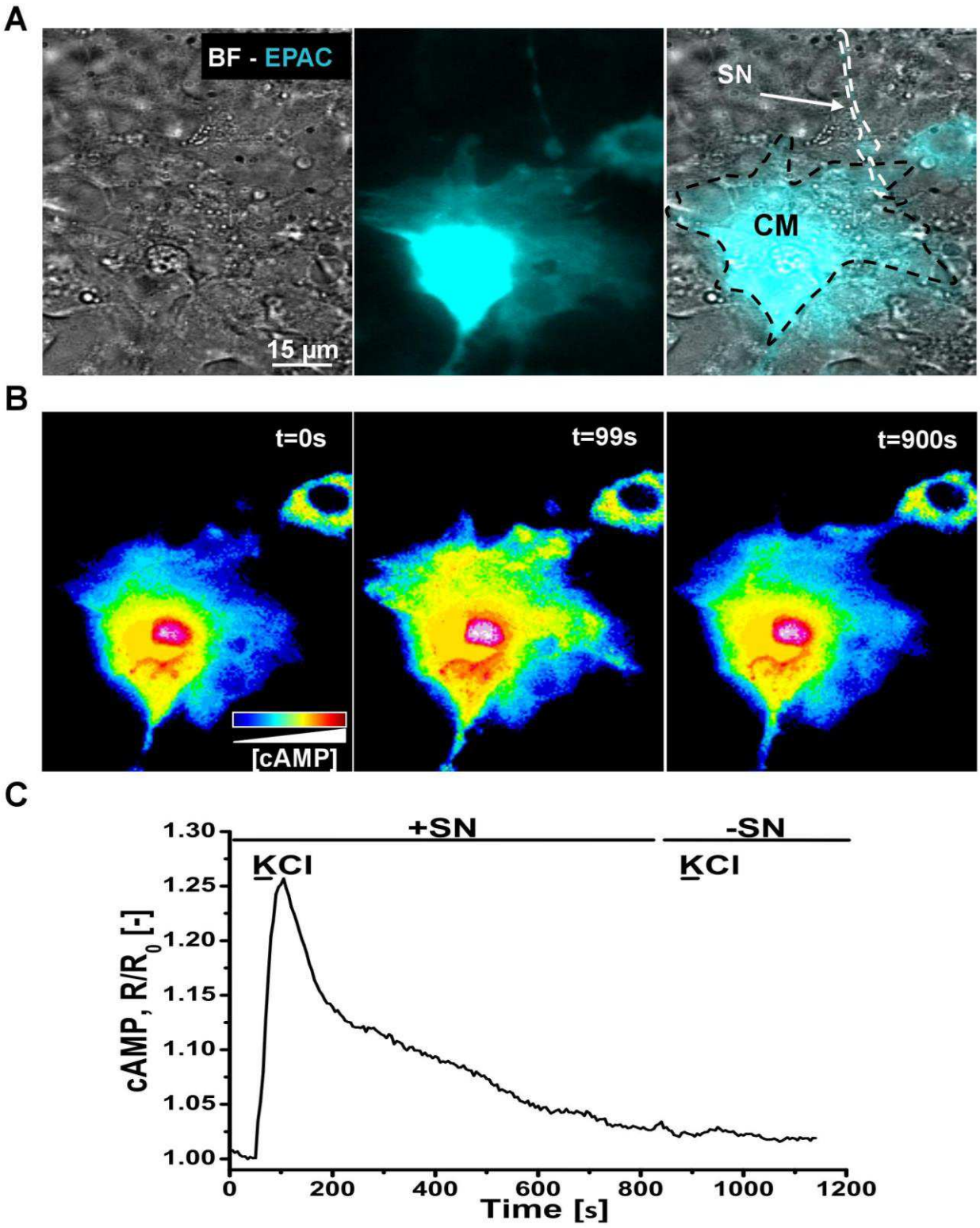

Figure 9. Selective signaling of sympathetic neurons to target innervated cardiomyocytes.

(A) Bright-field images of EPAC-camps expressing CM in direct interaction with a SN. (**B**) variation in cAMP levels: in basal condition (left panel); upon KCl stimulation (middle panel); upon KCl stimulation after SN detachment (right panel). (**C**) Representative plot of cAMP responses upin KCl depolarization before and after SN detachment.

3.6 Sympathetic neurons communicate to cardiomyocytes in a restricted domain, *in vitro*

To address the spatial selectivity of the neuronal-activated CM signaling, we firstly investigated cAMP responses in couples of adjacent CMs, only one of which was in direct contact with the stimulated SN, and observed that activation of β-ARs was limited to the innervated cell ($\Delta R/R_0$, innervated CMs: 9.3±0.92; non-innervated CMs: 0.23±0.08, in %) (**Fig. 10A-B**). Interestingly, CM responses to neurostimulation were unaffected by the rapid perfusion of the cells with normal saline solution, during the imaging experiment. Altogether, these data indicate that SNs communicate to target CMs by discharging NE in a 'diffusion-restricted' extracellular signalling domain, at the interface between the two cell types, outlined by the close apposition of the two cell membranes. These results, have also been confirmed in mouse SN-CM co-cultures, and are in line with the recent demonstration that, in co-cultures between hiPSC-derived SNs and CMs, the SN-CM physical contact is required for the modulation of CM beating rate (Oh *et al.*, 2016). Previous results obtained by the Kobilka lab. (Shcherbakova *et al.*, 2007) demonstrated that β-ARs accumulate on the portion of CM membrane contacted by SN varicosities. Consistently, we observed that upon neuronal depolarization, the cAMP increase was faster and higher in proximity to the neuro-cardiac interaction site, than in the areas of the same CM, far from the SN varicosity ($\Delta R/R_0$, proximity CM area: 176.51±26.94 *vs* distal CM area: 97.90±5,17, in %) (**Fig. 10C-D**). However, the cAMP change, elicited by NE added in the culture medium, was the same in all CM sub-cellular regions ($\Delta R/R_0$, proximity CM area: 106.04±1.89 *vs* distal CM area: 99.82±1.51, in %).

Thus, this experiment suggested the existence of a "similar synaptic cleft" in which neuronally-released NE activates only a confined pool of β-ARs/adenylyl cyclases in the post-synaptic CM membrane.

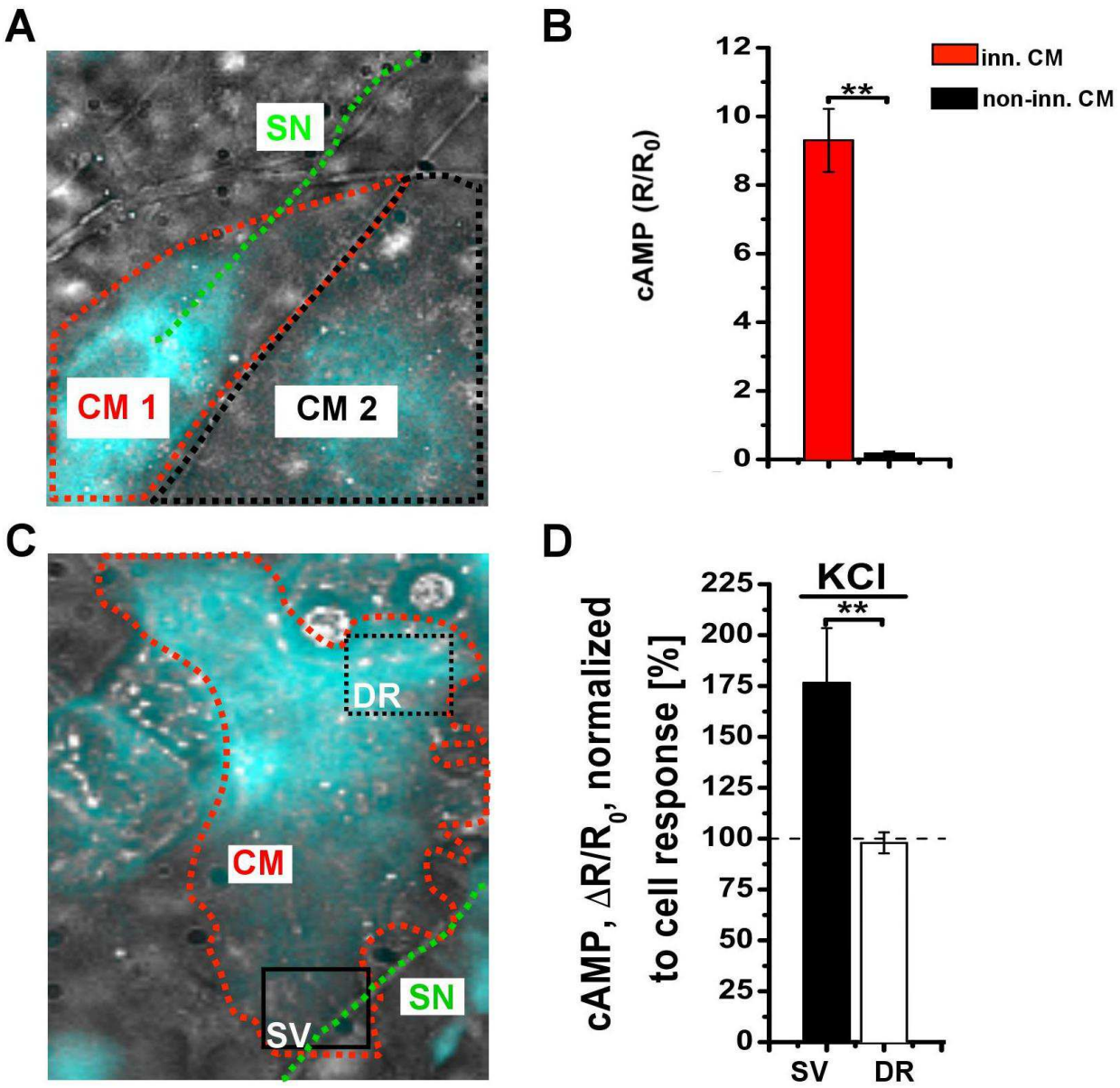

Figure 10. Spatial discrimination of target cell responses
(**A**) Bright-field (left panel) images of two adjacent EPAC-camps expressing CMs, one of which (CM1, red line) is in direct interaction with a SN (green line). (**B**) Statistics of cAMP responses in innervated CM compare to non-innervated (**C**) Bright-field image highlighting the topology of sub-cellular cAMP variations in cardiomyocytes innervated by sympathetic neurons. (**D**) Statistics of cAMP changes upon SN depolarization by KCl near the SN varicosity (SV) and in the distal region (DR). Bars indicate s.e.m. (**, $p<0.01$; n=100 CMs for each group).

3.7 Direct cell-cell interaction allows potent and efficient neuro-cardiac coupling

The results presented above support the notion that neuronally-released NE reaches, into the synaptic cleft, a very high concentration to elicit cAMP increase into the innervated CM. If this were correct, we would expect that high doses of β-blockers are required to blunt the SN-induced CM cAMP response. To test this hypothesis, we pre-incubated co-cultures with the selective β1-AR blocker, metoprolol (100μM). Interestingly, while metoprolol significantly reduced the cAMP increase induced by NE added to the culture medium, it was un-effective in counteracting the neuronal-dependent CM response, which was comparable to that observed in the absence of β-blockers (**Fig. 11A-C**). Upon metoprolol removal, by cell washing, the neuronal-dependent CM cAMP increase was totally preserved, and the response to diffuse NE restored (**Fig. 11A-C**). On these bases, we next aimed to estimate the [NE] achieved by the activated neuron in the intercellular cleft. Based on our evidence that the neuronally released NE only activates a restricted fraction of CM β-ARs, we aimed at estimating the effective [agonist] independently from the number of activated receptors. We thus adopted the principle of competition binding assays and obtained inhibition curves, by measuring CM cAMP responses to neuronal activation, after pre-treating co-cultures with increasing concentration of the non-specific and well characterized β-AR blocker propranolol. The dose-inhibition kinetics were compared between responses to neuronal activation and those elicited by known amounts of NE (10, 100 and 1000, in nmol/L) (**Fig.12A**). The propranolol inhibition curve in neuronally-stimulated CMs overlapped the one obtained with direct stimulation with 100 nmol/L NE, indicating that $[NE]_{cleft}$ is within this order of magnitude (**Fig. 12B**).

Taken together, the spatial discrimination of target cell responses, the evidence that receptor dependent signaling is initiated at the contact site, and the high effective $[NE]_{cleft}$ support that neurotransmission occurs in a 'quasi-synaptic' fashion within a restricted intermembrane domain. All this data set was confirmed in co-culture between CMs and NGF differentiated PC12 cells. Based on the morphological evidence of our IF and electron microscopy analyses, we estimated the volume of the synaptic cleft in the order of $0.1\mu m^3$.

To infer whether the properties of intercellular coupling observed *in vitro* were reflected by the physiology of cardiac autonomic control *in vivo*, we next performed a series of experiments using SN optogenetics in living mice.

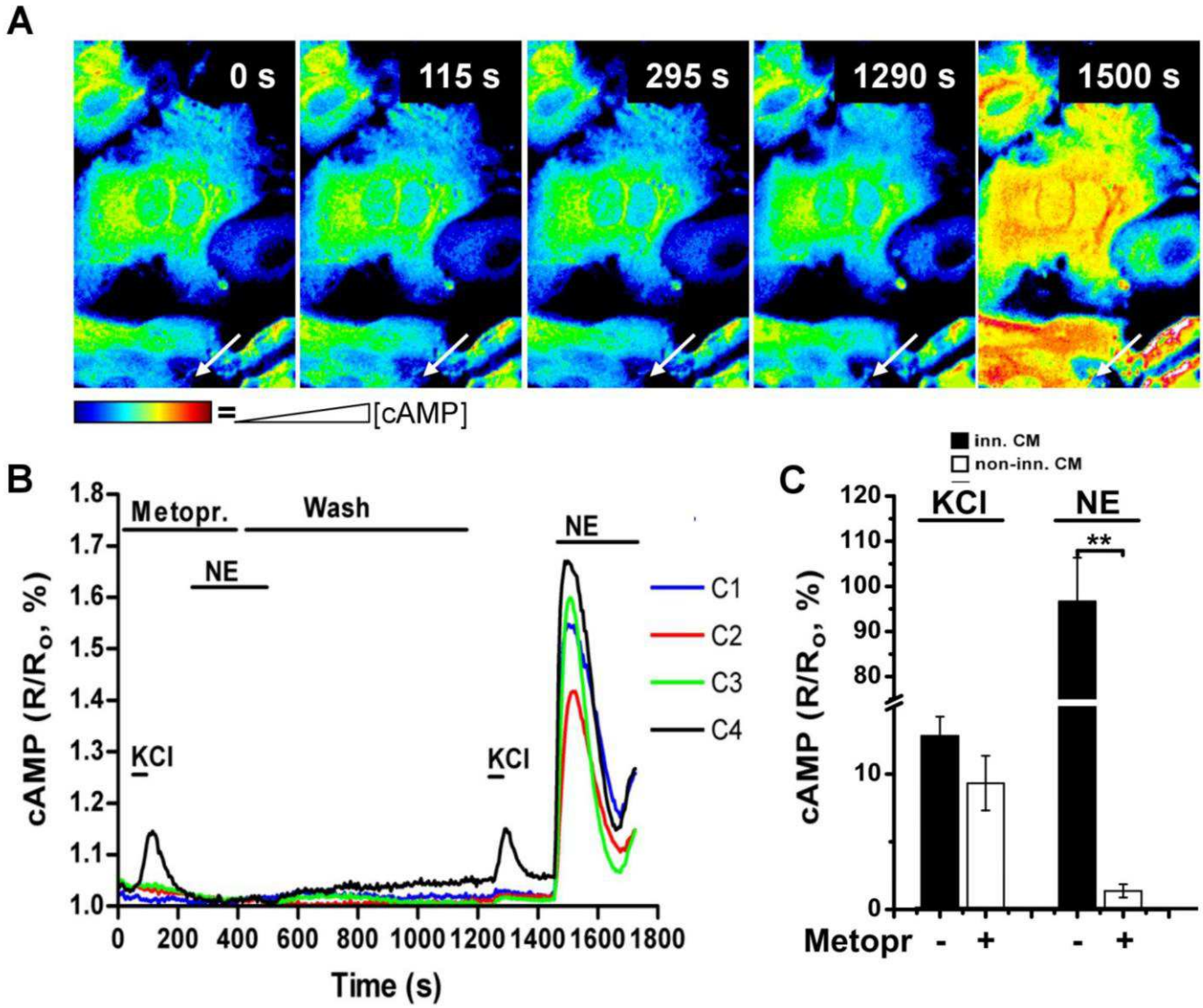

Figure 11. Neurons in direct coupling with cardiomyocytes overcome the effects of the competitive β-blockers

(**A**) Colorimetric map shows the variation in cAMP levels in cardiomyocyte, upon KCl stimulation, followed by direct administration of NE with or without metoprolol in the culture medium (**B-C**) Representative plot (**B**) and statistics (**C**) of cAMP responses in innervated CM compare to non-innervated with or without metoprolol. Bars indicate s.e.m. (**, $p<0.01$; n=60 CMs for each group).

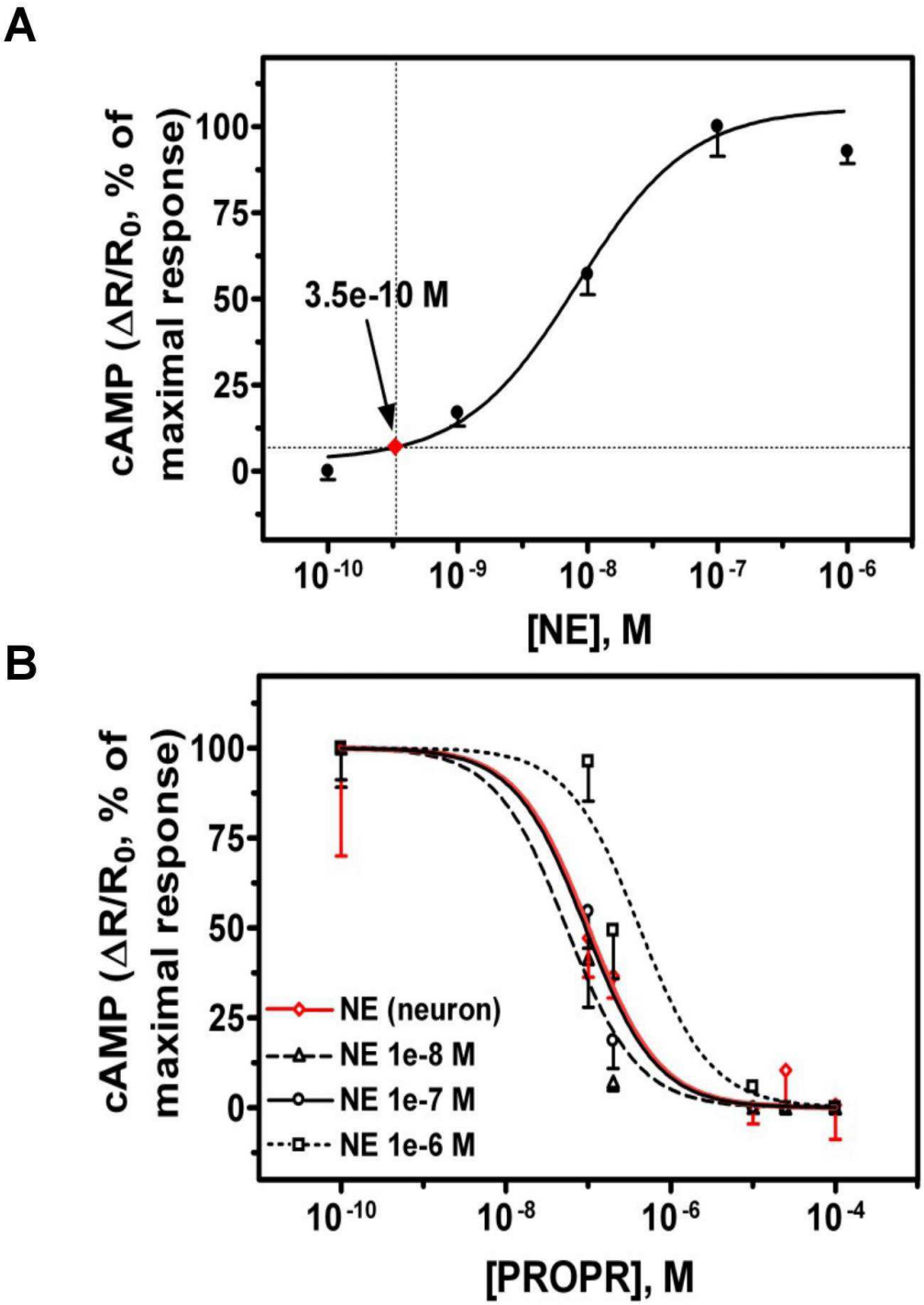

Figure 12. *In vitro* assessment of [NE] in the synaptic cleft
(**A**) Dose-effect curve of cAMP responses to NE directly applied to Epac1 expressing CMs. Arrow indicates the average cAMP response observed in co-cultures. (**B**) Propranolol inhibition curve of cAMP responses elicited by neuronal stimulation (red trace), overlapped to that resulting from direct treatment of CMs with known [NE].

3.8 Direct "neuro-cardiac" communication operates also in the maintenance of cardiomyocyte size *in vitro*

The evidence that neuro-cardiac interactions are stable in time, and that intercellular signaling is restricted to cells in direct contact, together with our previous observation that cardiac sympathetic activity regulates CM size (Zaglia *et al.*, 2013), suggests that upon prolonged SN stimulation, innervated cells would become larger than non-innervated ones. To assess this hypothesis, we compared the area of cells in contact with neuronal processes with that of non-contacted ones. To this purpose we used co-culture between CM and SNs differentiated from PC12 cells, since this cell line is highly prone to responde to nicotine stimulation and releases high amount of NE.

Nicotine was added to the co-culture to chronically increase NE release (Oh *et al.,* 2016; Shcherbakova *et al.,* 2007), and resulted in the selective enlargement of innervated CMs, with no changes in the area of non-innervated ones in the same dish (CM area, innervated CMs: 1197.03±84.46; non-innervated CMs: 844.47±59.38, in μm^2) (**Fig. 13A-B**). Nicotine treatment did not affect *per se* CM size (**Fig. 13C-D**).

These results further support that neuro-effector signaling is confined, even in the long term, to cells in direct contact, and demonstrate a negligible effect of the neurotransmitter leaked out of the NCJ.

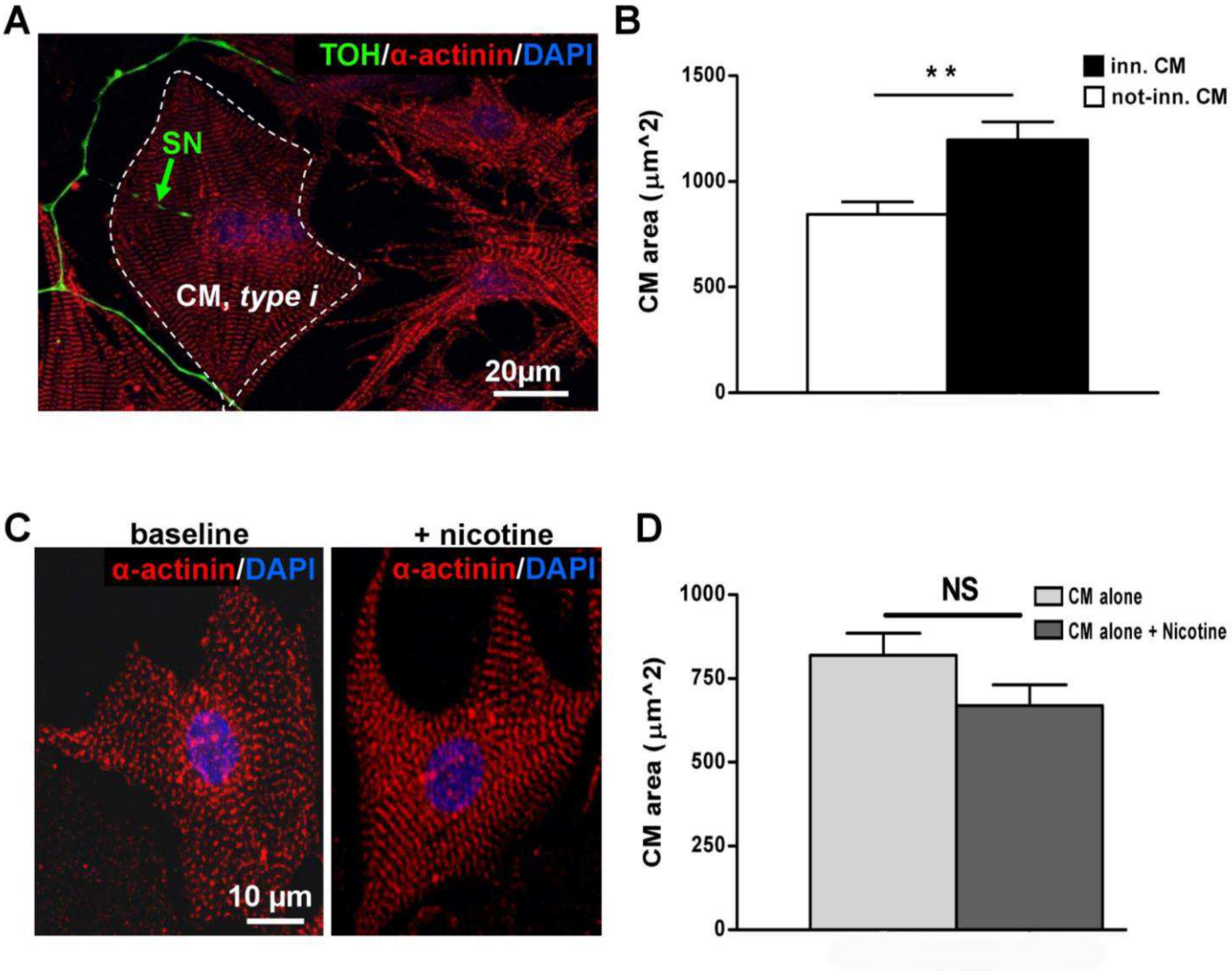

Figure 13. Long term effects of sympathetic neuron-cardiomyocyte coupling. (**A**) Confocal IF analysis on sympathetic neuron-cardiomyocyte (SN-CM) co-cultures co-stained with antibodies to tyrosine hydroxylase (TOH, green signal) and α-actinin (red signal). (**B**) Evaluation of the area of innervated *vs* not-innervated cardiomyocytes. (n=50 CMs for each study group). (**C**) Confocal IF analysis on cultured control *vs* nicotine-treated CMs, stained with an antibody to α-actinin (red signal). (**D**) Evaluation of the area of control *vs* nicotine-treated CMs. Bars indicate s.e.m. (NS: not significant; **, $p<0.01$; n=50 CMs for each group).

3.9 Optogenetic control of cardiac sympathetic neurons *in vivo*

Cardiac chronotropic responses triggered by the SNS are mediated by amplification of the inward current that underlays diastolic depolarization of pacemaker SAN cells, mostly through direct interaction of cAMP with HCN4 channels, responsible for I_f (DiFrancesco, 2010). To determine if the effects of sympathetic activation reflect, *in vivo*, the direct cell-cell communication observed in the *in vitro* system, we exploited optogenetics to control SN activity while monitoring HR. The method lets us to stimulate excitable cells, expressing Channel Rhodopsin 2 (ChR2) protein, with blue light flashes. ChR2, discovered in the green alga *Chlamydomonas*, in 2002, is a member of the rhodopsin family of proteins. ChR2 is a light-activated cations channel, mainly permeable to Na^+, that, upon blue light (470 nm) illumination, it changes its conformation and generates an inward depolarizing current and neurotransmitter release, with millisecond resolution (Boyden *et al.*, 2005; Zhang *et al.*, 2007; Wengrowski *et al.*, 2015). This approach has previously been adopted in isolated perfused hearts (Wengrowski *et al.*, 2015).

By using neuronal-specific promoters, as the TOH promoter, the expression of the channel, selectively in SNs, can be achieved. We thus generated transgenic mice expressing the *ChR2-H134R-tdTomato* gene under control of the TOH promoter (**Fig. 14A**). These mice had structurally and functionally normal hearts, with identical cSNs morphology and distribution to those of control hearts and showed specific expression of ChR2 in SNs, both in the atria and in the ventricles (**Fig. 14B-F and 15**). In addition, SCGNs isolated from TOH/ChR2 mice expressed both TOH and ChR2, the latter localized, as expected, on the plasma membrane, and had normal morphology (**Fig. 16A-B**). Photoactivation of the cells with blue light during whole cell voltage clamp activated the inward ChR2 photocurrent, and 10ms flashes were sufficient to trigger APs, undistinguishable from the spontaneous ones (**Fig. 16C-D**). These results suggested us that we could achieve control of the activity of TOH/ChR2 neurons *in vivo* by delivering blue light to the neuronal terminals with a fiber-optic.

We thus used the hardware and protocols previously developed for cardiac specific optogenetics (Zaglia *et al.*, 2015), to assess the effect of SN activation on HR (**Fig. 17A**). Thus, we calculated the resting HR and the HR reached upon photostimulation with a fiber optic probe (HR, basal: 426.25±0.41; upon

phostimulation: 539±16.28, in BPM). Then, we scanned the epicardial heart surface with the tip of a fiber optic probe, while delivering trains of light flashes. We observed that photoactivation of the right atrial *epicardium* reproducibly induced sinusal tachycardia, which was triggered by illuminating a very specific region of approximately 1-2 mm in diameter (**area #1**), and no increase in HR was ever elicited by illumination of the immediately surrounding of remote atrial parts (**area #2**) (**Fig. 17B-D**). The responsive atrial surface was marked with dermographic ink and analyzed with IF, which revealed CMs expressing the *bona fide* marker of SAN cells, HCN4 (Liu *et al.*, 2007), interacting closely with SNs (**Fig. 17E-F**). Maximal chronotropic responses were achieved with trains of light pulses at 10-20 Hz rate (HR, 20Hz: 506.0±2.5; 10Hz: 479.8±4.2; 5Hz: 471.2±6.1, in BPM; n=6), and ceased promptly when illumination was stopped. To further validate our approach, we performed a set of experiments aimed at excluding that non-specific ChR2 targeting to atrial CMs could be at the origin of false positive chronotropic responses. First, consistent with the physiology of cardiac sympathetic regulation, during photoactivated sinusal tachycardia the timing of light pulses and QRS complexes were unrelated, while identical illumination protocols in α-MyHC/ChR2 mice (Zaglia *et al.*, 2015) paced beats with fixed delay from the light flash in all atrial *epicardium* (flash/p-wave delay: 8±0.46 ms, n=8). Second, illumination of the SAN in TOH/ChR2 mice with long-lasting light pulses (100-500 ms) had no effect on HR, thus excluding that the chronotropic response could be due to photoactivation of the inward Na^+ current in SAN cells, directly increasing their diastolic depolarization rate.

Altogether, our optogenetic data demonstrate that rapid, selective and efficient modulation of pacemaker activity is achieved by the activation of a subset of cardiac SNs directly targeting the SAN myocytes, independent from effects on other sections of the conduction system.

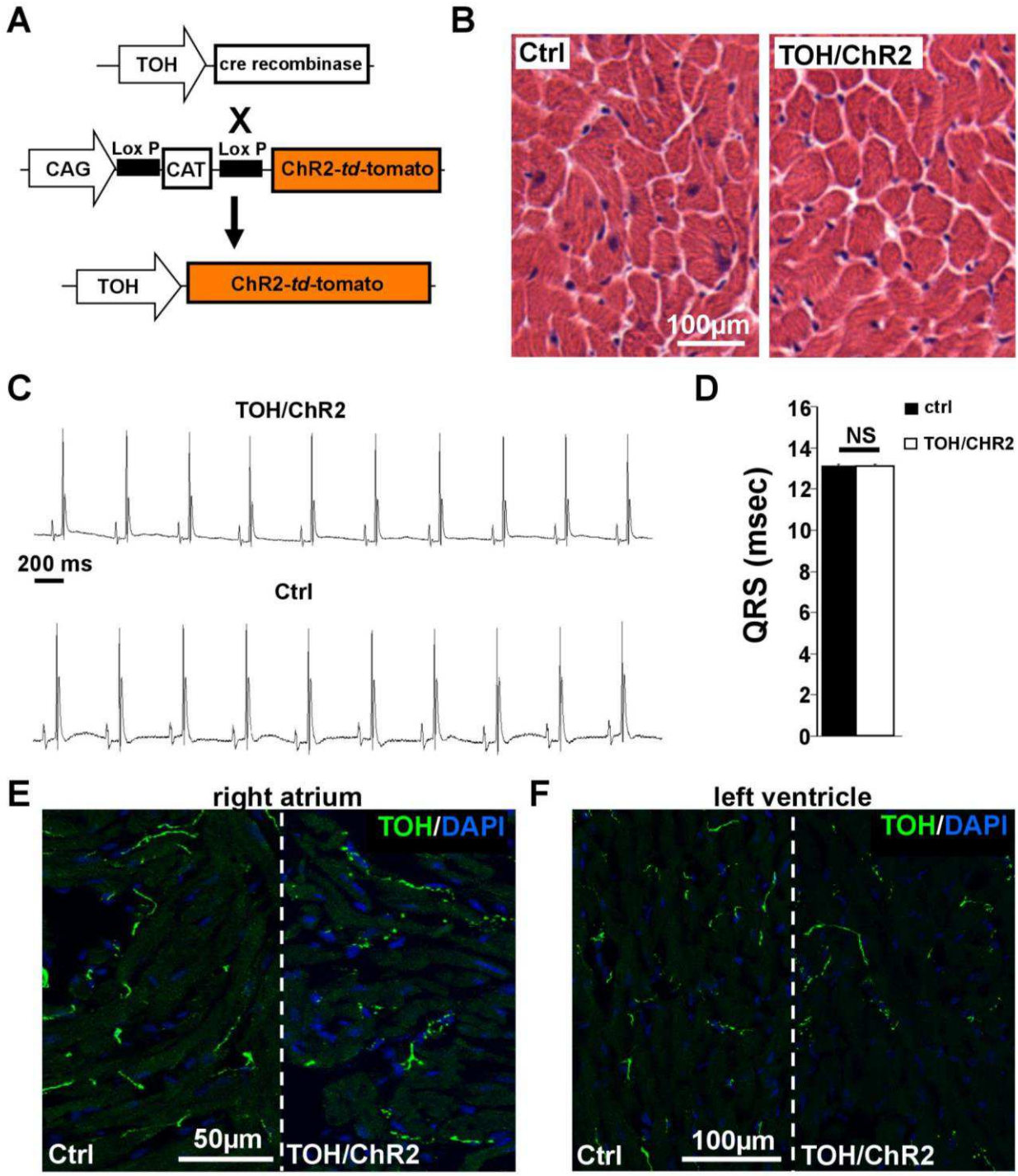

Figure 14. Heart phenotyping of TOH/ChR2 transgenic mice.
(**A**) Generation of transgenic mice expressing the fused protein ChR2-*tdTomato* under the control of the TOH promoter (TOH/ChR2). (**B**) Haematoxylin-eosin staining in heart cryosections from control and TOH/ChR2 mice. (**C**) ECG traces from TOH/ ChR2 and control mice. (**D**) Measurement of the QRS interval in transgenic mice and littermate controls. (n=6 mice for each group; NS=not significant). (**E-F**) Confocal IF analysis on heart sections from the right atrium (**E**) and left ventricle (**F**) of control and TOH/ChR2 mice, stained with an antibody to TOH. Nuclei were counterstained with DAPI.

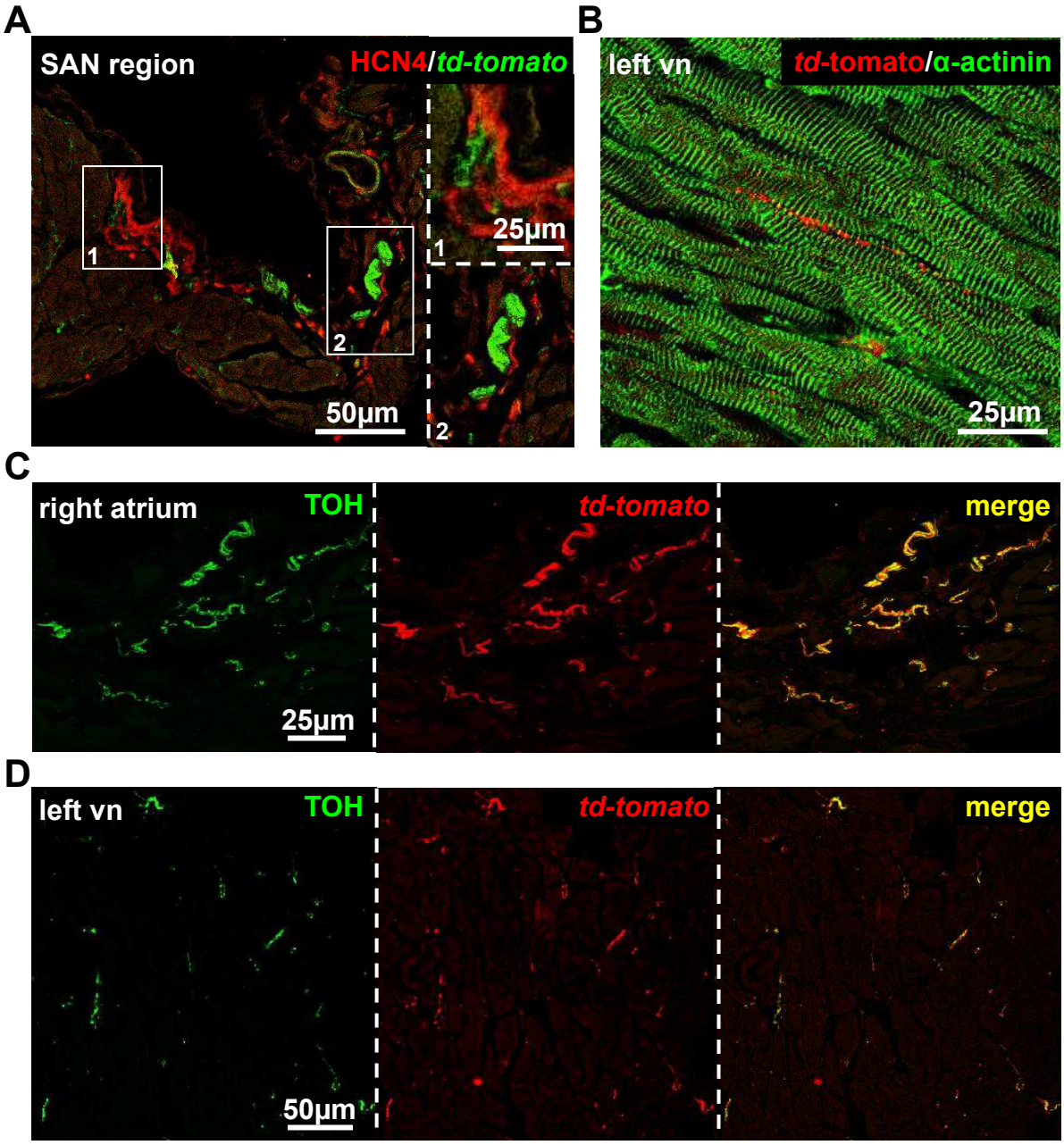

Figure 15. Characterization of cardiac autonomic innervation in TOH/ChR2 mice.

(**A**) Confocal IF analysis on right atrium sections co-stained with antibodies to HCN4 (red signal) and td-tomato (green signal). (**B**) Confocal IF analysis on left ventricle sections co-stained with antibodies to td-tomato (red signal) and -actinin (green signal). (**C-D**) Confocal IF analysis on right atrium (**C**) and left ventricle (**D**) co-stained with antibodies to td-tomato (red signal) and TOH (green signal).

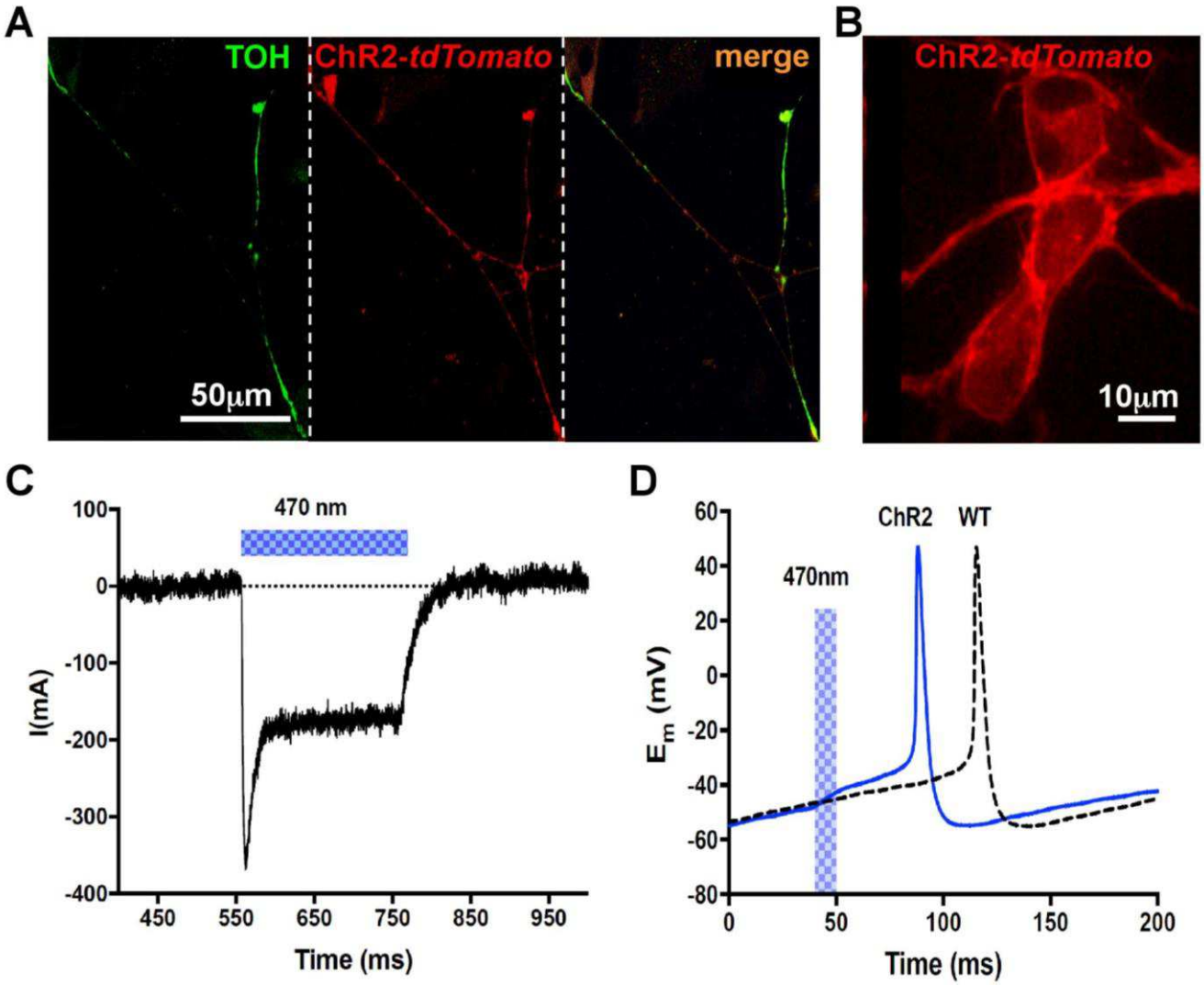

Figure 16. Optogenetic modulation of cultured sympathetic neurons.
(**A**) Confocal IF analysis on cultured sympathetic neurons from TOH/ChR2 mice stained with an antibody to TOH (left panel). The middle panel shows expression of td-tomato, while the right panel shows the merge of the two signals. (**B**) Confocal image analysis on cultured TOH/ChR2 SCGNs. (**C**) Patch clamp recording in cultured TOH/ChR2 SCGNs at baseline and during photostimulation (blue bar). (**D**) Comparison of spontaneous and light-induced (10 ms, 470 nm light pulse) APs in cultured TOH/ChR2 SCGNs.

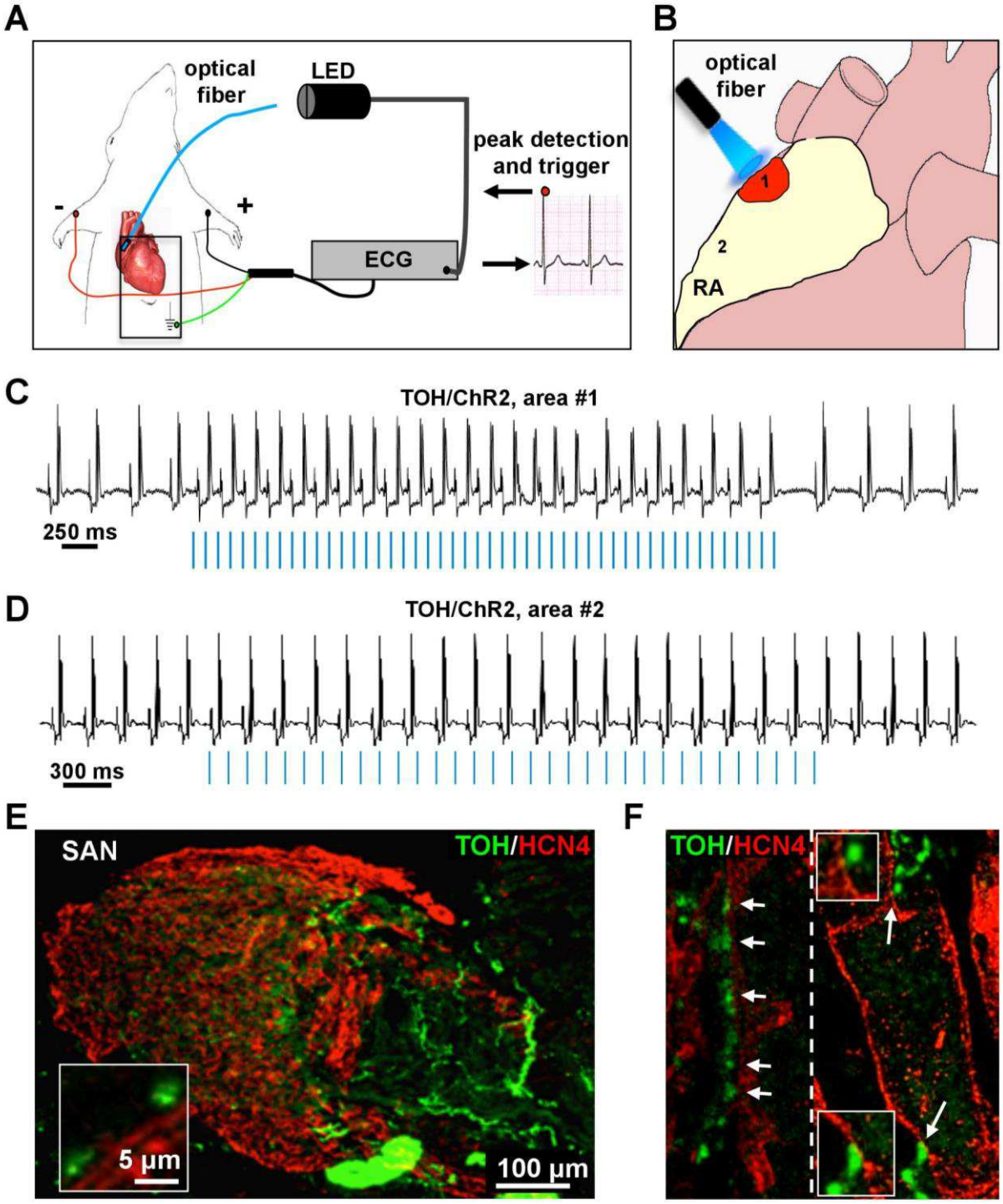

Figure 17. Optogenetic control of cardiac sympathetic neurons *in vivo*.
(**A**) Schematic illustration of the neuronal optogenetic experiment, showing the set up used for right atrium illumination in open-chest anesthetized mice, and (**B**) representation of the different atrial regions (areas #1-2) photostimulated. (**C**) ECG traces of the cardiac sympathetic optogenetic experiment, showing positive chronotropic response upon photoactivation (blue lines) of the right atrial region #1 in TOH/ChR2 mice. (**D**) Increase in HR was never elicited by illumination of regions #2. (**E-F**) Confocal IF with SAN (HCN4) and SN (TOH) markers. The magnified image (**F**) highlights the close interaction between SN varicosities and SAN myocytes (left) and an example of multiple neuronal processes interacting with the same myocyte (right).

3.10 Optogenetic assessment of neuro-cardiac communication *in vivo*

Our *in vivo* data indicate that SNs modulate heart electrophysiology with elevated target selectivity, which, based on our morphological and ultrastructural evidence (**Fig.4**) likely depends on direct interaction between SNs and CMs. By mimicking such interaction, our *in vitro* experiments indicate that intercellular signal transmission occurs through a restricted domain with high [NE]. To assess whether neuro-cardiac communication occurs with the similar dynamics in the intact heart, we analyzed the effects of propranolol on the chronotropic response to trains of neuronal photostimulation (20 pulses, 10 ms, 20 Hz). Propranolol (5mg/kg) decreased the resting HR, and fully inhibited the effect of systemically administered NE (1mg/kg i.p.) (**Fig. 18A**), at a dose which, in control conditions, caused an increase in HR comparable to that of photostimulation (ΔHR, resting conditions: 28.7±5.8 *vs* propranolol: 3.4±4.0, in %, n=6). Remarkably, propranolol, even at higher doses (10mg/kg), failed to reduce the response to photoactivation of SAN neurons, thus indicating that neuronal activation generates high $[NE]_{cleft}$, sufficient to overcome the antagonist at these doses. Consistently, blockade of neuronal responses required much higher [propranolol] (**Fig. 18A**).

To gain further insight on the dynamics of cardiac synapses, we determined the minimal number of neuronal APs required to decrease the interbeat interval, by gradually reducing the number of light pulses (from 5-to-1, 10 ms, 20 Hz). Neuronal photoactivation pulses shortened the interbeat interval within 100ms, which corresponded to two repeated pulses, and such effect was observed during the same or immediately following R-R cycle (**Fig. 18B**).

Moreover, we confirmed the same results using increasing concentration of Metoprolol (from 4mg/kg to 60mg/kg). Metoprolol was used because we would like to exclude that the decrease of the response to photoactivation of SAN neurons, which we observed also using propranolol, was not due to the blockage of Na^+ channels, that could occur at high doses of propranolol.

In summary, our *in vivo* data, showing the spatial selectivity of SN activation of SAN responses, the functional evidence of elevated $[NE]_{cleft}$, and the kinetics of neuro-effector coupling, are all in support of the working model whereby the establishment of a specialized extracellular domain enables sympathetic neurotransmission to the heart to occur in a ‘quasi-synaptic' fashion.

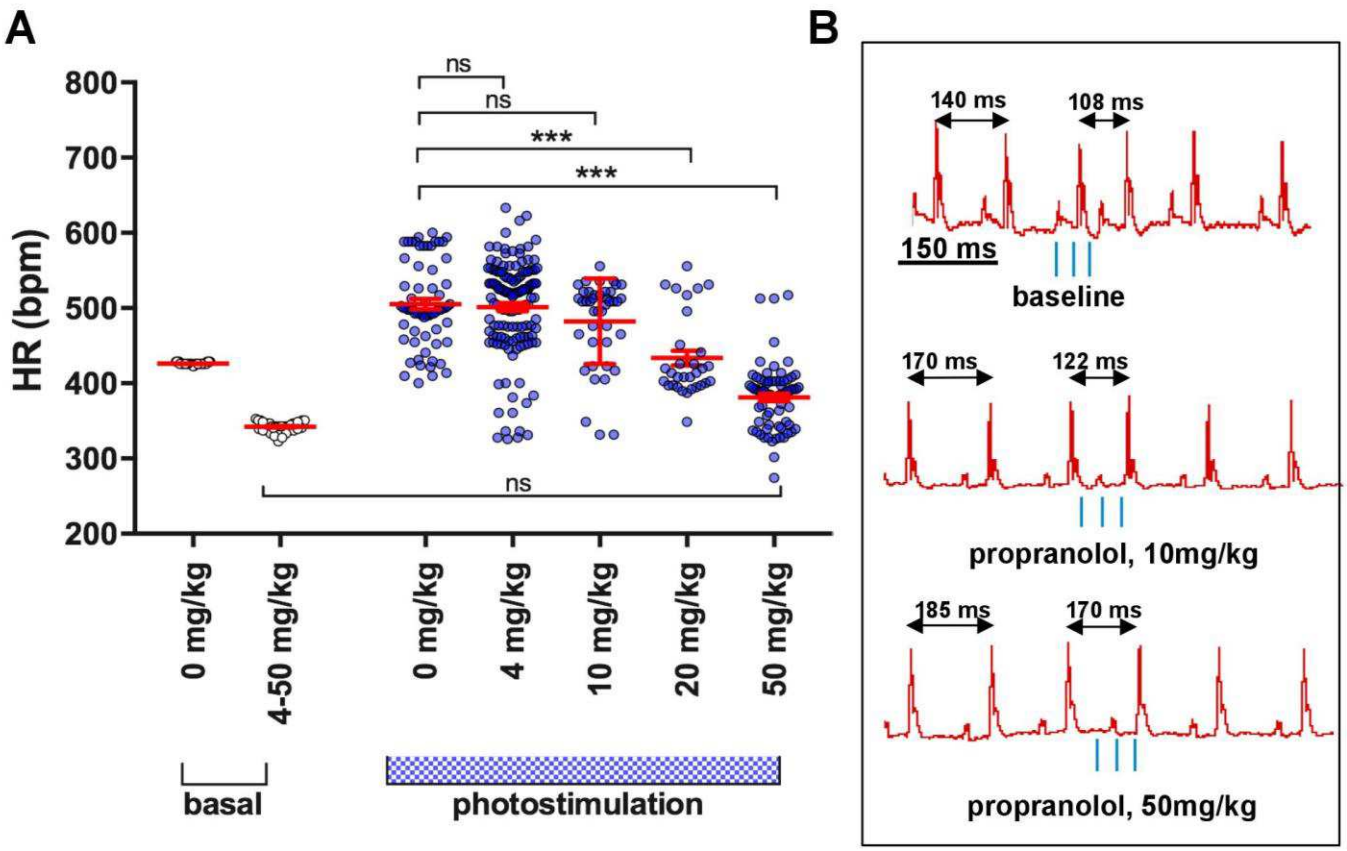

Figure 18. Assessment of the efficiency of neuro-cardiac coupling *in vivo*.
(**A**) Dose-effect analysis of the treatment with the β-AR antagonist, propranolol, on the chronotropic response to neuronal photostimulation. (**B**) Dose-effect analysis of the treatment with metoprolol on the chronotropic response to neuronal photostimulation. Bars indicate s.e.m. (ns=not significant; ***, $p<0.001$ n=100 CMs for each group).

4. Discussion

Cardiac SNs have a fundamental role in the control of cardiac physiology, and their dysfunction is a common finding in several heart diseases (Kaye and Esler, 2005; El-Armouche and Eschenhagen, 2009; Florea and Cohn, 2014; Franzoso *et al.*, 2016). Albeit decades of investigations have clarified the molecular entities underlying neuro-cardiac regulation and studied at high detail the intracellular signaling pathways dependent on adrenergic input, fundamental aspects of the neuro-cardiac communication remain elusive. Here, we investigated the SN-CM intercellular signaling dynamics, which were assessed *in vitro* by live imaging of cAMP in co-cultures, and *in vivo* using SN optogenetics.

Our *in vitro* data indicate that sympathetic modulation of CM signaling requires direct cell-cell contact, which brings together the neuronal NE-releasing and the CM NE-sensing membranes. Such interaction defines a low-volume extracellular space in which high [NE] is reached with only a few thousand molecules (i.e. few vesicles), as estimated by numerical simulation obtained in neuro-effector junctions with comparable geometry (Scepanovic, 2011). Such restricted signaling domains promote the activation of only a fraction of β-ARs within the contacted CM membrane, as supported by the stringent ***selectivity*** of neuronal target activation, and allow high ***efficiency*** enabling CM responses to minimal neuronal activation. These results fit well with the observation that signaling complexes of the cAMP/PKA pathway, including β1-ARs, as well as PKA anchoring proteins and targets, cluster within the CM membrane at the neuronal interaction site (Shcherbakova *et al.*, 2007). Our imaging data describe the consequences of such arrangement, showing that cAMP synthesis initiates, upon neuronal stimulation, at the innervated CM site, and identify the complex formed by the neuronal varicosity and post-synaptic CM membrane as the functional signaling unit in the neurogenic regulation of the heart. Our *in vitro* results were corroborated by our *in vivo* findings using optogenetics, which was exploited to achieve non-invasive control of cardiac SNs, avoiding direct effects on heart electrophysiology. The innovative aspects of this technique are represented by its structural simplicity, with light sensor element, its fast kinetic, the specificity of the stimulation obtained, its non-invasiveness and its spatial and temporal accuracy.

This properties provided a flexible tool to probe the function of restricted groups of cardiac neurons *in vivo*, and address neuro-effector signalling kinetics.

Although there are differences between the cellular environment *in vitro* and the intact innervated heart, the results of the *in vivo* experiments support the working model whereby neurogenic regulation of heart rhythm is underpinned by high-efficiency metabotropic synapses. The elevated speed and single beat precision of the neural control of SAN automaticity is further sustained by previous numerical modelling of agonist kinetics in a neuro-effector junction of comparable morphology, showing $[NE]_{cleft}$ rise and decay time of only few msec (Bennett *et al.*, 1995). Although our optogenetic investigations have been focussed on the sympathetic regulation of HR, and thus limited to the analysis of SAN function, our *in vitro* (**Fig. 8**) and *ex vivo* (**Fig. 4**) data, in both experimental and human hearts, support that tight neuro-cardiac coupling also takes place in the ventricles, suggesting that acute control of cardiac inotropism and long term modulation of CM structure, by SNs, may follow the same behaviour. Indeed, our *in vitro* data in co-culture suggested that the close CM-SN interaction is necessary to regulate CM size. These data are in line with the results of a parallel project, on-going in our laboratory, supporting that SNs regulate CM size by exerting a local control in the intact myocardium. Indeed, we demonstrated that, in the murine myocardium, SN density parallels with a transmural heterogeneity in CM size: CMs from the highly innervated EPI region are larger than cells from the less innervated ENDO area. Interestingly, such correlation holds true in other mammalian species, including human (Ieda *et al.*, 2007). (**Fig. 19,** Pianca *et al.*, manuscript submitted).

That SNs signal to target CM at the level of restricted extracellular domain implies that the activation of a limited CM membrane (and receptor) portion by a minute varicosity should provide enough adrenergic input to sustain cardiac stimulation during fight-or-flight reactions. However, in both the SAN and ventricular myocytes, each cell forms several junctional sites with the same neuronal process and may therefore receive NE simultaneously from multiple point sources, thus increasing the potency of adrenergic stimulation. In addition, as each cell is innervated by different processes, it is tempting to speculate that neuronal recruitment may be involved in modulating the degree of CM responses across the wide latitude of physiologic regulation, spanning from the fine tuning of heart rhythm to drastic increase in cardiac stimulation of fight-or-flight responses.

Our working model has several implications for cardiac pathology, including heart failure (HF), the first cause of cardiovascular mortality in Europe (47% of deaths). HF is commonly associated with altered function of cardiac autonomic control, but the underlying mechanisms are not entirely understood. The common tenet is that failing hearts have decreased responsiveness to β-AR agonists, reduced NE content in sympathetic endings, increased venous spillover of neuronal NE and interstitial NE accumulation (Kaye and Esler, 2005; El-Armouche and Eschenhagen, 2009; Florea and Cohn, 2014). All these features would be explained by effects of the structural remodeling of failing hearts on neuro-cardiac junction organization, which may lead to the disruption of the junctional cleft, with subsequent interstitial NE diffusion, reduced efficiency of cardiac β-adrenergic responses and decreased efficacy of pre-synaptic NE re-uptake. In further support of this, numerical modelling in similar neuro-effector junctions shows that the increase, by few microns, of the neuron-to-target intermembrane distance, causes neurotransmitter diffusion and a dramatic reduction (<15%) in the number of activated post-synaptic receptors (Bennett *et al.*, 1995). In addition, our unpublished data show that prolonged interference with the mechanisms of neuro-cardiac coupling causes *per se* SN degeneration, thus reducing the number of functional neuro-cardiac contacts, and subsequently the cumulative neuronal input to target cells.

In conclusion, by inspecting a seemingly overlooked system, under the new light of fluorescence imaging and optogenetics, we propose a model of cellular interaction to explain neuro-cardiac regulation, which has implications in the understanding of heart physiology and pathology.

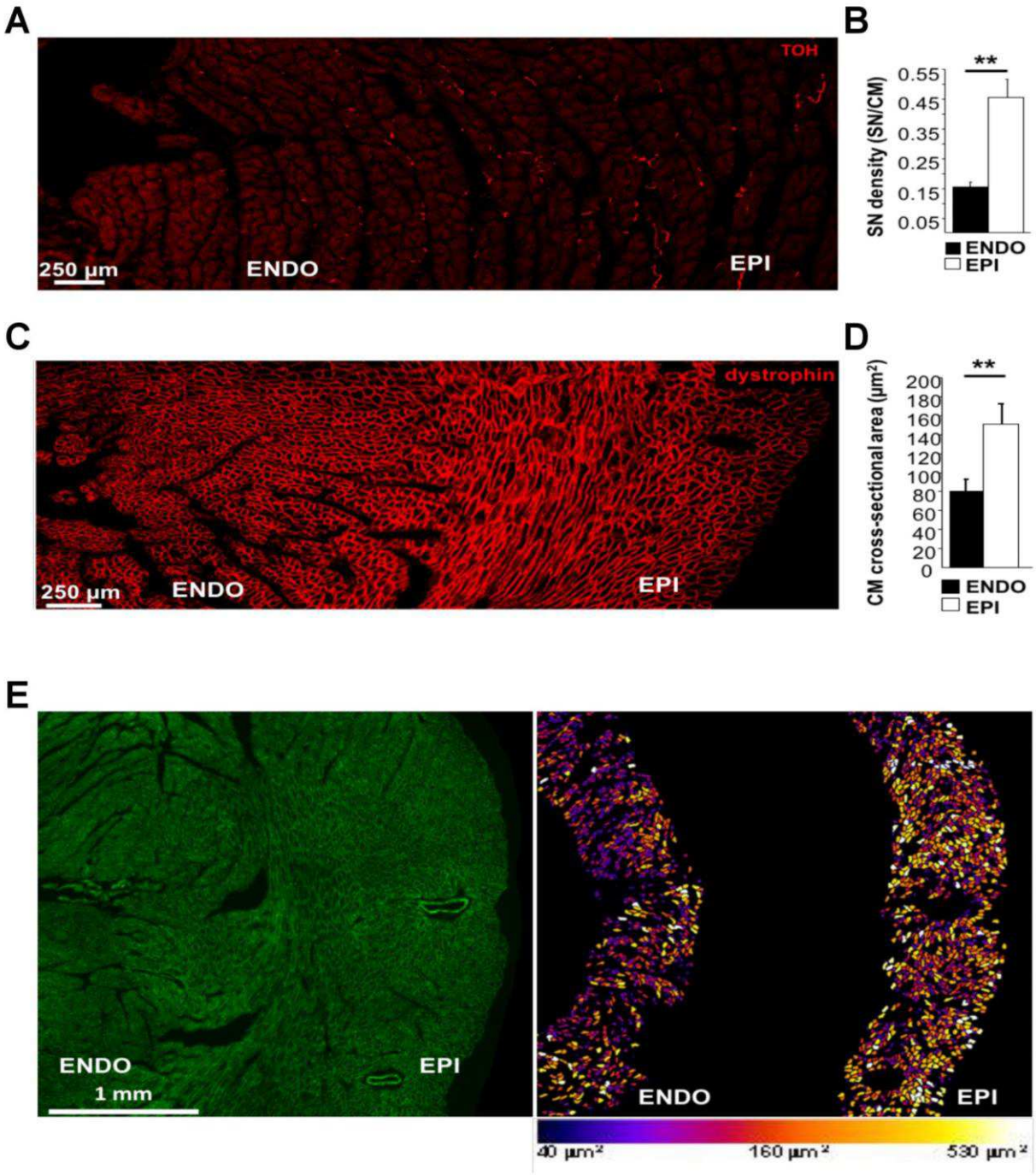

Figure 19. Neuronal-dependent regional control of cardiomyocyte size, *in vivo*.
(**A**) Confocal IF analysis on heart cryosections stained with an antibody to tyrosine hydroxylase (TOH). The image is a transmural detail of the left ventricle (LV). (**B**) Statistics of sympathetic neuron density in LV subepicardial and subendocardial regions. (n=6 hearts for each study group). (**C**) Confocal IF analysis on heart cryosections stained with an antibody to dystrophin. The image is a transmural detail of the left ventricle (LV). (**D**) Statistics of cardiomyocyte cross-sectional areas in LV subepicardial *vs* subendocardial regions. (n=6 hearts for each study group; **, $p<0.01$). (**E**) Images are details of the LV. The left panel show a confocal IF analysis on heart cryosections stained with an antibody to dystrophin. The right panel shows a colorimetric map in which the colors relate to the values of CM areas. White-yellow cells are bigger cells. Blue-purple cells are the smaller ones.

5. Overall conclusions and perspectives

Altogether our *in vitro* and *in vivo* data indicate that:

- The junctional site between sympathetic neurons and cardiomyocytes is the elementary unit of neuro-cardiac communication;
- Such interaction defines a low-volume extracellular space in which high [NE] is reached with only few thousands of molecules (i.e. few vesicles), promoting the activation of only a fraction of β-ARs within the contacted CM membrane.
- This concept supports the idea of a stringent *selectivity* of neuronal target activation, allowing high *efficiency* in cardiomyocyte responses with minimal neuronal activation.
- Optogenetics was a flexible tool to probe the function of restricted groups of cardiac neurons *in vivo*, and address neuro-effector signaling dynamics.
- Neurogenic regulation of heart rhythm by sympathetic neurons is underpinned by high-efficiency metabotropic synapses.

While proposing a novel interpretation on the physiology of neurogenic control of the heart, these results have opened several new questions, which are crucial in the basic understanding of neuro-cardiology and its clinical implications. To name a few questions:

1) the relation between the sympathetic network ad its function is still unresolved and we have not addresses yet whether a single CM may integrate the inputs received simultaneously by several neurons;
2) since we demonstrated that SN activity impacts on both CM contraction and signalling pathways, it will be interesting to evaluate how heart denervation, as occurring in transplant surgery, impacts on cardiac morphology and function. In addition, since re-innervation occurs few years after heart transplantation, it would be determinant to understand whether the physiologic innervation pattern and functional features are reconstituted.
3) Finally, our data suggest that neurogenic input to adrenergic receptors may be different from that of circulating catecholamines, and it will be relevant to

address whether differences may be identified in the effects of these two parallel adrenergic systems.

This dataset is part of a manuscript currently under review at the *Journal of Physiology* Valentina Prando*, Francesca Da Broi*, Mauro Franzoso* Anna Pia Plazzo*, Nicola Pianca, Maura Francolini, Cristina Basso, Matthew Kay, Tania Zaglia# and Marco Mongillo#. Dynamics of neuro-effector coupling at 'cardiac sympathetic' synapses. Journal of Physiology. UNDER REVISION, *JP-SRRP-2017-275693X*).

2nd PhD PROJECT: Role of the mitochondrial protein Opa1 in the regulation of the cardiac sympathetic neurons physiology.

1. Introduction

1.1 Mitochondria shape and function

Mitochondria, which were described for the first time by Rudolf Albrecht von Koelliker in 1857, are now well-recognized for their crucial role in several cellular functions and signalling pathways. Mitochondria are present, although in different number, in all the cell types of the bodies (es. 3-4 mitochondria for each plate; up to 1000-2000 mitochondria for hepatocytes), and display variable shape and size (with a diameter up to 1μm and a length varying from 2 to 10 μm). Their structure consists of i) an outer mitochondrial membrane (OMM), rich in pores allowing communication with the outside and ii) an inner mitochondrial membrane (IMM), impermeable and constituted by multiple folds called *cristae*, which increase the mitochondrial surface and delimit mitochondrial matrix.

The IMM homes enzymes which are responsible for electron transport and oxidative phosphorylation (OXPHOS), as well as various proteins involved in the transport of metabolites to and from the matrix. *Cristae*, which separate the matrix from the inter-membrane space, are involved in both OXPHOS and ATP synthesis, since most of the respiratory complex and cytochrome chains are concentrated on this site (**Fig. I**) (Bernardi & Azzone, 1981; D 'Herde *et al.,* 2000).

Mitochondria distribute in a complex network and their morphology governs mitochondrial function and the cytochrome C accessibility to the OMM. It has been shown that during apoptosis, the remodelling of the *cristae* causes a dramatic reorganization of IMM, which induces the mobilization of cytochrome C. During apoptosis, in particular, mitochondria integrate different stimuli and they induce the release of cofactors that trigger the activation, in the cytosol, of effectors caspases, leading to cell death (Danial *et al.*, 2004). Dysfunctions in these processes can be detrimental for the cell: several pathological conditions including cancer or neurodegenerative disease are indeed consequences of mitochondrial dysfunction (Schapira, 2000).

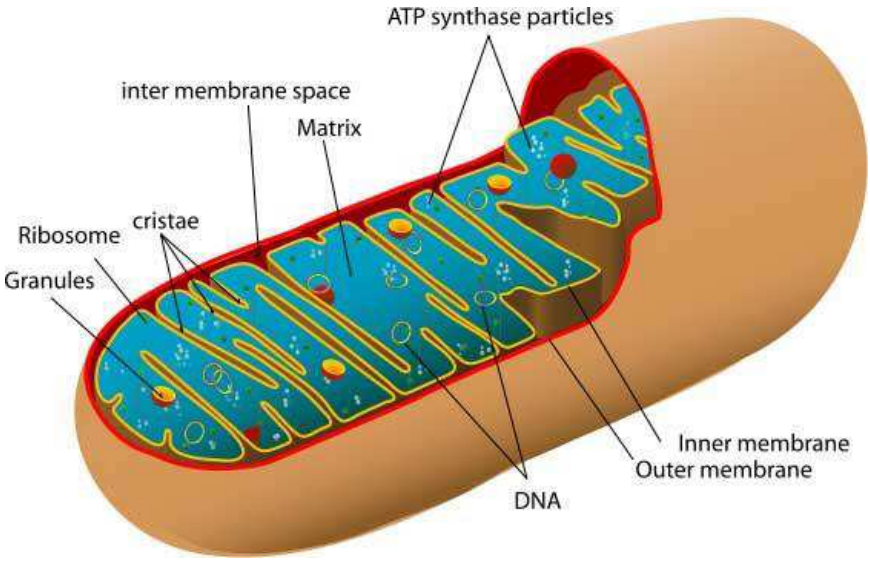

Figure I. Mitochondrion structure (*UNSW, Cell Biology*)

Interestingly, mitochondria are the only organelle that possesses its own DNA; in vertebrates mitochondrial DNA (mtDNA) consists of a double stranded covalently close circular DNA molecule of about 16.5 kb. The mtDNA encodes 13 mRNAs for the subunits of the OXPHOS complexes (Fernandez-Silva *et al.,* 2003). Proteins of mitochondrial origin are translated on mitochondria ribosome bound to the matrix site of the IMM and then they are delivered to the proper compartment. Mutations in mtDNA have been associated with a large number of genetic, multisystemic diseases thus strongly supporting that functional mitochondria are required to maintain the homeostasis of several tissues.

1.2 Mitochondria dynamics: fission and fusion processes

Mitochondria display a high plasticity, which is the result of mitochondria fission and fusion, which are two complex and finely controlled processes. Real-time imaging reveals that individual mitochondrial tubules continuously move back and forth along their long axes on radial tracks. Occasionally, two mitochondrial tubules encounter each other and fuse, end to end or head to site (Chen and Chan, 2006). On the other hand, these tubules can also undergo fission events, giving rise to two or more mitochondrial units. In particular, fission is the breakdown of the mitochondrial network in small isolated organelles. This process mainly occurs

in response to energy availability of tissues and during cell division, the latter to distribute mitochondrial genetic inheritance in newly formed cells.

The fission process is mediated by different proteins: Dynamin-related protein-1 (Drp-1), Mitochondrial Fission-1 protein (hFis-1) and endophyllin B1. Drp-1 belongs to the dynamin family. It is predominantly localized in the cytosol, but a fraction is also present at the level of the OMM (Smirnova *et al.,* 2001). During the fission phenomenon it interacts with hFis1 (James *et al.,* 2003), which is uniformly distributed on the OMM. Finally, endofilin B belongs to a family of proteins involved in the formation of endocytic vesicles. It is thought that its action takes place downstream of that of Drp-1, through a remodelling of the OMM (Karbowski *et al.,* 2004).

Regulated fusion of distinct mitochondria is required for the correct homeostasis of mitochondrial function, DNA (mtDNA), proteins and metabolites. This process is mediated by mitofusines isotype 1 and 2 (Mfn1.2), which are present in the OMM, and the optic atrophy factor-1 protein (Opa1), which is localized in the inter-membrane mitochondrial space, close to the IMM. MFN1 is responsible for the link between two adjacent mitochondria during the fusion process (Koshiba *et al.,* 2004), while MFN2 appears to be involved in mitochondria stabilization (Ishihara *et al.,* 2004). Interestingly, mutations in MFN2 were associated with peripheral neuropathy, Charcot-Marie-Tooth type Ia disease (Zuchner *et al.,* 2004). OPA1 plays an important role in mitochondrial fusion by interacting with MFN1 (**Fig. II**).

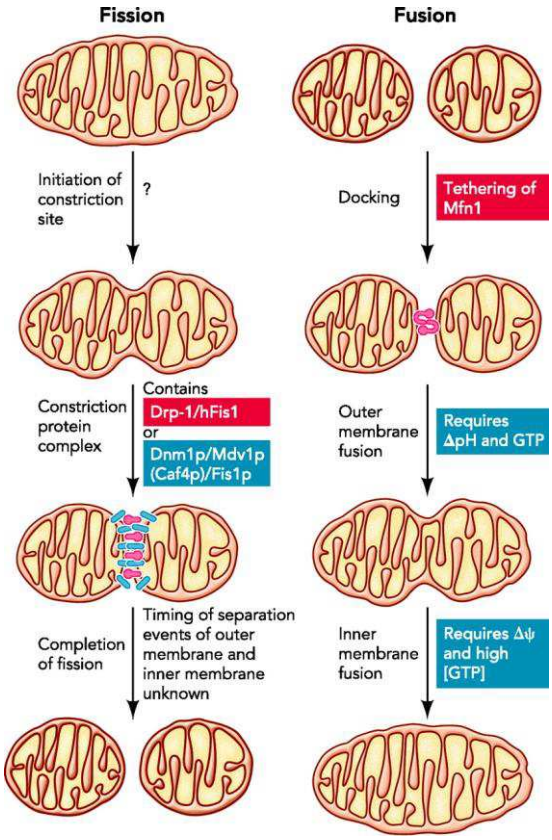

Figure II. Fission and Fusion processes (*Dimmer & Scorrano, 2006*)

1.3 Optic atrophy factor-1 protein

The Opa1 is a dynamin-related protein located in the intermembrane mitochondrial space closed to the IMM and is expressed in all tissues. The human gene encoding for Opa1 protein was identified in 2000 by two independent groups (Alexander *et al.*, 2000; Delettre *et al.*, 2000). Opa1 gene consisting of 30 exons that differ in the 3'UTR and in the open reading frame, by alternative splicing of exons 4, 4b and 5b. These several alternative splicing can encode for 8 mRNA isoforms in humans and 4 in the mouse (Akepati *et al.,* 2008).

The translated protein is composed by a coiled coil domain at the C-terminal and a GTPase domain at the N-terminal, where the protein exhibits the tagged signal for mitochondrial import (MTS). This MTS domain is subsequently removed by a peptidase (Olichon *et al.,* 2003) (**Fig. III**). The Opa1 protein is synthesized as a precursor that undergoes a number of post-translational modifications within the mitochondria (Herlan *et al.*, 2003). This process is regulated by several mitochondrial proteases including presenilin-associated rhomboid-like (PARL), mitochondrial ATPases associated with diverse cellular activities (m-AAA)

proteases (paraplegin and ATPase family gene 3-like protein 2-AFG3L2), the mitochondrial inner membrane AAA (i-AAA) protease yeast mitochondrial escape (YME1)-like 1 ATPase (YME1L) and the membrane-bound metallopeptidase with activities overlapping with the m-AAA protease (OMA1) (Cipolat *et al.*, 2006; Martinelli *et al*., 2010; Anand *et al.,* 2014).

After the removal of the IMS, matrix metalloproteases, give rise to the long form of IM-anchored L-Opa1, composed by 1014 AA, which can be further cleaved, leading to the production of S-Opa1 of 924 AA (Ishihara *et al.,* 2006; Herlan *et al.,* 2003). S-Opa1 interacts with un-cleaved forms of L-Opa1 to maintain *cristae* structure (Frezza *et al*., 2006). L-Opa1 is responsible for mitochondrial fusion, while S-Opa1 was shown to be involved in IMM fission (Anand *et al.,* 2014). The balance between the different Opa1 isoforms regulates mitochondrial morphology, dynamics and function (Cipolat *et al.*, 2006; Martinelli *et al*., 2010; Cogliati *et al.,* 2013; Belenguer *et al.,* 2013).

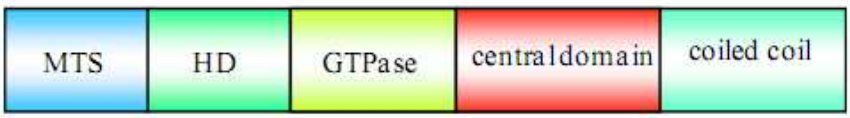

Figure III. Opa1 structure

Opa1 protein is involved in several cellular processes, such as mitochondrial fusion, the maintenance of mitochondrial *cristae* morphology and shape, OXPHOS and apoptosis. In line with this, cells with reduced Opa1 levels show alterations in mitochondrial *cristae* number, shape and size, block of the fusion process and of cellular respiratory function (Frezza *et al.,* 2006). In addition, the alteration of the *cristae* morphology, caused by the partial ablation of Opa1, causes cytochrome C release and the consequent activation of cell apoptosis. These data indicate that dysfunctional mitochondrial dynamics are causally linked to the development of neurodegenerative diseases with synaptic dysfunction, dendritic and axonal degeneration (Olichon *et al.,* 2003; Cho *et al.,* 2010).

Even *in vitro*, Opa1 downregulation in central neurons isolated from mouse cortex, leads to fragmentation of mitochondria, which are less abundant in the dendritic branches and also causes a deficit in synaptic growth and maturation.

This highlights the essential role of mitochondrial dynamics and mitochondria-associated proteins in maintaining the correct neuronal function (Bertholet *et al.,* 2013).

1.4 Neurons are high energy demanding cells

Neurons are postmitotic cells, uncapable to regenerate upon a damage. They are polarized cells constituted by a cell body from which originate numerous dendrites and a long axon, which can extend up to 1 meter, in the case of motor and sensory neurons (Matsuda *et al.*, 2009). However, the fine morphology of neurons differs depending on the specific neuronal population. While motor neurons dysplay a sole long axon, enlarging at the end in a bottom which establishes synaptic contacts with muscle cells, SNs develop axonal processess with a pearl-necklage morphology characterized by regular varicosities, close to target cells. Independently from their nature and function, neurons are highly active cells, as they: i) release neurotransmitters, to modulate the activity of target cells; ii) take-up the excess of the released neurotransmitter, to avoid exacerbated responses in target cells; iii) take-up neutrophins, released from target cells, which are then transported to the neuronal soma. All these functions, as well as other processes involved in the regulation of cell metabolism and trophism, require high amounts of ATP, which, as previously described, is provided by mitochondria (Harris *et al.,* 2012; Hall *et al.*, 2012; Morris *et al.*, 1993). On these bases, it follows that mitochondria have a key role for neuronal healthy and function (see previous paragraphs). Consistently, mitochondria concentrate in neuronal regions characterized by the highest energy consumption, such as the synaptic terminals and the regions of axonal sprouting (Brodin *et al.,* 1999). In mature neurons, the 20~30% of mitochondria, present into the axon, continuously move both anterogradely (from the soma to the synaptic terminals) and retrogradely (from the synaptic terminals to the soma). In addition, it has been demonstrated that about the 15% of mitochondria either briefly pause or dock at the synaptic site, where they are essential to maintain Ca^{2+} homeostasis and for the release and the re-uptake of neurotransmitter vesicles (Rizzuto *et al.,* 2000). Moreover, mitochondria provide the ATP necessary to sustain the retrograde transport of NGF, released by innervated cells (Mattson *et al.,* 2008). As an example, in the SNs innervating the heart, NGF, released by CMs binds to its receptor, TrkA, localized at the level of

neuronal varicosities, and once the TrkA-NGF complex is established, it is internalized into the varicosity and undergoes retrograte transport to the neuronal soma, where NGF activates signaling pathways specifically involved in cell growth and survival (Gallo & Letourneau, 1998; Lewin & Barde, 1996), Both NGF-TrkA internalization and retrograde transport require high amount of energy. As a consequence, when NGF is applied to axonal sites deprivated of mitochondria, results in the trapping of mitochondria undergoing transport into these sites and the triggering of axonal branching (Gallo & Letourneau, 1998).

Interestingly, both fission and fusion processes occur along neuronal axons (Yu *et al.,* 2016). The importance of the balance between fission and fusion in the regulation of axonal mitochondria is underscored by the observation that the transport of axonal mitochondria is inversely proportional to the length of the mitochondrion. In particular, in the neurons the maintenance of correct mitochondrial dynamics, and so the correct mitochondrial function, enable the cells to survive. Indeed, the partial ablation of Opa1 have been shown to induce alterations in morphology, number and size of mitochondria *cristae*, resulting in the remodeling of the IMM, the decrease in ATP energy production, the mobilization of cytochrome C and the consequent activation of apoptotic processes leading to neuronal cell death (Frezza *et al.,* 2006). The significance of mitochondria for neuronal viability and function is further supported by the implication of mitochondrial dysfunction, such as defective mitochondrial transport and altered distribution, in several neurodegenerative diseases (Exner *et al.,* 2012; Dutta *et al.,* 2012). In addition, during aging, a process associated to increased central and peripheral neurodegeneration, mitochondria are morphologically altered, broader and rounded and fragmented. As a result, they produce high concentrations of ROS and free radicals, that could impact on mtDNA, thus increasing the somatic mutations in the mtDNA, which are transmitted during cell division (Lenaz *et al.,* 2000).

1.5 Opa1 in disease: autosomal dominant optic atrophy

Mutations in Opa1 gene have been associated with autosomal dominant optic atrophy (ADOA), also known as Kjer type I disease. This neurodegenerative pathology is one of the two most common optic neuropathies, with an estimate prevalence from 1:50000 to 1:12000 (Kjer *et al.*, 1996; Yu-Wai-Man *et al.,* 2010).

The main form of ADOA is due to mutations in Opa1 gene. Over 300 Opa1 mutations, spread along the coding sequence in particular in the GTPase domain, have been described (Ferre *et al.,* 2009; Nasca *et al.,* 2017). These mutations are grouped into different categories depending on whether they predicted to cause the disease. In detail, single base-pair substitutions represent the most common mutational subtype, followed by deletions and insertions (Amati-Bonneau *et al.,* 2009; Ferre *et al.,* 2005). However, the majority of Opa1 mutations result in premature termination codons and unstable truncated mRNAs, indicating haploinsufficiency as the main pathogenic mechanism (Delettre *et al.*, 2000; Pesch *et al.*, 2001; Zanna *et al.,* 2008).

Moreover, missense Opa1 mutations affecting the catalytic GTPase domain in patients with ADOA, on the other hand, are more likely to exert a dominant-negative effect and these patients have a two-to three-fold increased risk of developing syndromic DOA compared to those with truncating mutation (Hudson *et al.,* 2008; Amati-Bonneau *et al.,* 2009; Yu-Wai-Man *et al.,* 2010).

ADOA affects retinal ganglion cells (RGC), whose axons form the optic nerves (Fuhrmann *et al.,* 2009). Thus, patients manifest decrease in visual acuity, tritanopia (dyschromatopsia characterized by confusion in the blue-yellow hues), loss of sensitivity in the central visual fields, and pallor of the optic nerve (Votruba *et al.,* 1998; Ferre *et al.,* 2005). Classic ADOA usually begins during childhood, with a large variability in the severity of clinical expression, which may range from non-penetrant unaffected cases up to very severe, early onset cases, even within the same family carrying the identical molecular defect (Delettre *et al.,* 2002). Histopathology studies have shown diffuse atrophy of the ganglion cell layer that predominates in the central retina and loss of myelin and nerve tissue within the optic nerve (Kjer *et al.,* 1996). This phenotypic diversity is closely related to the kind of Opa1 mutations and their identification allows further description of atypical clinical presentation.

Later extraocular features, complicating the ADOA pathology, lead to the description of “ADOA plus” phenotype, which is characterized by peripheral nervous system involvement, with the development of peripheral neuropathies and myopathies (Yu-Wai-Man *et al.*, 2010; Chao del la Barca *et al.*, 2016). In addition, heart rhythm abnormalities have been described, opening a new insight into the human disease (Spiegel *et al.*, 2016). Interestingly, it has been recently

demonstrated both in mouse model, but also in ADOA patients, the development of cardiomyopathy and cardiac rhythm abnormalities (Sarzi *et al.,* 2012; Liskova *et al.,* 2013; Spiegel *et al.,* 2016).

How Opa1 mutations cause such a wide range of clinical symptoms of ADOA remains to be clarified. Non-neuronal cells from patients with ADOA display aggregated, fragmented or normal mitochondria (Delettre *et al.,* 2000; Piquereau *et al.,* 2012). In addition, Opa1 mutations have been associated with reduced ATP production and reduced mtDNA content (Lodi *et al.,* 2004). Recent studies also suggest that abnormalities in Ca^{2+} homeostasis contribute to the pathogenesis of dominant optic atrophy (Fulop *et al.,* 2011). However, a fully comprehension of ADOA pathogenetic mechanisms are still lacking.

In this thesis, we will investigate the effect of Opa1 haploinsufficiency in cardiac sympathetic innervation morphology and physiology.

2. Material and Methods

2.1 In Vivo analyses

2.1.1 Animal models

TOH-Opa1$^{+/-}$ mice were obtained by crossing homozygous mice expressing cre-recombinase under the control of a tyrosine hydroxylase (TOH) promoter B6.129X1-Th<tm1(cre)Te>/Kieg (Emma Laboratories, KCTT/EMMA/Johannes Wilbertz Stockholm SWEDEN) with homozygous LoxPOpa1 mice. The cre-recombinase mediates recombination at the loxP sites, resulting in the deletion of Opa1 encoding gene. TOH-cre$^{+/-}$ lines were used to maintain the colonies and used as littermate controls. For the experiments were used adult (6mo.) and aged (24mo.) mice. The experimental procedures described in this manuscript were approved by the local ethical committee (Authorization number C54) and communicated to the relevant Italian authority (Ministero della Salute, Ufficio VI), in compliance of Italian Animal Welfare Law (Law n 116/1992 and subsequent modifications).

2.1.2 Genotyping

To characterize the genotype of transgenic animals, we used a protocol that takes place in three phases:

i) DNA Extraction from tissue;
ii) PCR (Polymerase Chain Reaction);
iii) Agarose gel electrophoresis;

• DNA extraction from tissue: DNA was extracted from a fragment of transgenic animal tissue and it was incubated for 5 hours at 56°C in the extract buffer (200mM Tris-HCl pH 8.4; 500mM KCl and Proteinase K (20mg / mL) (Invitrogen, Milan)). The proteinase K activity was subsequently blocked by incubating the samples at 99°C for 10 min. Then samples were centrifuged at 12000 rpm for 10 min., the supernatant withdrawn and the extracted DNA concentration was measured at the spectrophotometer.

• PCR (Polymerase Chain Reaction): PCR is a molecular biology technique used to amplify DNA fragments by designing specific oligonucleotide sequences (primers) complementing regions that flank the gene sequence to be amplified. The reaction mixture was composed of: 200mM Tris-HCl pH 8.4, 500mM KCl, 50mM MgCl2, 10mM Primer FWD, 10mM Primer REV, 100mM Nucleotides, 0.4% Taq Platinum and 150ng/mL DNA all from Invitrogen, diluited in sterile water to reach a final volume of 25µL. The amplification reaction was the follow:

• denaturation 94°C for 4 min,

• denaturation at 94°C for 30 sec.,

• fixation at 57°C for 30 sec.,

• elongation at 72°C for 1 min. The cycles were repeated for 35 times.

• elongation at 72°C for 10 min.

The sequences of the primers used in this study are described in **Table 1**.

TOHcre	*Foward*	5'-CAC CCT CAG CCA AGC ACT
	Reverse	3'- CTT TCC TTC CTT TAT TGA GAT
	Cre- UD	GAT ACC TGG CCT GGT CTG
loXP Opa1	*Foward*	CAGTGTTGATGACAGCTCAG
	Reverse	CATCACACACACTAGCTTACATTTGC

Table 1. *primer* sequences

• Electrophoresis: For this purpose, a 2.5% agarose gel was prepared by dissolving agarose (Ultra Pure Agarose, Invitrogen, Milan, Italy) in a suitable volume of TAE 1X buffer (Tris-Acetate EDTA), supplemented with Syber Safe (20000X, Euroclone), which is a dye that intercepts the DNA bases and emits fluorescence. Samples were loaded on gel and the electrophoretic run was conducted at 100-120 volts for about 20 min. The loading buffer (6mL of H_2Omq, 4mL of glycerol, 600µL Tris-HCl 1M pH8, 0.02% Bromo phenol, Sigma), which was added to the sample prior to their loading, was a mixture of two dyes, xylene cyano and blue bromophenol, 10% SDS (SodioDodecylSulfate) and glycerol (Sigma, Milan, Italy). This buffer increased the density of the amplified DNA, facilitating its loading into the gel wells, as well as its displaing. The two dyes also

migrated in the same direction as the nucleic acids, thus serving as indicators of the progression of electrophoresis. The DNA ladder (Promega, Milan, Italy) was also loaded into the gel, which was a mixture of DNA fragments of known size to be compared with the fragment obtained from the PCR. In our case TOH was at 300-400 pairs of bases (bp) and loxPOpa1 was at 700-800 bp. The electrophoresis gel was observed using the Image Lab program, Bio-rad, where agarose gel was inserted and, after UV activation, through Quantity One software, DNA bands were displayed in the gel.

2.1.3 Echocardiography

Echocardiography is a non-invasive diagnostic tool necessary to evaluate the heart function. Echocardiographic analysis were performed both in anesthetized adult and aged TOH-Opa$^{+/-}$ mice and age- and sex-matched littermate controls, using a Vevo 2100™ (VisualSonics, Toronto, Canada) system equipped with a 30 MHz transducer (**Image 1**). Mice were anesthetized with 3-1.5% isoflurane (v:v in O_2), while monitoring the temperature, the respiration rate, and the electrocardiogram (ECG). Two-dimensional cine loops with frame rates of 200 frames per second of a long-axis view and a short-axis view at proximal, mid, and apical level of the left ventricle (LV) were recorded. Interventricular *septum* (IVS) and LV posterior wall thicknesses, LV internal diameter, and maximal LV length were measured in systole and in diastole from the long-axis B-mode image, according to standard procedures. We calculated:

i) the Ejection fraction (EF), which is an index of the heart pumping and was determined by the following *formula*: %EF = 100 × systolic LV volume/diastolic LV volume;

ii) the fractional shortening (FS), which can assess changes in LV shape.

Echocardiographic image acquisitions and analysis were performed by a single operator, blinded to the mouse genotype.

Image 1. *Echocardiographic instrument Vevo 2100™*

2.1.4 ECG recording and analysis

The electrocardiography allows the evaluation of electrical activity via Electrocardiogram (ECG) in an easiest, least expensive and practical way. The bases underling the measurement of the ECG is purely physiological: two electrodes, placed in a precise position on the chest wall and limbs, may record the maximum action potential (AP) differences, that vary in space and time, created by the generation of myocardial impulses, through the connection to the voltmeter. It provides information on the heart rate (HR) and on the direction of cardiac depolarization and repolarization during the different phases of the heartbeat. The normal ECG trace has a specific aspect, that varies only in pathological conditions, and it is characterized by several waves, positive and negative, which are repeated in each heart cycle. In particular, the first wave, in chronological order, is the "*p wave*", which is due to the atria depolarization, followed by the "QRS complex", which represents the depolarization of the ventricles and the IVS. Then there is the "T wave", which is the sign of the repolarization of the ventricles.

Here, we used telemetry-based ECG analysis, which allows ECG monitoring in conscious mice eliminating the possible side effects of the anesthetics. The telemeters (TA10ETA-F10, Data Science International (DSI), St. Paul, MN, USA)

are transmitters, which record vital parameters and communicate, via radio waves, with a receiving device placed on a recording plate (RPC-1, DSI). This is placed under the animal cage and it is also connected to a PC (**Image 2**).

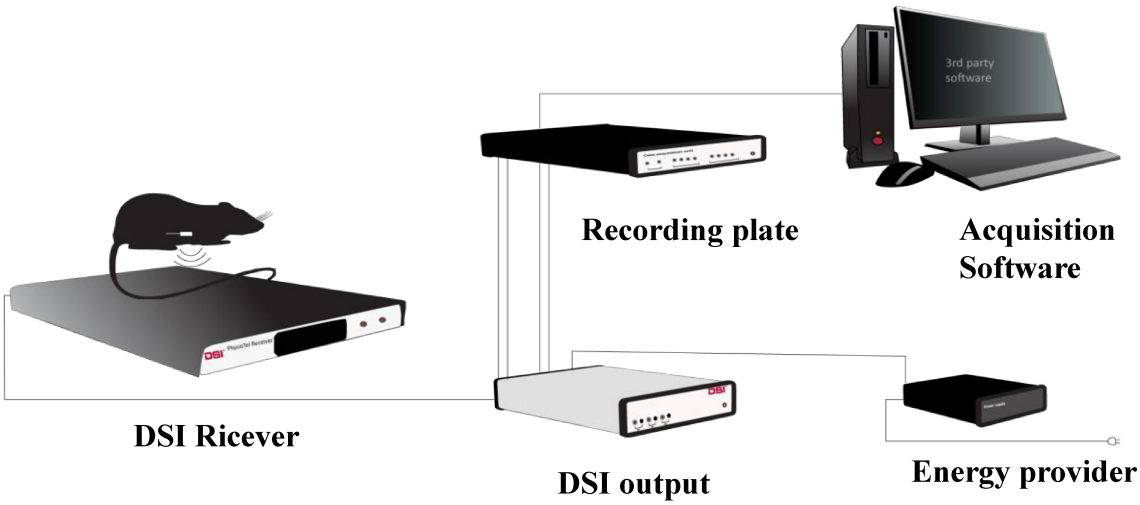

Image 2. *Telemetry apparatus*

For telemetry implantion control and TOH-Opa1$^{+/-}$, adult and aged mice, were anesthetized with Avertin 2.5% (5g Tribromoetanolo in 5ml of 2-methyl-2-butanol) in physiological water (400mg/kg, ip). The animal was placed in a supine postin and once shaved and disinfected, the skin and the abdominal muscles were cut. The viscera were exposed and the telemetry was inserted into the abdominal cavity. The abdominal muscles were closed with atraumatic wire (prolene 5/0) and the electrodes were positioned, through a subcutaneous tunnel, to the pectoral area. At the end of the procedure, the skin was closed with thread atraumatic (prolene6/0), disinfected with Betadine. Mice were treated, for the first three days after surgery, with 60 mg/Kg of Terramicina antibiotic, administered intraperitoneally, and 5 mg/kg of Contramal analgesic, administered intramuscularly twice a day (**Image 3**). The beginning of the ECG recordings started approximately one week after surgery. The recording was performed through the software "ART 4.2, Data Science International DSI", using a protocol that allowed to record fragments of 5min. every 30min. within 24h. Such recording mode has been used to monitor the ECG at baseline and during acute stress. During atropine administration experiments (2mg/kg, MONICO s.p.a.), a continuously recording was performed for the entire duration of the experiment.

The data acquired were processed through the software "LabChart 7, ADInstruments" and the following parameters have been analyzed: *i)* HR, *ii)* PR and QRS interval and *iii)* heart rate variability (HRV). The HRV can be expressed, in the time domain through the standard deviation (SDNN) of R-R intervals between beats.

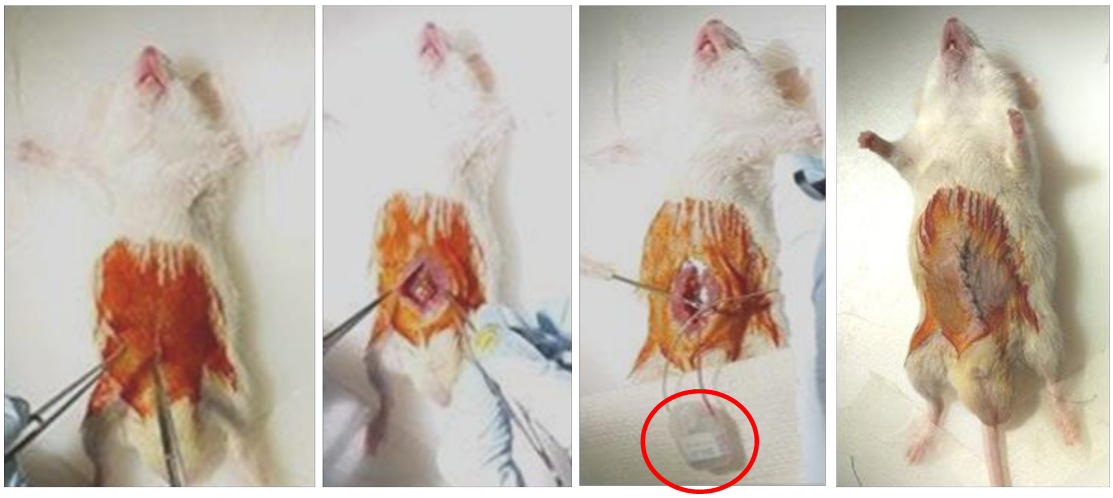

Image 3. *Telemetry implant*

2.2 Ex Vivo analyses

2.2.1 Tissue samples and immunofluorescence analysis

Hearts were harvested from adult (6 mo.) and aged (24 mo.) male transgenic and control mice, washed in 1X PBS to remove blood and cut transversally at the med portion of the ventricles. The apical portion of the heart was immediately frozed and used for molecular and biochemical analyses. The basal portion of the heart was processed for histological and IF analysis. In detail, hearts were fixed in 1% paraformaldehyde (PFA, v:v in 1X PBS) (Sigma, Milan, Italy) at room temperature (RT) for 15 min., after 3 washes in 1X PBS hearts were dehydrated in sucrose gradient embedded in OCT and frozen in liquid nitrogen. Ten-micron sections were obtained with a cryostat (Leica CM1850, Leica Microsystems GmbH, Wetzlar, Germany) and incubated with primary antibodies diluted in 1X PBS, supplemented with 1% BSA and 0.5% Triton-X100 overnight at 4°C. The primary antibodies used in this study are listed in **Table 2.** 488- and Cy3-conjugated secondary antibodies, all from Jackson lab (UK), were used to detect primary antibodies. These antibodies were diluted in 1X PBS, supplemented with 1% BSA and incubated at

37°C for 30 min. Heart sections were then analyzed at the confocal microscope (TCS SP5 Leica, Leica Mikrosysteme Vertrieb GmbH).
In a subset of mice we also harvested the liver and the brain which were directly frozen in liquid nitrogen for molecular and biochemical analyses.

2.2.2 Hematoxylin and Eosin staining

This standard histological staining was performed by using the (Bio Optica, Milan, Italy) kit, following the manufacturer instructions. Images were analyzed by the Leica DM5000B optical microscope equipped with a LEICA DFC300FX digital camera and IM1000.

2.2.3 Estimation of the density of the cardiac sympathetic neurons

The density of cardiac sympathetic neurons (cSNs) was assessed in mouse heart cryosections from adult and aged TOH-Opa1$^{+/-}$ mice and age- and sex-matched controls. In detail, five non-consecutive cryosections from the mid portion of the ventricles were stained with an antibody to TOH. Sections were analysed at the confocal microscope and the image of 8 randomly chosen fields (0,001 cm^2 area) were acquired from both the sub-endocardial (4 fields) and the sub-epicardial (4 fields) regions of the LV. To evaluate the SN density in the right atrium (RA) we analysed 4 non-consecutive sections and acquired images of 4 randomly chosen fiels. The percentage of the myocardial area occupied by TOH$^+$ fibers was then evaluated by using the software " IMAGE J J Volume 10.7b.".

2.2.4 Quantitative RT-qPCR

Total RNA was prepared using the SV Total RNA Isolation System (Promega Milan, Italy) according to the manufacturer's protocol. The single-strand cDNA was synthesized by SuperScript III (Invitrogen), according to the manufacturer's protocol. RT-qPCR was performed using a GeneAmp 9600 thermocycler, coupled with a GeneAmp 5700 Sequence Detection System (Applied Biosystems, Monza, Italy), according to the manufacturer's instructions, with the Power SYBR Green PCR Master Mix (Applied Biosystems). The relative quantification method, described by Pfaffl (Pfaffl *et al.,* 2001), was used to evaluate the differences in gene expression. Values in the experiments were normalized to the expression of the GAPDH internal reference, whose abundance did not change under the

experimental conditions used in the study. Gene-specific primer pairs were selected with Primer 3 software (http://frodo.wi.mit.edu/cgi-bin/primer3/primer3_www.cgi); sequences of distinct exons were chosen to avoid amplifying contaminant genomic DNA. The primer sequences used in this study are:

OPA1	*Foward*	5'-ATACTGGGATCTGCTGTTGG-3'
	Reverse	5'-AAGTCAGGCACAATCCACTT
GAPDH	*Foward*	CACCATCTTCCAGGAGCGAG
	Reverse	CCTTCTCCATGGTGGTGAAGAC

The results of RTqPCR are given in arbitrary units and expressed as fold changes in mRNA levels relative to controls.

2.2.5 Western Blotting analysis

One mm^3 heart blocks were homogenized by using the Tissue Lyser II (Qiagen) at 30 Hz for 1 min., followed by tissue incubation in Lysis Buffer (Tris 50mM, NaCl 150mM, $MgCl_2$ 10mM, DTT 0,5 mM, EGTA 1mM, Glycerol 10%, SDS 2%, Tryton 2%, anti-phosfatase and anti-protease 1X, in H_2O, pH 7,5)for 1h at 4°C.

At the end of protein isolation, samples were centrifuged at 12k rpm (10g) for 15 min. at 4°C. The pellet was discarded, the supernatant was collected and denaturated at 70°C and 1250 rpm for 10 min. Protein quantification was performed using the Bradford assay subsequently validated with a coomassie blue staining.

SDS–PAGE was performed on 4–12% gradient gels (Invitrogen) in MOPS 1X (invitrogen). Sixty mg protein were loaded for each lane in Loading Buffer (84% v:v SDS 1%, 30% v:v Sample Buffer 1X, 6% DTT v:v. The SeeBlue Plus2 (Life Technologies) was used as protein weight standard.

Proteins were transferred onto methanol-activated PVDF membrane (Invitrogen) by using Transfer Buffer at 4°C, 400 mA for 90 min. After that, membrane were processed and were stained with red ponceau dye (SIGMA) to check the transfer efficiency and quality. The membrane were blocked with 0.1% TTBS, supplemented with 5% milk for 1hour at RT, followed by incubation with the appropriate primary antibody (α-Opa1, mouse, (BD); α-actin, rabbit, (Sigma))

overnight at 4°C on a shaker. After three washes in 0.1% TTBS, the membranes were incubated with the appropriate secondary antibodies, conjugated to horseradish per- oxidase, diluted in 0.1% TTBS supplemented with 5% milk, for 90 min. Antibodies were the revealed t room revealed by enhanced chemiluminescence (ECL Plus, Pierce) and developed at Image Quant LAS4000mini. The semi-quantitative analysis of the relative protein content was performed using the ImageJ plug-in for densitometry that allows evaluating the optical density of protein bands in the photographic films.

2.3 Ex Vivo human biopsies

2.3.1 Skin biopsy and immunofluorescence

Skin biopsies of about three mm^3 were collected from the distal leg (10 cm above the lateral malleolus) and thigh (15 cm above the patella). Then, the samples were fixed in cold Zamboni fixative solution (2% PFA in saturated solution with picric acid) and kept at 4°C overnight. 50μm skin sections were obtained using a freezing sliding microtome (2000R; Leica, Deerfield, IL), and incubated overnight with primary antibodies (**Table 2**). In particular, we used serial sections in which we marked: in the first one, the sweat gland basement membrane, the epidermal/dermal border, the structure of muscle *erector pilorum* and the neurons; in the second one neuronal processes and sympathetic fibers. All antibodies used in this study were listed in the **Table 2**. In this way we are able to obtain a quantification of the SNs in skin biopsies distinguishing the sympathetic innervation in the sweat gland and in the *arrector pili* muscle. To reveal the staining, sections were labelled overnight with the alexa 488 and CY3 secondary antibodies (Jackson ImmunoResearch, West Grove, PA). We created a composite image that was viewed under a Zeiss fluorescent microscope (model Axioskop 40; Jena, Germany). Autonomic innervation density was quantified using the automated method described by Gibbons in 2010. The composite images were reviewed and scored semi-quantitatively on a 5 points scale. Scores of 0 (no identifiable nerve fibers), 1 (severely reduced nerve fiber density), 2 (moderately reduced nerve fiber density), 3 (mildly reduced nerve fiber density) and 4 (normal nerve fiber density) were provided for each image. All study images were analysed

in a blinded fashion twice to assess reliability and reproducibility. This method can differentiate groups of healthy patients from sick ones.

In addition, we quantify also the epidermal nerve fiber (ENF) density (number of un-myelinated fibers per linear millimeter of epidermis) that it was calculated by considering single PGP-immunoreactive (PGP-ir) epidermal nerve fiber crossings of the dermal-epidermal junction. Digital images were acquired using a laser-scanning confocal microscope Nikon A1, Tokyo, Japan. Each image was collected in successive frames of 1- to 2-μm increments on a *Z*-stack plan at the appropriate wavelengths for fluorophores, with a 40x or 60x plan apochromatic objective, and subsequently projected to obtain a 3-dimensional image by a computerized system (Nis Elements Viewer; Nikon).

2.4 Statistics

Data are shown as 'mean ± SEM', unless differently indicated. For the analysis of significance, unpaired Student's *t*-test was used, with P values <0.05 (*), < 0.01 (**) and < 0.001 (***) considered statistically significant.

For the skin innervation density it has been used the Mann-Whitney U test to compare 1) somatic (i.e. epidermal) and autonomic innervation scores between patients and controls; 2) somatic and autonomic scores between patients with somatic and autonomic peripheral neuropathies; and 3) autonomic scores between subgroups of autonomic neuropathy patients. The diagnostic yield of skin biopsy in evaluating somatic and autonomic innervation abnormalities was estimated using the area under the receiver operating characteristic curve. Correlations between somatic and autonomic innervation and between fiber density and length were assessed using Spearman correlation coefficient analysis. Interclass correlation coefficients were calculated to assess reliability within and between examiners of autonomic innervation method for both fiber density and length. A value of $p < 0.05$ was considered significant.

Table 2. Primary antibodies

Primary antibodies

Target	Company	Diluition	Host species
TOH policlonal	Millipore	1:600	rabbit
SYN1a policlonal	Millipore	1:1000	rabbit
Collagen I	Acris	1:100	rabbit
collagen IV	Millipore	1:800	mouse
PGP 9.3	Abcam	1:500	Mouse and rabbit
vasointestinal peptide (VIP)	Immunostar	1:1000	rabbit
ChAT	Chemicon	1:200	Anti-rabbit

3. Results

3.1 Generation and characterization of a novel transgenic mouse model with Opa1 haploinsufficiency in sympathetic neurons

To define the role of the mitochondrial protein Optic atrophy factor-1 (Opa1) in the regulation of cardiac sympathetic innervation, we generated a novel mouse model haploinsufficient for Opa1 selectively in tyrosine hydroxylase (TOH) expressing neurons. These mice were obtained by crossing homozygous mice expressing the cre-recombinase enzyme under control of the TOH promoter (B6.129X1-Th<tm1(cre)Te>/Kieg), with homozygous loxP-Opa1 mice. Both transgenic lines have previously been characterized (Lindberg *et al.,* 2004; Cogliati *et al.,* 2013). In our double transgenic mice, both transgenes are expressed in heterozygosity, and the expression of cre-recombinase, by promoting recombination at the loxP sites, caused the deletion of the Opa1 encoding gene, selectively in TOH expressing neurons (TOH-Opa1$^{+/-}$) (**Fig. 1A**). Consistently, these mice showed a reduction of about 50% of Opa1 mRNA level in sympathetic ganglia, and this was accompanied by a 40% decrease in Opa1 protein content (**Fig. 1B-C**). No changes in Opa1 mRNA and protein content were observed in other organs (i.e. liver), thus supporting the cell-specificity of our genetic approach (data not shown).

Our novel TOH-Opa1$^{+/-}$ mice were fertile and the life expectancy was unchanged, compared to sex- and age-matched controls. When we looked at heart function, echocardiographic analysis did not reveal significant changes in cardiac performance, which was assessed by evaluating the ejection fraction (EF, TOH-Opa1$^{+/-}$: 55.21±3.47 *vs* TOHcre$^{+/-}$: 46±2.98, in %; n=3 animals for each group) (**Fig. 2A**) and the fractional shortening (FS, TOH-Opa1$^{+/-}$: 32±5.98 *vs* TOHcre$^{+/-}$: 31.45±6.3, in %; n=3 animals for each group). In line with this, standard histological analyses did not reveal significant morphological alterations (i.e. no signs of CM death; fibrosis, etc) (**Fig. 2B-C**). Since these mice display haploinsufficiency of Opa1 in sympathetic neurons (SN), we evaluated whether this impacts on SN density and myocardial innervation pattern. Confocal IF analysis demonstrated an impairment of cSN morphology and myocardial distribution in adult (6mo.) TOH-Opa1$^{+/-}$, compared to relative controls. In detail,

Opa1 haploinsufficient cardiac SNs (cSNs) were more fragmented with increased sprouting of the neuronal processes limited to some focal myocardial areas (**Fig. 3A)**. In this study we focused our attention on the left ventricle (LV), and the morphometric analysis demonstrated a significant decrease of SN density (TOH positive fibers area/total myocardial area: adult TOH-Opa1$^{+/-}$: 1.14±0.036 *vs* TOHcre$^{+/-}$ mice: 1.86±0.081, in %; n=6 animals for each group) (**Fig. 3B**).

This phenotype resembles the myocardial innervation aspects observed during ageing, a physiological process associated to neurodegeneration (our unpublished data). Interestingly, the morphology of cSNs in aged (24mo.) TOH-Opa1$^{+/-}$ hearts was comparable to that described in the adult ones. Moreover, although in both control and TOH-Opa1$^{+/-}$ mice ageing caused a decrease in SN density, this worsened in the latter experimental group (TOH positive fibers area/ total area: aged mice TOH-Opa1$^{+/-}$: 0.83±0.09 *vs* TOHcre$^{+/-}$: 1.28±0.21, in %; n=6 animals for each group) (**Fig. 3B**).

Interestingly, by comparing the morphometric data from the different study groups, we observed that cardiac SN density in adult TOH-Opa1$^{+/-}$ mice was comparable to that measured in the normal aged myocardium. Thus, the alteration in SN structural phenotype and density suggests that reduction in Opa1 content by altering SN homeostasis, leads to heart precocius dysinnervation already in the adulthood.

The dysinnervation observed in the ventricles was confirmed in the atria, including the right one, where the sino-atrial node (SAN) is located (TOH positive fibers area/total myocardial area: adult TOH-Opa1$^{+/-}$: 1.28±0.075 *vs* TOHcre$^{+/-}$ mice: 2.67±0.31; aged mice TOH-Opa1$^{+/-}$: 0.79±0.09 *vs* TOHcre$^{+/-}$: 1.80±0.037, in %; n=6 animals for each group) (**Fig. 3C-D**).

In conclusion, we generated a novel transgenic mouse model of selective Opa1 haploinsufficiency in SNs, to dissect the role of this mitochondrial protein in cardiac innervation. Our results suggest that Opa1 is required for cSN to correctly develop and innervate the myocardium. To further assess this, we implemented the characterization of these mice by evaluating SN function, through functional assays based on the use of telemetry.

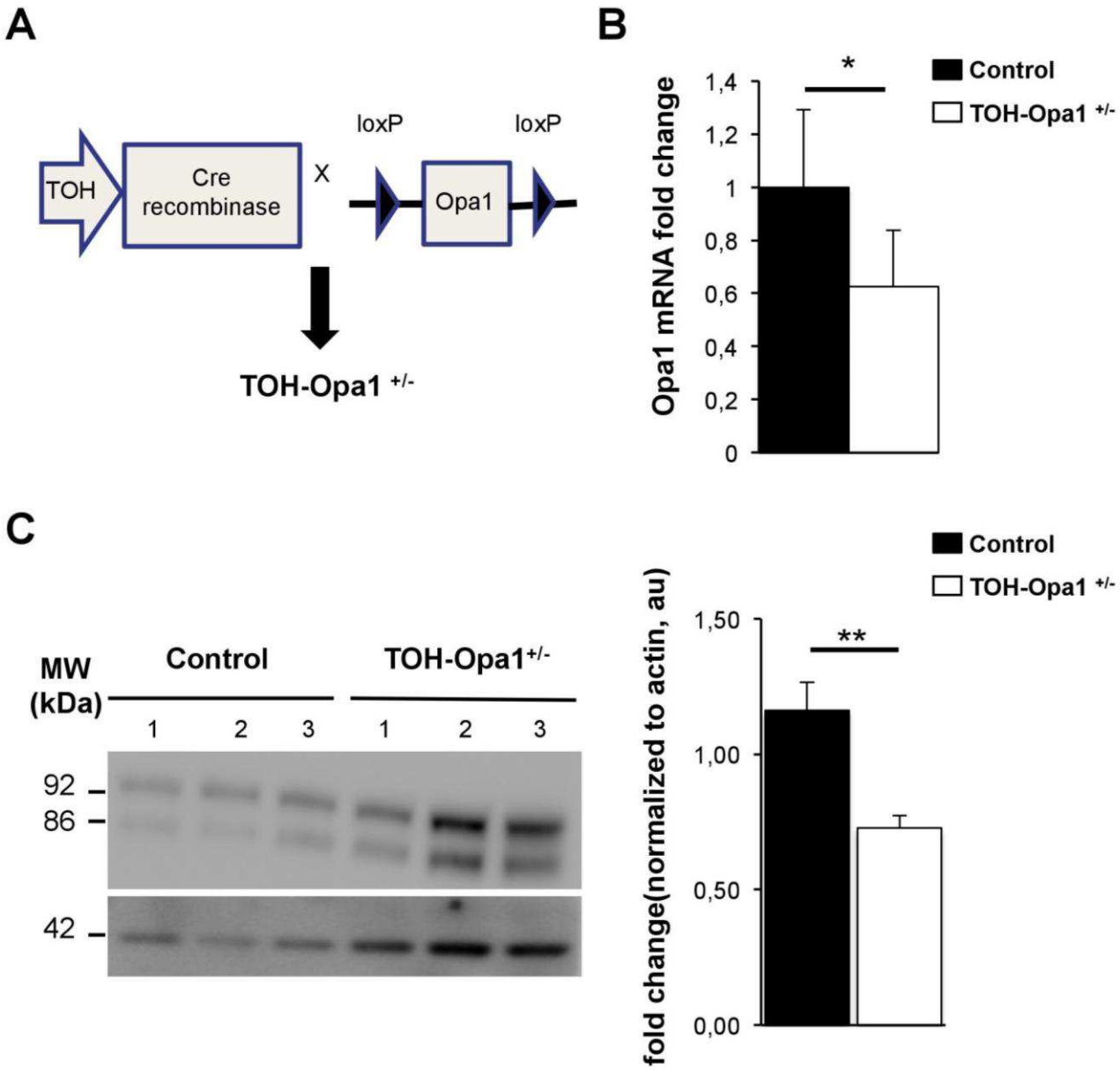

Figure 1: Generation of transgenic mice haploinsufficient for Opa1 in TOH neurons.

(**A**) Opa1 haploinsufficient mice (TOH-Opa1$^{+/-}$) have been generated by crossing homozygous mice expressing Cre-recombinase, under the control of tyrosine hydroxylase (TOH) promoter, with loxP-Opa1 homozygous transgenic mice. (**B-C**) RTqPCR (**B**) and western blotting (**C**) analyses on extracts from superior cervical ganglia. Bars in (**B**) and (**C**) represent s.e.m. (*, $p < 0.05$; **, $p < 0.01$; n=6 mice for each study group).

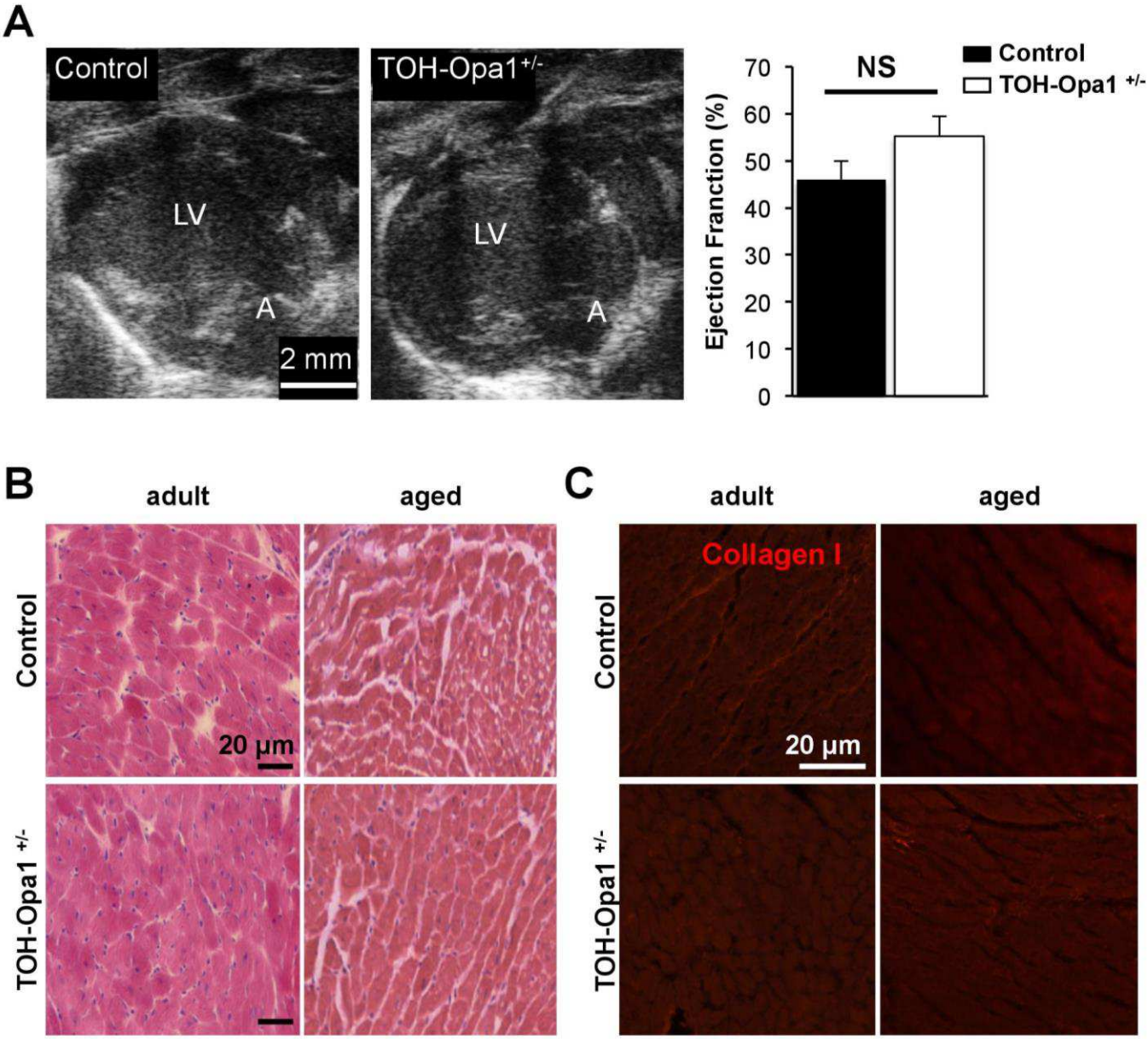

Figure 2. Characterization of cardiac function and morphology in TOH-Opa1$^{+/-}$ mice.

(**A**) Long-axis view (left panel), obtained during echocardiographic analysis, of control and TOH-Opa1$^{+/-}$ adult mice. (LV: left ventricle; A: atrium). The ejection fraction (right panel) was compared between control and transgenic mice. Bars represent the s.e.m. (NS: not significant; n=3 mice for each study group). (**B**) Haematoxylin-eosin staining on heart cryosections from adult and aged control and TOH-Opa1$^{+/-}$ mice. Images are details from the LV. (**C**) IF analysis on heart cryosections from adult and aged control and TOH-Opa1$^{+/-}$ mice stained with an antibody to collagen I. Images are details from the LV.

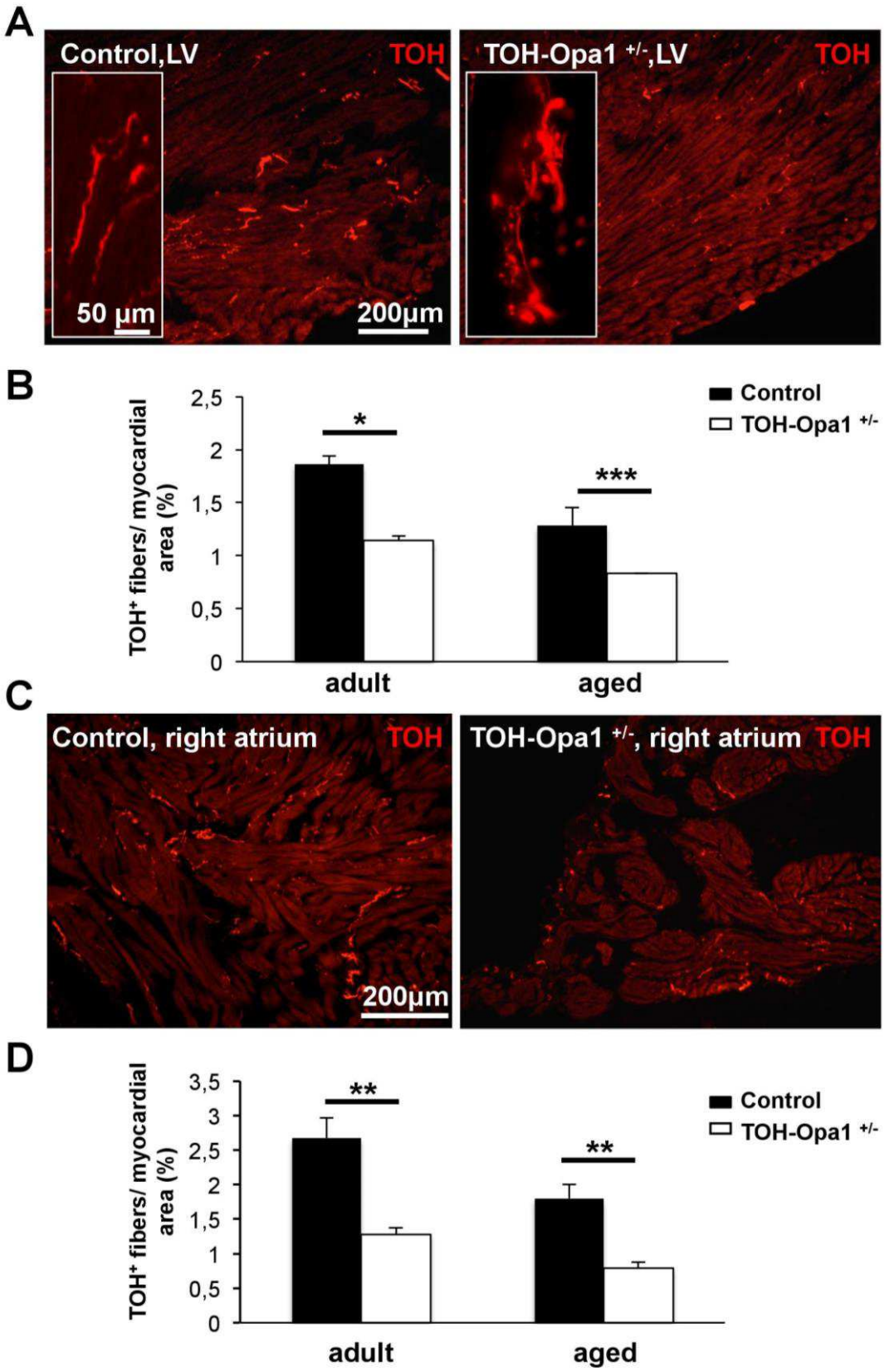

Figure 3. Characterization of cardiac autonomic innervation in TOH-Opa1$^{+/-}$ mice.

(**A** and **C**) IF analyses on ventricular (**A**) and right atrium (**C**) cryosections from adult control and TOH-OPA1$^{+/-}$ mice, stained with an antibody to TOH. (**B** and **D**) Evaluation of the percentage of myocardial area occupied by TOH-positive fibers in ventricular (**B**) and right atrium (**D**) sections from adult and aged mice. Bars represent the s.e.m. (*,$p<0.05$;**, $p<0.01$; ***,$p<0.0001$; n=6 mice for each study group).

3.2 Opa1 haploinsufficiency in sympathetic neurons leads to dysfunctional extrinsic control of cardiac rhythm

The autonomic nervous system (ANS) is the main extrinsic regulator of heart activity during stresses, such as exercise or emotions, but also in basal conditions. The noradrenaline (NE) input to SAN cells leads to increase in heart rate (HR), while NE binding to β–adrenoceptors (β-AR) expressed by working cardiomyocytes (CMs) results in the rise of the contraction force. In basal conditions, the constitutive SN input is required to modulate HR on a beat-to-beat basis. This parameter is known as Heart Rate Variability (HRV), and reflects the balance between the activity of the sympathetic and the parasympathetic branches of the ANS acting on the SAN cells.

To investigate the functional consequences of heart dysinnervation in TOH-Opa1$^{+/-}$ mice, we performed telemetry-based ECG analysis, and the following parameters were evaluated:

i) the HR during the entire day;

ii) the morphological phenotype of the depolarization waves (PR, QRS);

iii) the HRV.

Our analyses did not evidence significant differences in HR in adult and aged TOH-Opa1$^{+/-}$ mice, compared to age-matched controls (HR, adult, TOH-Opa1$^{+/-}$: 557.00±17.30 *vs* TOH-cre$^{+/-}$: 591±18.19; aged, TOH-Opa1$^{+/-}$: 633.76±31.60 *vs* TOHcre$^{+/-}$: 664.00±7.99, in BPM; n=3 animals for each group). Similarly, the morphology of PR and QRS segments was unchanged among our experimental groups (PR, adult TOH-Opa1$^{+/-}$: 35.73±0.41 *vs* TOH-cre$^{+/-}$: 35.13±0.46; aged TOH-Opa1$^{+/-}$: 34.20±0.02 vs TOH-cre$^{+/-}$: 35.31±5.30, in ms) (QRS, adult TOH-Opa1$^{+/-}$: 7.61±0.16 *vs* TOH-cre$^{+/-}$: 8.41±0.27; TOH-Opa1$^{+/-}$: 7.95±0.16 vs TOH-cre$^{+/-}$: 7.11±1.18, in ms; n=3 animals for each group) (**Fig. 4A-B**).

On the contrary, the HRV was significantly reduced in both adult and aged TOH-Opa1$^{+/-}$ mice, compared to controls (SDNN, adult TOH-Opa1$^{+/-}$: 3.62±0.46 *vs* TOHcre$^{+/-}$: 6.17±0.37; aged TOH-Opa1$^{+/-}$: 1.17±0.19 *vs* TOHcre$^{+/-}$: 3.86±0.60, in ms; n=3 animals for each group) (**Fig. 4C-D**). These results suggest a dominance of the parasympathetic branch of the ANS over the sympathetic tone and are in line with the sympathetic dysinnervation of the myocardium observed by immunofluorescence (IF) and morphometric analyses.

To confirm this data, we performed a pharmacological assay based on the use of atropine (2mg/kg, ip). Atropine is a muscarinic receptor antagonist, thus ablating the activity of the parasympathetic component on HR. As a consequence, in normal condition atropine administration results in HR increase (Zaglia *et al.,* 2013). When we compared the extent of HR increase in adult TOH-Opa1$^{+/-}$ *vs* control mice, we observed a significant reduction in the positive chronotropic response in TOH-Opa1$^{+/-}$ mice (Δ, adult TOH-Opa1$^{+/-}$: 13.68±1.68 *vs* TOH-cre$^{+/-}$: 19.89±2.23, in %; n=3 animals for each group). Such results were confirmed in the aged mice (Δ, aged TOH-Opa1$^{+/-}$: 6.7±1.2 *vs* TOH-cre$^{+/-}$: 11.3±3.2, in %; n=3 animals for each group) (**Fig. 5A**). In striking similarity with our morphological data, the response to atropine observed in the adult TOH-Opa1$^{+/-}$ mice was comparable to that observed in the control aged mice, thus confirming that Opa1 haploinsufficiency accelerates SN degeneration.

The analysis of ECG traces, acquired upon atropine administration, also revealed an increase in the incidence of Premature Ventricular Contractions (PVCs) in aged TOH-Opa1$^{+/-}$ mice (**Fig. 5B**). This latter evidence is consistent with the effect of altered cSN patterning, which has previously been associated to increased arrhythmogenesis (see INTRODUCTION,pag.48-49 Chen P.S. *et al.,* 2001).

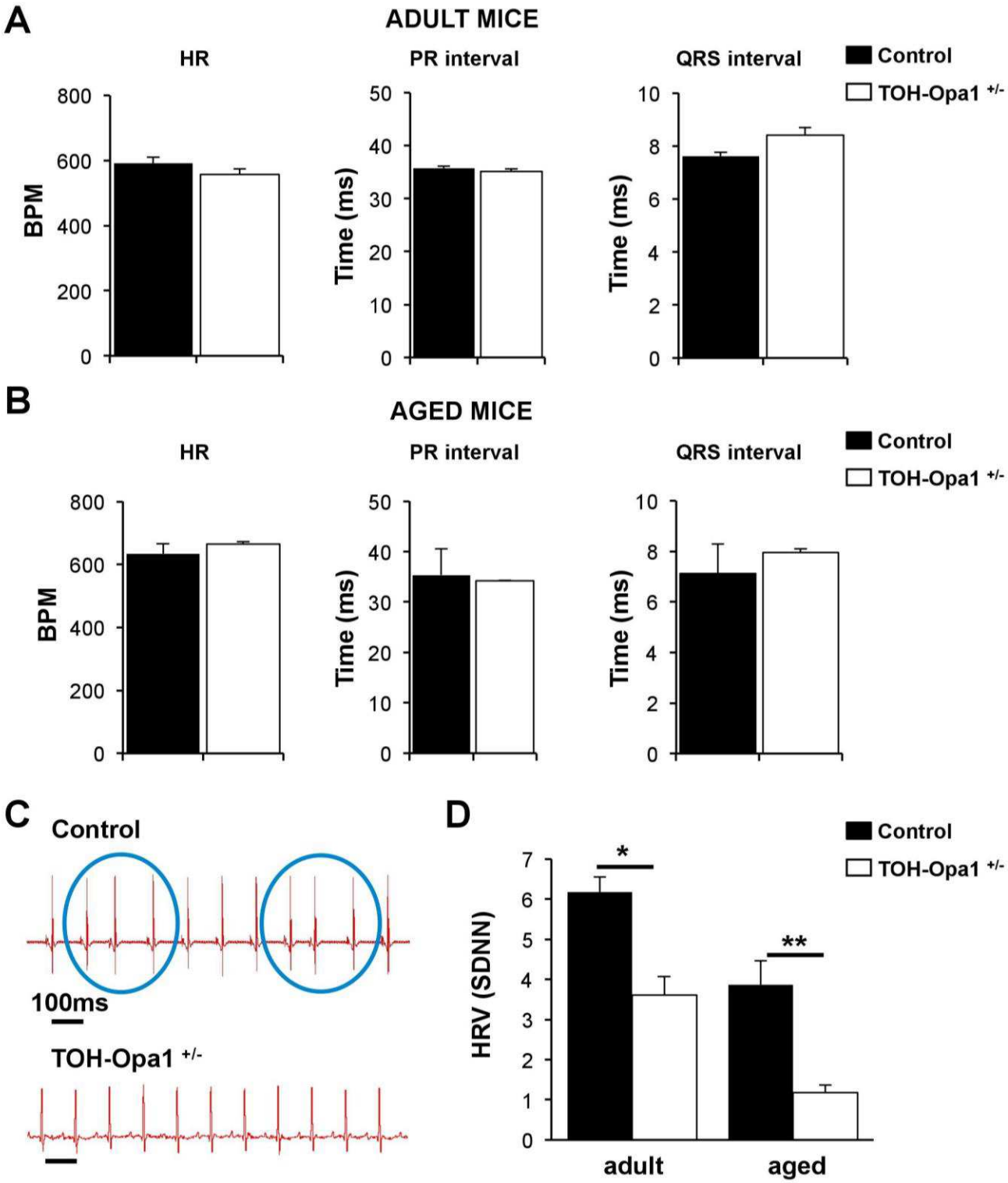

Figure 4: Electrocardiographic characterization of adult and aged TOH-Opa1$^{+/-}$ mice.

(**A**-**B**) Evaluation, performed by telemetry-based ECG analysis, of: heart rate (HR, in beats per minute, BPM); PR interval (in ms); QRS interval (in ms) in adult (**A**) and aged (**B**) control and TOH-OPA1$^{+/-}$ mice (**C**) Representative ECG traces from aged control and TOH-Opa1$^{+/-}$ mice. The blue circles evidence RR intervals of different duration. (**D**) Statistics of the evaluation of Heart Rate Variability (HRV), expressed in the time domain (ms) by the standard deviation (SDNN) of RR intervals between beats, in adult and aged control and TOH-Opa1$^{+/-}$ mice. The bars in (**A**), (**B**) and (**D**) indicate the s.e.m. (*, $p<0.05$; **, $p<0.01$; n=3 mice for each group;).

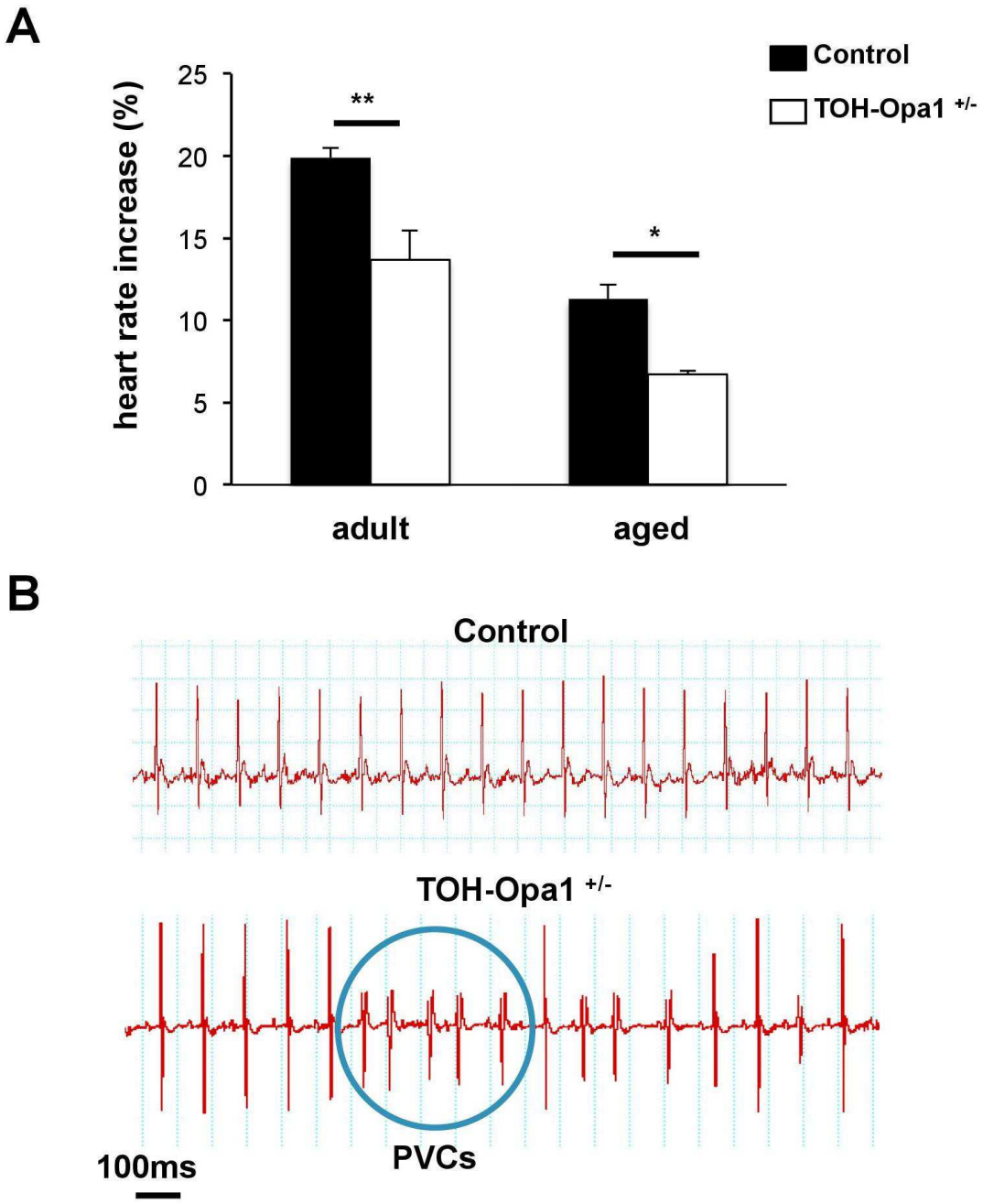

Figure 5: Functional assessment of autonomic cardiac innervation and arrhythmogenesis in TOH-Opa1$^{+/-}$ mice.

(**A**) Evaluation of the percentage of Heart Rate (HR) increase upon atropine administration (2mg/kg, IP) in control and TOH-Opa1$^{+/-}$ adult and aged mice (BPM, beats per minute). Bars indicate the s.e.m. (*, $p<0.05$; **,$p<0.01$; n=3 mice for each group). (**B**) ECG traces from aged control and TOH-Opa1$^{+/-}$ recorded upon atropine administration. The blue circle highlights a Premature Ventricular Contraction (PVC), occurring in TOH-Opa1$^{+/-}$ mice upon atropine administration.

3.3 ADOA patients display degeneration of cutaneous sympathetic neurons

Altogether, our findings, accrued in the murine model, show that reduced Opa1 content in cardiac SN neurons leads to their degeneration, resulting in altered neurogenic control of heart function and arrhythmias. This prompted us to evaluate whether this occurred also in Autosomal Dominant Optic Atrophy (ADOA) patients, potentially explaining the evidence of unexplained arrhythmias described in case reports.

To evaluate whether ADOA patients had signs of abnormal sympathetic innervation, we analyzed the morphology and density of peripheral SNs in skin biopsies collected from a cohort of 25 ADOA patients (from 20 to 70 years old) currently enrolled in clinical follow-up at the Istituto delle Scienze Neurologiche, Bologna. Skin biopsies represent an easily accessible viewpoint on peripheral autonomic innervation, as SNs innervate the sweat gland and the *arrector pili* muscles. In detail, we used IF staining in serial cryosections co-stained with a pan neuronal and anti-DA-β-OH antibodies (**Fig. 6A**).

In line with our preclinical data, the skin of ADOA patients showed a significant reduction in the density of SN fibers, which was more pronounced in the older subjects (**Fig. 6B**). Interestingly, this was accompanied by the decrease in epidermal nerve fiber density, which is a common biomarker for the diagnosis of small-fiber peripheral neuropathy (**Fig. 6C**). Although this data results from the analysis of the SNS in a sector different from the heart, it clearly demonstrates that sympathetic neurodegeneration takes place in ADOA patients. Together with our preclinical data, this evidence strongly supports that patients may develop cardiac dysinnervation, which could be the cause of increased arrhythmogenesis, and represent therefore a novel pathogenetic mechanism and clinical finding in ADOA.

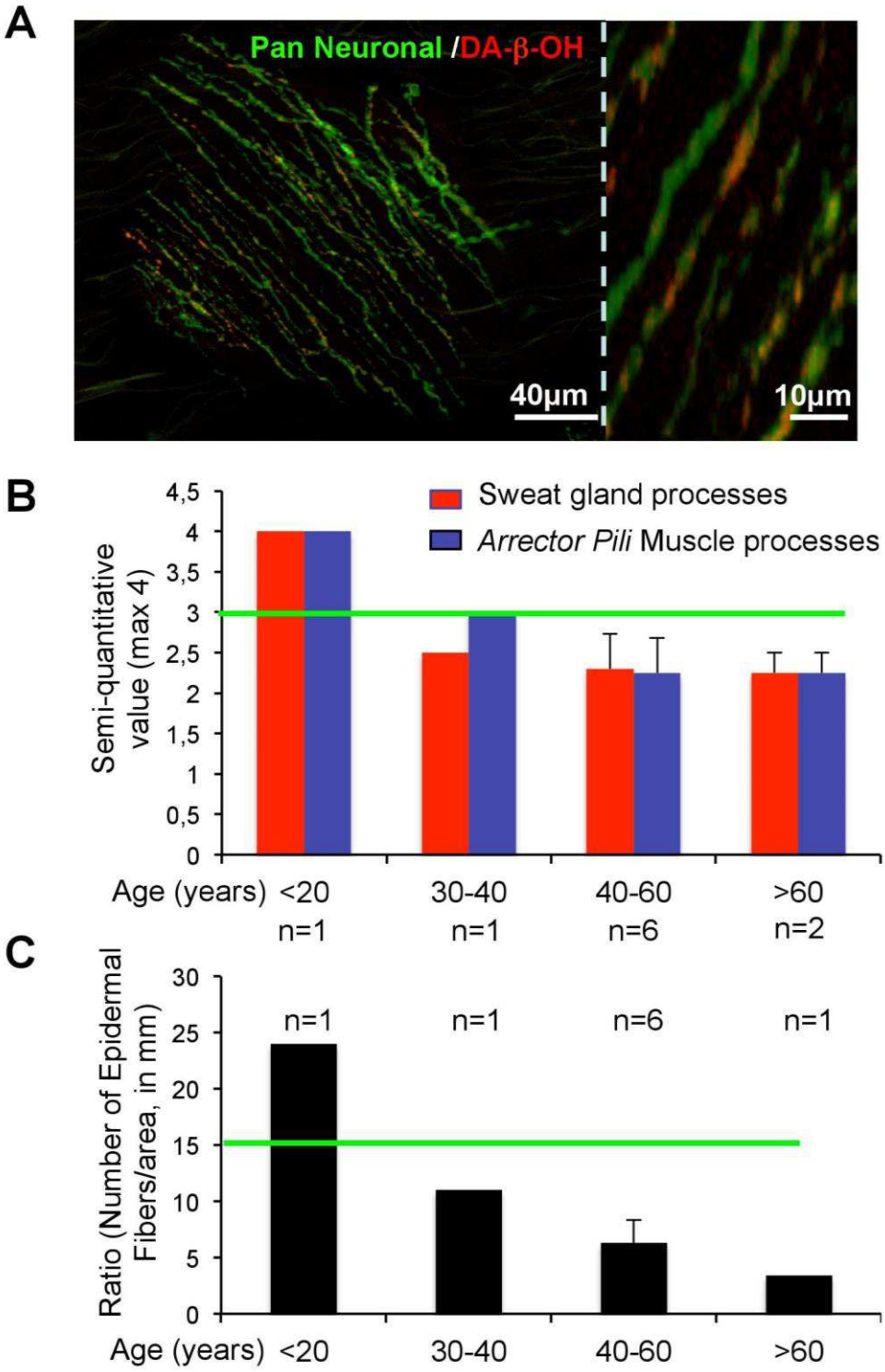

Figure 6: Characterization of skin autonomic innervation in biopsies from ADOA patients.

(**A**) Confocal IF analysis on human skin sections from healthy subjects, co-stained with antibodies to dopamine-β-hydroxylase (DA-β-OH) and neurofilament. The right panel shows a detail of the image in the left one. (**B**) Evaluation of the density of DA-β-OH positive fibers in skin biopsies from ADOA patients of different ages (from 20 to 60 years old). The green line identifies the threshold of the normal innervation density. (**C**) Evaluation of the density of neuronal epidermal fibers in the same samples analysed in (**B**). Bars indicate s.e.m. These analyses are in progress to increase the number of patients analysed.

4. Discussion and Perspectives

The results presented in this work demonstrate that a reduction in the cellular content of Opa1 affects cardiac sympathetic innervation, leading to dysfunction in the extrinsic control of heart rhythm and arrhythmias. Opa1 haploinsufficiency occurs in patients affected by Autosomal Dominant Optic Atrophy (ADOA), an autosomal genetic disease, which affects at least 1:25000 people in the population. The pathology leads to retinal ganglion cells degeneration causing blindness already in childhood (Fuhrmann *et al.,* 2009). Recent works demonstrated that ADOA patients also develop other systemic symptoms involving the peripheral nervous system, such as peripheral neuropathies, myopathies and heart rhythm abnormalities (Yu-Wai-Man *et al.*, 2010; Chao del la Barca *et al.*, 2016; Spiegel *et al*., 2016). The clinical finding that the degenerative consequences of ADOA are not confined to retinal ganglionic cells support the notion that Opa1 haploinsufficiency leads to damage of other peripheral neurons, including the autonomic neurons innervating the heart. Since alterations in cardiac sympathetic neurons (cSNs) are causally associated to arrhythmogenesis (Chen *et al.,* 2001), we made the hypothesis that heart dysinnervation may feature among the complex pathological manifestations occurring in ADOA and be responsible for heart rhythm disturbances.

This hypothesis was tested by generating a tissue specific murine model, in which Opa1 haploinsufficiency was limited to TOH-positive neurons. This model allowed isolate the effects of the same genetic mutation carried by all cells in ADOA patients, to the very restricted population of SNs which, importantly, are highly represented in the heart and responsible for the fine tuning of cardiac activity.

By combining morphological and functional assays, we demonstrated that Opa1 haploinsufficiency causes cSN degeneration, which appears in young mice and progresses with age. While the investigation of cardiac innervation is doable in experimental animal models, it is much more difficult to obtain such information in living patients. To translate our findings to the clinical scenario, we thus exploited the fact that the skin is highly innervated by SNs and biopsies can easily be obtained and studied. By comparing the morphology and density of skin SNs in healthy and diseased subjects, we demonstrated that peripheral sympathetic neurodegeneration occurs in ADOA patients. Interestingly imaging of neuronal

activity performed in few ADOA patients using scintigraphy, indicated the presence of dysinnervated areas of the myocardium.

Therefore, to strengthen the value of the comparison of the functional aspects of the neurogenic control of heart by SNs, we implemented in mice the same clinically accepted analysis of HRV indices. Our results indicated that there is a decrease in HRV, in line with the myocardial dysinnervation. In addition, consistent with the neuronal fragmentation and increased axonal sprouting, our transgenic mice displayed increase incidence of arrhythmic events. These analyses allow translate the functional evidence accrued in the mice to the human and, to this purpose, the same patient cohort enrolled for the analysis of skin innervation will undergo prolonged ECG Holter analysis to evaluate HRV and arrhythmias. Altogether our results expand the understandings on ADOA pathophysiology, providing the first piece of evidence that the decrease in Opa1 compromise not only central, but also peripheral autonomic neurons.

We are aware of the major limitations of our study, which will be subject of the immediate developments of the research. These include the ultrastructural analysis of the mitochondrial morphology in SNs, and the study *in vitro* of signalling pathways regulating cell survival. Considering this latter point, we will test the hypothesis that reduction in Opa1 content compromises the retrograde transport of neurotrophins, mainly NGF, from the neuronal varicosities to the soma, which is crucial for neuronal survival.

The results of the first project presented in this thesis demonstrated that SNs establish a structured junction (neurocardiac junction) with target cardiomycoytes (CMs), allowing a ‘quasi-synaptic’ intercellular communication. In a parallel project, we demonstrated that the neurocardiac junction not only mediates the communication from SN to target CM (anterograde signalling), but is also required for the efficient release of neurotrophins from CMs to the innervating neuronal varicosities. In detail, we demonstrated that CMs sustain neuronal viability and trophism by releasing NGF selectively into the synaptic cleft, where it reaches high concentration levels (Franzoso *et al.* manuscript in preparation). Upon binding to the TrkA receptors, which concentrate in the portion of the neuronal varicosity interacting with CM membrane, NGF is internalized into the neuron and transferred, by retrograde transport, to the neuronal soma, where it activates pro-survival signalling pathways (Kim *et al.,* 2014). All these processes require ATP.

Based on the evidence that Opa1 haploinsufficiency in central neurons compromises ATP synthesis (Lodi *et al.,* 2004), we will test whether SNs isolated from TOH-Opa1$^{+/-}$ mice show a difective NGF-TrkA retrograde transport. However, the alteration of this pathway could not be the sole mechanism responsible for SN degeneration in TOH-Opa1$^{+/-}$ mice. Alternative hypothesis, involving alterations in intracellular Ca^{2+} dynamics and increased ROS production will be considered. In addition, it will be interesting to assess whether Opa1 has a role in the correct SN-to-CM communication and in the maintenance of the structured neuro-cardiac junction.

Finally, we are aware that central SNs are involved in behavioural and movements control and as such our future studies will be focussed in the evaluation of the effects of cell-type specific central neurodegeneration.

OVERALL CONCLUSIONS

During my PhD training I had the opportunity to learn important techniques going from *in vitro* to *in vivo* methods. In particular, I have been involved in the development of neuronal optogenetics in the intact heart during the first project, but also I had the possibility to study a human genetic pathology and started a clinical study.

The collaboration with other groups, the feedback obtained during meetings followed and the interaction and discussion with my supervisors, offered me the possibility to carry on my scientific research project with new ideas and results interpretations.

In particular, *in vitro* data using SN-CM co-culture model and the achievement of the first example of *in vivo* optogenetic stimulation of sympathetic efferents in the intact heart, allowed to add further proves of the *quasi-synaptic* functional interaction between SNs and CMs. In the second project, I identified a possible pathological basis of cardiac involvement in dominant optic atrophy (ADOA), suggesting also a new insight in the possible pathological mechanisms involved in neurodegeneration, which it will be investigated in the near future experiments.

PhD COURSE ACTIVITIES

1. List of manuscripts

1. **Valentina Prando***, Francesca Da Broi*, Mauro Franzoso*, Anna Pia Plazzo*, Nicola Pianca, Maura Francolini, Cristina Basso, Matthew Kay, Tania Zaglia[#] and Marco Mongillo[#]. (2017). Dynamics of neuro-effector coupling at 'cardiac sympathetic' synapses. Under revision: *JP-SRRP-2017-275693X*; *,#, equal contribution

2. Zaglia T.*, Ceriotti P.*, Campo A.*, Borile G.*, Armani A., Carullo P., **Prando V.**, Coppini R., Vida V., Stølen T. O., Ulrik W., Cerbai E., Stellin G., Faggian G., De Stefani D., Sandri M., Rizzuto R., Di Lisa F., Pozzan T., Catalucci D. and Mongillo M. (2017). The content of mitochondrial calcium uniporter (MCU) in cardiomyocytes is dynamically regulated by miR-1 in physiologic and pathologic cardiac hypertrophy. Proc Natl Acad Sci USA (in press)

3. **Prando V.,** Pianca N., Di Bona A., Franzoso M., Campo A., Incensi A., Donadio V., Scorrano L., Carelli V., Mongillo M.* and Zaglia T.*. Role of the mitochondrial protein Opa1 in the regulation of cardiac sympathetic neurons physiology. Manuscript in preparation.

4. Pianca N., Di Bona A., **Prando V.,** Franzoso M., Armani A., Campione M., Basso C., Sandri M., Zaglia T.*, Mongillo M*. Sympathetic neurons shape myocardium trophism through a direct intercellular signalling with cardiomyocytes that acts on proteolysis rate. Manuscript submitted

5. Franzoso M., Zaglia T, Pianca N., Di Bona A., **Prando V.,** Basso C., Vitiello L. and Mongillo M. The neuro-cardiac interaction defines an extracellular microdomain required for neurotrophic signalling. Manuscript in preparation.

6. **Prando V**, Perry T., Pianca N., Franzoso M., Pesce P., Braghetta P., Willis M., Bonaldo P., Sandri M., Mongillo M. and Zaglia T. Muscle Ring Finger-1 (MuRF1) is required to prevent age-related cardiac hypertrophy and

interstitial remodeling. Manuscript submitted.

7. **Prando V***, Favaro G.*, Lo Verso F.*, Bertoli S., Di Mauro V., Soares R., Pianca N., Pesce P., Catalucci D., Mongillo M., Sandri M. and Zaglia T. Role of miR206 in the regulation of myocardial innervation and of targeted cardiomyocytes. Manuscript in preparation.

2. Selected Oral Presentations:

- Dysfunction in the mitochondrial Optic Atrophy-1 protein (Opa1) alters the neurogenic control of heart function. **ES-ISHR,** (July 2017, Hamburg, Germay)**.**
- Role of the mitochondrial protein Opa1 in the regulation of the cardiac sympathetic neuron physiology, **VIMM Retreat**, (February, 2017, Preganziol, Italy).
- Role of the mitochondrial protein Opa1 in the regulation of the cardiac sympathetic neuron physiology, **FCVB 2016**, (July, 2016, Florence, Italy).
- Role of the mitochondrial protein Opa1 in the regulation of the function and survival of cardiac sympathetic neuron. **Pre- congress ABCD meeting** (Sept, 2015, Bologna, Italy).

3. Awards:

- 2017: **Finalist for Young Investigator Award**, ES-ISHR Congress, Hamburg
- 2016: **Best Poster Presentation**, VIMM Retreat, TV
- 2015: **Travel grant** for ABCD Congress Bologna

Dynamics of neuro-effector coupling at 'cardiac sympathetic' synapses

Valentina Prando*, Francesca Da Broi*, Mauro Franzoso*, Anna Pia Plazzo*, Nicola Pianca, Maura Francolini, Cristina Basso, Matthew Kay, Tania Zaglia# and Marco Mongillo#

ABSTRACT

Aim: Cardiac sympathetic neurons (SNs), through the release of noradrenaline, finely tune the rate and strength of heart contractions to match the blood demand, both at rest and during acute stresses. Junctional sites at the interface between the two cell types have been observed, but whether direct neuro-cardiac coupling has a role in heart physiology has not been clearly determined thus far.

Methods and Results: The aim of this study has been to investigated the dynamics of SN/cardiomyocyte intercellular signaling communication, both by FRET-based imaging of cAMP in co-cultures, as a readout of cardiac β-AR activation, and *in vivo*, using optogenetics in transgenic mice with SN-specific expression of Channelrhodopsin-2. We demonstrate that SNs and cardiomyocytes interact at specific sites both in the human and rodent heart, and in co-cultures. Accordingly, neuronal activation elicited intracellular cAMP increases only in directly contacted myocytes and cell-cell coupling utilized a junctional extracellular signaling domain with elevated noradrenaline concentration. In the living mouse, optogenetic activation of cardiac SNs, innervating the sino-atrial node, resulted in the instantaneous chronotropic effect, which shortened the heartbeat interval with single beat precision. The dose of the β-blocker propranolol inhibiting the effect of photoactivation was much higher than that blocking circulating catecholamines, thus indicating that sympathetic neurotransmission in the heart occurs at locally elevated noradrenaline concentration.

Conclusions: Our *in vitro* and *in vivo* data suggest that the control of cardiac function by SNs, thanks to the establishment of a specific intercellular junctional-site, relies on 'quasi-synaptic' intercellular communication. The closely juxtaposed membranes of neurons and cardiomyocytes outline an extracellular signaling domain allowing activation of the β-ARs localized within the junctional space high

with [NE]. The very small volume of such domain allows a single neuronal action potential to release a [NE] sufficient to trigger detectable cAMP increase in the coupled cardiomyocytes.

(Journal of Physiology, UNDER REVISION, JP-SRRP-2017-275693X)

Role of the mitochondrial protein Opa1 in the regulation of the cardiac SN physiology.

Prando V., Pianca, N. Di Bona A., Franzoso M., Campo A., Incensi A., Donadio V., Scorrano L., Carelli V., Mongillo M. and Zaglia T.

ABSTRACT

Purpose: Cardiac sympathetic neurons (cSNs) are the main extrinsic regulators of heart function in physiologic and stress conditions. Neuronal viability and activity depend on the correct mitochondrial function. Opa1 controls mitochondrial fusion, ATP production and apoptosis and its haploinsufficiency causes Autosomal Dominant Optic Atrophy (ADOA), a neurodegenerative disease characterized by retinal ganglion cell death, leading to visual loss already in childhood. ADOA patients also display peripheral neuropathy and cardiac rhythm alterations but the mechanism linking Opa1 dysfunction and heart abnormalities has not been investigated yet. Our **purpose** is to establish the role of Opa1 in the neurogenic regulation of heart function.

Methods: We generated a mouse model haploinsufficient for Opa1 selectively in cSNs (TOHcre-Opa1$^{+/-}$). We performed telemetry-based ECG recording and pharmacological assays *in vivo*, confocal immunofluorescence and morphometric analysis to characterize sympathetic innervation in mouse hearts and skin biopsies from ADOA patients.

Results: Opa1 haploinsufficiency leads to a decrease in cSN density, which starts in the adulthood but it is also present during ageing. This is accompanied to alterations in cSN distribution patterning and morphology. Cardiac dysinnervation in TOHcre-Opa1$^{+/-}$ mice results in a significant decrease in heart rate variability and increased propensity to arrhythmias developments. Consistently, we detected decreased SN density in skin biopsies from ADOA patients, which progresses during ageing.

Conclusions: Our data demonstrate that the Opa1 is essential for cSN homeostasis and indicate that its haploinsufficiency leads to cSN degeneration. The cSN dysinnervation causes the dysfunction of the extrinsic control of cardiac rhythm. The mechanisms responsible for Opa1 haploinsufficiency-dependent cSN

degeneration will be assessed *in vitro*, with a focus on the NGF signalling. To translate our findings to the human pathology, we will analyse SN phenotype in skin biopsies from ADOA patients.

(1) Zaglia et al. Cardiovasc Res 2013

OTHER KEY PROJECTS FOLLOWED DURING THE PhD

Muscle Ring Finger-1 (MuRF1) is required to prevent age-related cardiac hypertrophy and interstitial remodeling

Prando V., T. Perry, N. Pianca, M. Franzoso, P. Pesce, P. Braghetta, M. Willis, P. Bonaldo, M. Sandri, M. Mongillo and T. Zaglia

Purpose: The Ubiquitin Proteasome System (UPS) is a selective degradation system mediating the removal of intracellular unfolded/misfolded proteins, and is essential for cardiomyocyte (CM) health. Substrate specificity and ubiquitination rate are ensured by E3 ubiquitin-ligases, such as Atrogin1 and MuRF1, which are specifically expressed in muscle cells. Perturbation of protein quality-control causes aggregation of misfolded proteins, leading to CM proteotoxicity. UPS dysfunction occurs in ageing, an important risk factor in the development of cardiac hypertrophy and heart failure. We recently demonstrated that correct proteostatic control, by Atrogin-1, is essential to maintain CM health during ageing (1). **Whether MuRF1 plays similar roles in heart adaptation to ageing is still unexplored, and different studies have yielded contrasting results.**

Methods: To assess the role of MuRF1 in the regulation of heart homeostasis, we combined echocardiography, histology, IF, TUNEL assay and electron microscopy on heart sections from MuRF1 knock-out (KO) mice, and littermate controls, at different ages (3, 10, 24 months). RTqPCR and WB assessed markers of UPS and extracellular matrix. Ex vivo heart perfusion using the Langendorff procedure was used to separate CMs from cardiac fibroblasts. Modulation of MURF1 was performed in cultured CMs, with the aim to uncover novel MuRF1 targets.

Results: Genetic ablation of MuRF1 leads to cardiac hypertrophy that, while still compensated in the young mice, progresses into maladaptive myocardial remodelling, during ageing, without affecting mouse lifespan. (CM areas in the LV: 3 mo., KO: 329.14±10.66 vs Ctrl: 296.25±5.43; 10 mo., KO: 399.73±7.64 vs Ctrl: 247.49±3.67; 24 mo., KO: 418.89±11.10 vs. Ctrl: 209.93±4.48, in μm2) (EF, 3 mo., KO: 62.50±3.82 vs Ctrl: 59.33±4.68; 10 mo., KO: 46.96±0.33 vs Ctrl: 53.45±2.50; 24 mo., KO: 29.55±8.82 vs Ctrl: 51.23±6.56, in %). Loss of MuRF1 increased

interstitial collagen I and collagen VI deposition, even before the onset of contractile dysfunction, and is followed by activation of Matrix MetalloProteinases, suggesting that such alterations may be responsible for the ageing-associated decreased cardiac performance in MuRF1 KO mice. Interestingly, interstitial fibrosis was not caused by increased CM apoptosis, nor myofibroblast activation and proliferation, supporting that MuRF1 has a role in CM-dependent regulation of the extracellular matrix dynamics. Modulation of MuRF1 in normal cultured neonatal CMs demonstrated that such ubiquitin ligase impacts on CM signalling pathways involved in the control of the homeostasis of the myocardial interstitium

Conclusions: Our data identify a novel role of MuRF1 in the control of CM proteostasis, unveil that in addition to cardiac fibroblasts, CM directly contribute to the regulation of ECM dynamics, and indicate that the correct function of MuRF1 is essential to heart adaptation to aging.

(1) Zaglia et al. JCI 2014

Role of miR206 in the regulation of myocardial innervation and of targeted cardiomyocytes

Prando V.*, Favaro G.*, Lo Verso F.*, Bertoli S., Di Mauro V., Soares R., Pianca N., Pesce P., Catalucci D., Mongillo M., Sandri M. and Zaglia T.

Background: The skeletal and the cardiac (i.e. myocardium) muscles are both striated muscles able to contract: skeletal muscle contraction underlies the voluntary locomotion, while heart contraction is required for the continuous supply of oxygen and nutrients to the different body tissues, including the muscle. As a consequence, the heart activity directly impacts on skeletal muscle performance. As an example, during exercise, the heart enhances its contractile activity to sustain the increased muscle oxygen requirement. Recently, several studies have brought to the light the concept whereby the skeletal muscle may influence, by acting through paracrine mechanisms, the structure and function of distal organs, including the heart. In particular, these researches strongly support the notion of the skeletal muscle as a secretory organ: indeed, these studies demonstrate that muscle fibers may release, into the bloodstream, microvesicles and exosomes containing myokines and microRNAs which impact on the homeostasis of distal tissues (*Pedersen, 2011*). The existence of a communication 'from the skeletal muscle to the heart' is also strongly supported by the evidence that patients affected by muscular (e.g. Duchenne Muscular Dystrophy) or neuro-muscular (e.g. Amiotrophic Lateral Sclerosis) diseases develop, in time, cardiomyopathies. However, at the time being, the molecular mechanisms underlying 'muscle to heart' communication are still unknown.

Recent work and preliminary observations, from the laboratory of our collaborator Prof. Sandri (Venetian Institute of Molecular Medicine, University of Padova), have shown that the muscle-specific genetic ablation of the autophagy-related protein, Atg7, leads to block of autophagy, which results in muscle sarcopenia and in the destabilization of the neuro-muscular junction (NMJ) (*Masiero et al., 2009; Carnio et al., 2014*). The block of autophagy leads to the increase in the secretion, by muscle fibers, of exosomes enriched in miR-206, a microRNA selectively expressed in the skeletal muscle and previously implicated

in the regulation of the NMJ structure and function (*Liu et al., 2012*). As a consequence, Atg7 knock-out mice show increased plasma levels of miR-206, NMJ destabilization accompanied to muscle denervation and, surprisingly, a significant increase in miR-206 expression in the myocardium.

Based on the literature, on our preliminary observations and on the evidence that the increase in the circulating miR-206 is a common denominator in several muscular disorders leading to cardiomyopathy, the aim of my work was ***to define the role of miR-206 in the 'skeletal muscle-to-heart' communication.*** In particular, the guiding hypothesis of this work is that increased plasma levels of miR-206, as occuring in pathologic conditions, result in miR-206 over-expression in the heart, where it compromises the myocardial autonomic innervation and, consequently, heart structure and activity.

Methods: To achieve this goal, we analyzed the function (by echocardiography and telemetry-based electrocardiography) and the structure (by histological and immunofluorescence analyses, morphometry, biochemical and molecular biology assays) of hearts from Atg7 knock-out mice and mice with increased miR-206 circulating levels, induced by intravenous injection of exosomes. To dissociate the signal pathways underling the phenotype observed in the intact heart, I performed *in vitro* assays (i.e. IF, western blotting, RTqPCR) in primary cultures of cardiomyocytes and cultures of sympathetic neurons.

Results: Overall, our findings demonstrate that miR-206 is a key mediator of the 'skeletal-to-cardiac muscle' communication. In particular, our data indicate that exosomes, released from damaged muscle fibers into the bloodstream, and containing miR-206, are captured in the heart by both cardiomyocytes (the contractile heart cells) and sympathetic neurons. Cardiac sympathetic neurons densely innervate the heart, moving within myocardial interstitium, and their activity is crucial to modulate heart activity, in both basal and stress conditions.
In cardiomyocytes, miR-206 over-expression causes: *i)* cell atrophy; *ii)* sarcomeric disorganization; *iii)* ultrastructural alterations mainly affecting the mitochondria and the sarcoplasmic reticulum and *iv)* alterations of the signal pathways downstream to □-adrenoceptors. Also in sympathetic neurons, the increased expression of miR-206 is accompanied by profound morphological alterations, including: *i)* atrophy of the active neurotransmitter release sites; *ii)* irregular distribution of the varicosities along the neuronal processes and *iii)* reduction in axonal sprouting. All

these alterations result, in the intact heart, in autonomic dysinnervation which causes a reduction in the extrinsic control of cardiac rhythm and an increased propensity to develop arrhythmias.

Conclusions: Thus, this work poses the bases for future studies aimed to define the signal pathways responsible for the miR-206-dependent structural and functional alterations in cardiomyocytes and sympathetic neurons. At present, we are focusing on the neuronal population and our preliminary data suggest that, in sympathetic neurons, miR-206 interferes with signal pathways essential for neuronal survival and function, such as those involved in the retrograde transport of NGF (Nerve Growth Factor) from sympathetic neuron varicosities to the neuronal soma. If successful, the results of these studies have the potential to define the molecular mechanisms involved in the 'muscle-to-heart' communication and to elucidate the pathogenesis of muscular and neuro-muscular disorders, associated to the development of cardiomyopathies. This latter aspect is of great scientific relevance, as there are no specific therapies effective in counteracting the progression of such diseases, that hesitate in the death of patients, already at a young age.

REFERENCES

1. Abilez O.J., Wong J., Prakash R., Deisseroth K., Zarins C.K., Kuhl E. Multiscale computational models for optogenetic control of cardiac function. *Biophys J.* 2011; **101**:1326-1334.
2. Akashi Y.J., Nef H.M., Lyon A.R. Epidemiology and pathophysiology of Takotsubo syndrome, *Nature reviews, Cardiology*. 2015;**12**:387–397.
3. Akepati V.R., Müller E.C., Otto A., Strauss H.M., Portwich M., Alexander C.J. Characterization of OPA1 isoforms isolated from mouse tissues. Neurochem.2008;**106(1)**:372-83.
4. Alexander C., Votruba M., Pesch U.E., Thiselton D.L., Mayer S., Moore A., Rodriguez M., Kellner U., Leo-Kottler B., Auburger G., Bhattacharya S.S. and Wissinger B. OPA1, encoding a dynamin-related GTPase, is mutated in autosomal dominant optic atrophy linked to chromosome 3q28. *Nat. Genet.*2000;**26**:211-215.
5. Allen M.D. and Zhang J. Subcellular dynamics of protein kinase A activity visualized by FRET-based reporters. *Biochem Biophys Res Commun*. 2006;**348**:716-721.
6. Amati-Bonneau P., Milea D., Bonneau D., Chevrollier A.,Ferré M., Guillet V., Gueguen N., Loiseau D., Pou de Crescenzo M-A., Verny C., Procaccio V., Lenaers G. and Reynier P. OPA1- associated disorders: Phenotypes and pathophysiology. *The international Journal of Biochemistry and Cell Biology*. 2009;**41**:1855-1865.
7. Anand R., Wai T., Baker M.J., Kladt N., Schauss A.C., Rugarli E., Langer T. The i-AAA protease YME1L and OMA1 cleave OPA1 to balance mitochondrial fusion and fission. *J Cell Biol.* 2014;**204**:919-929.
8. Anderson M.J. and Cohen M.W. Nerve-induced and spontaneous redistribution of acetylcholine receptors on cultured muscle cells. *J Physiol*.1977;**268(3)**:757-73.
9. Angeli S., Befera N., Peyrat J-M., Calabrese E., Johnson G.A. and Constantinides C. A high-resolution cardiovascular magnetic resonance diffusion tensor map from ex-vivo C57BL/6 murine hearts. *J Cardiovasc Magn Reson*.2014;**16**:77.
10. Anversa P., Ricci R. and Olivetti G. Quantitative structural analysis of the

myocardium during physiologic growth and induced cardiac hypertrophy: a review. *J Am Coll Cardiol.*1986;**7**:1140-1149.

11. Antzelevitch C., Sicouri S., Litovsky S.H., Lukas A., Krishnan S.C., Di Diego J.M., Gintant G.A. and Liu D.W. Heterogeneity within the ventricular wall. Electrophysiology and pharmacology of epicardial, endocardial, and M cells. *Circ Res*.1991;**69**:1427-1449.
12. Arrenberg A.B., Stainier D.Y., Baie, H. and Huisken J. Optogenetic control of cardiac function. *Science*.2010;**330**:971-974.
13. Baehr L. M., Tunzi M. and Bodine, S. C. Muscle hypertrophy is associated with increases in proteasome activity that is independent of MuRF1 and MAFbx expression. *Front Physiol.*2014;**5**:69.
14. Baker A.J. Adrenergic signaling in heart failure: a balance of toxic and protective effects. *Arch. Eur. J. Physiol*. 2014;**466**:1139–1150.
15. Baluk P. and Fujiwara T. Direct visualization by scanning electron microscopy of the preganglionic innervation and synapses on the true surfaces of neurons in the frog heart. *Neurosci Lett.* 1984;**51**:265–270.
16. Bandyopadhyay U., Sridhar S., Kaushik S., Kiffin R. and Cuervo A. M. Identification of regulators of chaperone-mediated autophagy. *Mol Cell.*2010;**39**:535-547.
17. Banghart M., Borges K., Isacoff E., Trauner D. and Kramer R.H. Light-activated ion channels for remote control of neuronal firing. *Nat Neurosci*.2004;**7**:1381-1386.
18. Baskin K.K., Rodriguez M.R., Kansara S., Chen W., Carranza S., Frazier O.H., Glass D.J., Taegtmeyer H. MAFbx/Atrogin-1 is required for atrophic remodeling of the unloaded heart. *J Mol Cell Cardiol*.2014; **72**:168-176.
19. Basser P.J., Mattiello J. and LeBihan D. MR diffusion tensor spectroscopy and imaging. *Biophys J*. 1994;**66**:259-267.
20. Bear M.F., Connors B.W. and Paradiso M.A. Chemicali control of the brain and behaviour. In: Neuroscience, Exploring the brain, 3rd ed. Philadelphia, Penn: Lippincott Williams and Wilkins, 2007; ch. 15.
21. Becker A.E. and De Wit A.P. Mitral valve apparatus. A spectrum of normality relevant to mitral valve prolapse. *Br Heart J*.1979;**42**:680-689.
22. Belenguer P., Pellegrini L. The dynamin GTPase OPA1: More than mitochondria?. *Biochimica at Biophysica Acta*.2013;**1833**:176-183.

23. Bennett M.R., Gibson W.G. and Robinson J. Probabilistic secretion of quanta: spontaneous release at active zones of varicosities, boutons, and endplates. *Biophysical journal*.1995;**69;**42-56.

24. Bernardi P. and Azzone G.F. Cytochrome c as an electron shuttle between the outer and inner mitochondrial membranes. *J Biol Chem*.1981;**256(14)**:7187-92.

25. Bernstein D., Faiardo G., Zhao M, Urashima T, Powers J, Berry G, Kobilka BK. Differential cardioprotective/cardiotoxic effects mediated by beta-adrenergic receptor subtypes. *Am J Physiol Heart Circ Physiol*.2005;**289**:H2441-2449.

26. Bers D.M. Calcium cycling and signaling in cardiac myocytes. *Annu Rev Physiol* 2008;**70**:23-49.

27. Bers D.M. and Despa S. Na/K-ATPase--an integral player in the adrenergic fight-or-flight response. *Trends Cardiovasc Med*.2009;**19**:111.

28. Bertholet A.M., Millet A.M.E., Guillermin O., Daloyan M., Davezac N., Miquel M.C. and Belenguer P. OPA1 loss of function affects *in vitro* neuronal maturation. *Brain*.2013;**136**:1518-1533.

29. Bierl M.A., Isaacson L.G. Increased NGF proforms in aged sympathetic neurons and their targets, *Neurobiol. Aging*.2007;**28**:122–134.

30. Bodine S.C. Latres E., Baumhueter S., Lai V.K., Nunez L., Clarke B.A., Poueymirou W.T., Panaro F.J., Na E., Dharmarajan K., Pan Z.Q., Valenzuela D.M., DeChiara T.M., Stitt T.N., Yancopoulos G.D., Glass D.J. Identification of ubiquitin ligases required for skeletal muscle atrophy. *Science*. 2001;**294**:1704-1708.

31. Boyden E.S., Zhang F., Bamberg E., Nagel G. and Deisseroth K. Millisecond-timescale, genetically targeted optical control of neural activity. *Nature neuroscience*.2005*;***8:**1263-1268.

32. Boyle P.M., Williams J.C., Ambrosi C.M., Entcheva E. and Trayanova N.A. A comprehensive multiscale framework for simulating optogenetics in the heart. *Nat Commun*. 2013;**4**:2370.

33. Boyle P.M., Karathanos T.V., Entcheva E. and Trayanova N.A. Computational modeling of cardiac optogenetics: Methodology overview & review of findings from simulations. *Comput Biol Med.* 2015; **65**:200-208.

34. Brodin L., Bakeeva L. and Shupliakov O. Presynaptic mitochondria and the temporal pattern of neurotransmitter release. *The royal Society*.1999;**354**:365-372.
35. Bruegmann T., Malan D., Hesse M., Beiert T., Fuegemann C.J., Fleischmann B.K., Sasse P. Optogenetic control of heart muscle in vitro and in vivo. *Nat Methods.* 2010;**7**:897-900.
36. Brutsaert D.L. The endocardium. *Annu Rev Physiol*. 1989;**51**:263-273.
37. Bucciantini, M. Giannoni E, Chiti F, Baroni F, Formigli L, Zurdo J, Taddei N, Ramponi G, Dobson CM, Stefani M. Inherent toxicity of aggregates implies a common mechanism for protein misfolding diseases. *Nature*.2002;**416**:507-511.
38. Busskamp V., Picaud S., Sahel J.A., Roska B. Optogenetic therapy for retinitis pigmentosa. *Gene Ther*. 2012; **19(2)**:169-75.
39. Carnio S., LoVerso F., Baraibar M.A., Longa E.,. Khan M.M, Maffei M., Reischl M., Canepari M., Loefler S., Kern H., Blaauw B., Friguet B., Bottinelli R., Rudolf R., Sandri M. Autophagy impairment in muscle induces neuromuscular junction degeneration and precocious aging. *Cell Rep*. 2014;**8**:1509–1521.
40. Carrier L., Schlossarek S., Willis M. S. and Eschenhagen T. The ubiquitinproteasome system and nonsense-mediated mRNA decay in hypertrophic cardiomyopathy. *Cardiovasc Res*. 2010;**85**:330-338.
41. Chao de la Barca J.M., Prunier-Mirebeau D., Amati-Bonneau P., Ferré M., Sarzi E., Bris C., Leruez S., Chevrollier A., Desquiret-Dumas V., Gueguen N., Verny C., Hamel C., Miléa D., Procaccio V., Bonneau D., Lenaers G., Reynier P. OPA1-related disorders: Diversity of clinical expression, modes of inheritance and pathophysiology. *Neurobiol Dis.* 2016;**90**:20-6.
42. Chen H. and Chan D. C. Critical dependence of neurons on mitochondrial dynamics. *Curr. Opin. In Cell Biology*.2006.**18**;453-459.
43. Chen L.S., Zhou S., Fishbein M.C., Chen P.S. New perspectives on the role of the autonomic nervous system in the genesis of arrhythmias. *J. Cardiovasc. Electrophysiol*.2007;**18**:123-7.
44. Chen P.S., Chen L.S., Cao J-M., Sharifi B., Karagueuzian H. S. and Fishbein M. C. Sympathetic nerve sprouting, electrical remodeling and the

mechanisms of sudden cardiac death. *Cardiovascular Research*.2001;**50**:409-416.

45. Choate J.K., Klemm M. and Hirst G.D. Sympathetic and parasympathetic neuromuscular junctions in the guinea-pig sino-atrial node. *Journal of the autonomic nervous system.1993;***44**:1-15.
46. Cho D.H., Nakamura T., Lipton S.A. Mitochondrial dynamics in cell death and neurodegeneration. *Cell Mol Life Sci*.2010;**67(20)**:3435-47.
47. Chow L.T., Chow S.S, Anderson R.H., Gosling J.A. Autonomic innervation of the human cardiac conduction system: changes from infancy to senility—an immuno- histochemical and histochemical analysis. *Anat. Rec.* 2001; **264**:169–182.
48. Chruscinski A.J., Rohrer D.K., Schauble E., Desai K.H., Bernstein D., Kobilka B.K. Targeted disruption of the beta2 adrenergic receptor gene. *J Biol Chem*.1999;**274**: 16694-16700.
49. Chu H.Y., Atherton J.F., Wokosin D., Surmeier D.J., Bevan M.D. Heterosynaptic regulation of external globus pallidus inputs to the subthalamic nucleus by the motor cortex. *Neuron*. 2015;**85**:364–376.
50. Cipolat S., Rudka T., Hartmann D., Costa V., Serneels L.,Craessaerts K., M etzger K., Frezza C., Annaert W., D'Adamio L., Derks C., Dejaegere T., Pel legrini L., D'Hooge R., Scorrano L., De Strooper B. Mitochondrial rhomboid PARL regulates cytochrome c release during apoptosis *via* OPA1-dependent cristae remodeling. *Cell.* 2006;**126**:163-175.
51. Clapham D.E. and Neer E.J. G protein beta gamma subunits. *Annu Rev Pharmacol Toxicol*.2007;**37**:167-203.
52. Clarke B. A. Drujan D., Willis M.S., Murphy L.O., Corpina R.A., Burova E., Rakhilin S.V., Stitt T.N., Patterson C., Latres E., Glass D.J. The E3 Ligase MuRF1 degrades myosin heavy chain protein in dexamethasone-treated skeletal muscle. *Cell Metab*.2007;**6**:376-385.
53. Cogliati S., Frezza C., Soriano M.E.,Varanita T.,Quintana-Cabrera R.M.,Cipolat S., Costa V., Casarin A., Gomes L.C., Perales-Clemente E., Salviati L., Fernandez-Silva P., Enriquez J. A. and Scorrano L. Mitochondrial Cristae Shape Determines Respiratory Chain

Supercomplexes Assembly and Respiratory Efficiency. *Cell*.2013;**155(1)**:160–171.

54. Cui G., Jun S.B., Jin X., Pham M.D., Vogel S.S., Lovinger D.M. and Costa R.M. Concurrent activation of striatal direct and indirect pathways during action initiation. *Nature*.2013;**494**:238–242.
55. Cunningham J. G. Textbook of veterinary physiology. (Saunders, 2002).
56. D'Herde K., De Prest B., Mussche S., Schotte P., Beyaert R., Van Coster R., Roels F. Ultrastructural localization of cytochrome c in apoptosis demonstrates mitochondrial heterogeneity. *Cell Death Differ.* 2000;**7**:331–337.
57. Danial N.N. and Korsmeyer S.J. Cell death: critical control points *Cell*. 2004;**116**: 205–219.
58. Dargemont, C. and Ossareh-Nazari, B. Cdc48/p97, a key actor in the interplay between autophagy and ubiquitin/proteasome catabolic pathways. *Biochim Biophys Acta*. 2012; **1823**:138-144.
59. Deisseroth K. Optogenetics. *Nat Methods.* 2011;**8**:26-29.
60. Delettre C., Lenaers G., Griffoin J.M., Gigarel N., Lorenzo C., Belenguer P., Pelloquin L., Grosgeorge J., Turc-Carel C., Perret E., Astarie-Dequeker C., Lasquellec L., Arnaud B., Ducommun B., Kaplan J. and Hamel C.P. Nuclear gene OPA1, encoding a mitochondrial dynamin-related protein, is mutated in dominant optic atrophy. *Nat. Genet*. 2000; **26**: 207-210.
61. Delettre C., Lenaers G., Pelloquin L., Belenguer P., Hamel C.P. OPA1 (Kjer type) dominant optic atrophy: a novel mitochondrial disease. *Mol Genet Metab.* 2002;**75(2)**:97-107.
62. DiFrancesco D. The role of the funny current in pacemaker activity. *Circulation research*.2010;**106:**434-446.
63. Dimmer K.S. and Scorrano L. (De)constructing mitochondria: what for?. Physiology (Bethesda). 2006;**21**:233-41.
64. Dutta D., Calvani R., Bernabei R., Leeuwenburgh C., Marzetti E. Contribution of impaired mitochondrial autophagy to cardiac aging: mechanisms and therapeutic opportunities. *Circ. Res*.2012;**110**:1125-1138.
65. El-Armouche A. and Eschenhagen T. Beta-adrenergic stimulation and myocardial function in the failing heart. *Heart Fail Rev*.2009;**14:** 225-241.

66. Evellin S., Mongillo M., Terrin A., Lissandron V., Zaccolo M. Measuring dynamic changes in cAMP using fluorescence resonance energy transfer. *Methods Mol. Biol.* 2004;**284**:259–270.
67. Exner N., Lutz A.K., Haass C. and Winklhofer K. Mitochondrial dysfunction in Parkinson's disease: molecular mechanisms and pathophysiological consequences *EMBO J*. 2012;**31(14)**:3038-62.
68. Fabiato A. and Fabiato F. Use of chlorotetracycline fluorescence to demonstrate Ca2+-induced release of Ca2+ from the sarcoplasmic reticulum of skinned cardiac cells. *Nature.*1979;**281**:146-148.
69. Fernández-Silva P., Enriquez J.A., Montoya J. Replication and transcription of mammalian mitochondrial DNA. *Exp Physiol*.2003;**88(1)**:41-56.
70. Ferre M., Amati-Bonneau P., Tourmen Y., Malthiery Y., Reynier P. eOPA1: an online database for *OPA1* mutations. *Hum Mutat.*2005;**25**:423-428.
71. Ferre M., Bonneau D., Milea D., Chevrollier A., Verny C., Dollfus H., Ayuso C., Defoort S., Vignal C., Zanlonghi X., Charlin J.F., Kaplan J., Odent S., Hamel C.P., Procaccio V., Reynier P., Amati-Bonneau P. Molecular screening of 980 cases of suspected hereditary optic neuropathy with a report on 77 novel *OPA1*mutations. *Hum Mutat*. 2009;**30**:e692–705.
72. Florea V.G. and Cohn J.N. The autonomic nervous system and heart failure. *Circulation research*.2014;**114:**1815-1826.
73. Franke W.W., Borrmann C.M., Grund C. and Pieperhoff S. The area composita of adhering junctions connecting heart muscle cells of vertebrates. I. Molecular definition in intercalated disks of cardiomyocytes by immunoelectron microscopy of desmosomal proteins. *Eur J Cell Biol*.2006;**85**:69-82.
74. Franzoso M., Zaglia T. and Mongillo M. Putting together the clues of the everlasting neuro-cardiac liaison. *Biochimica et biophysica acta*.2016;**863**(7 Pt B):1904-15.
75. Freeman S. Biological Scienze. 2nd Edition. *Pearson Prentice Hall*. 2005
76. Frescas D. and Pagano M. Deregulated proteolysis by the F-box proteins SKP2 and beta-TrCP: tipping the scales of cancer. *Nat Rev Cancer.*2008;**8**:438-449.

77. Frey N., Katus H.A., Olson E.N. and Hill J.A. Hypertrophy of the heart: a new therapeutic target? *Circulation*. 2004;**109**:1580-1589.
78. Frezza C., Cipolat S., Martins de B.O., Micaroni M., Beznoussenko G.V., Rudka T., Bartoli D., Polishuck R.S., Danial N.N., De S.B. and Scorrano L. OPA1 controls apoptotic cristae remodeling independently from mitochondrial fusion. *Cell*.2006;**126**:177-189.
79. Fuhrmann N., Alavi M.V., Bitoun P., Woernle S., Auburger G., Leo-Kottler B. Genomic rearrangements in OPA1 are frequent in patients with autosomal dominant optic atrophy. *Journal of Medical Genetics*.2009;**46**:136–144.
80. Fukuda K., Kanazawa H., Aizawa Y., Ardell J.L. and Shivkumar K. Cardiac innervation and sudden cardiac death. *Circ Res*.2015;**116**:2005-2019.
81. Fülöp L., Szanda G., Enyedi B., Várnai P., Spät A. The effect of OPA1 on mitochondrial Ca^{2+} signaling. *PLoS One*.2011;**6(9)**:e25199.
82. Furshpan E.J., Landis S.C., Matsumoto S.G., Potter D.D. Synaptic functions in rat sympathetic neurons in microcultures. I. Secretion of norepinephrine and acetylcholine. *J Neurosci.*1986;**6(4):**1061-79.
83. Gallo G. and Letourneau P.C. Axon guidance: GTPases help axons reach their targets. *Curr Biol.*1998;29:**8(3)**:R80-2.
84. Gibbons C.H., Illigens B.M., Wang N., Freeman R. Quantification of sudomotor innervation: a comparison of three methods. *Muscle Nerve.* 2010;**42(1)**:112-9.
85. Glajch K.E., Kelver D.A., Hegeman D.J., Cui Q., Xenias H.S., Augustine E.C., Hernandez V.M., Verma N., Huang T.Y., Luo M., Justice N.J., Chan C.S. Npas1+pallidal neurons target striatal projection neurons. *J Neurosci*.2016; **36**:5472–5488.
86. Glass D.J. Signalling pathways that mediate skeletal muscle hypertrophy and atrophy. *Nat Cell Biol*.2003;**5**:87-90.
87. Glebova N.O. and Ginty D.D., Heterogeneous requirement of NGF for sympathetic target innervation in vivo. J Neurosci. 2004;**24**:743–751.
88. Glickman M.H. and Ciechanover A. The ubiquitin-proteasome proteolytic pathway: destruction for the sake of construction. *Physiol Rev*.2002;**82**:373-428.

89. Gomes M.D., Lecker S.H., Jagoe R.T., Navon A. and Goldberg A.L. Atrogin-1, a muscle-specific F-box protein highly expressed during muscle atrophy. Proc Natl Acad Sci U S A. 2001;**98**:14440-14445.
90. Grazia, A. in Anatomy and physiology Ch. 20, 486-8332.
91. Gros D., Jarry-Guichard T., Ten Velde I., de Maziere A., van Kempen M.J., Davoust J., Briand J.P., Moorman A.F., Jongsma H.J. Restricted distribution of connexin40, a gap junctional protein, in mammalian heart. *Circ Res.*1994;**74**:839-851.
92. Guyton A.C. and Hall J.E. Textbook of Medical Physiology. 11th edition. Philadelphia, Penn: Elsevier/Saunders,2006.
93. Hall C.N., Klein-Flügge M.C., Howarth C. and Attwell D. Oxidative phosphorylation, not glycolysis, powers presynaptic and postsynaptic mechanisms underlying brain information processing. *J. Neurosci*. 2012;**32**:8940–8951.
94. Hanson J. and Huxley H.E. Structural basis of the cross-striations in muscle. Nature.1953;**172**:530-532.
95. Harris J.J., Jolivet R. and Attwell D. Synaptic energy use and supply. *Neuron*. 2012;**75**: 762–777.
96. Hasan W. Autonomic cardiac innervations and adult plasticity. *Organogenesis*.2013;**9(3)**:176-193.
97. Hasking G.J., Esler M.D., Jennings G.L., Burton D., Johns J.A., Korner P.I. Norepinephrine spillover to plasma in patients with congestive heart failure: evidence of increased overall and cardiorenal sympathetic nervous activity, Circulation. 1986; **73**:615–621.
98. Healy L.J., Jiang Y. and Hsu E.W. Quantitative comparison of myocardial fiber structure between mice, rabbit, and sheep using diffusion tensor cardiovascular magnetic resonance. *J Cardiovasc Magn Reson*. 2011;**13**:74.
99. Hegemann P. and Nagel G. From channelrhodopsins to optogenetics. *EMBO Mol Med.* 2013;**5**:173-176.
100. Heredia M., del P., Delgado C., Pereira L., Perrier R., Richard S., Vassort G., Bénitah J.P., Gómez A.M. Neuropeptide Y rapidly enhances [Ca2+]i transients and Ca2+ sparks in adult rat ventricular myocytes

through Y1 receptor and PLC activation. *J Mol Cell Cardiol*. 2005;**38(1)**:205-12.

101. Herlan M., Vogel F., Bornhovd C., Neupert W., Reichert A.S. Process ing of MGM1 by the rhomboid-type protease PCP1 is required for maintenance of mitochondrial morphology and of mitochondrial DNA. *J Biol Chem.* 2003; **278**:27781-27788.

102. Herzog H., Hort Y.J., Ball H.J., Hayes G., Shine J., Selbie L.A. Cloned human neuropeptide Y receptor couples to two different second messenger systems. *Proc Natl Acad Sci USA*.1992;**89(13)**:5794-8.

103. Hofmann B., Maybeck V., Eick S., Meffert S., Ingebrandt S., Wood P., Bamberg E., Offenhäusser A. Light induced stimulation and delay of cardiac activity. *Lab Chip*. 2010;**10**:2588-2596.

104. Hoppins S., Lackner L., Nunnari J. The machines that divide and fuse mitochondria. *Annu Rev Biochem*.2007;**76**:751–80.

105. Howe M.W. and Dombeck D.A. Rapid signalling in distinct dopaminergic axons during locomotion and reward. *Nature.* 2016;**535(7613)**:505-10.

106. Hoyt R.H., Cohen M.L. and Saffitz J.E. Distribution and three-dimensional structure of intercellular junctions in canine myocardium. *Circ Res.*1989;**64**:563-574.

107. Hudson G., Amati-Bonneau P., Blakely E.L., Stewart J.D., He L., Schaefer A. M., Griffiths P.G., Ahlqvist K., Suomalainen A., Reynier P., McFarland R., Turnbull D.M., Chinnery P.F. and Taylor R.W. Mutation of OPA1 causes dominant optic atrophy with external ophthalmoplegia, ataxia, deafness and multiple mitochondrial DNA deletions: a novel disorder of mtDNA maintenance. *Brain*.2008;**131**:329-337.

108. Ieda M., Kanazawa H., Kimura K., Hattori F., Ieda Y., Taniguchi M., Lee J-K, Matsumura K., Tomita Y., Miyoshi S., Shimoda K., Makino S., Sano M., Kodama I., Ogawa S. and Fukuda K. Sema3a maintains normal heart rhythm through sympathetic innervations patterning. *Nature Medicine*.2007;**5(13)**:604-612.

109. Ishihara N., Fujita Y., Oka T., Mihara K. Regulation of mitochondrial morphology through proteolytic cleavage of OPA1. *EMBO J*. 2006;**25**: 2966-2977.

110. Ishihara N., Eura Y., Mihara K. Mitofusin 1 and 2 play distinct roles in mitochondrial fusion reactions via GTPase activity. *J Cell Sci*.2004;**117**:6535-46.

111. James D.I., Parone P.A., Mattenberger Y., Martinou J.C. hFis1, a novel component of the mammalian mitochondrial fission machinery. *J Biol Chem*.2003;**278**:36373–9

112. Jansen A.S., Nguyen X.V., Karpitskiy V., Mettenleiter T.C. and Loewy A.D. Central command neurons of the sympathetic nervous system: basis of the fight-or-flight response. *Science (New York, NY).*1995; **270:** 644-646.

113. Jia Z., Valiunas V., Lu Z., Bien H., Liu H., Wang H.Z., Rosati B., Brink P.R., Cohen I.S., Entcheva E. Stimulating cardiac muscle by light: cardiac optogenetics by cell delivery. *Circ Arrhythm Electrophysiol.* 2011;**4**:753-760.

114. Jiang, Y., Pandya, K., Smithies, O. & Hsu, E. W. Three-dimensional diffusion tensor microscopy of fixed mouse hearts. *Magn Reson Med*.2004;**52**:453-460.

115. Jung T., Catalgol B. and Grune T. The proteasomal system. *Mol Aspects Med*. 2009;**30(4)**:191-296.

116. Karbowski M., Arnoult D., Chen H., Chan D.C., Smith C.L., Youle R.J. Quantitation of mitochondrial dynamics by photolabeling of individual organelles shows that mitochondrial fusion is blocked during the Bax activation phase of apoptosis.*J Cell Biol*.2004;**164(4)**:493-9.

117. Katz A. M. Physiology of the Heart. *Lippincott Williams & Wilkins*.2011

118. Kaye D. and Esler M. Sympathetic neuronal regulation of the heart in aging and heart failure. *Cardiovascular research.*2005;**66:**256-264.

119. Kedar, V., McDonough H., Arya R., Li H.H., Rockman H.A., Patterson C. Muscle-specific RING finger 1 is a bona fide ubiquitin ligase that degrades cardiac troponin I. *Proc Natl Acad Sci U S A*.2004;**101**:18135-18140.

120. Kim M.S., Shutov L.P., Gnanasekaran A., Lin Z., Rysted J.E., Ulrich J.D., Usachev Y.M. Nerve growth factor (NGF) regulates activity of nuclear factor of activated T-cells (NFAT) in neurons via the phosphatidylinositol 3-

kinase (PI3K)-Akt-glycogen synthase kinase 3β (GSK3β) pathway. *J Biol Chem.* 2014;**289(45)**:31349-60.

121. Kimura K., Ieda M., Kanazawa H., Yagi T., Tsunoda M., Ninomiya S., Kurosawa H., Yoshimi K., Mochizuki H., Yamazaki K., Ogawa S., Fukuda K.. Cardiac sympathetic rejuvenation: a link between nerve function and cardiac hypertrophy, *Circ. Res.* 2007;**100**:1755–1764.

122. Kimura K., Ieda M. and Fukuda K. Development, maturation, and transdifferentiation of cardiac sympathetic nerves. *Circ Res*.2012;**110**:325-336.

123. Kirchhoff S. Kim J-S., Hagendorff A., Tho¨nnissen E., Kru¨ger O., Lamers W.H., Willecke K. Abnormal cardiac conduction and morphogenesis in connexin40 and connexin43 double-deficient mice. *Circ Res*.2000;**87**:399-405.

124. Kjer B., Eiberg H., Kjer P., Rosenberg T. Dominant optic atrophy mapped to chromosome 3q region. II. Clinical and epidemiological aspects. *Acta Ophthalmol Scand.* 1996;**74(1)**:3-7.

125. Klarenbeek J., Goedhart J., van Batenburg A., Groenewald D. and Jalink K. Fourth-generation epac-based FRET sensors for cAMP feature exceptional brightness, photostability and dynamic range: characterization of dedicated sensors for FLIM, for ratiometry and with high affinity. PLoS One.2015;**10**:e0122513.

126. Klionsky D. J. The molecular machinery of autophagy: unanswered questions. *J Cell Sci*.2005;**118**:7-18.

127. Koshiba T., Detmer S.A., Kaiser J.T., Chen H., McCaffery J.M. and Chan D.C. Structural basis of mitochondrial tethering by mitofusin complexes. *Science*.2004;**305**:858-862.

128. Kurtz T.W., Griffin K.A., Bidani A.K., Davisson R.L., Hall J.E. Recommendations for blood pressure measurement in humans and experimental animals: part 2: blood pressure measurement in experimental animals: a statement for professionals from the Subcommittee of Professional and Public Education of the American Heart Association Council on High Blood Pressure Research. *Arterioscler Thromb Vasc Biol.* 2005b; **25**:e22–33.

129. Kuruvilla R., Zweifel L.S., Glebova N.O., Lonze B.E., Valdez G., Ye H., Ginty D.D. A neurotrophin signaling cascade coordinates sympathetic neuron development through differential control of TrkA trafficking and retrograde signaling. *Cell*. 2004;**118**:243-255.

130. Lakatta E.G. Deficient neuroendocrine regulation of the cardiovascular system with advancing age in healthy humans. *Circulation.*1993;**87**:631–636.

131. Landis S.C. Rat sympathetic neurons and cardiac myocytes developing in microcultures: correlation of the fine structure of endings with neurotransmitter function in single neurons. *Proc Natl Acad Sci U S A*.1976;**73(11)**:4220-4.

132. Lenaz G., D'Aurelio M., Pich M.M., Genova M.L., Ventura B., Bovina C., Formiggini G., Castelli Parenti G. Mitochondrial bioenergetics in aging. BBA.2000;**1459**;397-404.

133. Levitan I and Kaczmarek L. "Intercellular communication". *The Neuron: Cell and Molecular Biology (4th ed.). New York, NY: Oxford Univerty Press.*2015:153–328.

134. Levi-Montalcini R. and Angeletti P.U. Nerve growth factor. *Physiol. Rev*.1968;**48(3)**:534-69

135. Levy M.N. and Martin P.J. Physiology and Pathology of the heart: Autonomic neuronal control of cardiac function. *Springer (2nd edition).*1989:361-379.

136. Lewin G.R. and Barde Y.A. Physiology of the neurotrophins. *Annu Rev Neurosci.* 1996;**19**:289-317.

137. Li L., Desantiago J., Chu G., Kranias E.G., Bers D.M. Phosphorylation of phospholamban and troponin I in beta-adrenergic-induced acceleration of cardiac relaxation. *Am J Physiol Heart Circ Physiol*.2000;**278**:H769–H779

138. Li H.H. Kedar V., Zhang C., McDonough H., Arya R., Wang D.Z., Patterson C. Atrogin-1/muscle atrophy F-box inhibits calcineurin-dependent cardiac hypertrophy by participating in an SCF ubiquitin ligase complex. *J Clin Invest*. 2004;**114**:1058-1071.

139. Li H.H., Willis M.S., Lockyer P., Miller N., McDonough H., Glass D.J., Patterson C. Atrogin-1 inhibits Akt-dependent cardiac hypertrophy in

mice via ubiquitin-dependent coactivation of Forkhead proteins. *J Clin Invest.*2007;**117**: 3211-3223.

140. Lima S.Q. and Miesenbock G. Remote control of behavior through genetically targeted photostimulation of neurons. *Cell.* 2005;**121**:141-152.

141. Lindberg J., Usoskin D., Bengtsson H., Gustafsson A., Kylberg A., Soderstrom S., Ebendal T. Transgenic expression of Cre recombinase from the tyrosine hydroxylase locus. *Genesis*.2004;**40(2)**:67.

142. Liskova P., Ulmanova O., Tesina P., Melsova H., Diblik P., Hansikova H., Tesarova M., Votruba M. Novel OPA1 missense mutation in a family with optic atrophy and severe widespread neurological disorder. *Acta Ophthalmol*. 2013;**91**:e225–31.

143. Liu D.W., Gintant G.A. and Antzelevitch C. Ionic bases for electrophysiological distinctions among epicardial, midmyocardial, and endocardial myocytes from the free wall of the canine left ventricle. *Circ Res*. 1993;**72**:671-687.

144. Liu J., Dobrzynski H., Yanni J., Boyett M.R. and Lei M. Organisation of the mouse sinoatrial node: structure and expression of HCN channels. *Cardiovascular research*.2007;**73**:729-738.

145. Lockhart S.T., Turrigiano G.G. and Birren S.J. Nerva Growth Factor Modulates Synaptic Transmission between Sympathetic Neurons and Cardiac Myocytes. *The Journal of Neuroscience*.1997;**17(24)**:9573-9582.

146. Lodi R., Tonon C., Valentino M.L., Iotti S., Clementi V., Malucelli E., Barboni P., Longanesi L., Schimpf S., Wissinger B., Baruzzi A., Barbiroli B., Carelli V. Deficit of in vivo mitochondrial ATP production in OPA1-related dominant optic atrophy. *Ann Neurol*. 2004;**56(5)**:719-23.

147. Lombardi F., Malliani A., Pagani M. and Cerutti S. Heart rate variability and its sympatho-vagal modulation. *Cardiovascular research*.1996;**32**:208-216.

148. Luttrell, L. M. Transmembrane signaling by G protein-coupled receptors. *Methods Mol Biol.*2006;**332**:3-49.

149. Lyon A.R., Rees P.S., Prasad S.,. Poole-Wilson P.A, Harding S.E. Stress (Takotsubo) cardiomyopathy—a novel pathophysiological hypothesis

to ex- plain catecholamine-induced acute myocardial stunning. *Nat. Clin. Pract. Cardiovasc*. 2008;**5**:22–29.

150. Maejima Y., Usui S., Zhai P., Takamura M., Kaneko S., Zablocki D., Yokota M., Isobe M., Sadoshima J. Muscle-specific RING finger 1 negatively regulates pathological cardiac hypertrophy through downregulation of calcineurin A. *Circ Heart Fail*.2014;**7**:479-490.

151. Mattson M.P., Gleichmann M., Cheng A. Mitochondria in neuroplasticity and neurological disorders. *Neuron.* 2008;**60(5)**:748-766.

152. Martinelli P., Rugarli E.I. Emerging roles of mitochondrial proteases in neurodegeneration. *Biochim Biophys Acta.* 2010;**1797**:1-10.

153. Massey, A. C., Zhang, C. & Cuervo, A. M. Chaperone-mediated autophagy in aging and disease. *Curr Top Dev Biol*.2006;**73**:205-235.

154. Matsuda, W., Furuta, T., Nakamura, K.C., Hioki, H., Fujiyama, F., Arai, R. Single nigrostriatal dopaminergic neurons form widely spread and highly dense axonal arborizations in the neostriatum. *J. Neurosci*.2009;**29:**444–453.

155. McLeland C.B., Rodriguez J. and Stern S.T. Autophagy monitoring assay: qualitative analysis of MAP LC3-I to II conversion by immunoblot. *Methods Mol Biol*.2011;**697**:199-206.

156. Miguelez C., Morin S., Martinez A., Goillandeau M., Bezard E., Bioulac B., Baufreton J. Altered pallido-pallidal synaptic transmission leads to aberrant firing of globus pallidus neurons in a rat model of Parkinson's disease. *J Physiol*. 2012. **590**:5861–5875.

157. Miller G. Optogenetics. Shining new light on neural circuits. *Science*.2006; **314**:1674- 1676.

158. Miquerol L. Moreno-Rascon N., Beyer S., Dupays L., Meilhac S.M., Buckingham M.E., Franco D., Kelly R.G. Biphasic development of the mammalian ventricular conduction system. *Circ Res*. 2010;**107**:153-161.

159. Mitchell G.A.G. The innervation of the heart. *Br Heart J.*1953;**15**:159-171.

160. Mongillo M. and Marks A.R. Models of heart failure progression: Ca2+ dysregulation. *Drug Discovery Today: Disease Models*. 2007;**4(4)**:191-196.

161. Morris R.L. and Hollenbeck P.J. The regulation of bidirectional mitochondrial transport is coordinated with axonal outgrowth. *J. Cell Sci*.1993; **104(3)**:917–927.

162. Morselli E., Galluzzi L., Kepp O., Criollo A., Maiuri M.C., Tavernarakis N., Madeo F., Kroemer G. Autophagy mediates pharmacological lifespan extension by spermidine and resveratrol. *Aging* (Albany NY).2009;**1**:961-970.

163. Moseley M.E., de Crespigny A.J., Roberts T.P., Kozniewska E. and Kucharczyk J. Early detection of regional cerebral ischemia using high-speed MRI. *Stroke.*1993;**24**:I60-65.

164. Muhlfeld C., Papadakis T., Krasteva G., Nyengaard J.R., Hahn U. and Kummer W. An unbiased stereological method for efficiently quantifying the innervation of the heart and other organs based on total length estimations. *J Appl Physiol*.2010;**108**:1402–1409.

165. Myeku N. and Figueiredo-Pereira M.E. Dynamics of the degradation of ubiquitinated proteins by proteasomes and autophagy: association with sequestosome 1/p62. J Biol Chem.2011;**286**:22426-22440.

166. Myles R.C., Wang L., Kang C., Bers D.M. and Ripplinger C.M. Local □-adrenergic stimulation overcomes source-sink mismatch to generate focal arrhythmia. *Circ Res*.2012;**110**:1454-1464.

167. Nagel G., Szellas T., Huhn W., Kateriya S., Adeishvili N., Berthold P., Ollig D., Hegemann P., Bamberg E. Channelrhodopsin-2, a directly light-gated cation-selective membrane channel. *Proc Natl Acad Sci U S A*. 2003;**100**:13940-13945.

168. Nasca A., Rizza T., Doimo M., Legati A., Ciolfi A., Diodato D., Calderan C., Carrara G., Lamantea E., Aiello C., Di Nottia M., Niceta M., Lamperti C., Ardissone A., Bianchi-Marzoli S., Iarossi G., Bertini E., Moroni I., Tartaglia M., Salviati L., Carrozzo R., Ghezzi D. Not only dominant, not only optic atrophy: expanding the clinical spectrum associated with OPA1mutations. *Orphanet J Rare Dis.* 2017;12;**12(1)**:89.

169. Nave B. T., Ouwens M., Withers D.J., Alessi D.R. and Shepherd P.R.

Mammalian target of rapamycin is a direct target for protein kinase B: identification of a convergence point for opposing effects of insulin and amino-acid deficiency on protein translation. *Biochem J*. 1999;**344**(Pt 2):427-431.

170. Nikolaev V.O., Bunemann M., Hein L., Hannawacker A. and Lohse M.J. Novel single chain cAMP sensors for receptor-induced signal propagation. *The Journal of biological chemistry.*2004;**279:** 37215-37218.

171. Ogawa S., Barnett J.V., Sen L., Galper J.B., Smith T.W. and Marsh J.D. Direct contact between sympathetic neurons and ratmcardiac myocytes in vitro increases expression of functional calcium channels. *J Clin Invest*. 1992;**89**:1085–1093.

172. Oh Y., Cho G.S., Li Z., Hong I., Zhu R., Kim M.J., Kim Y.J., Tampakakis E., Tung L., Huganir R., Dong X., Kwon C. and Lee G. Functional Coupling with Cardiac Muscle Promotes Maturation of hPSC-Derived Sympathetic Neurons. *Cell stem cell*.2016;**19**:95-106.

173. Okabe S., Kim H.D., Miwa A., Kuriu T., Okado H. Continual remodeling of postsynaptic density and its regulation by synaptic activity. *Nat. Neurosci*. 1999;**2(9)**:804-11.

174. Olichon A., Baricault L., Gas N., Guillou E., Valette A., Belenguer P. and Lenaers G. Loss of OPA1 perturbates the mitochondrial inner membrane structure and integrity, leading to cytochrome c release and apoptosis. *J. Biol. Chem.*2003;**278**:7743-7746.

175. Opie L. H. Heart physiology, from cell to circulation. (Lippincott Williams and Wilkins, 2004).

176. Pauza D.H., Rysevaite K., Inokaitis H., Jokubauskas M., Pauza A.G., Brack K.E. and Pauziene N. Innervation of sinoatrial nodal cardiomyocytes in mouse. A combined approach using immunofluorescent and electron microscopy. *J Mol Cell Cardiol*. 2014;**75**:188–197.

177. Pesch U.E., LeoKottler B.,Mayer S., Jurklies B.,Kellner U., Apfelstedt Sylla E., Zrenner E., Alexander C., Wissinger B. OPA1 mutations in patients with autosomal dominant optic atrophy and evidence for semi-dominant inheritance. *Hum Mol Genet.* 2001;**10**:1359-1368.

178. Peters N.S. New insights into myocardial arrhythmogenesis: distribution of gapjunctional coupling in normal, ischaemic and

hypertrophied human hearts. *Clin Sci.*1996;**90**:447-452.

179. Pfaffl M.W. A new mathematical model for relative quantification in real-time RT-PCR. *Nucleic Acids Res.* 2001;**29(9):**e45.

180. Piquereau J., Caffin F., Novotova M., Prola A., Garnier A., Mateo P., Fortin D., Huynh L.H., Nicolas V. , Alavi M.V., Brenner C., Ventura-Clapier R., Veksler V. and Joubert F. Down-regulation of OPA1 alters mouse mitochondrial morphology, PTP function, and cardiac adaptation to pressure overload. *Cardiovascular Research*.2012;**94**:408-417.

181. Powell S.R. The ubiquitin-proteasome system in cardiac physiology and pathology. *Am J Physiol Heart Circ Physiol.* 2006;**291**:H1-H19.

182. Priori, S. G., Blomström-Lundqvist C., Mazzanti A., Blom N., Borggrefe M., Camm J., Elliott P.M., Fitzsimons D., Hatala R., Hindricks G., Kirchhof P., Kjeldsen K., Kuck K.H., Hernandez-Madrid A., Nikolaou N., Norekvål T.M., Spaulding C., Van Veldhuisen D.J. 2015 ESC Guidelines for the management of patients with ventricular arrhythmias and the prevention of sudden cardiac death: The Task Force for the Management of Patients with Ventricular Arrhythmias and the Prevention of Sudden Cardiac Death of the European Society of Cardiology (ESC)Endorsed by: Association for European Paediatric and Congenital Cardiology (AEPC). *Eur Heart J*. 2015;**17(2)**:108-70.

183. Protas L. and Robinson R.B. Neuropeptide Y contributes to innervation-dependent increase in I(Ca, L) via ventricular Y2 receptors. *Am J Physiol*.1999;**277**: H940-946.

184. Protas L., Barbuti A., Qu J., Rybin V.O., Palmiter R.D., Steinberg S.F., Robinson R.B. Neuropeptide Y is an essential in vivo developmental regulator of cardiac ICa, L. *Circ Res*. 2003;**93(10)**:972-9.

185. Randall WC, Szentivanyi M, Pace JB, Wechsler JS, Kaye MP. Patterns of sympathetic nerve projections onto the canine heart. *Circ Res.* 1968*;***22**: 315–323.

186. Richards M., Lomas O., Jalink K., Ford K.L., Vaughan-Jones R.D., Lefkimmiatis K., and Swietach P. Intracellular tortuosity underlies slow cAMP diffusion in adult ventricular myocytes. *Cardiovasc Res*. 2016;**110**:395–407.

187. Rizzuto R., Bernardi P. and Pozzan T. Mitochondria as all-round players of the calcium game. *J. Physiol*. 2000;**529(1)**:37–47.

188. Rochais F., Vandecasteele G., Lefebvre F., Lugnier C., Lum H., Mazet J.L., Cooper D.M. and Fischmeister R. Negative feedback exerted by cAMP-dependent protein kinase and cAMP phosphodiesterase on subsarcolemmal cAMP signals in intact cardiac myocytes: an in vivo study using adenovirus-mediated expression of CNG channels. *The Journal of biological chemistry*.2004;**279:** 52095-52105.

189. Robertson G.P. Functional and therapeutic significance of Akt deregulation in malignant melanoma. *Cancer Metastasis Rev*. 2005;**24**:273-285.

190. Rubart M. and Zipes D.P. Mechanisms of sudden cardiac death. Journal of Clinical Investigation.2005;**115(9)**:2305-15.

191. Sahu R. Kaushik S., Clement C.C., Cannizzo E.S., Scharf B., Follenzi A., Potolicchio I., Nieves E., Cuervo A.M., Santambrogio L. Microautophagy of cytosolic proteins by late endosomes. *Dev Cell*.2011;**20**:131-139.

192. Sanders T.H., Jaeger D. Optogenetic stimulation of cortico-subthalamic projections is sufficient to ameliorate bradykinesia in 6-ohda lesioned mice. *Neurobiol Dis.* 2016;**95**:225–237.

193. Sandri M., Sandri C., Gilbert A., Skurk C., Calabria E., Picard A., Walsh K., Schiaffino S., Lecker S.H., Goldberg A.L. Foxo transcription factors induce the atrophy-related ubiquitin ligase atrogin-1 and cause skeletal muscle atrophy. *Cell*. 2004;**117**:399-412.

194. Sandri M. and Robbins J. Proteotoxicity: an underappreciated pathology in cardiac disease. *J Mol Cell Cardiol.* 2014;**71**:3-10.

195. Sands G.B., Smaill B.H. and LeGrice I.J. Virtual sectioning of cardiac tissue relative to fiber orientation. *Conf Proc IEEE Eng Med Biol Soc*.2008;226-229.

196. Sarzi E., Angebault C., Seveno M., Gueguen N., Chaix B., Bielicki G., Boddaert N., Mausset-Bonnefont A-L., Cazevieille C., Rigau V., Renou J-P., wang J.J., Delettre C., Brabet P., Puel J-L., Hamel C.P., Reynier P. and Lenaers G. The Human OPA1$^{del\ TTAGN}$ Mutation induces premature

age-related systemic neurodegenration in mouse. *Brain. A Journal of Neurolgy*.2012;**135**:3599-3613.

197. Scepanovic D. A model of sinoatrial node cell regulation by the autonomic nervous system. Thesis (PhD), Massachusetts Institute of Technology. 2011. http://hdl.handle.net/1721.1/68457.

198. Schapira A.H.V. Mitochondrial disorders. *Current Opinion in Neurology*. 2000;**13(5)**:527-32.

199. Schmitt B. Fedarava K, Falkenberg J, Rothaus K, Bodhey NK, Reischauer C, Kozerke S., Schnackenburg B., Westermann D., Lunkenheimer P.P., Anderson R.H., Berger F. and Kuehne T. Three-dimensional alignment of the aggregated myocytes in the normal and hypertrophic murine heart. *J Appl Physiol.* 2009;**107**:921-927.

200. Seals D.R., Esler M.D., Human ageing and the sympathoadrenal system, *J. Physiol.* 2000;**528**:407–417.

201. Sharma N., Deppmann C.D., Harrington A.W., St Hillaire C., Chen Z.Y., Lee F.S., Ginty D.D. Long-distance control of synapse assembly by target-derived NGF. *Neuron*. 2010;**67(3)**:422-34.

202. Shcherbakova O.G., Hurt C.M., Xiang Y., Dell'Acqua M.L., Zhang Q., Tsien R.W., Kobilka B.K. Organization of beta-adrenoceptor signaling compartments by sympathetic innervation of cardiac myocytes. *J Cell Biol*.2007;**176(4)**:521-33.

203. Shen M.J. and Zipes D.P. Role of the autonomic nervous system in modulating cardiac arrhythmias, *Circulation research*.2014;**114**:1004-1021.

204. Slater C.R. Structural determinants of the reliability of synaptic transmission at the vertebrate neuromuscular junction. *J Neurocytol*.2003;**32:** 505-522.

205. Smirnova E., Griparic L., Shurland D.L., van der Bliek A.M. Dynamin-related protein Drp1 is required for mitochondrial division in mammalian cells. *Mol Biol Cell*. 2001;**12(8)**:2245-56.

206. Spiegel R., Saada A., Flannery P.J., Burté F., Soiferman D., Khayat M., Eisner V., Vladovski E., Taylor R.W., Bindoff L.A., Shaag A., Mandel H., Schuler-Furman O., Shalev S.A., Elpeleg O., Yu-Wai-Man P. Fatal infantile mitochondrial encephalomyopathy, hypertrophic cardiomyopathy

and optic atrophy associated with a homozygous OPA1 mutation. J Med Genet.2016;**53(2):**127-31.

207. Stieber J., Herrmann S., Feil S., Loster J., Feil R., Biel M., Hofmann F and Ludwig A. The hyperpolarization-activated channel HCN4 is required for the generation of pacemaker action potentials in the embryonic heart. *Proceedings of the National Academy of Sciences of the United States of America*.2003;**100:**15235-15240.

208. Thaemert J.C. Fine structure of neuromuscular relationships in mouse heart. 1969;**163(4)**:575–585.

209. Tritsch N.X., Ding J.B., Sabatini B.L. Dopaminergic neurons inhibit striatal output through non-canonical release of GABA. *Nature*. 2012;**490**:262–266.

210. Van Stee E.W. Autonomic innervation of the heart. *Environ Health Perspect.* 1978;**26**:151-8.

211. Van Kempen M. J. Vermeulen J.L., Moorman A.F., Gros D., Paul D.L., Lamers W.H. Developmental changes of connexin40 and connexin43 mRNA distribution patterns in the rat heart. *Cardiovasc Res*.1996;**32**:886-900.

212. Veeraraghavan R., Poelzing S. and Gourdie R.G. Intercellular electrical communication in the heart: a new, active role for the intercalated disk. *Cell Commun Adhes*.2014;**21**:161-167.

213. Volgraf M., Gorostiza P., Numano R., Kramer R.H., Isacoff E.Y., Trauner D. Allosteric control of an ionotropic glutamate receptor with an optical switch. *Nat Chem Biol*. 2006;**2**:47-52.

214. Votruba M., Moore A.T., Bhattacharya S.S. Clinical features, molecular genetics, and pathophysiology of dominant optic atrophy. *J Med Genet.* 1998;**35(10)**:793-800.

215. Weidmann S. Cardiac muscle: the functional significance of the intercalated disks. *Ann N Y Acad Sci*.1966;**137**:540-542.

216. Weingart R. The permeability to tetraethylammonium ions of the surface membrane and the intercalated disks of sheep and calf myocardium*. J Physiol.*1974; **240**:741-762.

217. Wengrowski A.M., Wang X., Tapa S., Posnack N.G., Mendelowitz D. and Kay M.W. Optogenetic release of norepinephrine from cardiac

sympathetic neurons alters mechanical and electrical function. *Cardiovascular research*. 2015;**105:**143-150.

218. Willis M.S. and Patterson C. Into the heart: the emerging role of the ubiquitinproteasome system. *J Mol Cell Cardiol*. 2006;**41**:567-579.

219. Willis M.S., Ike C., Li L., Wang D.Z., Glass D.J., Patterson C. Muscle ring finger 1, but not muscle ring finger 2, regulates cardiac hypertrophy in vivo. *Circ Res.*2007;**100**:456-459.

220. Willis, M. S. Rojas M., Li L., Selzman C.H., Tang R.H., Stansfield W.E., Rodriguez J.E., Glass D.J., Patterson C. Muscle ring finger 1 mediates cardiac atrophy in vivo. *Am J Physiol Heart Circ Physiol*.2009a;**296**:H997-H1006.

221. Willis, M. S. et al. Cardiac muscle ring finger-1 increases susceptibility to heart failure in vivo. *Circ Res.*2009b;**105**:80-88.

222. Wingerd K.L., Goodman N.L., Tresser J.W., Smail M.M., Leu S.T., Rohan S.J., Pring J.L., Jackson D.Y., Clegg D.O. Alpha 4 integrins and vascular cell adhesion molecule-1 play a role in sympathetic innervation of the heart. *J. Neurosci*. 2002;**22**:10772–10780.

223. Wong J., Abilez O.J. and Kuhl E. Computational Optogenetics: A Novel Continuum Framework for the Photoelectrochemistry of Living Systems. *J Mech Phys Solids.* 2012;**60**:1158-1178.

224. Woods R.I., Sir Lindor Brown F.R.S. The innervation of the frog's heart I. An examination of the autonomic postganglionic nerve fibres and a comparison of autonomic and sensory ganglion cells. *Pro. of the Roy. Soc. Lond. B*. 1970;**176**: 43-54.

225. Xie Y., Sato D., Garfinkel A., Qu Z. and Weiss J. N. So little source, so much sink: requirements for afterdepolarizations to propagate in tissue. *Biophys J*.2010;**99**:1408-1415.

226. Yu D.Y., Cringle S.J., Balaratnasingam C., Morgan W.H., Yu P.K., Su E.N. Retinal ganglion cells: Energetics, compartmentation, axonal transport, cytoskeletons and vulnerability. *Prog Retin Eye Res.* 2013;**36**:217-46.

227. Yu-Wai-Man P., Griffiths P.G., Gorman G.S., Lourenco C.M., Wright A. F., Auer-Grumbach M., Toscano A., Musumeci O., Valentino M.L., Caporali L., Lamperti C., Tallaksen C.M., Duffey P., Miller J., Whittaker

R.G., Baker M.R., Jackson M.J., Clarke M.P., Dhillon B., Czermin B., Stewart J.D., Hudson G., Reynier P., Bonneau D., Marques W. jr., Lenaers G., McFarland R., Taylor R.W., turnbull D.M., Votruba M., Zeviani M., Carelli V., Bindoff L.A., Horvath R., Amati-Bonneau P. and Chinnery P.F. Multi-system neurological disease is common in patients with OPA1 mutations. *Brain*.2010;**133**:771-786.

228. Yu-Wai-Man P., Votruba M., Burté F., La Morgia C., Barboni P.and Carelli V. A neurodegenerative perspective on mitochondrial optic neuropathies. *Acta Neuropathol.* 2016;**132(6)**:789-806

229. Zaccolo M. and Pozzan T. (2002). Discrete microdomains with high concentration of cAMP in stimulated rat neonatal cardiac myocytes. *Science (New York, NY).2002;* **295:**1711-1715.

230. Zaglia T., Milan G., Franzoso M., Bertaggia E., Pianca N., Piasentini E., Voltarelli V.A., Chiavegato D., Brum P.C., Glass D.J., Schiaffino S., Sandri M. and Mongillo M. Cardiac sympathetic neurons provide trophic signal to the heart via β2-adrenoceptor-dependent regulation of proteolysis. *Cardiovascular Research*.2013;**97**:240-250.

231. Zaglia T. Milan G., Ruhs A., Franzoso M., Bertaggia E., Pianca N., Carpi A., Carullo P., Pesce P., Sacerdoti D., Sarais C., Catalucci D., Krüger M., Mongillo M., Sandri M. Atrogin-1 deficiency promotes cardiomyopathy and premature death via impaired autophagy. *J Clin Invest*. 2014;**124**:2410-2424.

232. Zaglia T., Pianca N., Borile G., Da Broi F., Richter C., Campione M., Lehnart S.E., Luther S., Corrado D., Miquerol L. snd Mongillo M. Optogenetic determination of the myocardial requirements for extrasystoles by cell type-specific targeting of ChannelRhodopsin-2. *Proceedings of the National Academy of Sciences of the United States of America.*2015;**112**:E4495-4504.

233. Zaglia T., Di Bona A., Chioato T., Basso C., Ausoni S. and Mongillo M. Optimized protocol for immunostaining of experimental GFP-expressing and human hearts. *Histochem Cell Biol*.2016;**146(4):**407-19.

234. Zalk R. Clarke O. B., des Georges A., Grassucci R.A., Reiken S., Mancia F., Hendrickson W.A., Frank J., Marks A.R. Structure of a mammalian ryanodine receptor. *Nature*.2015;**517**:44-49.

235. Zanna C., Ghelli A., Porcelli A.M., Karbowski M., Youle R.J., Schimpf S., Wissinger B., Pinti M., Cossarizza A., Vidoni S., Valentino M.L., Rugolo M., Carelli V. OPA1 mutations associated with dominant optic atrophy impair oxidative phosphorylation and mitochondrial fusion. *Brain.* 2008*;***131**:352-367, 2008.

236. Zhang F., Wang L.P., Brauner M., Liewald J.F., Kay K., Watzke N., Wood P.G., Bamberg E., Nagel G., Gottschalk A. and Deisseroth K. Multimodal fast optical interrogation of neural circuitry. *Nature.*2007;**446:**633-639.

237. Zhang F., Vierock J., Yizhar O., Fenno L.E., Tsunoda S., Kianianmomeni A., Prigge M., Berndt A., Cushman J., Polle J., Magnuson J., Hegemann P., Deisseroth K. The microbial opsin family of optogenetic tools. *Cell.* 2011;**147**: 1446-1457.

238. Zhao S., Cunha C., Zhang F., Liu Q., Gloss B., Deisseroth K., Augustine G.J., Feng G. Improved expression of halorhodopsin for light-induced silencing of neuronal activity. *Brain Cell Biol*. 2008; **36**:141-154.

239. Zhou S., Chen L.S., Miyauchi Y., Miyauchi M., Kar S., Kangavari S., Fishbein M.C., Sharifi B. and Chen P.S. Mechanisms of cardiac nerve sprouting after myocardial infarction in dogs. *Circ Res.* 2004;**95**:76–83.

240. Zipes D.P., Heart-brain interactions in cardiac arrhythmias: role of the autonomic nervous system. Cleve Clin J Med. 2008;**75(2)**:S94-96.

241. Zipes D.P. Antiarrhythmic therapy in 2014: contemporary approaches to treating arrhythmias. *Nat. Rev. Cardiol*. 2015;**12**:68-9.

242. Züchner S., Vorgerd M., Sindern E., Schröder J.M. The novel neurofilament light (NEFL) mutation Glu397Lys is associated with a clinically and morphologically heterogeneous type of Charcot-Marie-Tooth neuropathy. *Neuromuscul Disord*.2004;**14(2)**:147-57.

ACKNOWLEDGMENTS

I would like to thank my supervisors, Prof. Marco Mongillo and Dr. Tania Zaglia for their scientific support with experiments, ideas and planning the activities, but also for discussions and for helping me to grow not only from a scientific point of view, but above all human. Indeed, they have always been able to motivate and stimulate me with attractive work activities and studies, proposing and then preparing me for international meetings and supporting me in challenging times with constant help.

I would also like to thank the group they have built over the years. These people have made it possible my thesis work and have always accompanied my scientific and personal growth. In particular, Francesca Da Broi and Anna Pia Plazzo, which started the work in the neuron-cardiomyocytes co-culture; Nicola Pianca, who helped me in both projects and in particular he taught me all about ECG analysis; Mauro Franzoso to the *in vitro* neuronal studies; Anna Di Bona to whole mount staining and human studies; Antonio Campo, that is my school-mate during the PhD training, who support me during these years; all other people of the lab, Silvia Bertoli, Arianna Scalco, Veronica Vita, Giulia Borile, Lolita Dokshokova to the support and discussion.

I would also like to thank the collaborators of the Opa1 project, in particular Luca Scorrano and Valerio Carelli.

Finally, I would like to thank the Ph.D. School and Professors, for the many opportunities offered for growth, training and scientific discussion.